This electronic thesis or dissertation has been downloaded from Explore Bristol Research, http://research-information.bristol.ac.uk

Author:
Bennett, Kathryn M

Title:
Neural Networks underlying Essential Tremor

Neural Networks underlying Essential Tremor

Kathryn Mary Bennett

Word count = 50,696

Abstract

Essential Tremor (ET) is a common movement disorder, causing a postural or kinetic tremor, and has an unknown aetiology. Accumulating evidence suggests abnormalities occurring within cerebellar circuits underlie the pathogenesis of ET, resulting in abnormal rhythmic output to the thalamocortical network.

The overarching aim of this thesis was to identify the neural dynamics of ET across the motor network in a rodent harmaline model of ET and in ET patients. Cerebellar local field potentials (LFPs) in anaesthetised and awake rats showed harmaline-induces theta frequency oscillations within the medial cerebellar nuclei. In the awake rat, tremor-correlated oscillations in the cerebellum were not modulated by movement, despite significantly increased behavioural tremor amplitude with movement. Conversely, neural oscillations recorded from the thalamus were modulated by movement. These findings suggest harmaline-induced cerebellar oscillations are independent of behavioural state and associated changes in tremor amplitude. By contrast, thalamic oscillations are dependent on behavioural state and related changes in tremor amplitude.

Visual feedback of tremor has been previously associated with increased tremor amplitude in ET. To examine whether this effect is mediated by synchronisation of cerebral cortical oscillations to the tremor, this thesis also assessed whether visually evoked steady-state electroencephalography (EEG) potentials influence tremor amplitude in ET patients. Rhythmic visual stimuli evoked EEG oscillations, however, these stimuli did not influence tremor amplitude. Natural but not artificial visual feedback of tremor increased tremor amplitude, however natural visual feedback was not associated with increased tremor frequency coherence between visual and motor brain sources.

Overall, this research shows that neural oscillations in thalamocortical, but not cerebellar circuits can be influenced by movement and/or behavioural tremor amplitude in the harmaline model. However, despite natural visual feedback increasing tremor amplitude in ET, this effect does not appear to be due to entrainment of cerebral cortical rhythms to the tremor via the visual system.

Abstracts associated with this work

Bennett, K.M., Cerminara, N., Goodfellow, M., Whone, A. & Apps, R. (2018). Examining cerebellar-thalamo-cortical network dynamics in the harmaline rodent model of Essential Tremor. *1st International Tremor Congress.*

Bennett, K.M., Cerminara, N., Goodfellow, M., Whone, A. & Apps, R. (2018). The effect of harmaline on coherent tremor oscillations across the cerebellar-thalamo-cortical network. 11th *Forum of Neuroscience, Federation of European Neuroscience Society.*

Bennett, K.M., Cerminara, N., Goodfellow, M., Whone, A. & Apps, R. (2019). Oscillatory motor network activity during rest and movement in the Harmaline rodent model of tremor. *Society for research on the cerebellum and ataxias.*

Bennett, K.M., Goodfellow, M., Cerminara, N., Apps, R., Whone, A. & Stothart, G. (2020). The effect of visual feedback and visual stimulation on tremor activity in Essential Tremor. *2020 Annual Meeting for the Society for the Neural Control of Movement.*

Acknowledgements

Authors Declaration

I declare that the work in this dissertation was carried out in accordance with the requirements of the University's *Regulations and Code of Practice for Research Degree Programmes* and that it has not been submitted for any other academic award. Except where indicated by specific reference in the text, the work is the candidate's own work. Work done in collaboration with, or with the assistance of, others, is indicated as such. Any views expressed in the dissertation are those of the author.

SIGNED: .... DATE: ..01/02/2021.........................

Contents

List of figures

xviii

List of tables

Abbreviations

5-HT	5-hydroxytryptamine
DBS	Deep brain stimulation
DICS	Dynamic modelling of coherence sources
EEG	Electroencephalography
EIB	Electrode interface board
EMG	Electromyography
ET	Essential Tremor
FFT	Fast fourier transform
GABA	Gamma-Aminobutyric acid
GAD-67	Glutamic acid decarboxylase 67
GluRδ2	Glutamate receptor delta 2
IAAFFT	Iterative amplitude adjusted fast fourier transform
i.p	Intraperitoneal
IO	Inferior olive
ISI	Inter-spike Intervals
LFP	Local field potential
LINGO1	Leucine rich repeat and Ig domain containing 1
M1	Primary motor cortex
MEG	Magnetoencephalography
MUA	Multi-unit activity
PB	Phosphate buffer
PBS-T	Phosphate-buffered saline with Triton X
PD	Parkinson's Disease
PET	Positron emission tomography
S1	Primary somatosensory cortex
SD	Standard deviation
SEM	Standard error of the mean
SMA	Supplementary motor area
SMC	Primary sensorimotor cortex
TMS	Transcranial magnetic stimulation
VA	Ventral anterior nucleus of the thalamus
VA/VL complex	Ventral anterior – ventral lateral complex of the thalamus

VGlut2	Vesicular glutamate transporter 2
VIM	Ventral intermediate nucleus of the thalamus
VL	Ventral lateral nuclei of the thalamus
VM	Ventral medial nucleus of the thalamus

Chapter 1.   **General introduction**

Tremors are defined as involuntary rhythmic movements of a body part, and so can be measured in terms of frequency and amplitude (Bhatia et al., 2018). Tremors can arise from different mechanisms and aetiologies and include physiological tremors which are observed in healthy individuals, as well as pathological tremors, which are a key symptom of different neurological disorders. Essential tremor (ET) is a pathological tremor that is the focus of this thesis.

1.1   Types of tremor

1.1.1   Physiological tremor

Physiological tremors are a natural phenomenon present in all individuals and are rarely visible to the human eye. These tremors are typically very low in amplitude and high in frequency (7–12Hz). Physiological tremors are thought to be partly influenced by mechanical properties of the limb, which include physical inertia and stiffness. The frequency of a mechanical tremor (f) of an object can be defined by $f = \sqrt{K}/I$, where K is the stiffness of the object and I is its inertia (Hallett, 1998). In the human body, this incorporates the mass of a limb interacting with the elasticity and stiffness of the muscle, tendons and joint. Mechanical tremors arise when a force is applied to an object (e.g. a relaxed and unsupported limb), causing the object to oscillate. Without sustained force, these oscillations dampen with each cycle, and with increased stiffness of the object, these oscillations dampen more rapidly (Allum & Young, 1976; De Groote et al., 2018; Walsh & Wright, 1987). Our limbs experience constant sources of external and internal force, such as gravitational force, passive vibrations from respiration and heart rate, as well as random motor unit firing (Christakos, 2005; Hallett, 1998). It is thought that these types of external and internal forces contribute to the mechanical tremors observed in our limbs. The contribution of mechanical properties to physiological tremor is illustrated by the phenomena that the frequency of tremor can be reduced by applying additional mass to the limb, which inherently changes the limbs mechanical properties in line with the equation provided above (Hallett, 1998; Homberg et al., 1987).

Physiological tremors are also thought to be affected by oscillations arising from synchronous motor unit activity within peripheral spinal reflex arcs. These oscillations arise from negative-feedback loops induced by a stretch of the extensor muscle, which in turn excites muscle spindle Ia afferent signals to the spinal cord, and after a conduction and synaptic time delay, the extrafusal muscle fibres receive synchronised motor unit inputs (Christakos, 2005). In such cases, the frequency of the tremor would depend on the length of the reflex arc. However, oscillations which are close together in terms of frequency can be entrained to the same rhythm, and so mechanical

and reflex tremors could modify or entrain one another (Rothwell, 2008). Entrained mechanical-reflex tremors may also be responsible for enhanced physiological tremors (Hallett, 1998; Young & Hagbarth, 1980). Physiological tremors may also be enhanced by prolonged muscle contraction, fatigue, anxiety, and a variety of tremor enhancing drugs (Bain, 2002; Homberg et al., 1987). Physiological tremors are therefore thought to arise from oscillations within the peripheral system, and not affected by central mechanisms.

1.1.2 Pathological tremor

Pathological tremors can arise from abnormalities occurring within longer feedback loops involving central neuronal motor networks, due to disease or injury, or abnormal changes in oscillatory activity occurring within central oscillators that are independent from the periphery (Deuschl et al., 2001). Pathological tremors can be classified by whether the tremor occurs when the limb is resting or used in action. A resting tremor refers to tremor occurring when the muscle is completely relaxed or supported (e.g. on a table/lap), whereas an action tremor occurs during voluntary contraction of muscles. Action tremors can be further subdivided into (1) postural tremor, where limbs are held in a sustained posture position, unsupported against gravity; (2) kinetic tremor, where limbs are voluntarily performing a movement; and (3) intention tremor, where a tremor occurs during intended movement towards an object (Bain, 2002). Table 1-1 provides examples of different neurological disorders that are associated with pathological tremors, and whether these tremors are typically classified as resting, postural, kinetic or intention tremors.

Essential tremor (ET) is the most common movement disorder and pathological tremor, affecting an estimated 0.4% of the population, or 4.6% of those aged 65 years and above (Louis & Ferreira, 2010). ET is increasingly being recognised as a syndrome without a known aetiology. Due to the high prevalence of this disorder, there is a demand for research that sheds light on the potential causes of ET. Tremor in ET occurs mainly under postural and kinetic conditions, but in some cases resting tremor may be present. However, it has been suggested that the latter is associated with advanced ET (Bhatia et al., 2018; Thenganatt & Jankovic, 2016). For a diagnosis of ET, according to criteria formulated by the Movement Disorder Society, a bilateral upper limb action tremor should be present for at least 3 years in duration. This can be accompanied by tremor affecting the head, voice, and less frequently, the lower limbs (Bhatia et al., 2018; Thenganatt & Jankovic, 2016). For diagnosis of ET, no other neurological signs, which may account for the tremor symptoms, should be present (Bhatia et al., 2018; Thenganatt & Jankovic, 2016). Supportive diagnostic criteria include a long duration since tremor onset, slow or no progression, a positive

family history and symptomatic relief with alcohol (Bhatia et al., 2018; Haubenberger et al., 2014). Additional "soft neurological signs" may also be present, but there is no consensus on which signs are acceptable within the diagnostic criteria for ET (Bhatia et al., 2018). The tremor task force proposed a diagnosis of "ET plus" for individuals with diagnostic features of ET in addition to other neurological signs such "*impaired tandem gait, questionable dystonic posturing, memory impairment, or other mild neurologic signs of unknown significance*" (Bhatia et al., 2018). The aim of this re-classification was to define a more homogenous group for future studies, which could exclude those classified as ET plus. However, a recent study, which re-classified patients using this criterion, found that out of 133 previously classified ET patients, only 20 would remain within this classification, where 110 would be classified as ET plus, due to various 'soft neurological signs' (Rajalingam et al., 2018).

Converging research suggests ET arises from abnormalities occurring within the cerebellar-thalamocortical network. However, there is much uncertainty underlying how and where these abnormalities may arise. This thesis will describe experiments examining the neural correlates underlying ET and the harmaline rodent model of ET, and how interactions within the cerebellar-thalamocortical network relate to changes in tremor amplitude.

Table 1-1 Neurological disorders associated with pathological tremor symptoms.
Table indicates the types of pathological tremors that can be associated with each of the listed neurological disorders.

Neurological disorders	Postural tremor	Kinetic Tremor	Intention tremor	Resting tremor
Essential Tremor	✓	✓		
Dystonic Tremor	✓	✓		
Cerebellar Tremor	✓	✓	✓	
Psychogenic tremor (functional tremor)	✓	✓	✓	✓
Parkinsonian Tremor				✓
Orthostatic Tremor	✓	✓		
Holmes Tremor	✓	✓	✓	✓
Palatal Tremor	✓	✓		
Tremor due to Multiple Sclerosis	✓	✓	✓	
Tremor due to Stroke	✓	✓	✓	✓

1.2   Anatomy and function of the cerebellar-thalamocortical pathway

The sections below provide a brief overview on the anatomy and functions of the key brain regions of the cerebellar-thalamocortical pathway that is associated with abnormal changes in ET.

1.2.1   The cerebellum

The cerebellum plays an important role in motor control, including the fine-tuning of movements and postures, and so abnormal involvement of the cerebellum is a likely candidate for the physiological changes observed in ET. The cerebellum has a consistent anatomical organisation across mammals (Sultan & Glickstein, 2007), and is located caudal to the cerebral cortex (Figure 1-1). In the longitudinal plane, the cerebellum can be divided into three parts: the vermis, the paravermis, and the hemispheres (Figure 1-2). In cross-sections of the cerebellum, the gross anatomical features of the cerebellum can be divided into a) the three layers of the cerebellar cortex which cover the surface of the cerebellum, and b) the cerebellar nuclei, which are embedded within white matter beneath the cerebellar cortex. The mammalian cerebellum has three nuclei; from medial to lateral these are the fastigial nucleus (known as the medial nucleus in rodents), the interposed nucleus (anterior and posterior), and the dentate nucleus (known as the lateral nucleus in rodents).

The layers of the cerebellar cortex from the pia towards the inner layer consist of the molecular layer, Purkinje cell layer and granule cell layer (Apps & Hawkes, 2009). The granule cell layer of the cerebellar cortex receives mossy fibres inputs from the pontine nuclei, which consist of descending inputs from the cerebral cortex (cortico-pontocerebellar pathway), as well as ascending inputs from Clarke's column and dorsal column nuclei (the spinocerebellar pathway) (Brodal & Bjaalie, 1997; Hantman & Jessell, 2010; Loutit et al., 2021). Mossy fibres synapse on granule cells in the cerebellar cortex, which in turn project long parallel fibres that run orthogonal to the longitudinal zones. It has been estimated that more than 100,000 parallel fibres can synapse on a single Purkinje cell (Napper & Harvey, 1988).

The other major inputs to the cerebellar cortex are climbing fibres, which arise exclusively from the inferior olive (IO) located in the caudal brainstem (De Gruijl et al., 2013; Reeber et al., 2012). Climbing fibre afferents are topographically organised, where climbing fibres originating in discrete regions of the IO target Purkinje cells located within longitudinally oriented zones of the cerebellar cortex, as illustrated in Figure 1-2 (see Apps & Hawkes, 2009 for review). The Purkinje cells are the only output cell from the cerebellar cortex. These cells are also highly topographically organised, as they send inhibitory projections to specific regions of the cerebellar nuclei thereby forming a series of olivo-cortical-nuclear modules (Apps & Hawkes, 2009). In brief, Purkinje cells in the vermal A zones of the cerebellar cortex (Figure 1-2) project to the medial nucleus; Purkinje cells in the paravermal zones project to the interposed nucleus; and Purkinje cells located in the hemispherical zones project to the lateral nucleus. The cerebellar nuclei then provide the final output from the cerebellum. Topographically organised climbing fibre afferents also give rise to collateral branches to the cerebellar nuclei, and the cerebellar nuclei possess reciprocal inhibitory cerebellar nuclear-IO projections, closing the loop on a tri-synaptic connection between the IO, Purkinje cells and cerebellar nuclei within the same topographic plane (Ruigrok & Voogd, 2000; van der Want et al., 1989; Wlklund et al., 1984).

Each Purkinje cell within the cerebellar cortex is innervated by only one climbing fibre, but each climbing fibre can have collateral branches which innervate 1-10 Purkinje cells arranged in parasagittal stripes. Each collateral branch of the climbing fibre wraps around the Purkinje cell dendritic tree and forms hundreds of synaptic contacts, to deliver a powerful excitatory input (Eccles et al., 1966; Silver et al., 1998). The result of this intense excitatory input produces an action potential with a complex waveform, known as a complex spike. This comprises an initial post-synaptic spike, followed by a high frequency burst of smaller spikelets. This distinct waveform makes climbing fibre afferent input to Purkinje cells easy to distinguish, as the second type of

afferent input, which arises from parallel fibres, produces an action potential with a conventional single spike waveform, known as a simple spike. As climbing fibre collateral branches can innervate a small number of Purkinje cells aligned in parasagittal stripes, the complex spikes that arise from these inputs occur synchronously (Lang et al., 1999).

Human Brain
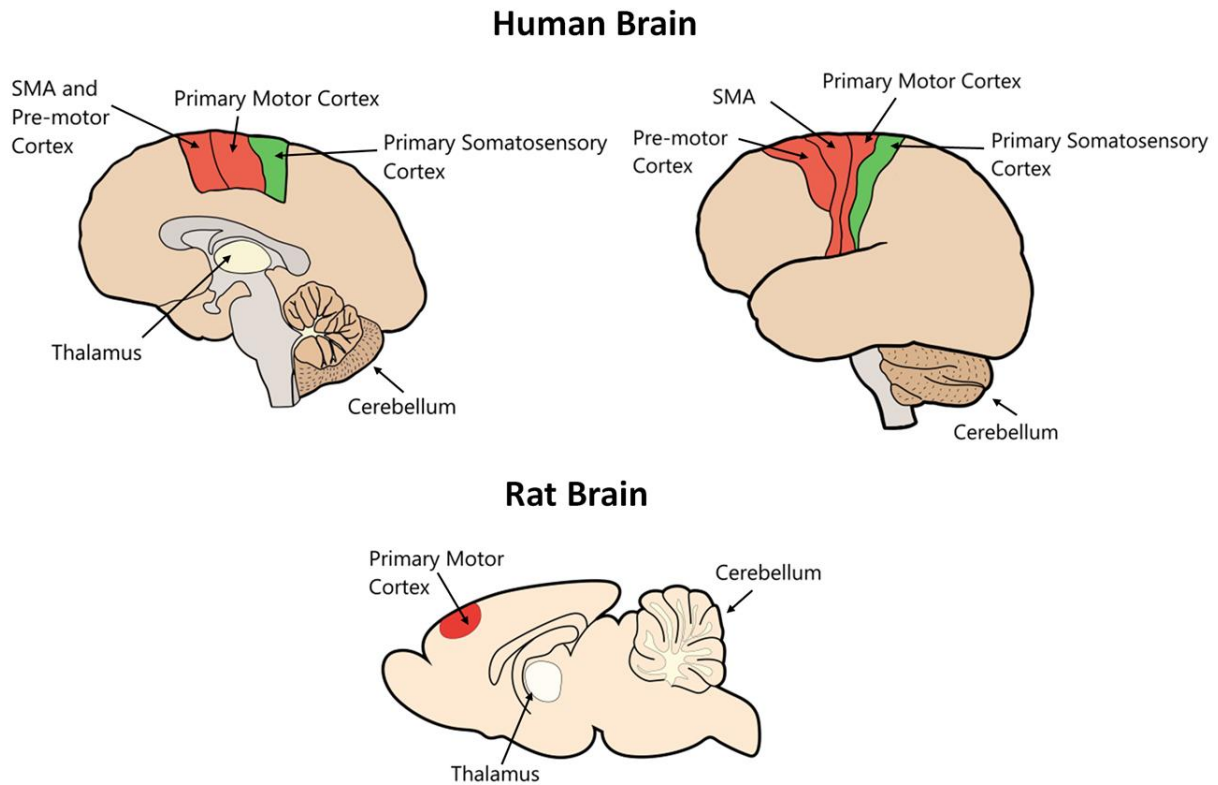
Rat Brain

Figure 1-1 Anatomical locations of the cerebellum, thalamus and motor cortex in the human brain and rat brain.
Schematic diagram of the sagittal (top left) and lateral (top right) views of the human brain, and a sagittal view of the rat brain (bottom).

	Hemisphere			Paravermis				Vermis				
D3	D0	D1	C3	C2	Cx	C1	A2	B	X	Ax	A	Cerebellar cortex zones
dlPO	dmPO	vlPO	vfDAO	rMAO	iMAO	vfDAO	cMAO	dfDAO	iMAO	cMAO	cMAO	Inferior Olive (input)
NL	DLH	NL	NIA	NIP	NIP	NIA	DLP	LVN	NIP	MedN	MedN	Cerebellar Nuclei (output)
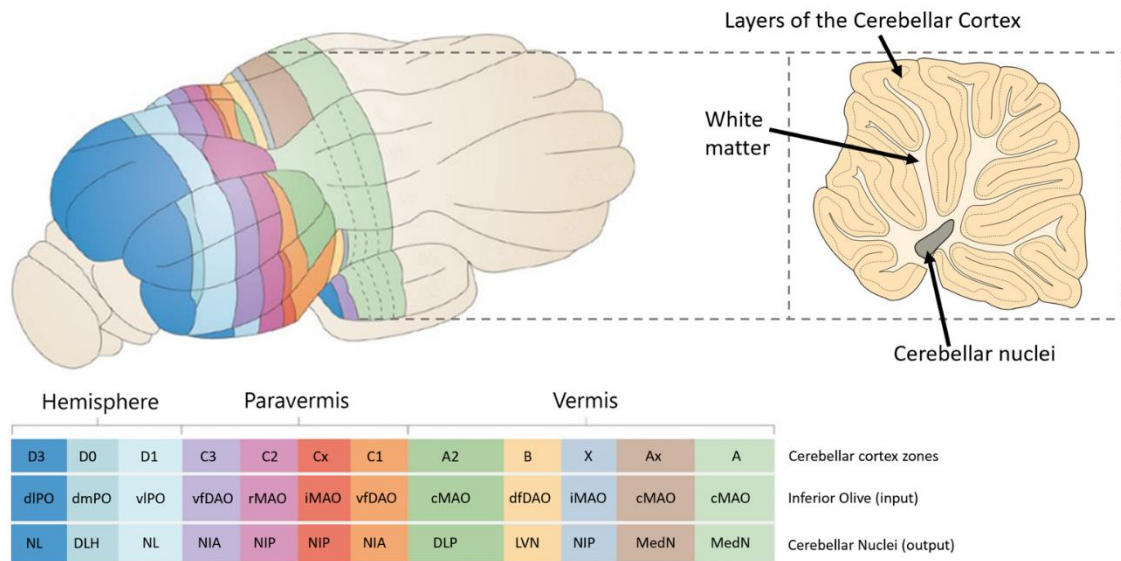
Figure 1-2 Longitudinal zones of the olive-cerebellar pathway.
The diagram shows a colour coded map of the olivo-cerebellar pathway in a rat. A posterior view of the rat cerebellum (top left) shows colour coded regions of the cerebellar cortex, and a cross-section of the vermal region of the cerebellar cortex (top right). The top half of the colour coded bar below the diagram approximately illustrates which regions of the cerebellar cortex receive inputs from the discrete regions of the inferior olive indicated in the middle bar. The bottom half of the colour coded bar illustrates approximately which cerebellar nuclei receives Purkinje cell projections from the colour coded region of the cerebellar cortex. Adapted from Apps & Hawkes, (2009).

cMAO = caudal medial accessory olive; dfDAO = dorsal fold of dorsal accessory olive; DLH = dorsolateral hump; DLP = dorsolateral medial nucleus; dlPO = dorsal lamella of the principal olive; dmPO = dorsomedial subnucleus of the principal olive; iMAO = intermediate medial accessory olive; LVN = lateral vestibular nucleus; MedN = medial nucleus; NIA = anterior interpositus nucleus; NIP = posterior interpositus nucleus; NL = lateral nucleus; rMAO = rostral medial accessory olive; vfDAO = ventral fold of dorsal accessory olive; vlPO = ventral lamella of the principal olive.

1.2.2 The thalamus

Regions of the lateral (dentate), interpositus and medial (fastigial) cerebellar nuclei send excitatory ascending projections to the thalamus (Asanuma et al., 1983; Hintzen et al., 2018; Sakai, 2013; Teune et al., 2000). The thalamus comprises a range of nuclei which relay information from subcortical structures to the cerebral cortex across functional brain networks. In addition, the thalamus contains association nuclei, which integrate a range of inputs from cerebral cortical and subcortical sources (Danos et al., 2003; Sherman, 2007). In humans the thalamus is a pair of egg-like shapes located in the midbrain above the brain stem (Figure 1-1). Bands of myelinated axons called the internal medullary lamina, divide the thalamus into three regions on each egg like structure: the anterior, medial, and lateral regions.

The lateral regions of the thalamus, specifically the ventral anterior (VA), ventral lateral (VL) and ventral medial (VM) nuclei of the thalamus, are involved in relaying information to the motor cortex from the cerebellum and basal ganglia, and vice versa (Habas et al., 2019; Hintzen et al., 2018). Immediately posterior to the motor regions of the thalamus are the ventral posterior nuclei of the thalamus, which are involved in relaying information through the somatosensory system (Diamond et al., 1992). The motor regions of the thalamus are largely conserved across mammals (Bosch-Bouju et al., 2013). However, in rodents, the distinction between VA and VL is more difficult, and so this region is often referred to as the VA/VL complex (Kuramoto et al., 2009b; Nakamura et al., 2014).

1.2.3   The motor cortex

In humans, the cerebral cortex is made up of the frontal, parietal, temporal and occipital lobes. Like the thalamic nuclei, different regions of the cerebral cortex have been associated with different specialised functions. The motor regions of the cerebral cortex consist of the primary motor cortex (M1), the supplementary motor area (SMA), and the pe-motor cortex (Figure 1-1). M1 is located anterior to the central sulcus which separates the frontal and parietal lobes, and is involved in the initiation of movements, as neural activity within this region reflects movement patterns, and this area has direct projections to spinal motoneurons (Cowper-Smith et al., 2010; Hamed et al., 2007; Yokoi et al., 2018). Furthermore, neurons within this region have been shown to be somatotopically organised, such that different regions of the motor cortex map to different regions of the body (Indovina & Sanes, 2001; Rao et al., 1995). The SMA and pre-motor cortex are located anterior to M1 where the pre-motor cortex is located caudal to the SMA (Tanji, 1994). SMA is thought to be involved in the planning and co-ordination of movements (Makoshi et al., 2011; Picard, 2003), and the premotor cortex is thought to be responsible for coding goal-directed movements (Gremel & Costa, 2013; Kantak et al., 2012). Located immediately posterior to the central sulcus and M1 is also the primary somatosensory cortex (S1), which receives somatosensory inputs relayed from the thalamus, and is also organised somatotopically with different regions of S1 mapping to different regions of the body (Kaas et al., 1979; Omori et al., 2013; Overduin & Servos, 2004). Sensory feedback of movements is thought to play an important role in motor control, as impaired sensorimotor integration has been associated with different movement disorders (Abbruzzese & Berardelli, 2003).

Neurons across the cerebral cortex are organised into six layers. From the pia to the inner layer, this includes 1) the molecular, 2) external granular, 3) external pyramidal, 4) internal granular, 5) internal pyramidal and 6) multiform layers. Intracortical inputs are typically located in the

superficial layers (1-3) of the cerebral cortex, and evidence has shown extensive intercortical connections between M1, SMA and the premotor cortex in these layers (Dum & Strick, 2005; Matelli et al., 1986; Morecraft & van Hoesen, 1992; Takada et al., 2001; Tokuno & Tanji, 1993). Thalamocortical relay neurons located in motor regions of the thalamus receive input from both the cerebellum and basal ganglia, and in turn have excitatory projections to layers 4 in the motor cortex (Bosch-Bouju et al., 2013; Gaidica et al., 2018). Corticothalamic neurons project back to motor regions of the thalamus from deep layers (5-6) of the motor cortex (Guillery, 1995; Yamawaki & Shepherd, 2015). In rodents, the cytoarchitecture of the cerebral cortical layers are conserved, whereby humans and rodents show similarity in the somatotopic organisation of M1 and S1 (Chapin & Lin, 1984; Donoghue & Wise, 1982; Narayanan et al., 2017; Neafsey et al., 1986).

1.3 What are the neural substrates of Essential Tremor?

1.3.1 Cerebellar involvement

1.3.1.1 *ET is associated with cerebellar-dependant motor symptoms*

Accumulating behavioural research suggests ET is associated with impaired cerebellar-dependant behaviours, implicating cerebellar abnormality as an underlying cause. Most compelling is evidence that known damage to the cerebellum is associated with movement related tremors, and ataxia, amongst other movement related disturbances (Benito-León & Labiano-Fontcuberta, 2016; Diener & Dichgans, 1992; Fahn, 1984; Holmes, 1939; Marek et al., 2015). Intention tremor, which is a tremor that worsens when reaching the endpoint of a goal-directed movement, is a cardinal symptom of cerebellar dysfunction, resulting from disturbances to cerebellar output pathways (Fahn, 1984; Holmes, 1939). Intention tremor is also a 'sometimes prevalent' rather than distinguishing symptom of ET, where the prevalence of intention tremor has been associated with more severe or advanced cases of ET (Deuschl et al., 2000; Louis et al., 2009; Sternberg et al., 2013). For example, some patients slowly develop an intention tremor from a postural tremor, and the amplitude of postural tremor in ET with intention tremor may be greater than for ET without intention tremor (Deuschl et al., 2000; Marsden, 1984). ET patients with intention tremor also performed similar to patients with cerebellar disease in a reach-to-grasp task, where both groups showed increased amplitude of hand path curvature and significant overshooting of the wrist movement when grasping (Deuschl et al., 2000). These findings suggest that ET with intention tremor is accompanied by cerebellar-related deficits in the co-ordination and speed of goal-directed multi-joint movements. ET patients without intention tremor also showed a trend towards similar abnormalities when compared to control subjects (Deuschl et al., 2000).

Non-tremor motor symptoms have also been reported in ET groups, such as mild bradykinesia (i.e. slowness of movement) and ataxia (Arkadir & Louis, 2013; Duval et al., 2006; Singer et al., 2004; Stolze et al., 2001). Ataxia describes disturbances in movement co-ordination, including gait and balance, and is also a symptom of cerebellar dysfunction, or damage to descending motor pathways. Dystonia, which is an uncontrollable muscle spasm, has also been reported in 47% of ET patients in a study comprehensively examining clinical symptoms in 350 ET patients. (Lou & Jankovic, 1991). A wealth of evidence has shown that ataxia and dystonia are related to abnormalities with cerebellar physiology (Shakkottai, 2014), and so there is a strong indication that cerebellar-abnormalities are associated with symptoms of ET.

1.3.1.2   Abnormal changes in motor timing and motor adaption

The olivo-cerebellar circuit is thought to play a central role in motor timing, as well as with motor adaption and motor learning. Involvement of this pathway in motor learning is supported by evidence from eye-blink conditioning. Eye-blink conditioning is a classical conditioning paradigm which involves pairing a conditioned stimulus, such as a visual or auditory cue, with an unconditioned stimulus, such as a puff of air delivered to the eye. Delivery of an unconditioned stimulus (e.g. puff of air) will elicit an unconditioned response, such as an eye-blink. Over repetitive pairings of the conditioned and unconditioned stimulus, the participants will learn to respond to the conditioned stimulus with an unconditioned response, producing a conditioned response. Eye-blink conditioning is therefore a form of motor learning, and physiological experiments have shown that eye-blink conditioning is a cerebellar-dependant behaviour, as lesions to the cerebellum can abolish the conditioned response without affecting the unconditioned response (Clark et al., 1984; McCormick et al., 1982; Yeo et al., 1985). Using this classical conditioning paradigm, evidence has suggested ET patients show an impaired ability to learn conditioned eye-blink responses (Kronenbuerger et al., 2007, 2008). Studies examining oculo-motor function in ET also identified abnormal hand-eye co-ordination (Trillenberg et al., 2006), impaired ocular smooth pursuit, and abnormal vestibulo-ocular reflex in ET (Helmchen et al., 2003). Furthermore, ET patients have shown impaired performance on a visuo-motor adaption task (Hanajima et al., 2016). Taken together, impairments of eye-blink conditioning and motor adaption in ET points towards the involvement of cerebellar dysfunction.

Behavioural studies have also shown that ET patients may have difficulties performing voluntary rhythmic movements, which intrinsically involve motor timing abilities associated with olivo-cerebellar function. For example, Farkas, Szirmai, & Kamondi, (2006) demonstrated that ET patients had a reduction in their regularity of finger tapping movements at speeds paced by a

metronome, suggesting ET patients were not able to synchronize repetitive movements to extrinsic timing cues. ET patients were also slower to perform rhythmic thumb to forefinger tapping movements, and showed greater variability in these movements, with longer touch duration and reduced inter tapping intervals (Avanzino et al., 2009; Jiménez-Jiménez et al., 2010). Work by Pedrosa et al., (2016) also showed that ET patients performed worse on a task that involved observing and reproducing the length of time a stimulus was displayed on-screen. Taken together, this suggests ET may be associated with impairments in predictive temporal perception as well as motor timing.

1.3.1.3 *Neuropathological changes in the cerebellum*

Although ET is not considered to alter life expectancy (Rajput et al., 1984), there is increasing evidence from post mortem ET brains that suggests ET may be a slowly progressing neurodegenerative disorder involving the cerebellum. This is accompanied by reports of worsening objective and subjective measures of tremor symptoms in ET overtime (Gironell et al., 2015; Gutierrez et al., 2016; Louis et al., 2011). For example, research has identified signs of cerebellar atrophy and Purkinje cell degeneration in ET compared to healthy controls (Benito-León et al., 2009; Louis, 2016), although significant Purkinje cell loss has not been detected in all studies (Louis, 2016). Other Purkinje cell related pathological changes include an increased number of Purkinje cells displaced in the molecular layer of the cerebellum, a reduction in the size of Purkinje cell dendritic arbors and dendritic spine density, increased axonal swellings, axon terminal sprouting and axonal branching (Babij et al., 2013; Kuo et al., 2011; Louis, 2016; Louis et al., 2014; Yu et al., 2012). There is also evidence for increased density of basket cell branching in ET (Erickson-Davis et al., 2010). Basket cells are inhibitory interneurons, which form a branching network of synapses around Purkinje cell bodies, and so increased branching density may suggest an increased number of inhibitory basket-Purkinje cell synaptic connections. Research has also identified an overall reduction in the density of climbing fibre-Purkinje cell synapses, and a change in the distribution of climbing fibre synapses, where greater number of climbing fibre synapses are found on distal dendritic spines (Kuo et al., 2017; Lee et al., 2018; Lin et al., 2014; Pan et al., 2020). This is opposed to normal development and distribution of Purkinje cell synapses, where parallel fibres develop synaptic territories on distal branches of the Purkinje cell dendritic arbour, and climbing fibres develop synaptic territories on the thick proximal branches (Ichikawa et al., 2016). In a healthy subject, the vast number and location of climbing fibre synaptic inputs on proximal branches of Purkinje cell dendritic tree likely play an important role in the very high probability of action potential generation.

Neuroimaging has shown that ET was associated with increased activation of the dentate nucleus in the cerebellum, as well as in the red nucleus which receives cerebellar projections (Bucher et al., 1997). Conversely, healthy individuals who mimicked tremor movements of their upper limbs did not show increased activation in these nuclei (Bucher et al., 1997). Diffusion tensor imaging has also shown abnormalities occurring in superior and inferior cerebellar peduncles in ET, which are white matter tracts carrying efferent and afferent information to the cerebellum (Klein et al., 2011; Nicoletti et al., 2010). The integrity of these fibres may be related to tremor generation, or a consequence of hyperactivity. Positron emission tomography (PET) has also suggested abnormal hyper-metabolism of the IO, cerebellum and red nucleus (Boecker et al., 1996; Wills et al., 1994). Overall, behavioural, neuropathological and neuroimaging evidence suggests cerebellar dysfunction in ET.

1.3.2 Thalamic involvement

Electrophysiological recordings from the thalamus have provided convincing evidence for thalamic involvement in ET. In particular, Hua et al. (1998) identified cells within the ventral intermediate nucleus (VIM) of the thalamus that fire periodically at rates that correlate with the tremor recorded via electromyography (EMG). The VIM of the thalamus is part of the ventral lateral thalamic nuclei and is thought to receive direct inputs from the cerebellum (Lierse, 1993). Individuals, who do not respond to pharmacological treatment for ET, can receive symptomatic relief from deep brain stimulation (DBS) to this area, suggesting its direct involvement in tremor pathways (Vaillancourt et al., 2003). Stimulation of the VIM and nearby subthalamic regions are thought to reduce tremor by disrupting or masking the underlying pathological inputs from the cerebellum (Kiss et al., 2002). Cagnan et al., (2013) also showed thalamic stimulation at near-to-tremor frequency could entrain the tremor frequency. Furthermore, near-to-tremor frequency stimulation also significantly amplified or suppressed tremor amplitude, depending on the phase of tremor oscillation when stimulation was applied (Cagnan et al., 2013). This suggests the thalamus plays an important role in propagated tremor oscillations through the cerebellar-thalamocortical pathway.

Research has also shown thalamic activity at the tremor frequency is only present during tremor periods. For example, Hua & Lenz (2005) identified neurons within the VIM that showed rhythmic firing of action potentials during periods of postural tremor and not during periods of resting without tremor. Coherence is a measure used to examine the linear correlation between signals in the frequency and time domain and has been used to examine whether neural signals correlate with the tremor as recorded via EMG. Local field potential (LFP) recordings from the VIM have

been shown to be highly coherent with EMG activity at the tremor frequency during tremulous periods (He et al., 2016; Pedrosa et al., 2012). To examine whether thalamic-EMG coherence occurred before or after tremor onset, Pedrosa et al., (2014) recorded thalamo-muscular coherence in patients during a task that involved moving arms and hands from a resting/supported position to holding arms and hands elevated and outstretched. This revealed that thalamo-muscular coherence at the tremor frequency occurred 220 ± 460ms following the onset of posture-induced tremor, suggesting somatosensory input may be important to the onset of thalamocortical coherence. This may be because the integration and entrainment of both motor and sensory tremor inputs to neighbouring sub-nuclei of the thalamus play a role in amplifying and spreading the tremor oscillation.

1.3.3   Motor cortex involvement

Evidence for the involvement of the motor cortex in ET is uncertain, as previous research has shown that cortico-muscular coherence is sporadic (Hellwig et al., 2001; Raethjen et al., 2007). Raethjen et al., (2007) found sensorimotor cortico-muscular coherence can appear intermittently, and it has been observed that sensorimotor cortico-muscular coherence is more likely to be present when tremor intensity increases (Hellwig et al., 2001; Raethjen et al., 2007). Intermittent cortico-muscular coherence has also been observed when the peripheral tremor activity remains constant, suggesting motor cortex tremor rhythms may be influenced by tremor intensity but the motor cortex may not be driving the tremor itself (Raethjen et al., 2007).

Hellwig et al., (2001, 2003) found that cortico-muscular coherence could occur exclusively contralaterally or both contralaterally and ipsilaterally. Additionally, coherence could switch between being exclusively contralateral to both contralateral and ipsilateral, therefore showing intermittent ipsilateral cortico-muscular coherence, and suggesting tremor oscillations on either side of the body occurs independently at times. This is further corroborated by evidence that EMG tremor measures did not significantly cohere between the right and left side of the body (Lauk et al., 1999). The authors proposed that intermittent activity may be indication of separate oscillating systems, which are intermittently entrained to the same phase and frequency and identified the thalamus as a potential key component in entraining these oscillators. Conversely, cortico-muscular coherence was not detected in a study using magnetoencephalography (MEG) (Halliday et al., 2000), and in some ET patients using EEG (Hellwig et al., 2001). This may be due to differences in the underlying physiology, low tremor amplitudes or signal-to-noise ratios.

To examine the involvement of the cortico-spinal tract in tremor generation and transmission, studies have also examined the influence of motor cortex stimulation on the rhythm of tremor

bursts. These studies have shown that transcranial magnetic stimulation (TMS) applied to M1 as well as the SMA can interrupt the tremor rhythm (Britton et al., 1994; Lu et al., 2015). Invasive stimulation of the motor cortex, as well as continuous theta-bust stimulation, has also shown some success in reducing tremor amplitude in patients (Chuang et al., 2014; Hellriegel et al., 2012; Moro et al., 2011). These studies provide clear evidence that the motor cortex is involved in modulating tremor oscillations at the muscles but does not necessarily imply the motor cortex is driving these oscillations.

1.3.4   Neural changes at the network level

Research has suggested that neural connectivity across the motor network is important for maintenance of tremor oscillations. Evidence from case studies of ET patients who have had a stroke within any region of the cerebello-thalamocortical network, or the pontine nucleus within the brain stem (part of the cortico-pontocerebellar pathway), can eradicate tremor symptoms (Dupuis et al., 2010). Work by Schnitzler et al., (2009) has suggested that ET can be characterised by hyper-synchronised oscillations occurring within cerebellar-thalamocortical network at the tremor frequency. This study used MEG and a source localisation technique known as dynamic modelling of coherence sources (DICS) to examine the network dynamics of tremor rhythms in ET. This identifed significant M1-EMG coherence at tremor frequency, and significant cortico-cortical coherence between M1 and ipsilateral premotor cortex, ipsilateral thalamus, the contralateral cerebellum, and the brainstem at the same frequency. Taken together, this suggests that although abnormal changes within the cerebellum are likely candidates for the development of abnormal tremor-related oscillations, the entire cerebello-thalamocortical circuit is important for the maintenance and propagation of these abnormal oscillations in ET.

1.4   Genetic link with Essential Tremor

The prevalence of ET increases in the elderly population (Louis & Ferreira, 2010). However, there is evidence of a bimodal distribution in the age of onset of ET, reflecting a young onset subgroup of ET and another subgroup for onset of ET in later-life (Louis & Dogu, 2008). Various studies have reported around 17-65% of sampled individuals with ET had a positive family history of the disorder, suggesting ET has a genetic basis in at least a subset of individuals (Critchley, 1972; Hornabrook & Nagurney, 1976; Lou & Jankovic, 1991; Louis & Ottman, 2006; Mengano et al., 1989; Rajput et al., 1984; Salemi et al., 1994). ET cases that onset during childhood were also more likely to have a positive family history of ET (Louis, Clark, & Ottman, 2015). Evidence has suggested that in some families ET may have autosomal dominant inheritance, which means that if the dominant abnormal gene is inherited from one parent, the condition will be passed onto the child. However,

this is evidently not the case for all familial cases of ET, as the expectancy rates in first degree relatives would be 50%. Despite evidence for ET heritability, progress in identifying genetic determinates of ET has been limited due to genotypic heterogeneity.

Genome-wide linkage analyses have shown some success in identifying chromosome locations of candidate ET-related genes (Gulcher et al., 1997; Higgins et al., 1997; Shatunov, 2006). However, the causal gene mutations within these loci have not been established, and study replication is poor due to the identification of different loci across different families and populations (Blair et al., 2008; Deng et al., 2005; Jeanneteau et al., 2006; Tan et al., 2007). However, the most recent genetic candidate identified using genome-wide mapping, the leucine rich repeat and Ig domain containing 1 (LINGO1) gene on chromosome 15q24.3, has been associated with ET in European and American families with an estimated population-attributable risk of 20% (Stefansson et al., 2009). This association has now been replicated by more than one large scale study, demonstrating a link with some European, American and Asian populations (Clark et al., 2010; Jiménez-Jiménez et al., 2012; Tan et al., 2009), but not with some Spanish and French-Canadian populations (Bourassa et al., 2011; Lorenzo-Betancor et al., 2011). LINGO1 expression is associated with neuronal damage and significantly increased LINGO1 protein levels have been found in the cerebellum of ET brains, which was also associated with disease duration (Delay et al., 2014). Increased LINGO1 expression has also been located on the axons of basket cells and Purkinje cells has also been found in ET brains and as well as on basket collateral synapses on/around the Purkinje soma (Kuo et al., 2013). LINGO1 expression was also correlated with the number of Purkinje cell axonal torpedoes and basket cell pathology, suggesting LINGO1 expression may contribute to cerebellar pathology and dysfunction associated with ET (Kuo et al., 2013). Taken together, research has indicated a promising link between ET and LINGO1 expression in some ET patient subgroups, which is likely linked to cerebellar pathologies.

1.5   Animal models of action tremor

As the causes of ET are unknown, animal models provide an opportunity to elucidate the pathological mechanisms underlying tremor. Several rodent models of tremor have been identified that originate from spontaneously occurring mutant genes with a tremor and ataxia phenotype (Miwa, 2007; Pan et al., 2018). These rodent models exhibit prominent pathological abnormalities within cerebellar circuits, such as Purkinje cell degeneration. Four of the most promising models of tremor showing ET-like characteristics are reviewed briefly below.

1.5.1 The harmaline model

The most widely used model of action tremor is the harmaline model. This is a pharmacological model of tremor, that involves administration of a β-carboline alkaloid known as harmaline. Harmaline is a reversible inhibitor of monoamine oxidase-A, and is found naturally in the seeds of the Pegamum harmala flower (Herraiz et al., 2010). The tremorgenic effect of harmaline has been reported within scientific literature since the 1950's, and has been shown to reliably produce a tremor in mice, rats, cats and monkeys that is more apparent during movement (Cheng et al., 2013). Harmaline induces a tremor by increasing the frequency and synchronicity of climbing fibre inputs from the IO to the cerebellum (De Montigny & Lamarre, 1973; Llinás & Volkind, 1973). This effect of harmaline on olivo-cerebellar activity is observed *in vivo* through systemic delivery of harmaline, as well as following microinjection of harmaline directly into the IO, and via perfusion of harmaline through the vertebral artery in a brainstem-cerebellum *in vitro* preparation (De Montigny & Lamarre, 1973; Llinás & Mühlethaler, 1988). The frequency of these tremors can vary slightly across species, where for smaller mammals (e.g. rats and mice) the frequency is generally higher (10-16Hz) than for larger mammals (e.g. monkeys show a tremor frequency of 7-12Hz)(Lamarre et al., 1975; Martin et al., 2005). However, an exception to the relationship between animal size and tremor frequency was found when administrating harmaline to pigs, which induced a tremor at a frequency of 10-16Hz (Lee et al., 2018).

Harmaline's effect on increasing the frequency and synchronicity of IO neuron firing is likely mediated by more than one mechanism and is linked to important physiological features of the IO. Specifically, the IO has a very high-density of gap junctions on dendritic spines, which gives the IO intrinsic oscillatory properties (Leznik & Llinás, 2005). The dendritic spines located on neighbouring IO neurons cluster together to form "glomeruli", which consist of dendro-dendritic gap junctions and chemical synaptic terminals bundled together within an astrocytic sheath (DeGruijl et al., 2014). The gap junctions provide electrical coupling of neighbouring neurons, by the bi-directional flow of current from one neuron to another (Faber & Pereda, 2018). This coupling is responsible for generating spontaneous 'subthreshold' oscillations in neuron membrane potential, which can influence the precise timing of action potentials elicited by synaptic inputs, and govern the synchrony of coupled IO neuron clusters (Chorev et al., 2007; De Gruijl et al., 2014; Long et al., 2002). This is evidenced by reduced synchrony between intracellular oscillations recorded from IO neurons, as well as between Purkinje cell complex spikes following intra-IO infusion of gap junction blockers (Blenkinsop & Lang, 2006; Leznik & Llinás, 2005). Research has also shown that gap-junction blockers carbenoxolone and mefloquine, suppress harmaline tremor (Martin & Handforth, 2006). This suggests that gap junctions in the IO play a

vital role in increasing the synchrony of complex spike firing in response to harmaline. Conversely, mice which have a knockout of the connexin 36 neuronal gap junction protein and reduced electrical coupling of IO, still show a tremor response to harmaline (Kistler et al., 2002). However, evidence has shown that the IO in connexin 36 deficient mice develop structures resembling gap-junctions and IO neurons still show sub-threshold oscillations, suggesting these mice develop structural and electrophysiological compensatory changes to persevere the rhythmic properties of the IO (De Zeeuw et al., 2003).

The glomeruli also receive GABAergic and glutamatergic inputs, which have been shown to influence the electrical coupling of IO neurons. For example, optogenetic induction of GABAergic input to the IO, suppressed subthreshold oscillations and reduced the voltage change coupling between the pre- and post-junction neurons (Lefler et al., 2014). Furthermore, low frequency (1Hz) stimulation of excitatory NMDA synaptic inputs to the IO can reduce the coupling of paired IO neurons (Mathy et al., 2014), whereas higher frequency stimulation (9Hz) of NMDA receptors, can increase the coupling of paired IO neurons (Turecek et al., 2014). Intra-IO infusions of picrotoxin, a GABA antagonist, and NBQX, a AMPA agonist, have also been shown to increase complex spike synchrony and alter the distribution of this synchronous activity within the cerebellar cortex (Lang et al., 1996; Lang, 2002). Taken together this evidence suggests GABAergic and glutamatergic inputs play a vital role in modulating the electrical coupling of IO neuron clusters, to alter the degree and pattern of synchronous, rhythmic activity in cerebellar circuits.

Despite harmaline belonging to a family of alkaloids known to be $GABA_A$ inverse agonists, research has shown that harmaline does not bind to $GABA_A$ receptors (Deecher et al., 1992). Harmaline has been shown to displace the binding of benzodiazepine, but only at a low affinity, and so is unlikely to be the driving mechanism in which harmaline modulates the electrical coupling IO neurons (Glennon et al., 2000; Robertson, 1980). However, administration of the $GABA_A$ receptor agonist, muscimol, suppresses harmaline-tremor, and the $GABA_B$ receptor agonist baclofen was shown to increase harmaline-tremor (Paterson et al., 2009). The $GABA_A$ agonist ethanol has also been shown to effectively reduce harmaline-induced tremor, but did not prevent increased levels of cerebellar cGMP, caused by increased cerebellar activation (Rappaport et al., 1984). Therefore, modulation of GABAergic inputs can impact harmaline-induced tremor, but the tremorgenic effects of harmaline is not likely driven by binding of harmaline to IO $GABA_A$ receptors.

Harmaline has also been shown to interact with glutamatergic receptor antagonists. For example, harmaline displaces the non-competitive NMDA receptor antagonist MK-801 (also known as dizocilpine) in the rabbit IO (Du et al., 1997). Non-competitive NMDA receptor antagonists

memantine and MK-801 were shown to reduce harmaline tremor, whereas competitive receptor NMDA receptor antagonist d-CPPene and competitive AMPA antagonist NBQX dose-dependently blocked harmaline-induced tremor (Iseri et al., 2011; Paterson et al., 2009). Furthermore, memantine was shown to reduce caspase-3 marker of neuronal damage in IO neurons and Purkinje cells, indicating that the NMDA receptor antagonist dampened harmaline's excitotoxic effect on the olive-cerebellar pathway (Paterson et al., 2009). Therefore, one mode in which harmaline may modulate IO activity is via its interaction with glutamatergic receptors.

Another mechanism by which harmaline may alter IO activity is via its interaction with calcium channels. Both low and high-threshold voltage-gated calcium channels have been shown to influence the generation, amplitude and frequency of IO subthreshold oscillations in the neuronal membrane potential, and these oscillations are inhibited by the blockade of the low-threshold T-type calcium channel CaV3.1 subunit (Bazzigaluppi & de Jeu, 2016; Choi et al., 2010). Harmaline has been shown to reduce voltage-gated calcium currents into the cell (Splettstoesser et al., 2005; Zhan & Graf, 2012). This attenuation is accompanied by broadened spike waveforms due to slower action potential repolarisation and attenuated afterhyperpolarization, which may be due to reduced activation of $Ca2+$ activated $K+$ channels (Llinás & Yarom, 1981; Zhan & Graf, 2012). Intra-IO infusion of T-type calcium channel blocker mibefradil, suppresses harmaline-tremor, as well as a range of T-type channel antagonists delivered systemically (Handforth et al., 2010; Park et al., 2010). Mice lacking the T-type CaV3.1 calcium channel ($CaV3.1^{-/-}$) do not show increased oscillatory activity in the IO or medial cerebellar nuclei in response to harmaline, or a harmaline-induced tremor (Park et al., 2010). Taken together, this evidence suggests calcium channels play an important role in mediating harmaline-induced changes in IO firing.

Harmaline also acts on the IO via the serotonergic route, as harmaline has been shown to increase 5-hydroxytryptamine (5-HT) levels in both IO and cerebellum, and depletion of 5-HT has been shown to inhibit harmaline tremor (Mehta et al., 2003; Sjölund et al., 1977). Harmaline is a monoamine oxidase-A inhibitor and therefore reduces the breakdown of serotonin, along with other biogenic amine neurotransmitters such as norepinephrine, and dopamine (J. H. Meyer et al., 2006). Intra-IO infusion of 5-HT induces complex spike synchrony whereas 5-HT antagonist reduced complex spike synchrony (Sugihara et al., 1995). Furthermore, administration of the serotonin agonist 5-methoxy-N,N-dimethyltryptamine and serotonin precursor L-tryptophan resulted in rhythmic complex spike firing and a whole body tremor (Wiklund et al., 1981). The topographic distribution of serotonergic innervation of the IO also aligns with the topographic distribution of the IO which display rhythmic firing in response to harmaline. This includes caudal

regions of the medial accessory olive and the dorsal accessory olive, but not the principal olive (De Montigny & Lamarre, 1973; Sjölund et al., 1977; Wiklund & Björklund, 1980). Harmaline's effect on increasing synchronous and rhythmic activity within the olive-cerebellar circuit is therefore likely to be a complex combination of several modes of action.

Many pharmacological treatments that alleviate tremor in ET, also reduce harmaline-induced tremor. This includes the first line ET treatment propranolol, which is a non-selective beta-blocker that is thought to exert effects peripherally on muscle spindles via blockade of β-2 receptor (Abila et al., 1985; Hedera et al., 2013; Martin et al., 2005; Paterson et al., 2009). Many first and second line ET treatments such as primidone, topiramate and benzodiazepine act by increasing GABAergic transmission (Ferreira et al., 2019; Taylor, 1997; Zesiewicz et al., 2013). Research has shown that primidone and gabapentin reduces harmaline-induced tremor, in addition to the GABA-agonist muscimol (Paterson et al., 2009). There is also evidence that T-type calcium channel blockades such as zonisamide can be clinically effective at reducing tremor in ET as well as harmaline-induced tremor (Deuschl et al., 2011; Handforth et al., 2010; Zesiewicz et al., 2013). Harmaline therefore provides a model of tremor which shares a similar phenotype and pharmacological profile to ET and is known to involve cerebellar circuits. This provides a useful tool for examining the contribution of altered cerebellar activity to the generation of an action tremor.

1.5.2   The GABA hypothesis and GABA$_A$ receptor α-1 subunit knockout mouse model

As reported above, some ET patients respond to medications which increase GABAergic transmission. This led to the hypothesis that GABAergic dysfunction may underlie the aetiology of ET. This is supported by evidence that ET patients showed reduced GABA$_A$ and GABA$_B$ receptors in the cerebellar dentate nuclei (Paris-Robidas et al., 2012). Patients with ET were also shown to have reduced levels of GABA in cerebral spinal fluid (Málly et al., 1996). Research suggests that close to 50% of ET patients show improved tremor symptoms follow alcohol consumption (Hopfner et al., 2015). Alcohol is a central nervous system depressant and increases GABAergic release in the cerebellum (Luo, 2015). Evidence from PET illustrated that alcohol-consumption in ET was also associated with decreased cerebellar blood flow and increased blood flow in the IO, whereas healthy controls showed decreased cerebellar blood flow but no changes in the IO (Boecker et al., 1996). In line with the GABA hypothesis, this may suggest that tremor suppression is related to increased cerebellar-IO GABAergic transmission. PET has also revealed increased cerebellar binding of [11C]flumazenil in ET, where [11C]flumazenil selectively binds to GABA$_A$ receptors (Boecker et al., 2010). This increased binding potential reflects increased receptor availability which may indicate reduced endogenous GABA. Binding of [11C]flumazenil within the

cerebellum has also been shown to positively correlate with tremor severity in ET (Gironell et al., 2012). GABAergic dysfunction may therefore underlie ET, where decreased GABAergic inhibition of cerebellar circuits, including Purkinje cell inhibition of cerebellar nuclei, and/or cerebellar nuclear inhibition of the IO, result in overactive cerebellar output. However, an important caveat is that these patient studies are limited by small sample sizes.

The GABA hypothesis has been further investigated by breeding GABA$_A$ receptor α-1 subunit knockout mice. These mice exhibit incoordination and a postural and kinetic tremor at around 17–21Hz, which is a higher frequency than tremors observed with harmaline (~16Hz in mice) and ET. Similar to the harmaline model, these mice also show reduced tremor symptoms in response to ET treatments including primidone, propranolol, gabapentin, and ethanol (Kralic et al., 2005). A limitation of this model is that the GABA$_A$ receptor α-1 subunit knockout is not specific to the cerebellum, and involves ~50% loss of GABA$_A$ α-1 subunit across the brain, including the thalamus and basal ganglia (Kralic et al., 2002, 2005). More recently, however, a transgenic mouse strain has been developed with selective knockout of the GABA$_A$ α-1 subunit in Purkinje cells, which left GABA$_A$ inhibition in the molecular layers of the cerebellar cortex intact (Nietz et al., 2020). These mice exhibit a similar tremor phenotype as the global GABA$_A$ α-1 subunit mice but did not show the same deficits in motor co-ordination as measured by the rotarod test. The GABA$_A$ receptor α-1 subunit knockout mice therefore provide a useful genetic model of tremor, lending support to the GABA hypothesis.

1.5.3 TRM/Kyro genetic rodent model

The TRM/Kyro rodent model is another genetic tremor model, bred from a sub-strain of Wistar rats with a tremor phenotype (Ohno et al., 2015). These rats are reported to develop a 7-8Hz postural and kinetic tremor, which is reduced by ET treatments propranolol and phenobarbital which is a GABA agonist (Ohno et al., 2015). Research has identified a possible genetic mutation of the hyperpolarization-activated cyclic-nucleotide-gated (HCN) 1 channel which may underlie the tremor phenotype, which was supported by evidence that HCN1 channel blockade induced tremor in a sub-strain of TRM rats that did not develop the tremor phenotype (Ohno et al., 2015). HCN1 channel function has been implicated in spontaneous rhythmic activity (Hao et al., 2019) and these channels are expressed in the IO and Purkinje cells in the cerebellum (Garden et al., 2018; Nolan et al., 2003). Bilateral lesion of the IO in the tremor-phenotype TRM rat significantly reduced but did not completely abolish tremor (Ohno et al., 2015). These rats also show elevated Fos expression in areas of the motor network that include the IO, and sensorimotor cortex, implicating overactivity of these regions. Fos expression within the cerebellum was not examined.

Taken together, this may suggest that genetic mutation of the HCN1 channel in the IO and possible IO over-activity as a result, may partly underlie tremor development in TRM rats. However, further research is needed to investigate the implications of the HCN1 mutation on olivo-cerebellar activity, and the effects of this mutation on other brain regions.

1.5.4 GluRδ2 deficient (hotfoot17J) mouse model

As mentioned above, pathological evidence has revealed changes in the distribution of climbing fibre synapses on cerebellar Purkinje cells in ET, where increased climbing fibre synapses were found on distal branches of the Purkinje cell dendritic arbour (Kuo et al., 2017; Lee et al., 2018; Lin et al., 2014; Pan et al., 2020). Post-mortem ET brains showed 75% reduction in the expression of glutamate receptor delta 2 (GluRδ2), a protein involved in the regulation of Purkinje cell synaptic wiring (Pan et al., 2020). This suggests deficient GluRδ2 expression may be associated with the development of tremor pathophysiology. Spatial alterations to these climbing fibre inputs may therefore reduce the probability or modulate the timing of Purkinje cell action potentials.

The Glurδ2 deficient (hotfoot17J) genetic mouse model has partially preserved Glurδ2 expression, and increased climbing fibre synapses in the parallel fibre territory. These mice exhibit a 20Hz action tremor which develops at three months of age (Pan et al., 2020). Optogenetic manipulation to silence climbing fibre synaptic input in the cerebellar cortex was shown to suppress tremor in these mice. This was achieved using viral vectors to inhibit climbing fibre synaptic vesicle protein docking and release through optogenetic stimulation of the cerebellar surface. Conversely, optogenetic silencing of climbing fibre synapses on the cerebellar nuclei did not reduce tremor. This suggests climbing fibre synapses on distal Purkinje cell dendrites was specifically related to tremor generation. Treatment with anti-ET drugs primidone, propranolol and ethanol were also shown to reduce tremor in Glurδ2 deficient mice. Deficiency of Glurδ2 expression and changes in the distribution of climbing fibre synapses therefore provides a viable mechanism of ET pathogenesis.

1.6 Inferior olivary hypothesis vs. Purkinjopathy

Early research identified ET as having a central mechanism, as application of an additional weight to the limb does not reduce the frequency of the recorded tremor (Homberg et al., 1987). If tremor were peripherally generated, an additional weight to the limb would change the biophysical properties of limb and reduce the frequency of the tremor. Emerging physiological research at that time also identified that the IO had an intrinsic ability to spontaneously oscillate (Headley & Lodge, 1976; Llinás, 1988, 1989), which led to the hypothesis that ET may be driven by a central oscillator. The IO hypothesis of ET posited that enhanced synchrony of IO rhythms may underlie

tremor in ET (Hallett & Dubinsky, 1993; Lamarre, 1984; Lamarre et al., 1975). However, this theory was developed from the harmaline model of tremor rather than clinical evidence. In support of this theory, evidence from PET has indicated overactivity within a region of the brainstem in ET which may be indicative of IO overactivity (Boecker et al., 1996; Hallett & Dubinsky, 1993). Conversely, a similar PET study did not find evidence to suggest overactivity of the IO in ET (Wills et al., 1994). fMRI revealed a reduction in IO activation during finger tapping in ET compared to healthy controls, which may indicate dysfunction of the IO during performance of voluntary rhythmic movements (Buijink, Broersma, et al., 2015). Evidence for IO dysfunction in ET has therefore been minimal and with small samples sizes. However, the location and size of this brain structure makes it difficult to examine in humans *in vivo*. Post-mortem analysis revealed no differences in IO density or evidence of IO neuronal damage in ET compared to controls (Louis et al., 2013). However, tremor caused by hyperactivity of the IO would require the IO to be intact. Currently, there is no evidence to indicate whether there are changes in the rhythmicity or firing rates of the IO in ET.

A competing but not mutually exclusive theory of ET tremor is the "Purkinjopathy" theory (Grimaldi & Manto, 2013). This theory posits that ET develops due to neurodegenerative changes occurring within the cerebellar cortex. As reported in section 1.3.1.3 of this Chapter, neurodegenerative changes have been observed in ET brains that are Purkinje cell related, and include Purkinje cell loss and changes in Purkinje cell morphology and connectivity at both axonal and dendritic compartments (Kuo et al., 2011, 2013; Kuo, Wang, et al., 2017; Louis et al., 2014; Yu et al., 2012). The heterogeneous nature of reported Purkinje cell related ET pathologies also corresponds with the heterogenous ET phenotype (Whaley et al., 2007), as illustrated by the proposal of extending ET diagnostic classifications to "ET" or "ET plus" (Bhatia et al., 2018), as well as the heterogenous genetic profile (Tio & Tan, 2016). This supports the notion that ET can be characterised as a collection of diseases in which abnormal changes within cerebellar circuits result in a postural and/or kinetic tremor. Evidence for axonal connectivity alterations of Purkinje cells in ET include increased axonal recurrent collaterals into the cerebellar cortex, as well as increased axonal branching and terminal sprouting (Babij et al., 2013; Louis, 2014). An important observation within the literature is that some of these observed pathological changes may be the result of secondary regenerative changes, such as increased axon recurrent collaterals to inhibit an overactive cerebellar cortex or increased axonal branching and terminal sprouting to compensate for Purkinje cell loss. It is thought that this combination of degenerative and regenerative changes within the cerebellum leads to inadequate re-wiring of the cerebellum, which may result in abnormal cerebellar output and tremor (Louis, 2014). However, there has

been no research examining whether these changes are disease-specific (i.e. ET-specific) or whether they occur as a general response to cerebellar-injury (e.g. with spinocerebellar ataxia) or in response to tremor (e.g. with PD).

Both the IO and "Purkinjopathy" theories of ET tremor posit abnormal changes within cerebellar circuits lead to abnormal cerebellar output. Due to the organisation of the olivo-cerebellar circuits into longitudinal zones, increased synchrony of Purkinje cell complex spikes is likely to produce increased synchrony of cerebellar nuclear output. Furthermore, an increased number of synaptic contacts between surviving Purkinje cells and cerebellar nuclei neurons may also increase the synchrony of cerebellar nuclei output in ET (Handforth & Lang, 2020). The GABAergic hypothesis of ET posits that cerebellar nuclear disinhibition results in increased rhythmic output to the thalamus (Boutin et al., 2015). There is no evidence of a straight-forward relationship between cerebellar nuclear disinhibition and rhythmicity. There is, however, evidence for a relationship between abnormal rhythmicity of Purkinje cells and rhythms in cerebellar nuclear neurons (Cheron et al., 2018). Two-photon calcium imaging has also revealed that the GluRδ2 knockout mouse showed enhanced synchrony of calcium transients in neighbouring Purkinje cells (Hashizume et al., 2013). Simultaneous electrophysiological recordings indicated that these calcium transients correlated with Purkinje cell complex spikes and abnormal clustered firing of Purkinje cells, which may have been the result of abnormal climbing fibre input (Hashizume et al., 2013). The harmaline model of ET has been critical in demonstrating the capacity of the olivo-cerebellar circuit to generate pathological oscillations leading to tremor. Whether abnormal rhythms within the cerebellum are caused by IO hypersynchrony, or neurodegeneration and regenerative alterations, all models and theories of ET pathogenesis assume dysregulation and/or increased rhythmic cerebellar nuclear output.

1.7 Summary

The aetiology of ET is currently unknown, but it is generally agreed that ET is a tremor syndrome which may have one of numerous causes. Considerable research, however, suggests this syndrome involves abnormalities within the cerebellar-thalamocortical network, and that there may be a genetic link. Evidence suggests that abnormalities such as Purkinje cell neurodegeneration and neuronal re-wiring within the cerebellum may be the catalyst for symptom development in ET. Electrophysiological studies have indicated that the thalamus plays a key role in the transmission of abnormal rhythms, as neural signals recorded from the thalamus is tightly synchronised with tremor signals recorded at the muscle (Hua & Lenz, 2005). Furthermore, DBS of the thalamus has been an effective treatment for reducing tremor symptoms

in ET patients (Shih & Pascual-Leone, 2017). Evidence suggests that somatosensory input to thalamus may also play an important role in modulating neural tremor rhythms. There is uncertainty regarding the role of the M1 in the transmission and generation of tremor oscillations in ET. Stimulation of M1 has been shown to interrupt tremor rhythms, but M1 coherence with tremor has been shown to be intermittent, suggesting the M1 tremor rhythms do not drive tremor. Furthermore, little research has examined the influence of altered cerebellar nuclear rhythmic output on thalamocortical activity, despite theories emphasising the importance of the cerebellar nuclei-thalamic projections on tremor activity in ET (Buijink, van der Stouwe, et al., 2015).

1.8   The current study

1.8.1   Aims and objectives

The overall aims of the research were to identify the neural network dynamics of ET across the motor system, and to examine the relationship between neural oscillations and tremor amplitude. To achieve this aim, *in vivo* electrophysiological recordings across the cerebellar-thalamocortical circuit will be examined using the harmaline rodent model of tremor, which is known to produce a pathological tremor by increasing the synchronicity of climbing fibre inputs to the cerebellum. This research aims to further elucidate on thalamic and motor cortical involvement in the pathological tremor oscillations. The research will also examine how these neural network dynamics correspond with EEG correlates of ET in patients, and to enhance understanding on the cortical involvement in ET.

Objectives of the project:

1) Using a harmaline rodent model of ET, examine the neural network dynamics of tremor in the motor network, and examine neural coherence to muscle activity.
2) To examine the EEG signatures of ET in patients, and to further elucidate on the mechanisms and conditions in which enhanced EEG coherence with the tremor may be present.

1.8.2   Organisation of the thesis

The methods and results of experiments carried out as part of the thesis are reported in three results chapters. Chapter 2 will describe *in vivo* electrophysiological experiments examining the effect of harmaline of cerebellar oscillations in the anaesthetised rat. Chapter 3 will examine the effect of harmaline on oscillations across the cerebellar-thalamocortical circuit in the awake behaving rat. Chapter 4 will examine neural correlates of tremor in ET patients, and Chapter 5 will provide a General Discussion of the work and summarise the principal findings.

Chapter 2. **Effect of harmaline on cerebellar nuclear oscillations in the anaesthetised rat**

2.1 Introduction

The effect of harmaline on the olivo-cerebellar system has been studied in anaesthetised animals since the early 1970s and has provided our current understanding on the mechanisms of harmaline's tremorgenic effects (De Montigny & Lamarre, 1973; Llinás & Volkind, 1973). As outlined in the General introduction, harmaline has a prominent effect on IO neurons, by inducing a sustained increase in rhythmic activity of neurons in mainly the caudal regions of both the medial accessory olive and caudal accessory olive (De Montigny & Lamarre, 1973, 1975). This in turn, increases the regularity and synchrony of complex spikes in the cerebellar vermis, with a complete suppression of simple spikes, which is likely to be a secondary effect of the increased activation of climbing fibre inputs and complex spike generation (Bernard et al., 1984; De Montigny & Lamarre, 1973). Research has also shown that harmaline-induced rhythmic activation of climbing fibres extends to regions of the paravermal cortex, but not the cerebellar hemisphere (Bernard et al., 1984).

The cerebellar nuclei, in addition to the vestibular nuclei, are the only source of output from the cerebellum and have multiple central nervous system targets including projections to the cerebral cortex via the thalamus. As outlined in the General introduction, the thalamus is thought to play a key role in propagating neural tremor rhythms in ET. Therefore, the cerebellar nuclei likely play a central role in propagating abnormal tremor-related neural oscillations to the rest of the brain including thalamocortical circuits. Rhythmic burst firing of neurons has been recorded in the fastigial (or medial in rodents) nucleus and interpositus cerebellar nucleus in response to harmaline, but not in the dentate (or lateral in rodents) cerebellar nucleus (Batini, Bernard, et al., 1981; De Montigny & Lamarre, 1973; Llinás & Volkind, 1973). This finding corresponds with previously reported topographical projections of harmaline-induced activation of the olivo-cerebellar pathways. Further work carried out by Lorden et al., (1992) suggests that only a small proportion of recorded cells in the interpositus nuclei showed a burst-firing response to harmaline, but this effect was shown in nearly all cells recorded within the medial nucleus (De Montigny & Lamarre, 1973). The effect of harmaline on LFP rhythms in the cerebellar nuclei of the rat have not been examined, and these rhythms can give insights into local population activity of neurons within the cerebellar nuclei. The interpositus nucleus is involved in the control of forelimb movements (Garwicz & Ekerot, 1994), and ET largely affects the upper limbs in patients

(Bhidayasiri, 2005). Therefore, changes in interpositus rhythms may provide translational insights into tremor in ET.

2.1.1 Aims

This Chapter examines the effect of harmaline on LFP oscillations in the interpositus and medial cerebellar nuclei in the anaesthetised rat. Preliminary data on effects of harmaline on multiunit (MUA) activity in the medial cerebellar nuclei is also reported. The effect of harmaline on individual Purkinje cells is examined as a positive control. Additionally, this Chapter will examine whether harmaline can induce detectable changes in brain regions involved in higher levels of sensorimotor processing, by recording EEG activity simultaneously from the motor cortex. This first experimental Chapter examines neural oscillations in the anaesthetised rat, as anaesthesia removes the confounds of behavioural tremor, where electrodes may be sensitive to the mechanical movement of tremor, as well as sensory afferents associated with tremor.

2.2 Methods

2.2.1 Animals

All procedures were performed in accordance with the United Kingdom Animals (Scientific Procedures) Act 1986 and the University of Bristol Animal Welfare and Ethical Review Body. Experiments were performed on 20 adult male Lister Hooded rats (300–450g). All animals were housed in groups under normal environmental conditions (~20°C and 45–65% humidity) maintained on a 12/12 h light/dark cycle and provided with food and water ad libitum.

2.2.2 Surgical procedures

Animals were initially anaesthetised with isoflurane (5%, delivered in oxygen) and maintained with 1.2g/kg Urethane (Sigma-Aldrich) dissolved in 25% distilled water, administered via an intraperitoneal (i.p) injection. Additional doses of anaesthetic (at 10% the initial dose) were given every 15 minutes until the animal was under a surgical level of anaesthesia, indicated by loss of pedal reflex (toe pinch) and eye blink reflex. Urethane anaesthesia was used as previous research has demonstrated harmaline-induced neural rhythmicity using Urethane in rodents (Ledoux & Lorden, 2002; Park et al., 2010). The rat's head was shaved in a non-sterile area, before being transferred to the sterile surgical table. A rectal probe was inserted to monitor body temperature and maintained at 37°C with the aid of a homoeothermic blanket (Harvard). Sterile saline (5ml) was given via a subcutaneous injection to keep the animal adequately hydrated during surgery. Local anaesthetic (Xylocaine ®, 10mg, AstraZeneca) was sprayed onto the scalp and in the ears before rats were fixed in place in a stereotaxic frame with atraumatic ear bars and mouthpiece to

26

hold the head in place. A midline scalp incision was made to expose the skull, and connective tissue was cleared using blunt dissection. A silver screw was implanted over the right M1 to record EEG (distance from Bregma: anterior-posterior, +2 mm, medial-lateral, +3 mm, Paxinos & Watson, 2005). A craniotomy was performed to expose the posterior-cerebellum and to allow access to the cerebellar nuclei.

2.2.3   Electrophysiological recordings

A Tungsten wire microelectrode 76 µm tip diameter, expoyxlite insulation, 300-500KΩ impedance, FHC), painted with the fluorescent maker DiI (3% in absolute ethanol) was inserted on one side of the brain into either the anterior interpositus nucleus (distance of from Bregma: anterior-posterior, -11.16 mm, medial-lateral, -2.5 mm, dorsal-ventral, -3.7 to -4 mm, from the surface of the cerebellum, Paxinos & Watson, 2005) or the medial cerebellar nucleus (distance from Bregma: anterior-posterior, -11.3 mm, medial-lateral, 1 mm, dorsal-ventral, -4 to -4.4 mm, from the surface of the cerebellum, Paxinos & Watson, 2005), contralateral to the EEG screw. A hydraulic micro-drive manipulator was used to insert a second tungsten microelectrode (76µm tip, expoyxlite insulation, 300-500KΩ impedance, FHC) into the cerebellar cortex of the vermis in eight of the 20 rats to isolate Purkinje cell single units. Agarose solution (0.4g in 20ml 0.9% saline) was placed over the exposed cerebellum to keep the surface of the brain moist.

2.2.4   In vivo acute electrophysiological recordings with anaesthetised rats

Differential recordings were made using a micro 1401 A/D device (Cambridge Electronic Design) and Spike2 version 7 acquisition software. A wire electrode placed between the skin and the skull served as the reference. LFP from the nuclei and EEG recordings were band-pass filtered (0.1Hz-500Hz) and LFP signals were digitised and stored at a sample rate of 10kHz, whereas EEG signals were digitised and stored at 5khz. Single or multiunit activity (MUA) from the nuclei and cerebellar cortex were band-pass filtered (300Hz-5kHz) and MUA from the nuclei were digitised and stored at a sampling rate of 20kHz, whereas single unit activity from the cerebellar cortex was digitised and stored at a sampling rate of 10khz. 50Hz electrical interference from LFP recordings was removed by a Humbug™ noise eliminator (Digitimer).

2.2.5   Drug delivery and experimental procedure

Baseline recordings were obtained for an average of 20 minutes prior to administration of Harmaline hydrochloride (Sigma-Aldrich, St Louis, MO, USA). Harmaline was dissolved in 1ml/kg of sterile saline and administrated via an i.p. injection at a dose of either 10mg/kg (n=5) in earlier experiments examining interpositus nucleus LFP or 20mg/kg (n=11) in later experiments

examining medial nucleus LFP and Purkinje cell activity. Recordings were measured for around 60 minutes following harmaline administration.

2.2.6   Histological procedure

At the conclusion of the experiments, the rat was euthanised by cervical dislocation whilst still under surgical levels of anaesthesia. The cerebellum was removed and post fixed in 4% paraformaldehyde for a minimum of 24 hours, and then transferred into a 30% sucrose solution for 4-6 days.

The cerebellum was cut with a freezing microtome in the sagittal plane at a thickness of 100 µm and mounted onto gelatinised slides. The sections were examined on an Axioskop 2 Plus microscope (Zeiss) and images were acquired using AxioVision software for confirmation of electrode placement. Only rats that had histological confirmation of recording electrodes in the targeted nuclei were included within the analyses. This included all five rats where the interpositus nucleus was targeted, and eight out of 11 rats where the medial nucleus was targeted. Examples of histological confirmation of electrode positioning in the nuclei are provided in Figure 2-1, and a summary of the on target positioning of recording electrodes within the nuclei are provided in Figure 2-2.
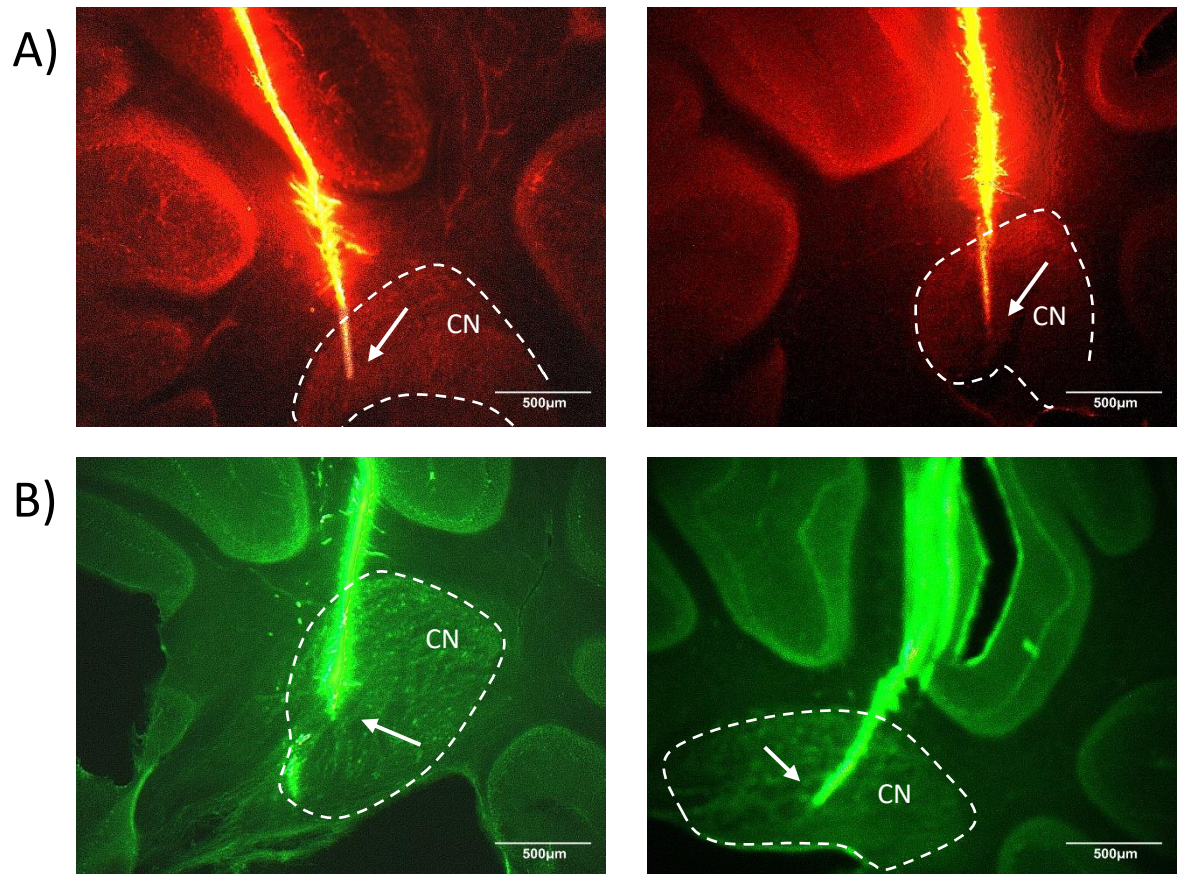
Figure 2-1. Histological confirmation of recording electrode site.
Electrodes were painted with fluorescent DiI solution before insertion into the cerebellum and tracts were visualised under a fluorescent microscope. A) and B) provide examples of electrode positioning in the anterior interpositus nucleus and medial nucleus, respectively. Examples are from four different rats. White arrows indicate the position of electrode tips and white dashed lines outline the cerebellar nuclei (CN).
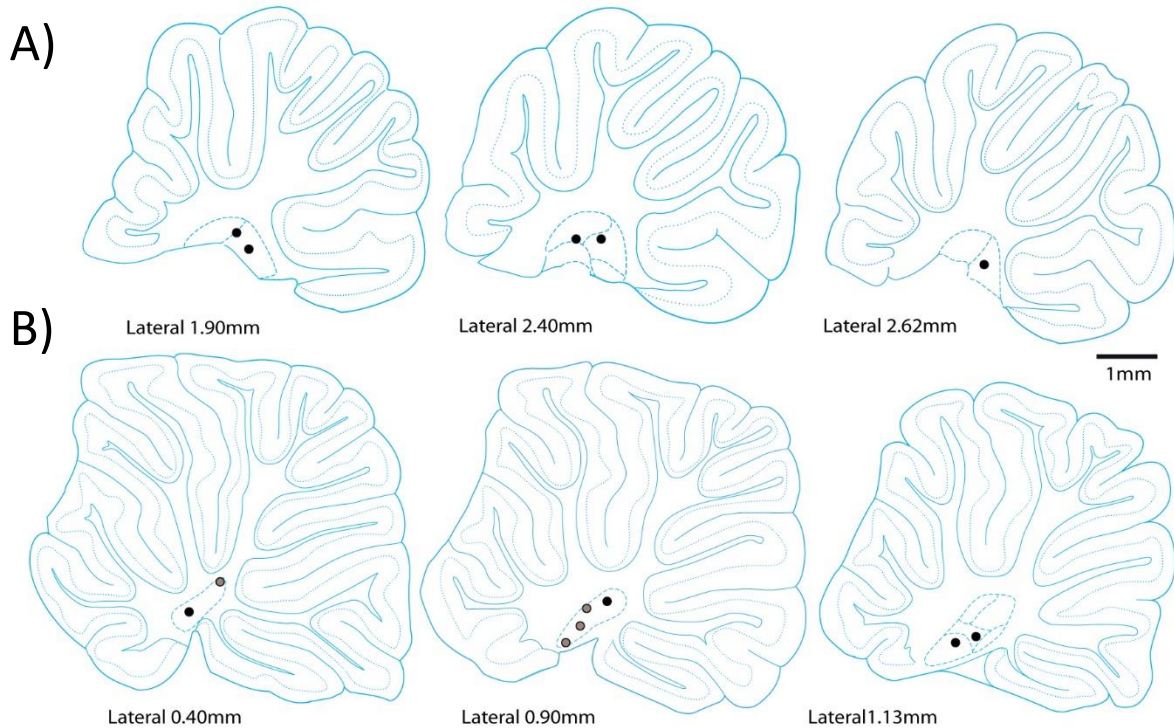
Figure 2-2. Standard sagittal sections of cerebellum summarising the approximate position of the electrode recordings sites within the target cerebellar nucleus.
A) and B) provide approximations of electrode positions within the interpositus (n=5) and medial cerebellar nuclei (n=8), respectively. Each dot represents the approximate electrode positioning per rat. Adapted from Paxinos & Watson (2005).

2.2.7 Data pre-processing

2.2.7.1 LFP and EEG data

Analysis was performed offline using custom MATLAB scripts. LFP and EEG data were bandpass filtered (1-49Hz), down-sampled to 1kHz and segmented into two second epochs. This epoch size was chosen as it provides adequate frequency resolution of 0.48Hz and captured at least seven cycles of the lowest tremor-related frequency of interest (4Hz). Single-sided amplitude spectrum was calculated by applying the MATLAB discrete fast fourier transforms (FFT) function to each individual epoch. The ratio of signal amplitude within discrete frequency bands were examined in comparison to summed amplitude in the low frequency range (1.5-45hz). The following frequency bands were examined: delta (1.5-4Hz), theta (4-15Hz), beta (15-30Hz) and low gamma (30-45Hz). The boundaries of the theta band were chosen to capture changes within tremor-related frequencies reported for harmaline model and ET (Bhidayasiri, 2005; Pan et al., 2018). The ratio of signal amplitude in these frequency ranges is defined by equation 2.1, where Sxx represents the single-sided amplitude spectrum. This measure was compared across baseline and harmaline

conditions. Similar methods have been applied by previous research to examine changes in the distribution of amplitude in low frequency bands in tremor recordings (Iseri et al., 2011).

$$Amplitude\ ratio = \frac{\sum Sxx(frequency\ band\ range)}{\sum Sxx(low\ frequency\ range)}$$ Equation 2.1

Statistical differences in the mean ratio of amplitude for each frequency range following harmaline were examined using pairwise t-test analyses. As the sample size of these proportions were low (n<30 animals), a Shapiro-Wilk normality test was first carried out to examine whether the differences of the paired data followed a normal distribution. If the differences did not follow a normal distribution (i.e. if the null hypothesis of the Shapiro-Wilk normality test is rejected, and p<0.05), a paired samples Wilcoxon signed-rank test was used to compare the median difference of paired observations.

Single-sided fast Fourier transform spectrograms were also computed using the MATLAB spectrogram function, with a 10 second window size and 50% overlap to examine neural oscillations over time.

2.2.7.2   Single and multi-unit data

Single and multi-unit recordings were analysed offline in Spike2, and single-unit activity was isolated using template matching and principal component analysis. Purkinje cell single units were identified by the presence of both simple spikes and complex spike complex waveforms that were followed by a short pause in spiking activity. Purkinje cell simple spikes and complex spikes were sorted separately using the manual template matching function in Spike2, whereby action potentials with a single spike waveform were manually categorised as a simple spike, and action potentials that had an initial spike followed by smaller spikelets and a post-complex spike pause were categorised as complex spikes. For cerebellar nuclei multi-unit activity (MUA), a spike detection threshold of 50µV was applied.

Spike-times and waveforms were exported from Spike2 to MATLAB for further analysis. Inter-spike intervals (ISI) were examined by calculating the difference between spike times in milliseconds, to compute ISI histograms with a bin size of 0.5ms. Changes in the rate of neuronal spikes times per second in response to drug delivery were examined by computing firing rate time histograms using the MLIB MATLAB toolbox (Stüttgen, 2020), with a bin size of 1000ms. To examine changes in the rhythmicity of firing rates, binary spike trains were computed at the millisecond resolution using

the MLIB toolbox, and autocorrelations of these spike trains were computed using the MATLAB *xcorr* function. Autocorrelations were normalised to provide a measure of similarity between zero and one for the spike train and itself at lagged time-intervals, such that the autocorrelation coefficient at zero lag (i.e. correlation for identical copies) is equal to one. Peaks in the autocorrelation at lagged intervals indicate periodicity at that time interval.

2.3 Results

2.3.1 Harmaline did not induce changes in interpositus LFP activity in anaesthetised rat

The first aim was to examine the effect of harmaline on LFP activity centred on the interpositus. In five rats the mean amplitude spectrum (± standard error of the mean, SEM) of LFP recorded from each rat before (blue) and after (red) harmaline is displayed in Figure 2-3. No significant change in the ratio of LFP amplitude in the delta, theta, beta, and gamma frequency ranges were found in response to harmaline (Figure 2-4, all p value's > 0.5). These findings suggest that 10mg/kg of harmaline administered to urethane anaesthetised rats do not affect interpositus LFP activity.

2.3.2 Assessment of changes in Purkinje cell activity in response to harmaline reported as a positive control

As there were no systematic differences detected in the amplitude spectrum of the LFPs recorded in response to harmaline, Purkinje cell single unit activity was examined as a positive control to verify that harmaline (20mg/kg) was acting to increase climbing fibre activity. Changes in Purkinje cell activity in response to harmaline were recorded in five out of eight rats; two Purkinje cells were adequately isolated and maintained for the duration of the recording in two of these animals. Figure 2-5 A and B illustrates one-second raw traces recorded from the same Purkinje cell before and after harmaline and shows a clear change in the firing rate of simple spikes and complex spikes. An example of the average simple spike and complex spike waveforms from a recorded Purkinje cell are shown in Figure 2-5 E and F. The change in Purkinje cell firing rate is further illustrated in Figure 2-5 C and D, which displays firing rate time histograms for simple spikes and complex spikes across the duration of the recording. Prior to harmaline administration, mean simple spike firing rate was 35.23Hz for Purkinje cell 1 and 62.32Hz for Purkinje cell 2, and mean complex spike firing rate was 0.22Hz for Purkinje cell 1 and 0.27Hz for Purkinje cell 2. Approximately 10 minutes following the injection of harmaline, there was a dramatic suppression of simple spike activity (mean firing rate of 0.91Hz for cell 1 and 2.22Hz for cell 2), and an increase

in complex spike firing rates (mean firing of 3.41Hz for cell 1 and 6.02Hz for cell 2), and this firing rate pattern was maintained for the remainder of the recording session.

Complex spike time autocorrelations (binned by 1ms and lags up to ±500ms) also revealed a change in the rhythmicity of complex spike firing in response to harmaline. Figure 2-5 G shows an increase in autocorrelation at 160ms following harmaline administration for Purkinje cell 1, indicating increased rhythmicity of complex spike firing at around 6.25Hz. For Purkinje cell 2 a peak in the autocorrelation emerged at 250ms, indicating increased rhythmicity of complex spike firing at around 4Hz. These analyses correspond with previously reported effects that harmaline increases the average firing rate and rhythmicity of the climbing fibre activation in methohexital and pentobarbital anaesthetised cats (De Montigny & Lamarre, 1973; Llinás & Volkind, 1973). Therefore, despite observing no changes in the recorded interpositus LFP, harmaline had a marked impact on Purkinje cell single unit activity at 20mg/kg.
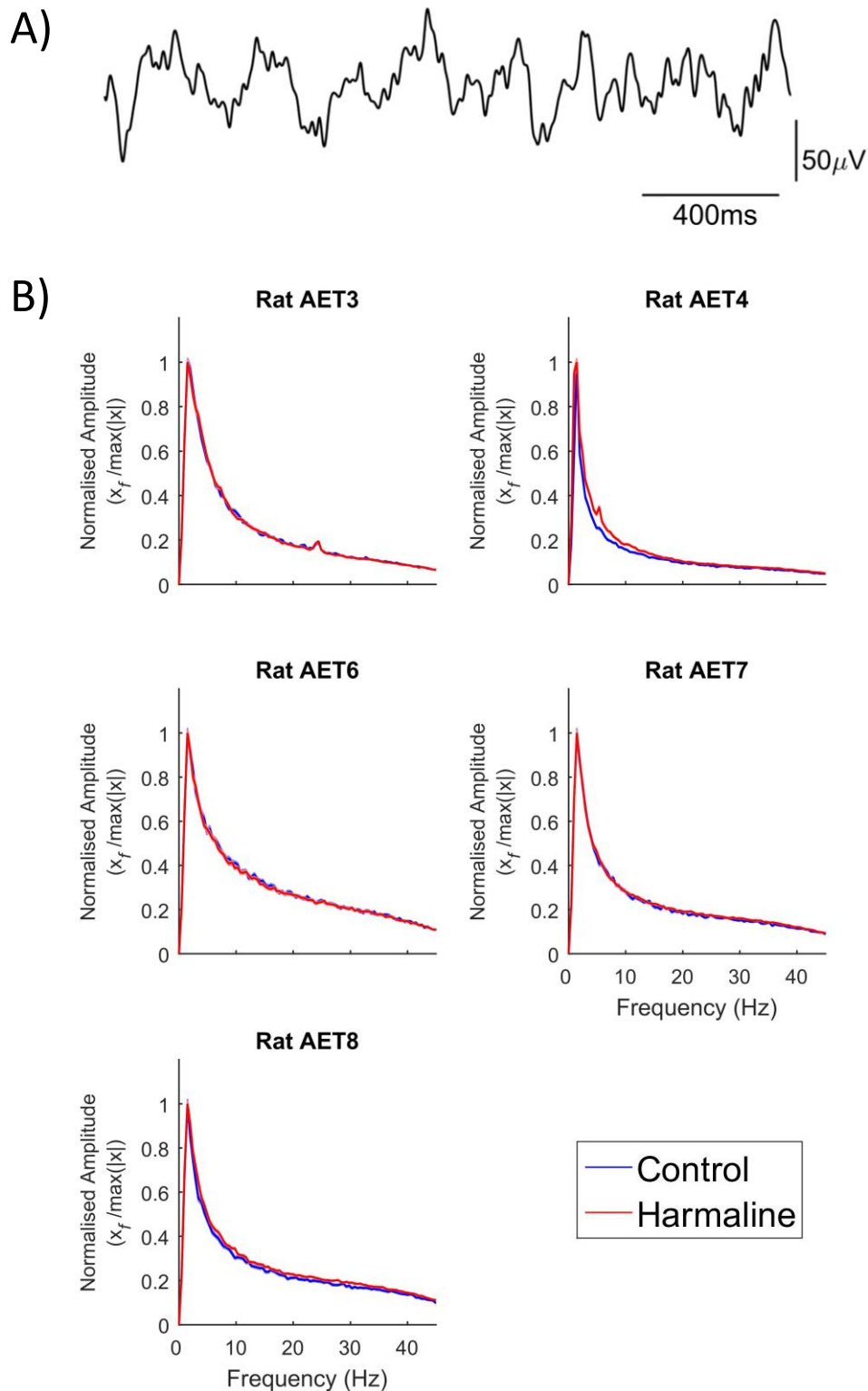
Figure 2-3. No systematic change in interpositus nuclei LFP amplitude spectrum in response to harmaline.
A) Example 2-second interpositus nuclei LFP after harmaline and B) interpositus nuclei LFP amplitude spectra. Each panel in B) illustrates the mean amplitude spectrum ±SEM across 2-second epochs during control (in blue) and harmaline (in red) conditions per animal. Animal ID is indicated above each panel. Y-axis gives relative signal amplitude normalised to the maximum amplitude.
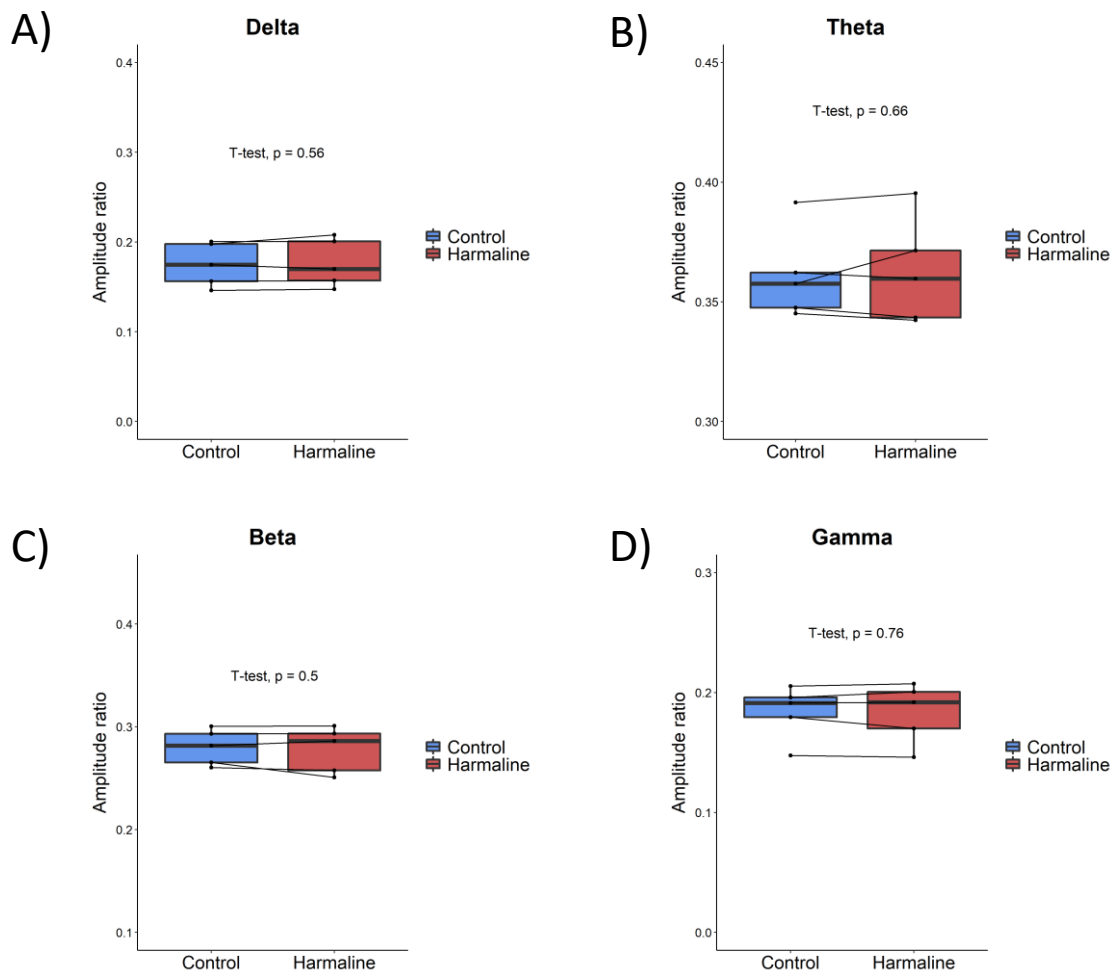
Figure 2-4. No significant change in the ratio of interpositus nuclei LFP amplitude in the delta (1.5-4Hz), theta (4-15Hz), beta (15-30Hz) and low gamma (30-45Hz) frequency ranges in response to harmaline.
Boxplots illustrate median and interquartile range of the ratio of amplitude before (blue) and after (red) harmaline (n=5), where each individual point and line marked on the boxplots represents individual rats.
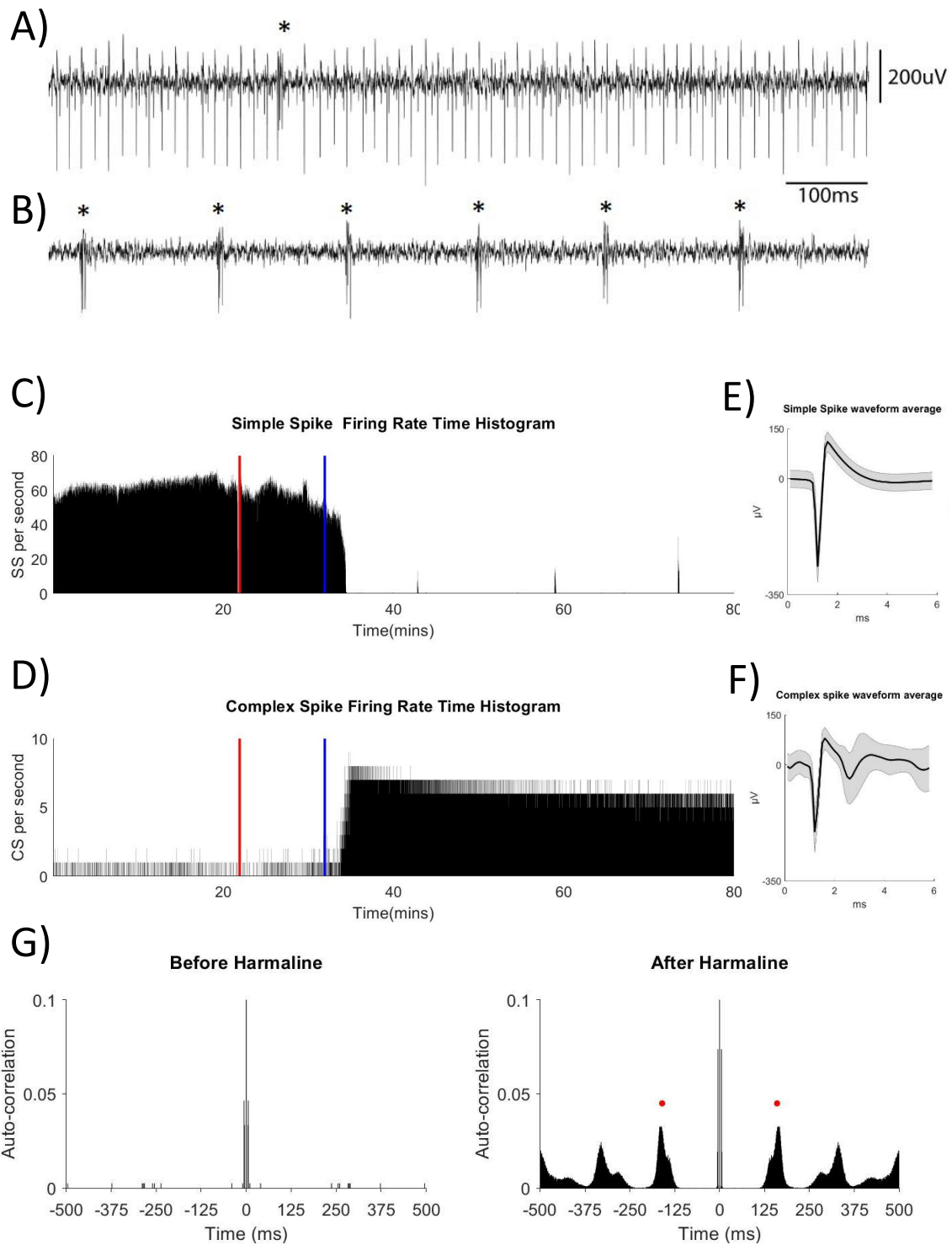
Figure 2-5. Change in Purkinje cell firing patterns and complex spike rhythmicity following harmaline.
All data displayed in this figure were recorded from the same Purkinje cell. A) Single unit recording from the Purkinje cell before and B) after harmaline administration. Complex spikes are indicated by an asterisk. The scale bar corresponds to both A) and B). C) Simple spike and D) complex spike firing rate time histograms (1000ms bin size). The red vertical line indicates the time-point when harmaline (20mg/kg, i.p.) was given; blue line indicates ten-minutes following harmaline onset. E) Average simple spike and F) complex spike waveforms. Solid black line displays average waveforms, and the shaded areas represent the SD. G) Autocorrelations of complex spikes before and after harmaline. Following harmaline, a peak in autocorrelation emerged at 160ms indicated by the red dots. Auto-correlation coefficients are normalised to give a measure between zero and one.

2.3.3 Proportional change in theta activity in the medical nucleus LFP

The amplitude spectrum of LFP recorded from the medial nucleus across individual rats (n=8) is shown in Figure 2-6. This figure illustrates that the LFP rhythmic activity varied greatly across animals. For example, peaks in beta oscillations (~20-25Hz) were recorded from two rats (rat ID's AET16 and AET19), and a peak in gamma oscillations (~40Hz) were recorded from another rat (AET21). Two rats (rat ID's AET13 and AET20) displayed small peaks in the theta frequency range at 5.5Hz and 6.5Hz after drug delivery, with small harmonic peaks in the spectra at 11Hz and 13Hz, respectively. An expanded view of the medial nuclei LFP amplitude spectrum for these two rats are displayed in Figure 2-7.

The mean ratio of amplitude in the delta, theta, beta, and low gamma frequency ranges before (blue) and after (red) harmaline was also examined across rats (n=8, Figure 2-8). These analyses revealed no significant changes in the ratio of amplitude within delta, beta and low gamma frequency bands following harmaline (paired t-test; all p value's > 0.33). However, a Wilcoxon signed-ranked test showed a significant change in the ratio of amplitude in the theta frequency range (4-15Hz) in response to harmaline (W test-statistic=33, z=-2.1, p=0.039, r=0.73), whereby the median ratio of amplitude was greater after vs before drug administration. These findings indicate that harmaline increases the ratio of amplitude in theta frequency in medial nucleus LFP, which is the same frequency range of tremor activity recorded in awake behaving rats (Pan et al., 2018).
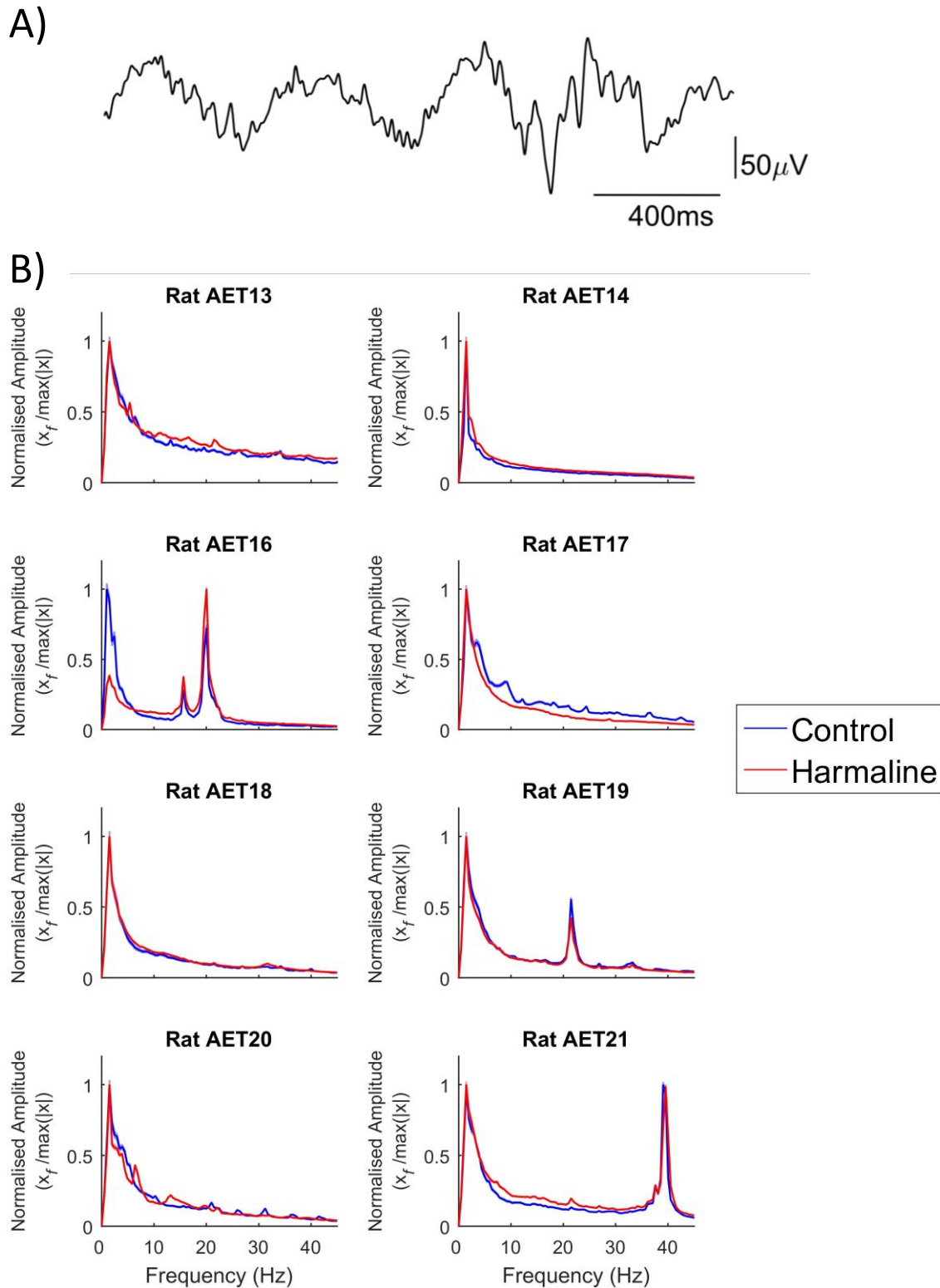
Figure 2-6. Variability in medial nucleus LFP potential in response to harmaline administration.
A) Example 2-second medial nuclei LFP after harmaline and B) medial nuclei LFP amplitude spectra. Each panel in B) illustrates the mean amplitude spectra ± SEM across 2-second epochs during control (in blue) and harmaline (in red) conditions per animal. Animal ID is indicated above each panel. Y-axis gives relative signal amplitude normalised to the maximum amplitude.

38
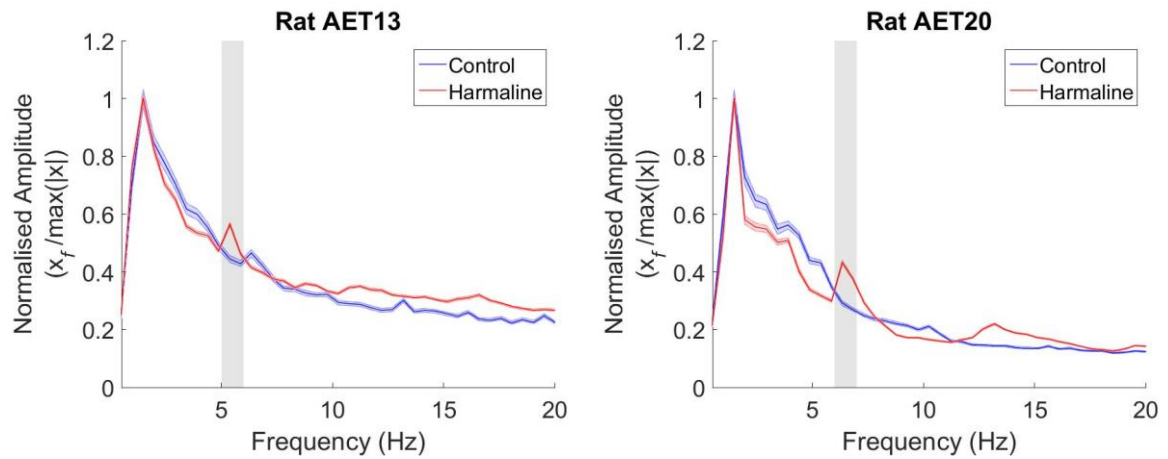
Figure 2-7. Increased oscillations at 5-7Hz in the medial nuclei LFP.
Mean amplitude spectrum ± SEM across 2-second epochs taken before (in blue) and after (in red) harmaline administration, for two different rats. Animal ID is indicated above each panel. Y-axis gives relative signal amplitude normalised to the maximum amplitude.
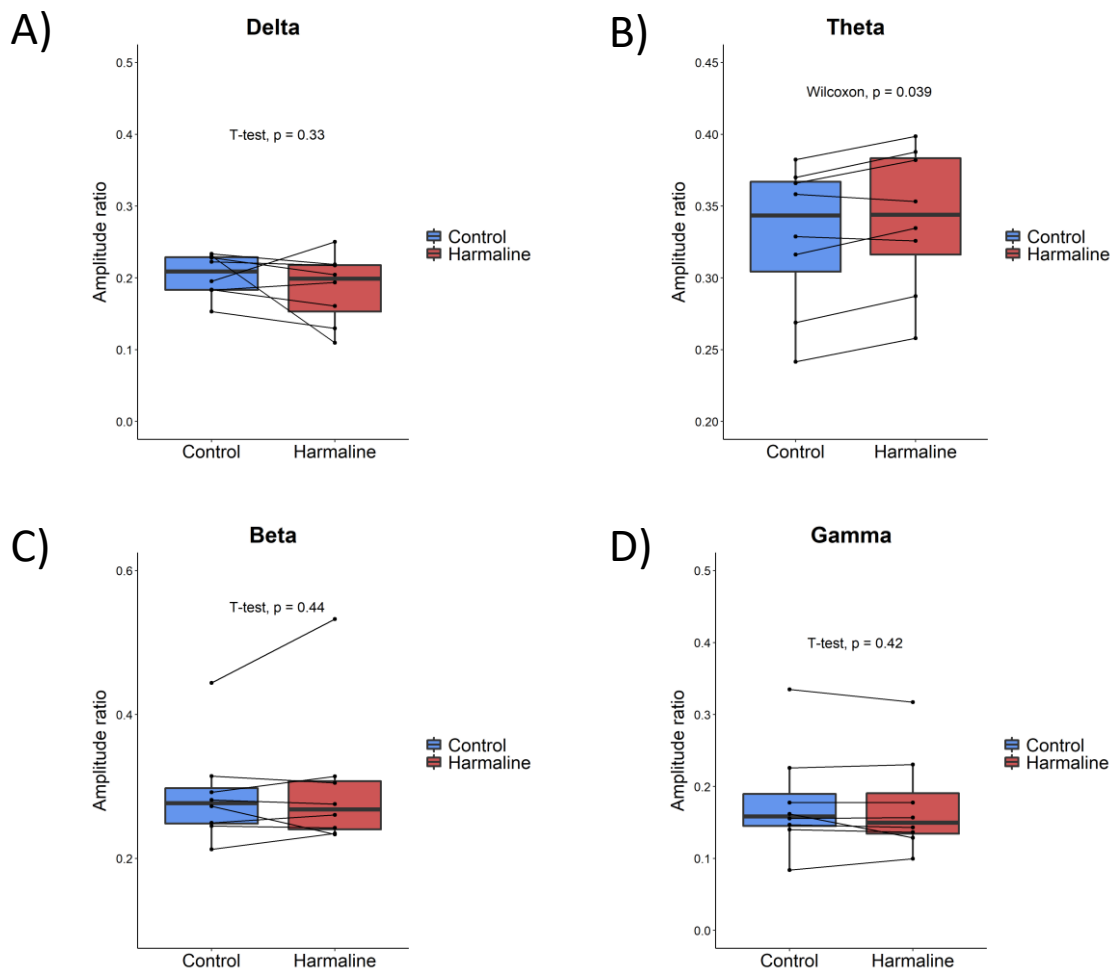
Figure 2-8. Significant increase in the ratio of summed theta (4-15hz) amplitude in the recorded LFP of the medial nucleus in response to harmaline.
Boxplots illustrate the median and interquartile range of the ratio of amplitude before (blue) and after (red) harmaline (n=8) at delta, theta, beta, and low gamma frequency ranges. Each individual point and line marked on the boxplots represents an individual rat.

2.3.4 Preliminary findings on the effect of harmaline of medial nucleus MUA

To examine whether the increase in theta-range activity of the medial nucleus LFP corresponds with changes in MUA, the rhythmicity of medial nuclei MUA was examined in two rats. Figure 2-9 provides an example of MUA recorded from the same rat before and after harmaline. The autocorrelations displayed in Figure 2-10 show that changes in the MUA rhythmicity were variable across the two rats. In both rats, there was an increase in the frequency of the MUA, indicated by a shift in peak autocorrelation from ~12ms to ~8ms in the first rat (Figure 2-10 A), and a shift in peak autocorrelation from ~72ms to ~64ms in the second rat (Figure 2-10 B). However, in the first rat only (Figure 2-10 A) there was also a second slower rhythmic oscillation emerging at 6.5Hz in the autocorrelation during harmaline conditions, which corresponds to periodic activity every 150ms or 6.67Hz. This slower rhythm corresponds with a peak in LFP activity at 6.5Hz simultaneously recorded from the same rat (Rat AET20; Figure 2-7). As reported in section 2.3.5, a peak in theta LFP activity emerged following harmaline in only two out of eight rats, despite the overall ratio of theta activity increasing in response to harmaline across all rats (Figure 2-7). In sum, these preliminary findings illustrate a variable change in rhythmic activity in medial cerebellar nuclear activity in response to harmaline.

As previous research has suggested that the disinhibition of cerebellar nuclei in response to reduced Purkinje cell inhibition may be a key feature of ET, changes in the frequency of MUA activity over time was also examined. Inspection of the frequency of MUA across the two rats revealed that in one rat, there was a significant increase in MUA in response to harmaline (baseline: 170.2Hz±18.5, harmaline: 204.6Hz±9.2; unpaired t-test, t(4198)=-79.8, p<0.001), but there was no significant difference in MUA for the second rat (baseline 60.6±11.1, harmaline: 60.12Hz±5.1 unpaired t-test, t(2597)=1.1, p=0.282). Inspection of the MUA time histograms displayed in Figure 2-11 also illustrates that prior to harmaline delivery, there was a large variation in the frequency of MUA. However, ten minutes following harmaline delivery, which is the time-point when changes were observed in Purkinje cell activity, the variability in firing rates were reduced (Figure 2-5). This is indicated by a reduction in the mean coefficient of variation (CD) from 14.6% (±5.2) at baseline to 6.5% (±2.8) for activity recorded ten-minutes post drug delivery. This indicates an increase in the regularity of medial nuclei MUA in response to harmaline.
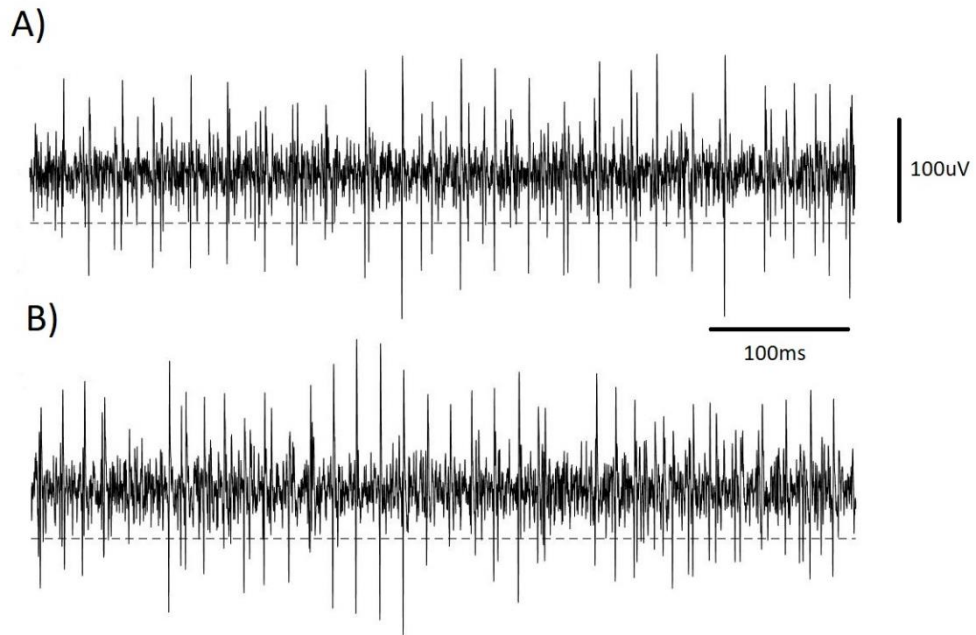
Figure 2-9. Example medial nucleus MUA recording.
A) MUA before harmaline administration, and B) MUA maintained from the same animal following harmaline administration. The scale bar corresponds to both A) and B), and the dashed line indicates the crossing threshold taken at -50µV.
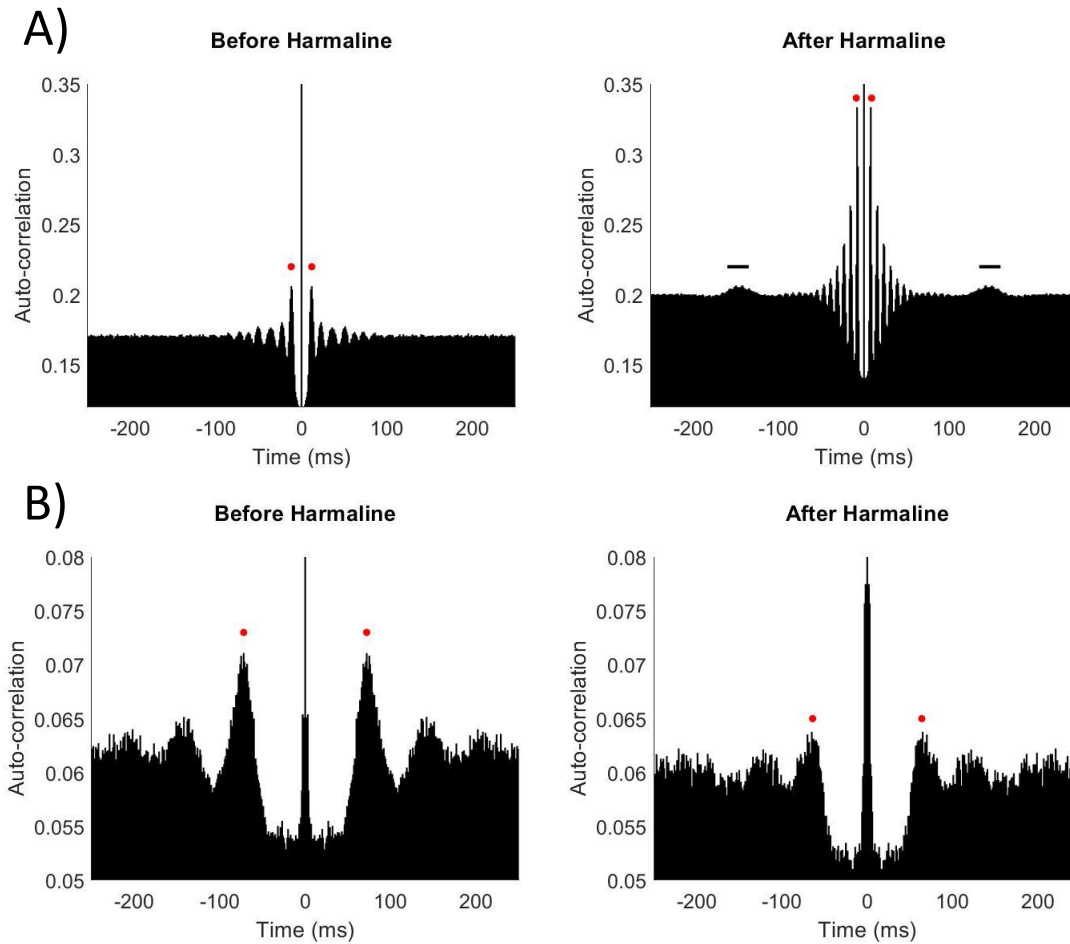
Figure 2-10. Variable change in rhythmicity of MUA in response to harmaline.
Autocorrelations of medial nuclei MUA before and after harmaline for two rats A) and B) Non zero-lag peaks in autocorrelation are indicated by the red dots, and auto-correlations coefficients are normalised to give a measure of similarity between zero and one. A) Before harmaline there was a peak in autocorrelation at 12ms, and after harmaline there was a peak in correlation at 8ms, as well as a slower rhythmic oscillation emerging at 150ms, indicated by the black horizontal line. B) Before harmaline there was a peak in autocorrelation at 72ms, and after harmaline there was a peak in correlation at 64ms.
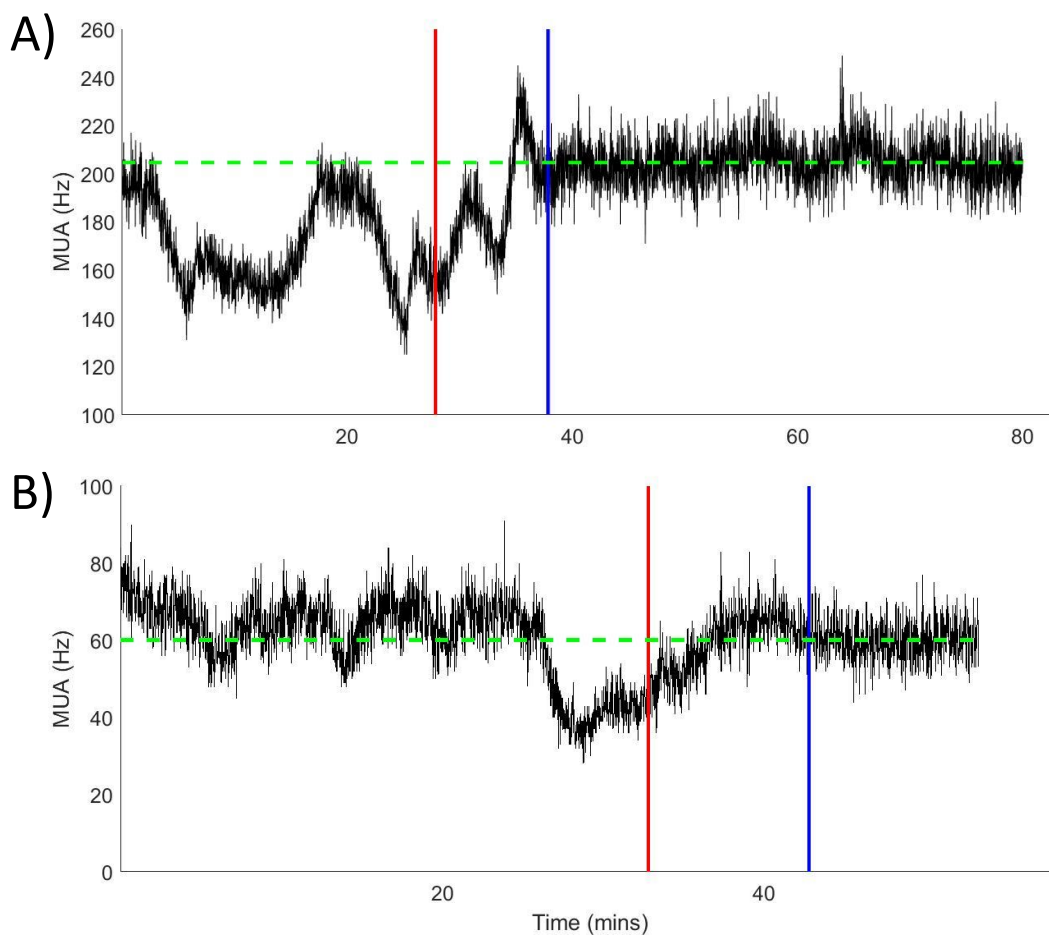
Figure 2-11. Stabilisation of MUA 10 minutes following harmaline delivery.
MUA time histograms for two different rats A) rat AET20 and B) rat AET21, respectively. The red vertical line indicates the time-point when a 20mg/kg dose of harmaline was given i.p., and the blue line indicates ten-minutes following harmaline onset. The dashed green line represents average MUA from ten minutes post drug delivery, to the end of the recorded activity.

2.3.5 Harmaline did not induce any changes in EEG activity in the anaesthetised rat

To examine whether harmaline can induce detectable rhythmic neural activity in M1 in the anaesthetised rat, EEG was recorded from subdural electrodes placed over M1. The mean amplitude spectrum (± SEM) of the EEG recorded from each rat (n=8) before and after harmaline is displayed in Figure 2-12. Inspection of the individual EEG amplitude spectrum across rats indicates variation in the EEG activity across rats (n=8) as well as no consistent change in EEG activity in response to harmaline. Figure 2-13 displays individual and group level changes in the ratio of amplitude in the delta, theta, beta, and low gamma frequency bands before and after harmaline for the EEG. Pair-wise analyses revealed no significant change in the ratio of amplitude within these frequency bands before versus after harmaline (paired t-test; all p values > 0.44). This revealed that there was no clear qualitative or quantitative change detectable in the amplitude of the low-frequency (1.5-45Hz) activity in recorded EEG in response to harmaline in the anaesthetised rat.

2.3.6 Urethane up/down states

Urethane anaesthesia has been previously used as an animal model of sleep, as it induces cycles of slow wave oscillations (~1Hz) alternating with higher frequency oscillations (~4Hz), which resemble rapid eye movement and non-rapid eye movement sleep. These up/down states are observed across a timeframe of 5-10-minute periods (Clement et al., 2008). To examine whether systematic effects of harmaline on EEG and LFP rhythms are removed due to averaging across up/down states, EEG and LFP spectrograms were inspected. Figure 2-14 shows examples of simultaneously recorded EEG and medial nucleus LFP spectrograms from two rats (A: rat AET13, & B: rat AET18), that showed very different EEG amplitude spectra as shown in Figure 2-12.

Figure 2-14 A provides evidence that despite EEG showing somewhat intermittent rhythms at ~1.5Hz, 3Hz, 4.5Hz, 9Hz following harmaline delivery, a consistent 6Hz rhythm was seen in the spectrogram of simultaneously recorded medial nucleus LFP, from 20 minutes after harmaline until the end of the recording. Furthermore, this same rhythm was identified in the LFP amplitude spectrum (reported in section 2.3.3, Rat AET13; Figure 2-7) where LFP spectra were averaged over time. Figure 2-14 B provides a more representative example of recorded EEG rhythms recorded across animals, where there was a prominent down state in EEG rhythms was observed across the entire recording, indicated by a high amplitude rhythm at 1-2Hz. This rhythm in the EEG was accompanied by an intermittent slow rhythm in the medial nucleus LFP at 1-2Hz. Inspection of these spectrograms therefore suggest a lack of alternating up/down states following harmaline

administration, and therefore the reported effects of harmaline on EEG and LFP rhythms should not be impacted by averaging across time and potential urethane up/down states.
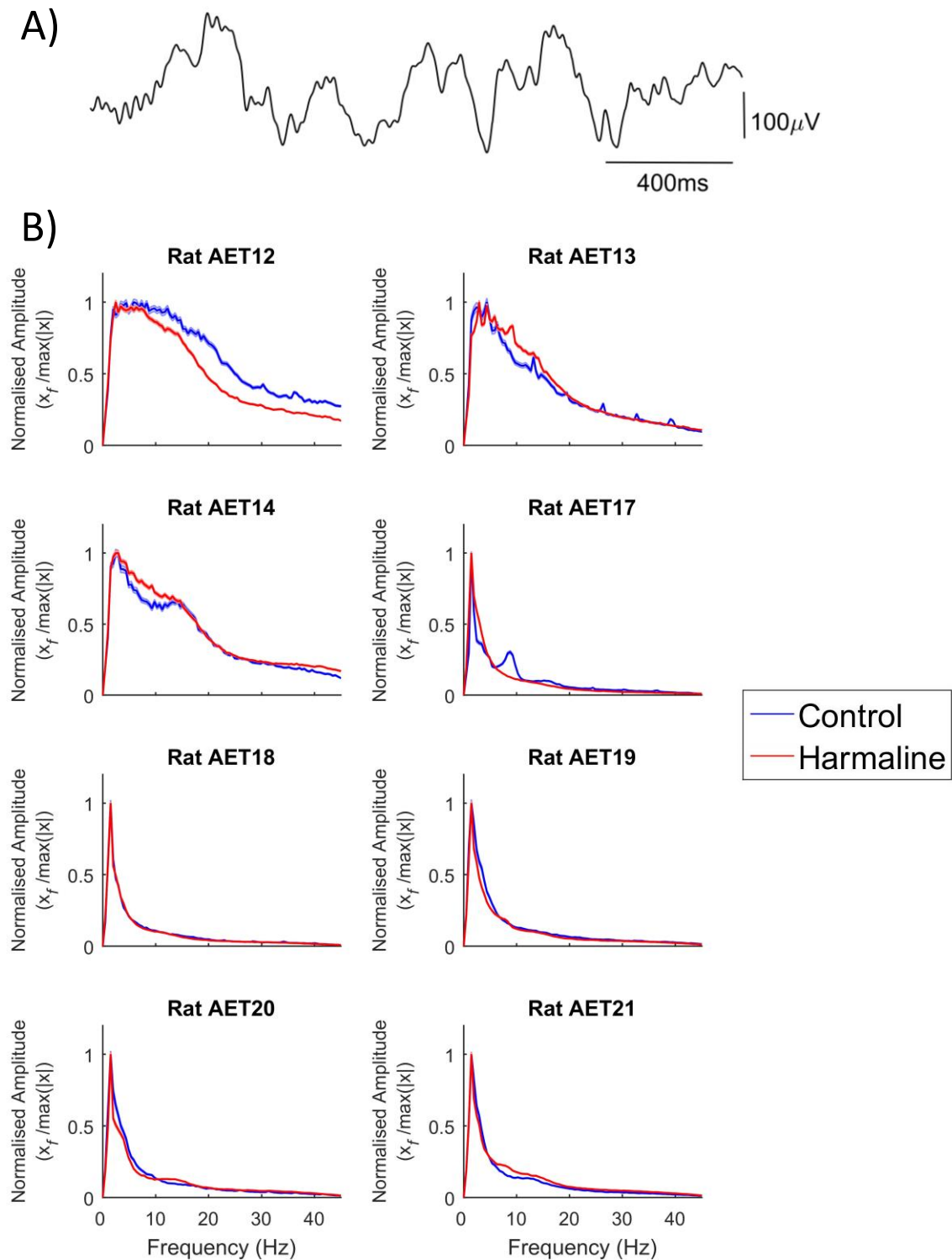
Figure 2-12. EEG amplitude spectrum in response to harmaline.
A) Example 2-second EEG recording after harmaline and B) EEG amplitude spectra. Each panel in B) illustrates the mean amplitude spectra ±SEM across 2-second epochs during control (in blue) and harmaline (in red) conditions per animal. Animal ID is indicated above each panel. Y-axis gives relative signal amplitude normalised to the maximum amplitude.
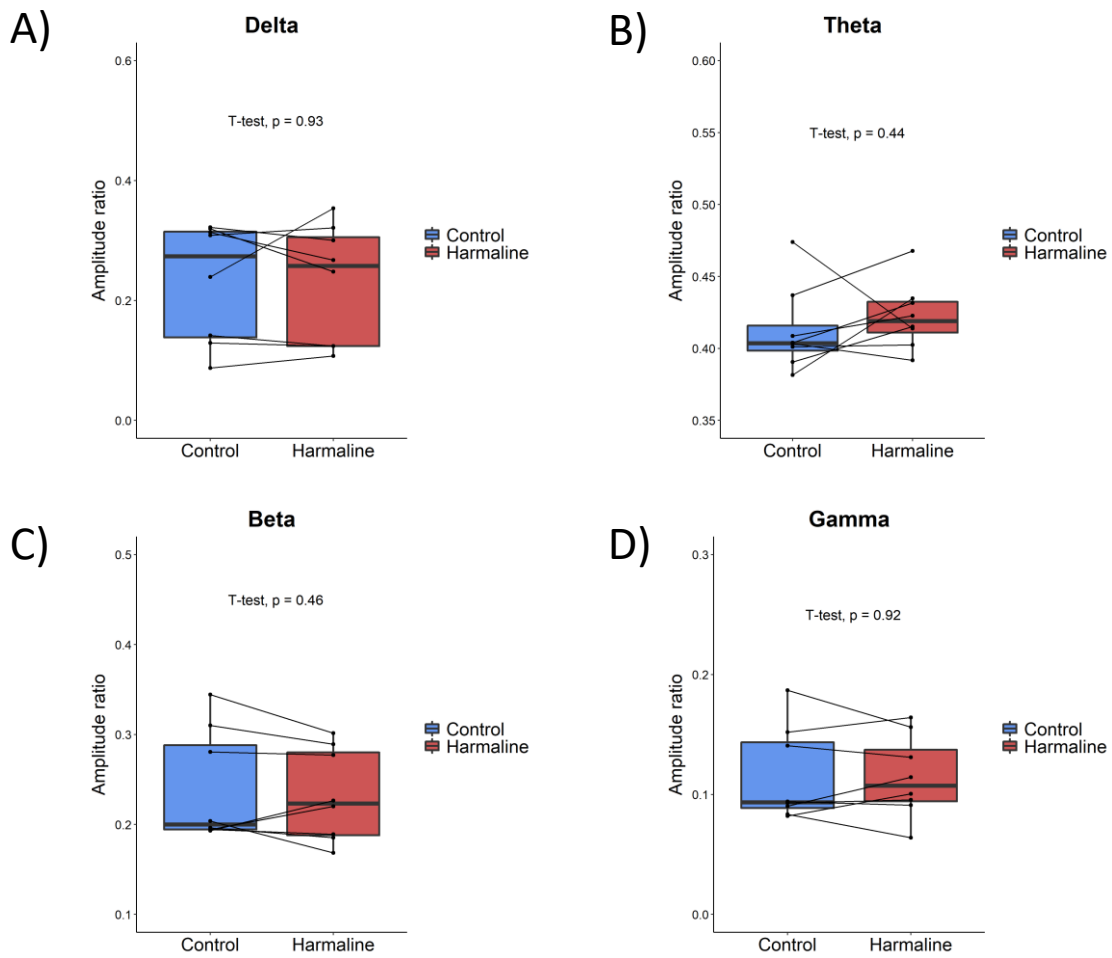
Figure 2-13. No significant changes in the ratio of EEG amplitude in the delta (1.5-4hz), theta (4-15hz), beta (15-30hz) and low gamma (30-45hz) frequency ranges in response to harmaline.
Boxplots illustrate median and interquartile range of the ratio of amplitude before (blue) and after (red) harmaline (n=8), where each individual point and line marked on the boxplots represents individual rats.
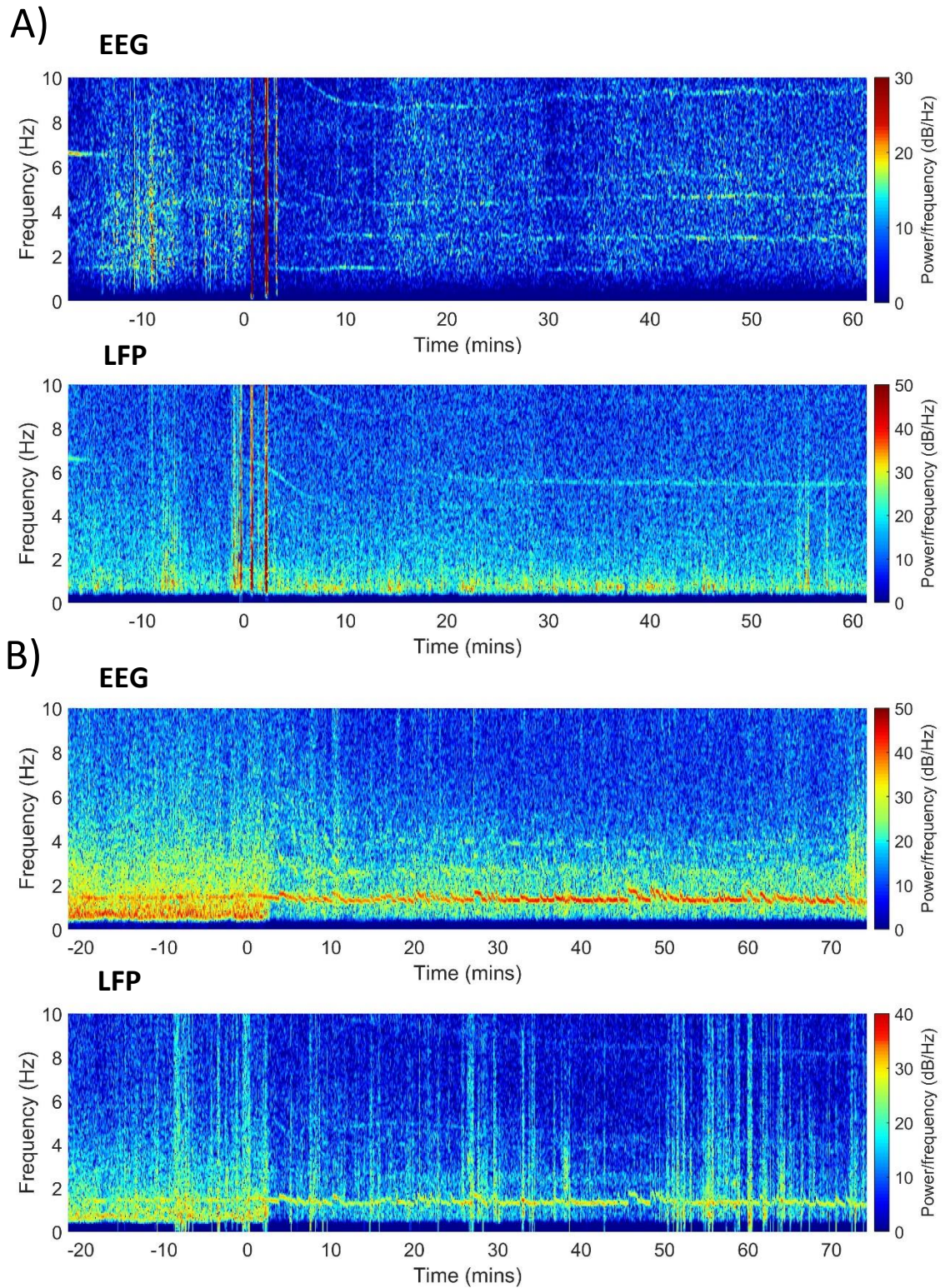
Figure 2-14. No evidence of systematic changes in urethane up/down states following harmaline administration.
Examples of simultaneously recorded EEG and medial nucleus LFP spectrograms from different rats A) rat AET13 and B) rat AET18, respectively. At time point zero harmaline (20mg/kg) was given i.p.

2.4 Discussion

The main aim of the experiments reported in this Chapter was to examine the effect of harmaline on cerebellar nuclear LFP in the anaesthetised rat. The results revealed that there were no detectable changes in interpositus LFP activity or M1 EEG activity. However, small increases in the amplitude of 5-7Hz LFP oscillations were detected in the cerebellar medial nucleus in two out of eight rats. Furthermore, increases in 5-7Hz LFP oscillations coincided with changes in the rhythmicity of simultaneously recorded MUA. On a group-level, there was also a significant increase in the ratio of theta amplitude (4-15Hz) LFP recorded from the medial nucleus following harmaline delivery. Individual-level inspection of MUA recordings also revealed a change in the regularity of MUA frequency in response to harmaline. Therefore, changes in cerebellar nuclear population activity can be detected in the urethane anaesthetised rat, but these changes appear to be confined to the medial nucleus.

2.4.1   No changes in EEG activity in the anaesthetised rat.

No consistent changes in EEG activity were recorded in urethane anaesthetised rats associated with harmaline, including activity in the theta-range. As anaesthesia inhibits harmaline-induced behavioural tremor, this may imply that anaesthetic also suppresses the transmission of harmaline-related neural rhythms in the thalamocortical network. Alternatively, harmaline-related thalamocortical rhythmicity may depend on sensory feedback of the behavioural tremor.

2.4.2   Harmaline induces rhythmic changes in medial cerebellar nuclei

The results in this Chapter show that under urethane anaesthesia, harmaline did not elicit oscillations in the interpositus nuclei. However, there was evidence for increased theta oscillations (4-15Hz) in the medial cerebellar nuclei. This corresponds with previous research which showed a greater proportion of medial compared to interpositus nuclei neurons displaying rhythmic burst firing in response to harmaline, in urethane anaesthetised Spague-Dawley rats (Lorden et al., 1992). These findings also correspond with previous research which recorded medial nuclei LFP from harmaline-treated urethane anaesthetised mice, which showed that harmaline induced an increase in theta oscillations at around 5Hz (Park et al., 2010).

Biophysical modelling and simultaneous spike-LFP recordings suggest synchronous (or near synchronous) bursts of neurons correlate with oscillations in LFP at the inter-burst frequency. This is evidenced by units firing at specific phases of the LFP (Constantinou et al., 2015; Lalla et al., 2017; Siapas et al., 2005). However, most research examining the relationship between unit spiking and LFP involves cerebral cortical or hippocampal activity, where there is uniform

alignment of sinks and sources (dendrites and axons). From what is known about the structure of cerebellar nuclear neurons, large projection neurons have a large dendritic field (41.8±1.9 ×10³μm² in humans; Ristanović et al., 2010) with dendritic branches emerging from the entire radial circumference of the soma (Ristanović et al., 2010; Sotelo & Angaut, 1973). Therefore, the alignment of cerebellar nuclear neurons may not be sufficient for generating LFP rhythms, as the morphology of these neurons may cancel out synaptic currents. However, the results from this Chapter highlight the capability of the medial nuclei to produce oscillations in the beta (~20-25Hz) and low gamma range (~40Hz) with a high signal to noise ratio compared to lower frequencies.

The results from this Chapter also showed low amplitude peaks in medial nuclear LFP theta oscillations during harmline conditions, which was the same frequency as harmaline-induced Purkinje cell complex spike firing (5-7Hz) and coincided with changes in the rhythmicity of MUA. It is therefore likely that these changes in medial nuclear LFP activity can be attributed to burst firing of medial nucleus neurons due to harmaline-induced rhythmic complex spike inhibition. In support of this, a previous study has shown rhythmic burst firing of cerebellar nuclear neurons coincided with increased complex spike discharges during pauses in cerebellar nuclear activity (Lang & Blenkinsop, 2011).

2.4.3 The topographical impact of synchronous complex spike activity on medial and interpositus nuclei activity

Previous research examining the topography of harmaline-responding Purkinje cells in rats have shown that Purkinje cells located in the vermis, particularly lobules II-VIII, exhibited sustained rhythmic complex spike activity with suppression of simple spikes (Bernard et al., 1984). However, Purkinje cells located further from the cerebellar midline were much less likely to display sustained rhythmic complex spike activity. Instead these cells tended to show complex spike rhythmicity interrupted with periods of simples spike activity, or increased complex spike activity without the rhythmicity, or no change at all (Bernard et al., 1984). Harmaline-induced climbing fibre activation of regions in the cerebellar cortex have also been examined using 14c2-deoxyglucose and Fos labelling, which indicates vermis and paravermis, but not cerebellar hemisphere involvement (Batini, Buisseret-Delmas, et al., 1981; Beitz & Saxon, 2004). Based on single-unit topographic assessment of harmaline-activated climbing fibres, the interpositus nuclei may receive less synchronised inhibitory input from paravermal Purkinje cells, in comparison to the medial nucleus.

In vitro experiments have illustrated that the synchrony of inhibitory inputs to cerebellar nuclei has a significant impact on the timing and firing rate of cerebellar nuclear activity (Person & Raman, 2011; Wu & Raman, 2017). For example, delivery of 50% synchronous vs 100%

asynchronous inhibitory post synaptic potentials, equivalent to the inhibitory inputs from 40 Purkinje cells at 50 spikes per second, significantly increased the probability of cerebellar nuclear firing every 20ms (Wu & Raman, 2017). Furthermore, computational modelling has shown synchronous pauses in inhibition increases the synchrony of cerebellar nuclear firing (Sudhakar et al., 2015). This suggests tremor-related bursting of cerebellar nuclei neurons is dependent on synchronous rhythmic inhibition from converging Purkinje cells. Therefore, the lower probability of harmaline-induced rhythmic climbing fibre activation in paravermal regions, reduces the probability of rhythmic interpositus nuclei activity. Conversely, synchronous rhythmic climbing fibre activation in the vermis would produce rhythmic output of the medial cerebellar nuclei at the same frequency.

2.4.4   Stabilisation of medial cerebellar nuclei MUA

The results from this Chapter verify previous reports that harmaline increases the frequency of complex spike firing in the cerebellar vermis, with almost complete suppression of simple spikes (De Montigny & Lamarre, 1973; Stratton et al., 1988). This large change in Purkinje cell activity onset around 10 minutes post intra-peritoneal injection, corresponds with previous reports of dose-dependent delays in IO and cerebellar nuclei oscillations (Park et al., 2010). Moreover, in the same timeframe as harmaline-induced rhythmic activation of climbing fibres, the variability in MUA was greatly reduced and stabilised at a steady firing rate. The reduction in medial nucleus MUA variability may be specifically related to the suppression of variable simple spike Purkinje cell inputs, which is replaced by highly regular and synchronised complex spike inputs.

As reported above, the synchrony of pauses in Purkinje cell inputs is thought to affect the timing of cerebellar nuclear firing, but also the firing rates of cerebellar nuclear neurons have been shown to increase during the synchronous pauses (Sudhakar et al., 2015). This effect is thought to be mediated in the cerebellar nuclei rebound firing, where the cell membrane returns to a more depolarised state during synchronised pauses, producing a transient increase in firing rate (Alvĩa et al., 2008; Sudhakar et al., 2015). This also corresponds with previous reports on harmaline's effect on medial cerebellar nuclear burst activity. For example, the firing rate of medial nuclei neurons increased during harmaline-induced burst activity compared to spontaneous activity prior to harmaline administration, such that overall firing rate increased from around 13 to 23Hz (Lorden et al., 1992). The results in this Chapter also report a similar effect for one of two MUA recordings from the medial cerebellar nuclei. These findings also correspond with current theories of cerebellar nuclear involvement in ET, which suggest that the pathophysiology of ET is due to cerebellar nuclear disinhibition, which results in altered cerebellar output propagated to

subcortical and cortical motor loops to produce pathological tremor oscillations (Boutin et al., 2015; Paris-Robidas et al., 2012). These theories suggest that cerebellar nuclear disinhibition is related to defective GABAergic transmission in the cerebellum rather than an increase climbing fibre activation. However, an increase in complex spike firing and suppression of simple spike firing may reduce the overall frequency of inhibitory input to the cerebellar nuclei, producing a similar effect of cerebellar nuclear disinhibition.

2.5   Chapter Summary

This Chapter has shown that harmaline induces changes in theta range (4-15Hz) LFP oscillations in the medial but not interpositus nuclei, in the anaesthetised rat. Furthermore, changes in Purkinje cell activity coincided with changes in the variability of medial cerebellar nuclei MUA. The nuclei form a gateway between abnormal olivo-cerebellar input and cerebellar output to brainstem and mid-brain nuclei, which also play a key role in motor control. To examine whether altered cerebellar output can induce tremor-related activity in thalamocortical circuits, Chapter 3 will examine changes in neural oscillations in this circuit in response to harmaline in awake behaving rats.

Chapter 3. **Effect of harmaline on neural oscillations across the cerebellar-thalamocortical network in awake behaving rats**

3.1 Introduction

ET and harmaline-induced tremor are identified as action tremors, where tremor onsets or increases in amplitude with movement. Movement-related oscillations have been reported in the granular cell layer of the cerebellar cortex in the theta and beta range (4-25Hz) (Courtemanche et al., 2013). For example, theta frequency oscillations (~14Hz in monkeys, ~7Hz in rats) in the granule cell layer have been associated with periods of immobility in awake animals, where these rhythms are reduced during movement (Hartmann & Bower, 1998; Pellerin & Lamarre, 1997). Purkinje cell simple spike firing patterns have also been associated with encoding different movement parameters (e.g. movement onset, limb position, velocity), which may account for the reduction in granule cell layer rhythms in response to movement (Ebner et al., 2011; Hewitt et al., 2015; Laurens & Angelaki, 2020). Purkinje cell complex spikes have also been associated with encoding movement parameters (Ebner et al., 2002; Streng et al., 2018). As harmaline-activation of climbing fibres completely disrupts the natural rhythmicity of the cerebellum, it is likely that harmaline would have a disruptive impact on cerebellar movement-related encoding. The findings reported in Chapter 2 of this thesis, in corroboration with previous research, have shown that harmaline-induced changes in cerebellar oscillations are prevalent during anaesthetised states. However, research to date has not examined whether harmaline-induced rhythms in the cerebellum are altered during movement versus inactivity.

Previous research has hypothesised that tremor-onset with action in ET is due to disrupted cerebellar output (Buijink, van der Stouwe, et al., 2015). The cerebellar nuclei transmit integrated sensorimotor signals to the wider motor network (Armstrong & Edgley, 1984; Giuffrida et al., 1981), and optogenetic stimulation of the interpositus cerebellar nucleus has been shown to disrupt the accuracy of forelimb reaching movements (Low et al., 2018). Furthermore, bilateral rhythmic optogenetic stimulation of the interpositus nucleus has been shown to induce a tremor in mice at the same frequency of stimulation, where a range of stimulation frequencies between 1-20Hz were examined (Brown et al., 2020). This underscores the importance of increased cerebellar nuclear rhythmicity in generating and propagating tremor rhythms. As outlined in the General Introduction, the cerebellar nuclei project to the motor cortex via the thalamus and are thought to play a key role in ET pathophysiology. However, research to date has not examined the impact of altered cerebellar projections to ascending thalamocortical pathways in the harmaline

model, and whether these pathways further contribute to changes in tremor amplitude with movement.

3.1.1 Aims

The research presented in this Chapter aimed to examine the neural network dynamics of tremor in the motor network, in the awake behaving rat using the harmaline model, and to examine how neural oscillations in the central network thought to be critically involved in ET, relate to behavioural tremor. There has been substantial evidence showing harmaline induces rhythmic oscillations in the olivo-cerebellar circuit in the anaesthetised animal, but harmaline's effect on the cerebello-thalamocortical circuit, which is implicated as being hyper-synchronised in ET patients, is unknown. Furthermore, as ET and harmaline-induced tremors are characterised as action-induced tremors, this Chapter aims to examine how neural network interactions are modulated by movement.

3.2 Materials and methods

3.2.1 Animals

All procedures were performed in accordance with the United Kingdom Animals (Scientific Procedures) Act 1986 and the University of Bristol Animal Welfare and Ethical Review Body. Experiments were performed on 16 adult male Lister Hooded rats (300 - 600g). All animals were housed in groups under normal environmental conditions (~20°C and 45 - 65% humidity), maintained on a 12/12hr light/dark reverse lighting cycle and provided with food and water ad libitum. Rats were handled daily to acclimatise to the experimenter for at least one week prior to surgery. Following surgery, the animals were housed separately, and their health was monitored closely with daily observational assessments and monitoring of weight.

3.2.2 Targets for electrophysiological recordings

This experiment simultaneously recorded across the cerebello-thalamocortical network using microdrives assembled to target the medial cerebellar nuclei and thalamus, as well as EEG screws implanted over motor cortex, and simultaneous EMG and accelerometer recordings to monitor movement and tremor. Further details on target co-ordinates and surgical procedures are provided below.

3.2.3 Microdrive construction prior to implantation

Custom-made microdrives were used which allowed simultaneous multi-brain site MUA and LFP recordings from the cerebellum and the thalamus. For each brain site, microdrives included two-to-four tetrodes with independently moveable drives per tetrode.

3.2.3.1 Microdrive design type 1

Experiments carried out on the first six rats involved lightweight microdrives custom made using single row Mill-Max inter connector strips (Mill-Max Manufacturing Corp). Prior to implantation, independently moveable microdrives were created using three interconnector strips, each containing four pinholes (see Figure 3-1). Two of these interconnector strips were used as outer structural components, and the third was used as the inner adjustable component. When building the drive prior to surgery, two support screws were fixed into the first and third pinholes of the interconnector stripes, such that these support screws were fixed securely into the outer structural components but fitted loosely within the inner adjustable component. This allowed the inner adjustable component to move up and down the support screws with ease, whilst the support screws held the drive together. Once the support screws were fixed into place, the heads of the screws were removed using a Dremel rotatory power tool. The main screw was threaded through the pinhole in between the two support screws, such that the screw fitted loosely within the outer structural components, and secularly screwed into the inner adjustable component. A nut was then screwed onto the bottom of the main screw, beneath the drive, and soldered into place. When the main screw was then turned using a screwdriver, the inner adjustable component moved up or down the thread of the screw. A stainless-steel rod cannula was then threaded through the final pinhole in the interconnectors and superglued only to the adjustable inner component of the drive. This moved the stainless-steel rod cannula up/down when the main screw was turned using a screwdriver. The microdrives were then positioned such that the cannula from each microdrive was guided through a central guide tube to converge at a centre point. The microdrives were then fixed together to the central guide-tube using dental cement. To avoid cementing the inner moveable component and the moveable cannula, these parts were first covered with Vaseline to prevent contact with the dental cement. Tetrodes (see 3.2.3.3 below) were inserted into each of the cannula and superglued into place at the top of the cannula. An electrode interface board (EIB-16, Neuralynx) was cemented above the drives. The wires from each tetrode were pinned onto the electrode interface board using gold pins, to provide the signal connection between the electrode wires and the Neuralynx headstage.
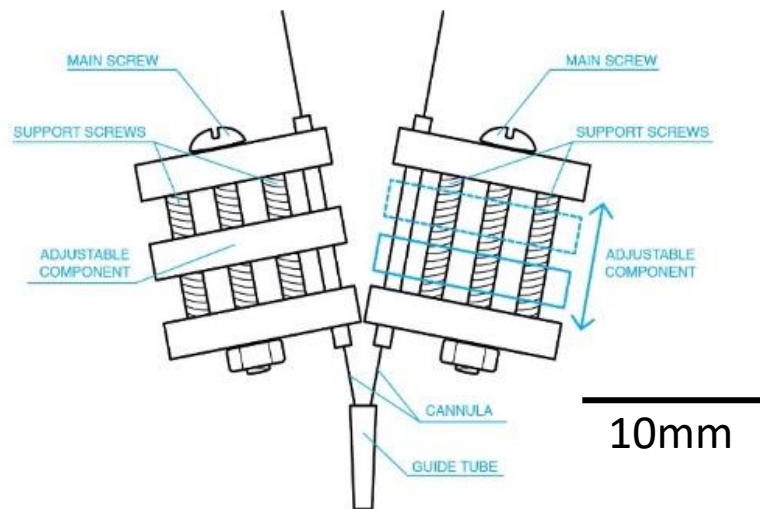
Figure 3-1. Diagram of custom-made microdrives.
Each microdrive consists of three strips of Mill-Max interconnectors (two for outer structural support, and one inner adjustable component), three screws (two for structural support, and one main adjustable screw), and a tetrode cannula.

3.2.3.2 Microdrive design 2

For the remaining experiments, the drive design was further developed with the use of 3D software (Fusion 360) and 3D printing. The new design, illustrated in Figure 3-2, comprised three or four microdrives fixed together at the base, which ensured a fixed angle and spacing of the drives. Each microdrive had a fixed outer structure, and a separately printed moveable inner component, which slotted into the central groove of the micro-drive. Each microdrive had two pinholes (one large and one small pinhole) which passed through the micro-drive and inner moveable component. A screw was threaded though the larger pinhole, and nut was fastened underneath the drive and soldered into place. A clockwise turn of the screw functioned to move the inner components down, allowing tetrode depths to be adjusted post-surgery. The cannula was threaded through the smaller pinhole, and then each cannula was then threaded through a larger guide tube beneath the drives. The tetrode for each microdrive was inserted into the cannula and superglued into place at the top, and the cannula were superglued to the smaller pinhole of the inner moveable component. Dental cement was used to fix the drives to the guide tube, as well as to the electrode interface board (EIB-16).

3.2.3.3 Tetrodes, EMG and EEG wires

Both designs involved hand-made tetrodes that were crafted using insulated tungsten wire (5μm diameter, California Fine Wire Co.). For each tetrode, a length of tungsten wire was folded fourfold

and spun together using the Neuralynx tetrode spinner (80 turns forward and 40 turns backwards), and then fused together using a heat gun. Prior to surgery, the tetrode tips were cut to size (approx. 7.5mm), and tetrode impedance levels were checked before implantation. For 7 out of 16 rats, one of the cerebellar tetrodes were cut ~2mm shorter, by adjusting the tetrode depth with the independently moveable microdrives before cutting. To identify the site of the recordings post-mortem, the tips of the tetrodes were dipped in florescence DiI solution (3% in absolute ethanol). Insulated stainless-steel wires (~127µm dimeter, Cooner wire) were additionally soldered to the EIB board for EEG and EMG recordings.
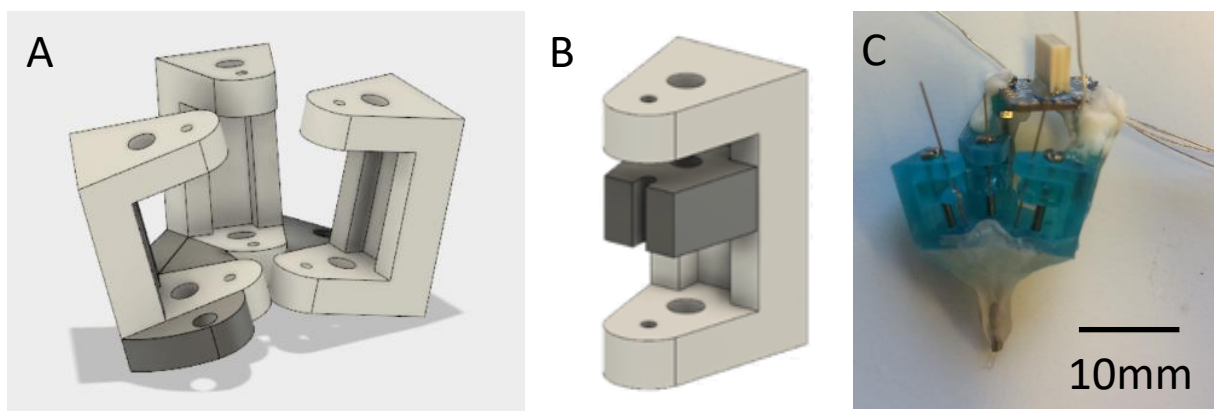
Figure 3-2. 3D designed microdrives.
A) shows a diagram of the fixed microdrives without the inner moveable component, B) shows a diagram of a single micro-drive with the inner moveable component slotted into place, and C) shows microdrives fixed to guide tube and EIB-16 (scale bar for C only).

3.2.4 Surgery and implantation of the electrodes for chronic experiments

Rats were anesthetised with a combination of ketamine (50%) and medetomidine (30%) in saline (20%), which was administered via an i.p. injection at a dose of 1ml/kg. Once anesthetised, the rats were transferred to a non-sterile preparation area where their head and limb were shaved and cleaned with antibacterial scrub. Rats were then transferred to the sterile surgical table and placed on a heated mat with a rectal thermometer to maintain temperature at 36-37°C. Saline (5ml) was given via a subcutaneous injection to keep the animal adequately hydrated during surgery. Local anaesthetic lidocaine (10% Xylocaine®) was sprayed onto the scalp and in the ears before mounting onto a stereotaxic frame with ear and mouth bars to hold the head in place. Surgical levels of anaesthesia were checked regularly during procedures via pedal reflex (toe

pinch) and eye blink reflex, and additional doses of 0.1ml of the ketamine/medetomidine/saline solution were given when required. A scalp midline incision was made to expose the skull, and the connecting tissue was cleared using blunt dissection and the skull was cleaned. Screws that had been pre-soldered with a section of insulated stainless-steel wire (127µm diameter, Cooner wire) were fixed into the skull that covered the M1 and S1 to provide four subdural EEG recordings (M1 co-ordinates: 3mm lateral and 2mm anterior of bregma, and S1 co-ordinates: 3mm lateral and 0.5mm posterior to bregma, Paxinos & Watson, 2005). A reference screw pre-soldered to insulated silver wire and was fixed into the right parietal skull plate, and a support screw was fixed into the left parietal skull plate. A ground screw soldered to an insulated silver was fixed over the right occipital skull plate. All skull screws had a head diameter of 1mm and a thread diameter of ~0.7mm.

A burr hole was drilled through the skull covering the cerebellum (ML 1mm, AP -11.3mm to target the medial cerebellar nucleus, Paxinos & Watson, 2005). For 15 of the 16 rats, a second burr hole was drilled through the skull to allow implantation of tetrodes into the motor thalamus, contralateral to the cerebellar implant. The VA, VL, and VM nuclei of the thalamus have been identified as the motor thalamus in the rodent brain (Kuramoto et al., 2009a, 2011; Nakamura et al., 2014). The top of the VA/VL complex of the thalamus was therefore targeted during implantation of thalamic tetrodes (ML 1.8mm and AP -2.28mm). For each craniotomy, the dura was removed to exposure the surface of the brain before tetrodes were inserted. The tetrodes were then lowered to the appropriate depths (medial cerebellar nucleus DV 4.1mm from the surface of the cerebellum; motor thalamus DV, 5.1mm from the surface of the cerebral cortex, Paxinos & Watson, 2005). A diagram illustrating the surgical implantation sites is illustrated in Figure 3-3. The drives were cemented in place on the top of the skull and skull screws using dental cement containing gentamicin. The wires connected to the EEG, reference and ground screws were then soldered to the electrode interface board (EIB-16, Neuralynx) and the excess wire incorporated into the implant with dental cement.

Two EMG wires were secured into the neck muscle, using non-absorbable stitches, and two wires were tunnelled under the skin from the back of the neck to the forelimb or hind limb on the ipsilateral side of the cerebellar implant. EMG wires were then secured into the clavotrapezius neck muscle, triceps brachii or biceps femoris, using non-absorbable stitches. Skin incisions were closed with absorbable stitches, and a tin cone was cemented around the circumference of the microdrives for protection. On completion of the surgery procedure, 1ml dose of analgesic

carprofen (5% in saline) was given subcutaneously followed by 0.1ml of atipamezole 20% in saline given via i.p. injection, to reverse the effects of the medetomidine.
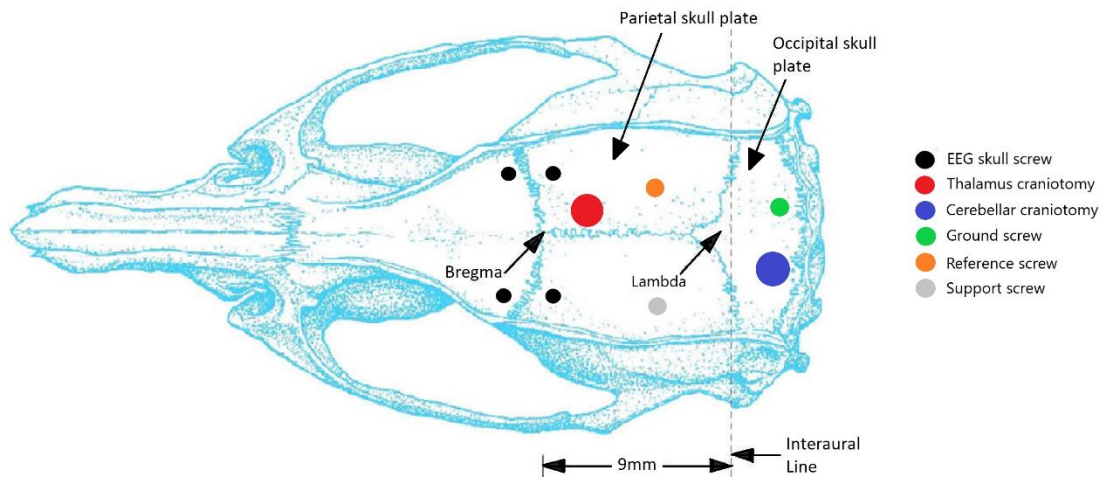
Figure 3-3. Surgical implantation of electrodes *in vivo.*
Four skull screws were fixed into the skull covering M1 and S1 to provide subdural EEG recordings (M1 co-ordinates: 3mm lateral, and 2mm anterior or bregma; S1: 3mm lateral and 0.5 posterior of bregma). A small craniotomy was performed over the parietal skull plate (1.8mm lateral and 2.28mm posterior of bregma) and a second over the occipital skull plate (1mm lateral, 11.3mm posterior of bregma) to allow implantation of thalamus and cerebellar tetrodes, respectively. A reference skull screw electrode and support screw were placed on the parietal skull plates, and a ground skull screw was inserted into the occipital skull plate. All skull screws had a head diameter of 1mm and a thread diameter of ~0.7mm.

3.2.5 Experimental protocol

Following a recovery period (between 2-7 days), chronically implanted rats were connected to the tethered Blackrock Microsystem to collect electrophysiological recordings. Data were collected while rats were able to freely move around their home cage, and this data was collected before (i.e. control condition) and after administration of harmaline hydrochloride (10mg/kg, i.p.). Baseline control data was collected across several days. Animals were temporally disconnected from the recording system during harmaline administration. After harmaline administration, data was continuously recorded until any visible deficits in motor function were completely recovered.

3.2.6 In vivo chronic electrophysiological recordings in awake behaving rats

Neural and EMG signals were sampled whilst the animal moved freely around the home cage. The EIB boards were connected to the tethered Blackrock CerePlex μ Headstage, and differential neural and EMG signals were sampled and digitised using a Cereplex acquisition system (Blackrock Microsystems). Raw data was continuously recorded at a sampling rate of 30kHz across all

channels. MUA from each tetrode was also recorded, sampled at 10kHz and band-pass filtered 250Hz-5000kHz. Low pass filtered EEG and EMG data (<500Hz) were sampled at 2kHz. Continuously recorded raw data allowed tetrode LFP to be examined off-line. The Blackrock CerePlex μ Headstage also enabled 3-axis accelerometer recordings, which were low pass filtered data (<500Hz) sampled at 2kHz.

3.2.7 Histological preparation

Rats were killed by transcardial perfusion under deep anaesthesia with an overdose of Euthatal (1ml, i.p.). The recording site was additionally marked whilst rats were under anaesthesia by an electrolytic lesion (3μA for 30 seconds). For each recording site, the tetrode recording units with the best signal to noise ratio (SNR) was chosen. Rats were then transcardially perfused with 0.9% saline, followed by 0.1m phosphate buffer (PB) that contained 4% paraformaldehyde. After perfusion, the whole brain was extracted, and the tissue was post fixed in 4% paraformaldehyde for 24-72 hours, and then transferred into 30% sucrose solution 3-4 days before cutting and mounting sections. A freezing microtome (SM2000R, Leica) was used to section the brain tissue using Cryomatrix as the embedding medium (Thermo Scientific). The cerebellum was detached from the rest of the brain, and cerebellar tissue was cut into sagittal sections of either 40 μm (n=10 rats) or 100 μm (n=6 rats) thickness. The thalamus was sectioned either in the coronal (n=5 rats; 100 μm section thickness) or sagittal plane (n=10 rats; 40 μm section thickness). The tracks of the inserted tetrodes marked with DiI within the cerebellum and motor thalamus were visualised with a fluorescent Axioskop 2 Plus microscope (Zeiss) fitted with a CoolLED pE-100 excitation system and images acquired using AxioVision software.

To further aid identification of the motor nuclei of the thalamus, immunofluorescent labelling of glutamic acid decarboxylase 67 (GAD-67) and vesicular glutamate transporter 2 (VGluT2) was performed on 40μm sagittal sections of the thalamus in 10 of 15 rats. This is based on previous research, which showed GAD-67 and VGluT2 immunoreactivities provide a clearer distinction between the regions of the motor thalamus that receive inhibitory input from the basal ganglia and excitatory input from the cerebellum (Nakamura et al., 2014). To achieve this, every third thalamic section was first washed three times in 0.01m PB before being incubated overnight at room temperature in the primary antibody solution. The primary antibody solution was made up of a mixture of Guinea Pig anti-vGluT2 (AB2251-I, Millipore) and mouse anti-GAD67 (MAB5406, Millipore) in a dilution of 1:1000 in phosphate-buffered saline with Triton X (PBS-T) containing 5% normal goat serum. After an overnight incubation at room temperature, sections were then washed again three times in 0.01m PB. Sections were then incubated for two hours in the

secondary antibody mixture, which contained goat anti-Guinea Pig IgG (A-110776, Alexa Fluor 594, Thermo Fisher Scientific) and goat anti-mouse IgG (A32723, Alexa Fluor 488, Thermo fisher Scientific) in a dilution of 1:1000 in PBS-T. Following incubation in the secondary antibody mixture, sections were again washed three times in 0.01m PB before mounting onto glass slides. The mounted sections were cover slipped with the antifade medium FluorSave.

3.2.8 Data processing

Processing of raw data was performed offline using MATLAB. Bipolar referencing configurations were used for all EMG, EEG, and tetrode LFP recordings. Bipolar referencing of LFP channels removes EEG signal picked up by the skull-screw reference, as well as providing a better voltage representation of correlated sources of noise (including 50Hz noise, and movement artefacts) across the reference and recorded sites. In addition, bipolar referencing removes any discrepancy between the reference and recorded sites, in terms of electrode size, impedance, and physical distance from the recorded site (Ludwig et al., 2009). Bipolar local referencing of recording sites also prevents recording of volume-conducted signals or mechanical movement-related artefacts. Where multiple tetrodes were inserted into a brain site, the tetrodes with the least amount of background noise and/or SNR of MUA were selected for group analysis of changes in LFP rhythms. EEG screw electrodes fixed over the sensorimotor cortex (M1 and S1) were also bipolar referenced, where single EEG channels on bilateral sides of the sensorimotor cortex were referenced against each other. For EEG, LFP and EMG analysis, data were band-pass filtered between 1-49Hz, and then down-sampled to 1Khz. Data were then z-scored, to standardise epoch rejection, as reported below. For analyses performed on the tri-axial accelerometer data, a principal component analysis was first computed to combine measurements in three directions into one principal component or axis to captures the axis with maximal variance.

3.2.9 Division of data into 'rest' and 'move' epochs

To examine how neural network interactions are modulated by movement, electrophysiological data were divided into epochs where the rats were either 'resting' or 'moving'. This was achieved by applying a global movement-threshold value to a measure of total acceleration, which was taken as a proxy of overall movement, to distinguish between any periods in which the animal was quietly resting versus moving. Total acceleration, A, was calculated using Equation 3.1. Here, x, y, and z represent the three axes of the accelerometer, which was positioned on the rats' head.

$$A = \sqrt{(x^2 + y^2 + z^2)}$$
<div style="text-align: right">Equation 3.1</div>

Total acceleration was then smoothed using a moving average filter with a window size of 100 samples. A global movement threshold of $1m/s^2$ was applied to distinguish quiet resting from movement. Similar methods have been employed previously to distinguish periods of immobility and movement (Guitchounts et al., 2020; Meyer et al., 2018; Pasquet et al., 2016). This threshold was verified against video recordings and performed well at identifying time points when rats begin to move around the cage or move to adjust their resting position. For an epoch to be classified as either 'resting' or 'moving', rats needed to be immobile or moving for the entire epoch duration. This introduced a trade-off when choosing epoch length. A shorter epoch size increased the number of total epochs in which the animal was either active or resting for the entire epoch duration, whereas a longer epoch size would increase the low frequency resolution of recorded signals but decrease the number of epochs in total. A two-second-long epoch was chosen as it captured eight cycles of 4Hz, which is the lowest tremor frequency recorded in patients, as well as providing a reasonable number of epochs for analysis. Figure 3-4 illustrates the threshold applied to total acceleration data to distinguish period of resting and movement.
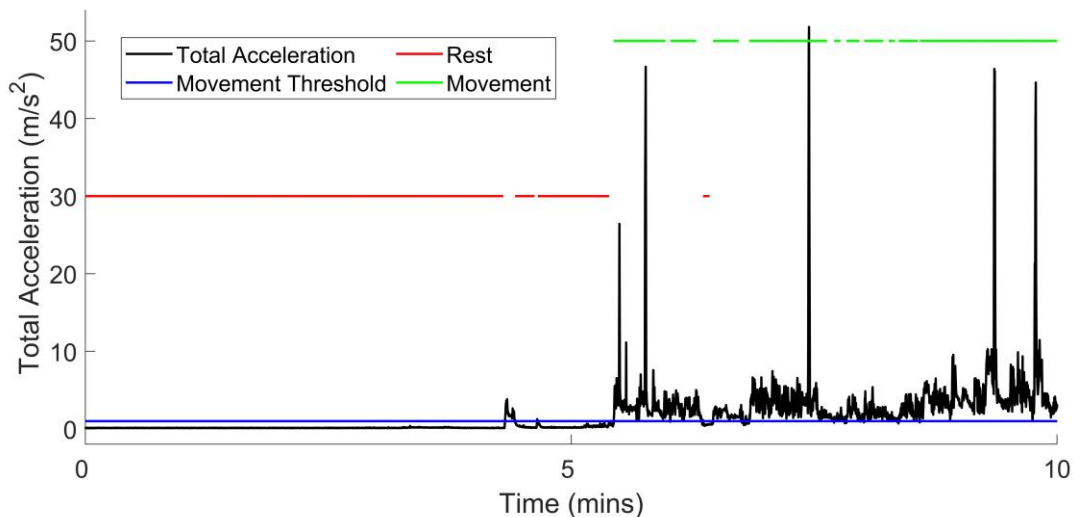
Figure 3-4. Division of data into 'move' and 'rest' epochs.
The data in black illustrate smoothed total acceleration of the rat over time and the applied movement threshold ($1m/s^2$) is shown in blue. Red lines demonstrate time points categorised as 'rest', and green lines demonstrate time points categorised as 'movement'.

1.1.1 Epoch rejection

Visual inspection of the neural data and video recordings identified large amplitude global artefacts that appeared across multiple channels and recording sites, which were mostly identified as chewing or movement-related artefacts (e.g. grooming and scratching behaviours that knocked the tethered wires and headpiece). Following visual inspection of z-scored neural data, these

artefacts were removed by rejecting epochs containing data points larger than or equal to four standard deviations (SD) of the mean from further analysis. The use of a z-score threshold criterion to remove epochs containing high-amplitude artefacts has been applied in similar studies examining changes in network dynamics (West et al., 2018).

Visual inspection of the data also highlighted the presence of spontaneous high amplitude spike-wave discharges, which occurred intermittently within EEG recordings of all rats. These waveforms have been previously associated with brief periods of absence seizure-like events. Unlike convulsive seizures, absence-seizures are non-convulsive and are associated with behavioural arrest, which corresponds with observed immobility of the rats during these events. During baseline pre-harmaline conditions, these discharges oscillated at around 7-8Hz (Figure 3-5). This activity was accompanied by bursting of MUA in some of the thalamic recording channels. Interestingly, following harmaline administration, these periods increased in frequency, to the same frequency as the tremor (9-15Hz), and were also accompanied by an increase in tremor oscillations recorded within the accelerometer (Figure 3-5). It is speculated that this may be a result of rhythm entrainment. As these rhythms occurred within tremor frequency range, it was important to exclude these periods from further analyses, to assess whether neural oscillations recorded out-side of these periods also oscillate at the tremor frequency.

As these periods of absence seizure-like discharges were easily identified by visual inspection, a MATLAB graphic user interface was created to allow user identification of the onset and offset these periods. This enabled the timings of all user-defined absence seizure-like discharges to be logged for all recordings and enabled the exclusion of any epochs containing these discharges from the final data sets before analysis. After identifying epochs containing artefacts or spike-wave discharges, raw data was pre-processed in the steps described above, with the exception that data was not z-scored before dividing into epochs. Instead, after epoch rejection, all epochs within rat were collated across conditions and collated data were z-score normalised within rat. This allowed comparison of spectral amplitude across conditions and rats.

A) Control
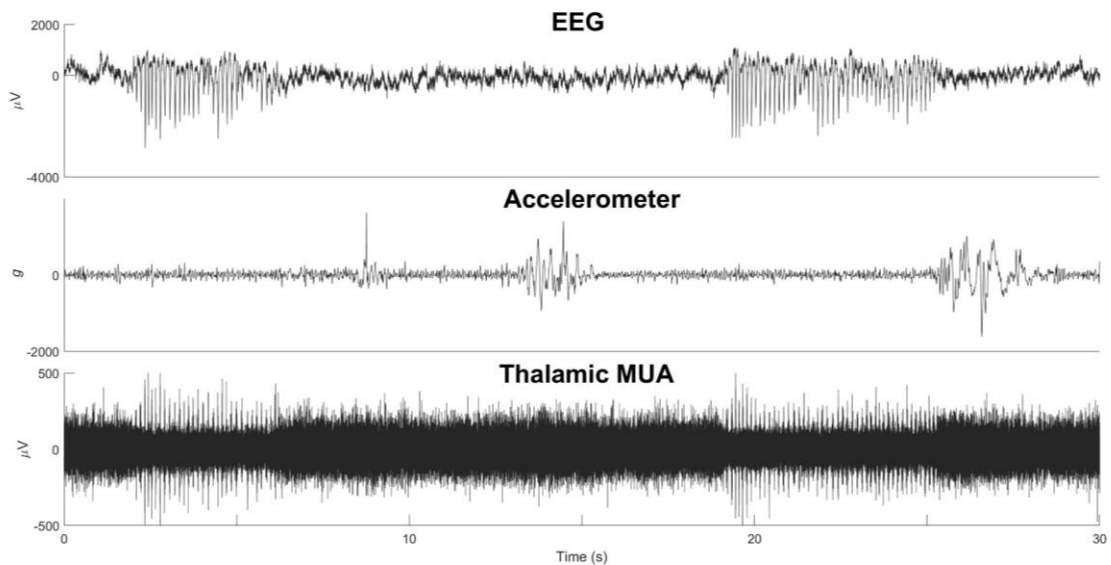
B) Harmaline
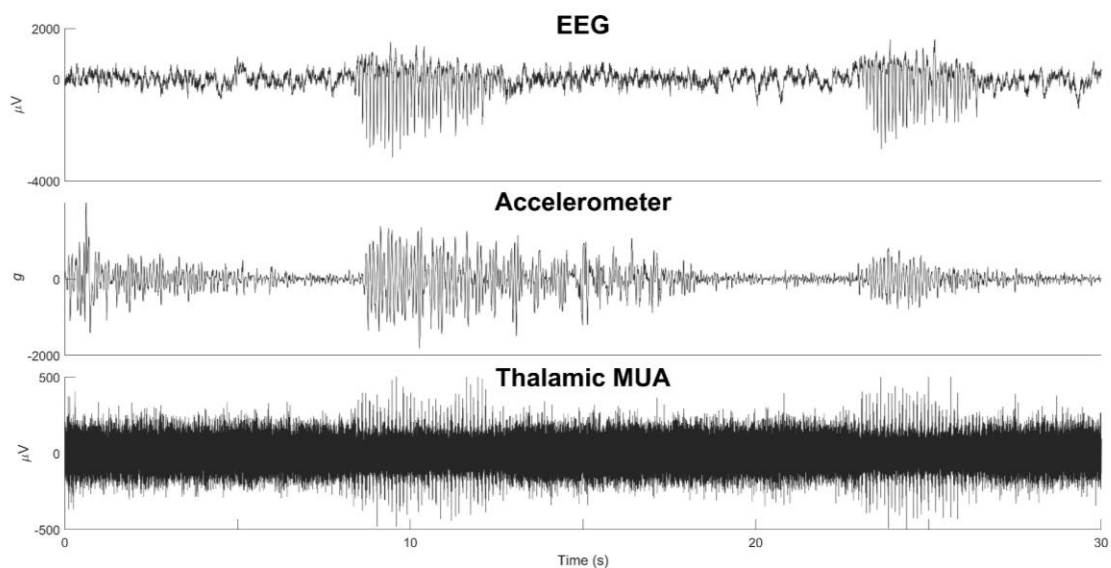
Figure 3-5. Large amplitude spike-wave discharges in the subdural EEG occurred alongside MUA burst firing.

Simultaneously recorded EEG, accelerometer activity, and thalamus MUA during A) control (pre-harmaline) and B) harmaline conditions. During control, there were no changes in accelerometer activity associated with spike-wave discharges in EEG and busting in thalamus MUA. During harmaline, spike-wave discharges in EEG and busting in thalamus MUA was also accompanied by increased tremor activity in the accelerometer.

3.2.10 Spectral analyses

FFTs were applied to each epoch, to decompose the time-series signals into the frequency domain, where the number of FFT points calculated was 1024. As reported in Chapter 2 of this thesis, the ratio of signal amplitude within the tremor frequency range (9-15Hz), in comparison to total amplitude in the low frequency range (0-15hz), were calculated for each epoch. This is defined by Equation 3.2, where Sxx represents the amplitude spectrum obtained from the FFT. Similar methods have been previously employed to examine changes in the distribution of power at tremor specific frequencies (Iseri et al., 2011).

$$Amplitude\ ratio = \frac{\sum Sxx(9 - 15\text{Hz } bins)}{\sum Sxx(0 - 15\text{Hz } bins)}$$ Equation 3.2

Signal frequency coherence was computed by examining the magnitude-squared coherence (C_{xy}) for each epoch using the 'mscohere' function in MATLAB described in Equation 3.3.

$$C_{xy} = \frac{|P_{xy}(f)|^2}{Pxx(f)P_{yy}(f)}$$ Equation 3.3

Here C_{xy} represents coherence, P_{xy} represents the cross-spectrum of the two signals and P_{xx} and P_{yy} represent the separate amplitude spectrum of the two signals. This function outputs a quotient number between zero (no coherence) and one (very coherent), representing the correlation between two signals for each frequency bin.

Surrogate analyses were applied to examine the significance of coherence. Surrogate analysis tests the null hypothesis that the two signals are independent Gaussian linear stochastic processes, and that means and variances in coherence values derived from the same probability distribution should be the same. For each epoch, 99 surrogate data sets were generated using the iterative amplitude adjusted fast fourier transform algorithm (IAAFFT) using MATLAB (Venema et al., 2006). IAAFFT generates surrogates from the original time series, where surrogate data sets maintain the same amplitude distribution and power spectrum of the original data but the phase relationship between the two time series is random (Schreiber & Schmitz, 1996). Signal coherence was then computed on each of the 99 surrogate epochs, and statistical significance of coherence was examined by comparing mean coherence at the tremor frequency (9-15Hz) for each recorded epoch against the mean coherence at 9-15Hz for the 99 surrogate epochs. Spurious coherence

can arise due to the spectral content of both signals showing independent oscillations at the same frequency, signal amplitude correlation or as an artefact of epoch length (Lee et al., 2012; Srinath & Ray, 2014). Therefore, surrogate-corrected mean coherence values, *C*, was calculated using Equation 3.4 (Rummel et al., 2015), which corrects for spurious coherence.

$$C = \frac{P - P(surr)}{1 - P(surr)} \, S \qquad\qquad \text{Equation 3.4}$$

Here *P* represents the mean coherence coefficient across the tremor frequency coherence bins (9-15Hz) of the real data, and *P(surr)* represents the mean coherence at the tremor frequency across 99 surrogate epochs. If *P* is greater than *P(surr),* then the null hypothesis that the two signals are independent can be rejected, and *S* takes a value of 1. Else, the null cannot be rejected, *S* takes on the value of 0.

3.2.11 Cross-correlations

Time-lagged relationships between electrophysiological signals recorded from each brain site, as well as with EMG measures of tremor, were calculated using cross-correlations. Data were first band-pass filtered at the tremor frequency range (9-15Hz) before dividing into epochs as described above. Only data recorded during harmaline conditions when the rat was categorised as 'moving' were selected for further analysis. For each epoch and pair of signals, cross-correlations were calculated using the 'xcorr' function in MATLAB, and the time-lag with the maximum correlation coefficient were extracted. For each animal and pair of signals, time-lags showing maximum correlation coefficients were pooled across epochs, and the normalised probability of maximum cross-correlation at binned time-lags was calculated (± 100ms lags with a 2ms bin width). For each animal and pair of signals, the time-lag with greatest probability of maximum cross-correlation was identified. A measure of peak probability was calculated by taking the probability at the bin with the max probability value and adding this to the sum of the adjacent two bins. If time-lagged relationships followed a uniform distribution, the probability of maximum cross-correlation at each binned time-lag would be 0.01. Therefore, peak probabilities that surpassed a threshold value of 0.1 or higher were included within summary statistics examining time-lagged relationships between tremor signals recorded across the network.

3.2.12 Statistics

A multi-level regression model was specified to examine the relationship between a) harmaline and signal amplitude at the tremor frequency, and b) motor activity and signal coherence at the tremor frequency. Multi-level modelling for repeated measures designs involves modelling data with hierarchically structured random factors. These random factors include two levels of sampling: at the highest level (level 2) is the subject (i.e. rats), and at the lower level (level 1) the occasions (i.e. 2-second epochs) at which the dependant variable was sampled. The design also includes fixed factors which are the independent variables (i.e. harmaline vs control, or moving vs resting).

The advantage of choosing a multi-level model to statistically examine relationships, is that this model yields a higher power in statistical testing than a repeated measures ANOVA, due to a more accurate assessment of the variance at each sampling level (Bell et al., 2019; Quené & Van Den Bergh, 2004). This method can also address unbalanced data, as the number and timing of sampled observations can vary between subjects.

3.2.12.1 The multi-level model

To examine the relationship between harmaline or movement conditions and the dependant variable, *DV* (i.e. signal amplitude or coherence), a baseline simple variance model (Model 1) without any independent variables, was compared to a fixed effects model (Model 2) which declared either harmaline or movement as a categorical independent variable, *IV*. The simple variance (Model 1) and more complex predictor (Model 2) models were statistically compared using the likelihood ratio test, which examines whether the more complex model (Model 2) provides a better fit of the data.

Model 1   Level 1:
$$DV_{ij} = \beta_{0ij}$$
            Level 2:
$$\beta_{0ij} = \beta_0 + u_{0j} + e_{ij}$$
Equation 3.5

Model 2   Level 1:
$$DV_{ij} = \beta_{0ij} + \beta_1 IV_{ij}$$
            Level 2:
$$\beta_{0ij} = \beta_0 + u_{0j} + e_{ij}$$
Equation 3.6

Model 3   Level 1:
$$DV_{ij} = \beta_{0ij} + \beta_{1j} IV_{ij}$$
            Level 2:
$$\beta_{0ij} = \beta_0 + u_{0j} + e_{ij}$$
Equation 3.7
$$\beta_{1j} = \beta_1 + u_{1j}$$

$$\chi 2 = [-2LL(simple\ model)] - [-2LL(complex\ model)] \qquad \text{Equation 3.8}$$

Model 1 and Model 2 are displayed in Equation 3.5 and Equation 3.6, respectively. Here, DV_{ij}, is the dependant variable for rat j at sampled epoch i. Model 1 estimates the grand mean value of the *DV*, represented by β_0, and the variability in the grand mean value of *DV* across rats, u_{0j}, and across sampled epochs e_{ij}. Model 2 additionally includes a regression coefficient β_1 for the dummy coded *IV* {0, 1}. The regression coefficient for the intercept β_{0ij} represents the reference group, which is either the control condition when harmaline is included as the *IV* or resting when movement is included as the *IV*. If Model 2 provided a significantly better fit than Model 1, the fixed effects model (Model 2) was then statistically compared to a mixed effects model (Model 3). Model 3 is displayed in Equation 3.7 and specifies that the effect of the *IV* on the *DV* varies across rats, u_{1j}. Inclusion of this level 2 variation can provide a more accurate estimate of the standard error (Bell et al., 2019). Multi-level models were assessed using MLwiN (v3.05, Centre for Multilevel Modelling, University of Bristol, UK).

Models were statistically compared using the likelihood-ratio chi-squared test in Equation 3.8. This examines the difference in the 2*log-likelihood (-2LL) deviance statistic between the simple and complex model. The degrees of freedom for the chi-squared probability, $\chi 2$, is the difference in the number of parameters included in the model, which include the fixed, variance, and co-variance parameters. If the more complex model provided a significantly better fit of the data, findings were reported in comparison to the simplest model and a Wald chi-squared test was applied to statistically compare fixed parameter estimates of the *DV* across each level of the IV (i.e. harmaline vs control, or moving vs resting). If diagnostic checks revealed a non-normal distribution of the residuals in the model, a generalised linear model with an approximate Poisson distribution of the response data was applied and the final model was re-run (Green, 2020; Leyland et al., 2020). A Poisson distribution assumes a natural logarithmic relationship between the DV and IV and can provide a better estimation if the response variable is heavily skewed due to non-negative response values.

3.2.13 Network analysis

To examine changes in coherence across the recorded neural network, the area under the mean coherence curve at the tremor frequency (9-15Hz) was measured for each condition for both the recorded and surrogate data sets. For each condition, statistical analyses compared the area under the coherence curve for the recorded and surrogate data sets using one-tailed paired t-tests. Holm-Bonferroni adjusted p-values were applied to counteract the problem of multiple

comparisons. Analyses comparing the area under the coherence curve has been examined in previous research (Omlor et al., 2011) which aimed to compare the magnitude of coherence values within a specific frequency range, and this provided a straightforward approach to quantity and summarise the differences observed in the coherence spectra presented in the results sections below.

3.3 Results

3.3.1 Histology – identification of recording sites

Recording site locations of cerebellar tetrodes were identified by following florescence DiI electrode tracks from the surface of the cerebellar cortex and identifying electrolytic lesions. In four out of 16 rats, electrode tracks ended in both the medial cerebellar nuclei and as well as more dorsally in the cerebellar cortex, whereas in another five rats, electrode tracks were only seen to end in the medial cerebellar nuclei. In another five rats, electrode marks were only seen to end in the cerebellar cortex, and for the final two, electrode tracts were seen to end in white matter in between the cerebellar cortex and cerebellar nuclei. In total, approximate histological identification of tetrode tracks grouped 9 rats with tetrodes in the medial nucleus and 9 with tetrodes within the vermis of the cerebellar cortex, where four of these rats were allocated in both groups. For the four rats with tetrodes located in both the medial nucleus and cerebellar cortex, the tetrode cut to a shorter length prior to surgery was taken to be the tetrode located in the cerebellar cortex. Data recorded from the shorter tetrode were therefore included within cerebellar cortex group data, and data recorded from one of the longer tetrodes was included within the medial nucleus group data (see section 3.2.8). Figure 3-6 provides example sagittal cerebellar sections and a summary diagram indicating approximate tetrode positions.

In 5 of 15 rats, recording site location of thalamus tetrodes were identified by following florescence DiI electrode tracks from the surface of the cortex in 100 μm coronal sections of the brain. Example histological sections showing tetrode positioning within the thalamus are shown in Figure 3-7. In the other 10 rats, thalamus tetrode recording site location were identified by following florescence DiI electrode tracts in sagittal sections of the brain, alongside examining GAD67 and vGluT2 immunoreactivity. Corresponding with previous research (Nakamura et al., 2014), regions of intense GAD67 immuno-reactivity were identified within anterior-ventral regions of the thalamus, which align with regions of the VA and VM thalamic nuclei (Figure 3-7 B&C). Previous research identified that intense GAD67 immunoreactivity in ventral regions of the VA/VL complex and VM thalamic nuclei reflect inhibitory basal ganglia input, whereas intense vGluT2 immunoreactivity in dorsal regions of the VA/VL complex reflect excitatory cerebellar input

(Nakamura et al., 2014). However, vGluT2 immunoreactivity within the thalamus was not detected by visual inspection of the sections. Therefore, the location of tetrode marks just above the thalamic regions showing intense immunoreactivity to GAD67 were considered as being positioned within the cerebellar receiving zone of the VA/VL complex. Histological identification of thalamic tetrode tracks indicated that tetrodes were approximately positioned within the VA/VL complex of the motor thalamus in 10 out of 15 rats. For the other five rats, tetrodes were positioning either within the reticular, posterior, or laterodorsal-dorsomedial nuclei of the thalamus. Estimated tetrode positioning in the thalamus is shown in Figure 3-8.
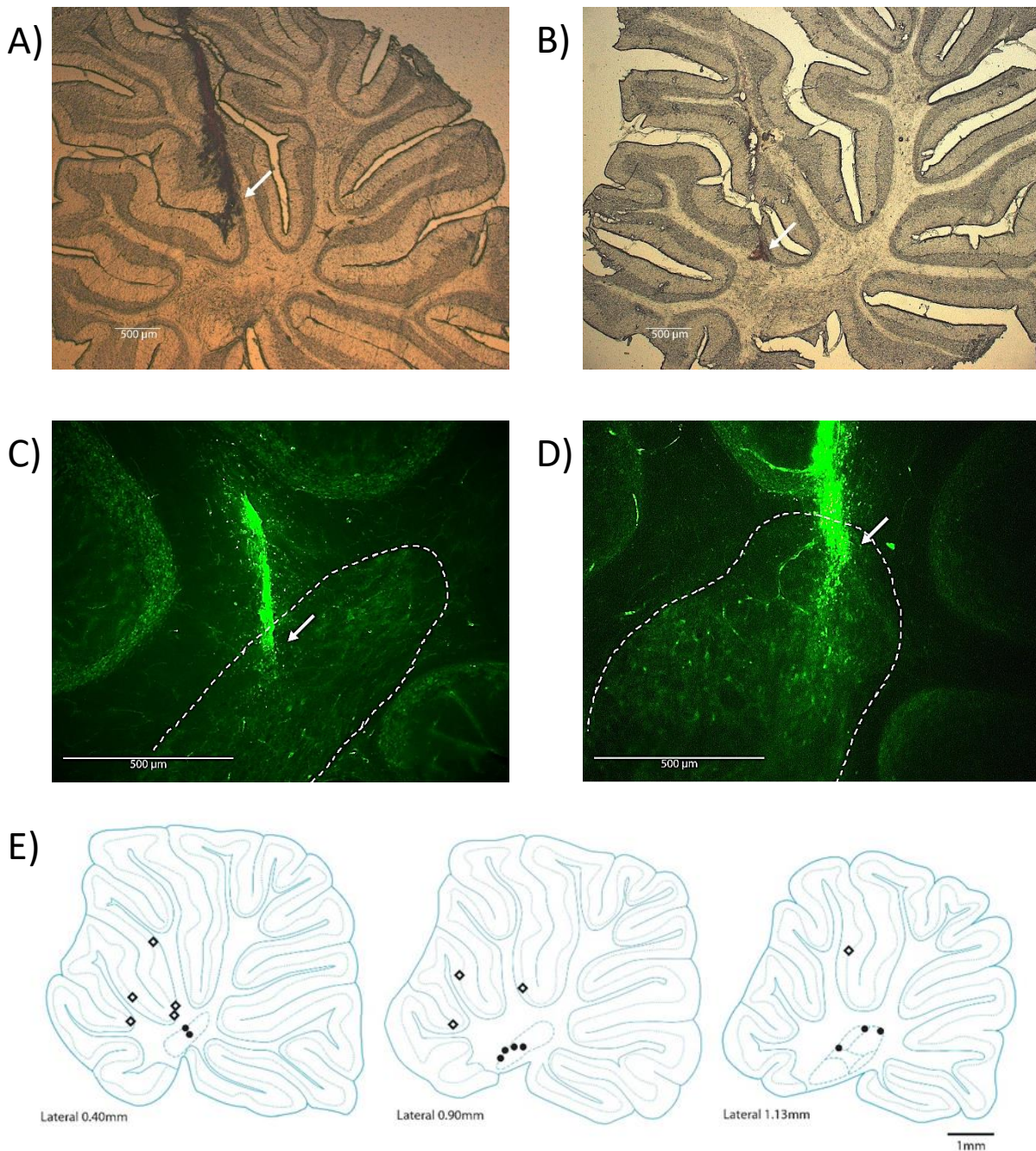
Figure 3-6. Histological confirmation of recording sites in the cerebellum.
Electrodes were painted with fluorescent DiI solution before insertion into the cerebellum and tracks were visualised with fluorescence microscopy. In some cases, electrode tracks could be clearly localised under light microscopy. White arrows show estimated final recording location. A&B) Examples of sagittal cerebellar sections with tetrode tracts in the cerebellar cortex from two different rats. C&D) Two examples of sagittal cerebellar sections with tetrode tracts in the medial cerebellar nuclei. The white dotted line approximately outlines the medial cerebellar nucleus. E) Summary diagram illustrating approximate electrode positions on sagittal sections of the cerebellum (adapted from Paxinos & Watson, 2005). Black dots represent approximate electrode positioning per rat in the medial cerebellar nuclei, and diamond symbols represent approximate electrode positions per rat in the cerebellar cortex.
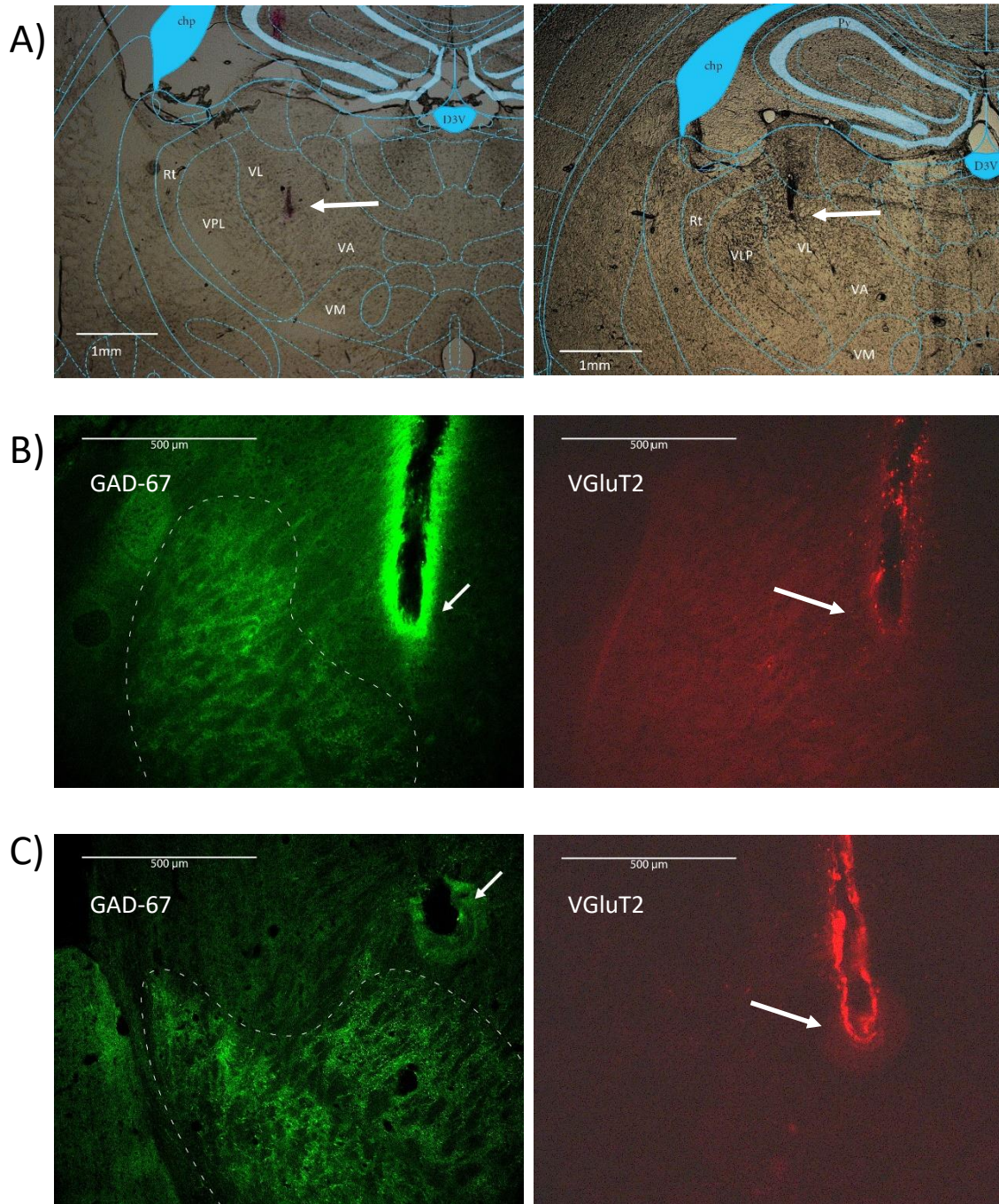
Figure 3-7. Histological confirmation of recording sites in the thalamus.
Electrodes were painted with fluorescent DiI solution before insertion into the cortex and tracks were visualised with fluorescence microscopy. White arrows show estimated final recording location. A) Examples of coronal sections with electrodes approximately located in the VA/VL complex of the thalamus from two different rats. B&C) Fluorescent images of sagittal sections showing GAD67 and VGluT2 immunoreactivity from another two rats (the left and right image are from the same rat). The white dotted line outlines regions of increased GAD-67 immunoreactivity in anterior-ventral regions of the motor thalamus (left). No VGluT2 immunoreactivity (right) was found.

Thalamic nuclei: VL = ventral lateral, VA = ventral anterior, VPL = ventral posterolateral, VM = ventromedial, Rt = reticular nucleus. D3V (blue) = dorsal part of the 3rd ventricle, chp = choroid plexus
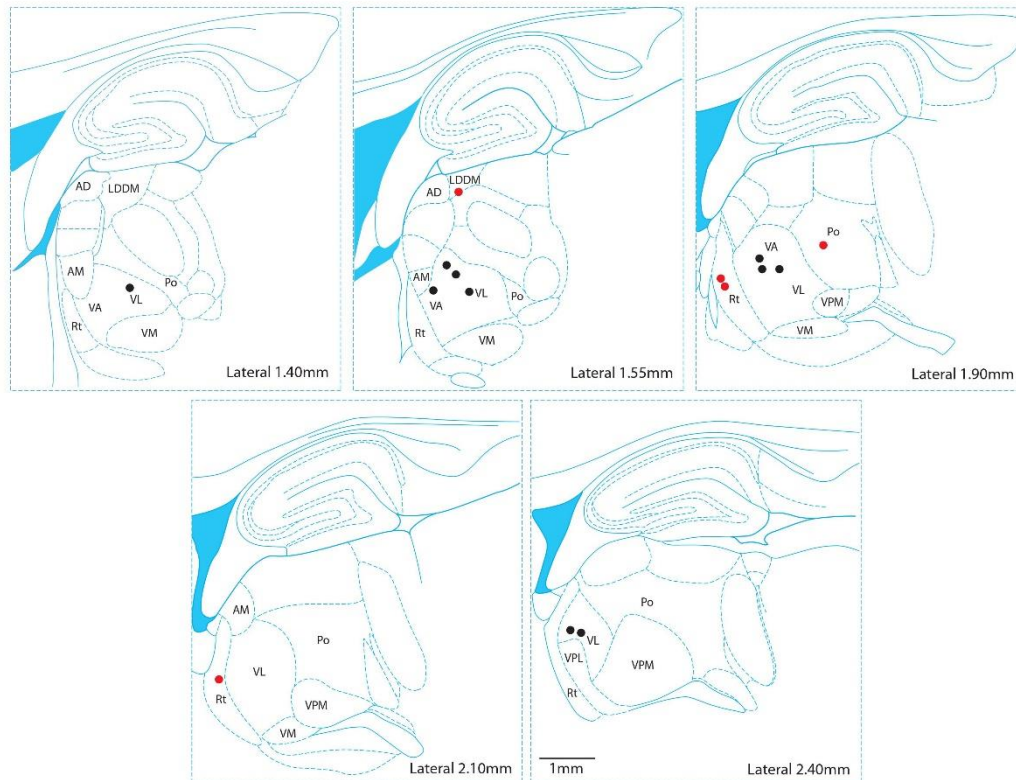
Figure 3-8. Diagram summarising the approximate positioning of electrode tracks in the thalamus.

The diagram illustrates sagittal sections of the thalamus, adapted from Paxinos & Watson (2005), where each black dot represents the approximate electrode positioning per rat in the VA/VL complex of the thalamus. Red dots represent off-target positioning of electrodes outside the VA/VL complex.

Thalamic nuclei: VL = ventral lateral, VA = ventral anterior, VPL = ventral posterolateral, VM = ventromedial, Rt = reticular nucleus, Po = Posterior nucleus, VPM = ventral postero-medial, AD = antero-dorsal, AM = antero-medial, LDDM = Latero-dorsal dorsomedial.

3.3.2 Harmaline induces a tremor at 9-15Hz

Tremor was measured using EMG and accelerometer recordings. An example of simultaneously recorded EMG and accelerometer activity during control (no harmaline) and harmaline conditions is presented in Figure 3-9 (A&B). Harmaline-induced tremor can be identified by the presence of regular short bursts of EMG, accompanied by an increase in oscillatory activity recorded by the accelerometer. To identify the frequency of harmaline-induced tremor, FFTs were applied to the limb EMG and head accelerometer data. The average amplitude spectra of EMG and accelerometer data recorded across rats during control and harmaline conditions are shown in Figure 3-9 (C&D). These figures demonstrate harmaline-induced tremor occurred at a frequency of 9-15Hz (shaded grey region; Figure 3-9 C&D) in both EMG and accelerometer recordings

72

compared to the control condition. This tremor frequency corresponds with previous reports of harmaline-induced tremor frequency in rats (8-12Hz; Pan et al., 2018).

To quantify the change in rhythmic limb muscle activity and head movement at the tremor frequency, the ratio of signal amplitude at the tremor frequency (9-15Hz) was extracted from each epoch during control and harmaline conditions for both the EMG and accelerometer. The ratio of tremor frequency signal amplitude in the EMG and accelerometer were modelled separately with harmaline included as a predictor variable. Analyses revealed that inclusion of harmaline in the model significantly improved model fit over the simple variance model when predicting the ratio of tremor frequency signal in the EMG (change in log-likelihood $\chi^2(3)$ = 7470.98, p<.001), as well as the accelerometer (change in log-likelihood $\chi^2(3)$ = 17847.21, p<.001). The violin plots displayed in Figure 3-9 (E&F) show the distribution of the ratio of tremor frequency amplitude in the EMG and accelerometer data recorded during harmaline and control conditions pooled across all epochs, where individual data points represent means per rat. A Wald test was applied to statistically compare the estimated fixed effects parameters for mean amplitude of rhythms at 9-15Hz during harmaline versus control conditions. As illustrated in Figure 3-9 (E&F), these analyses revealed significantly increased amplitude of rhythms at 9-15Hz during harmaline conditions (EMG: b = 0.36, SE = 0.01, Accelerometer: b = 0.53, SE = 0.03) vs control (EMG: b = 0.24, SE = 0.01, $\chi^2(1)$ = 4.385, p=0.036, n=7 rats, Accelerometer: b = 0.30, SE = 0.01, $\chi^2(1)$ = 75.633, p<0.001, n=12 rats) for both EMG (Figure 3-9 E) and accelerometer recordings (Figure 3-9 F). These figures also illustrate a greater difference in relative tremor amplitude for harmaline vs control when tremor was recorded via the accelerometer than EMG, where there is also less overlap in the distributions presented in Figure 3-9 F than Figure 3-9 E. This may indicate that the accelerometer provides a measure of tremor with greater SNR than the EMG, as the accelerometer was more sensitive in picking up a difference in tremor frequency amplitude. These figures may also suggest that tremor recorded via the EMG was intermittent at times, as a sizeable proportion of epochs did not show increased tremor rhythms during harmaline compared to control, indicated by the overlap in the EMG distributions (Figure 3-9 E). This may suggest that the accelerometer can provide a more reliable and sensitive measure of tremor than the EMG.
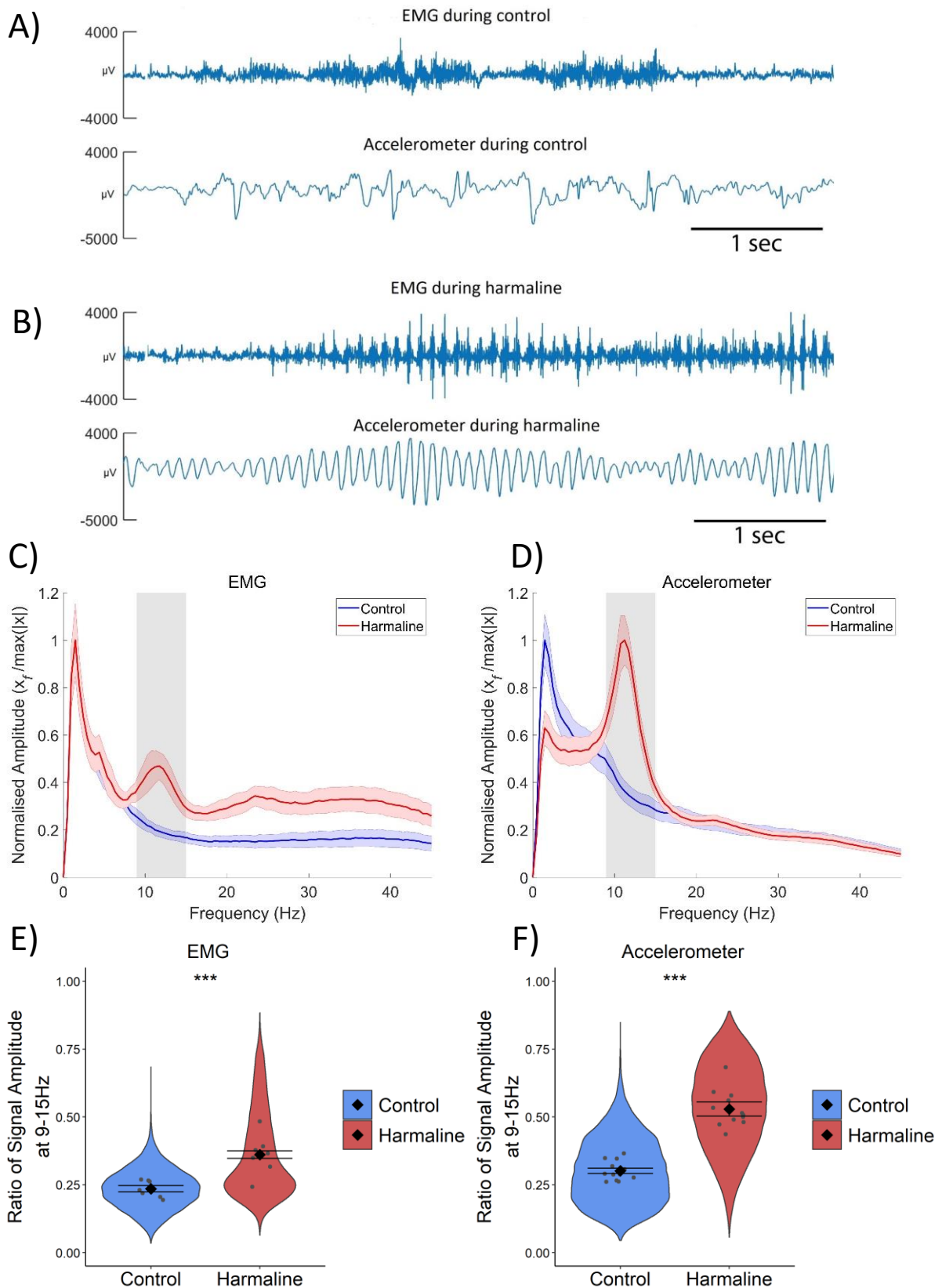
Figure 3-9. Harmaline induces a 9-15Hz tremor.
A&B Example EMG and accelerometer recording during A) control and B) harmaline. Upper trace is EMG, and lower trace is accelerometer. C&D Mean (± SE) amplitude spectrum for C) EMG (n=7) and D) accelerometer (n=12) during control and harmaline. The solid line represents mean amplitude, and the coloured shaded areas represent SE. The grey area represents the tremor frequency (9-15Hz). E&F Ratio of amplitude at the tremor peak for E) EMG and F) accelerometer, where the violin plots show the distribution of this ratio across all epochs (pooled across rats). Individual grey data points represent mean per rat. Fixed effects parameter estimates (± SE) representing predicted mean estimates are shown by ◆ and corresponding error bars. *** indicates p<.001.

3.3.3 Harmaline induces a change in neural rhythms in cerebellar circuits

To identify harmaline-induced changes in cerebellar rhythms, LFP recorded from the vermis of the cerebellar cortex and from the medial cerebellar nuclei were compared. The average amplitude spectra of LFP recorded from the cerebellar cortex and cerebellar nuclei across rats during control and harmaline conditions are shown in Figure 3-10 (A&B). These figures demonstrate a very clear and specific increase in rhythmic activity in the tremor frequency range (9-15Hz; shaded grey region in Figure 3-10 A&B) in both the cerebellar cortex and cerebellar nuclei during harmaline compared to the control condition. Harmonic oscillations were also present at twice the tremor frequency (~23Hz, arrows in Figure 3-10 A&B). Harmonic oscillations are frequencies that are a multiple of the fundamental frequency and can emerge when the fundamental frequency is a non-sinusoid waveform (Erickson et al., 2001).

To quantify the change in oscillatory activity in the cerebellum, the ratio of LFP amplitude at the tremor frequency range (9-15Hz) was modelled with harmaline as a predictor variable. Separate models were carried out for LFP recorded from the cerebellar nuclei and cerebellar cortex. Inclusion of harmaline in the model significantly improved model fit compared to the simple variance model when predicting the ratio of tremor frequency LFP amplitude in the cerebellar nuclei (change in log-likelihood $\chi^2(3) = 11198.41$, p<.001), and the cerebellar cortex (change in log-likelihood $\chi^2(3) = 14043.59$, p<.001). Wald analyses revealed a significant increase in relative tremor frequency LFP amplitude during harmaline (cerebellar cortex: $b = 0.35$, SE = 0.02, cerebellar nuclei: $b = 0.30$, SE = 0.03) vs control conditions (cerebellar cortex: $b = 0.22$, SE = 0.01, $\chi^2(1) = 32.14$, p<0.01, n= 9 rats, cerebellar nuclei: $b = 0.23$, SE = 0.01, $\chi^2(1) = 4.65$, p=0.031, n= 9 rats) for LFP recorded from both the cerebellar cortex (Figure 3-10 C) and cerebellar nuclei (Figure 3-10 D).

Figure 3-10 C illustrates that there was a greater (i.e. elongated) distribution in the relative amplitude of tremor frequency oscillations recorded from the cerebellar cortex during harmaline vs control. Furthermore, the mode relative amplitude during control (i.e. widest part of the distribution) was lower than the relative amplitude recorded across the majority of harmaline epochs, suggesting a consistent increase in tremor frequency rhythms. For the cerebellar nuclei (Figure 3-10 D), the distribution in the relative amplitude of tremor frequency oscillations was also greater, illustrated by the elongated violin plot during harmaline vs control. However, there was also greater overlap between the modal regions of the control and harmaline distributions (i.e. the widest part of the distributions) for the cerebellar nuclei compared to cerebellar cortex. This may suggest that increased tremor-frequency oscillations in the cerebellar nuclei during

harmaline vs. control was more intermittent. Inspection of Figure 3-10 D also indicates that one rat showed a much larger increase in harmaline-induced tremor frequency rhythms in the cerebellar nuclei. To examine the influence of this outlier on the statistics and underlying distribution, a second model was examined with this outlier removed. Figure 3-10 E illustrates that removal of this outlier did not change the increased upper tail of the data distribution, and Wald analyses still revealed a significant increase in tremor-frequency rhythms in the cerebellar nuclei during harmaline (b = 0.26, SE = 0.01) vs. control (b = 0.23, SE = 0.01, χ^2(1) = 8.32, p=0.004, n=8). These analyses therefore suggest that harmaline induces tremor frequency (9-15Hz) oscillations in the vermis of the cerebellar cortex and medial cerebellar nuclei, where this increase in tremor-frequency oscillations in the cerebellar nuclei may be more intermittent than the cerebellar cortex.
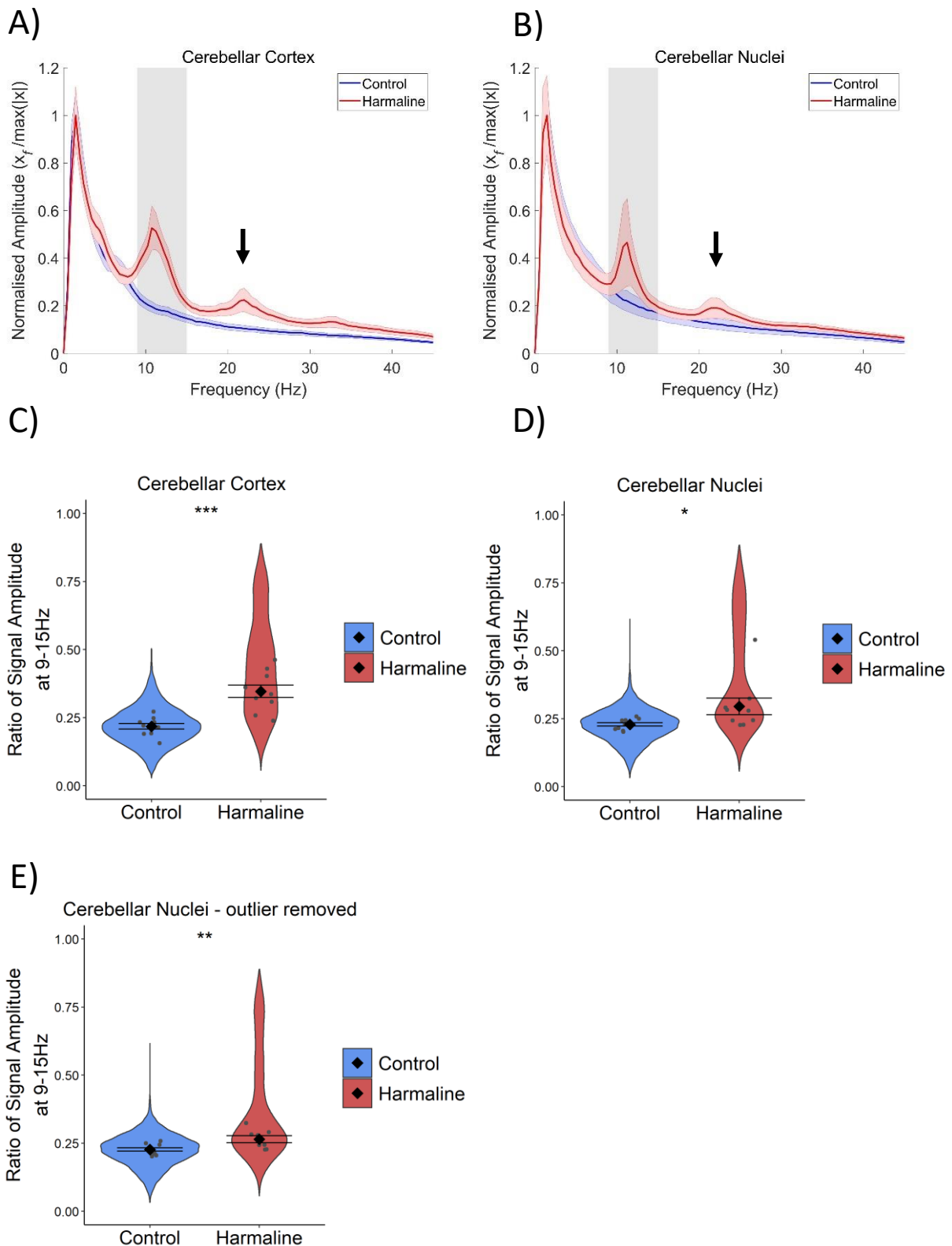
Figure 3-10. Harmaline increases oscillatory activity in the cerebellum at the tremor frequency.
A&B Mean (± SE) amplitude spectrum for A) Cerebellar cortex (n=9) and B) cerebellar nuclei (n=9) during control and harmaline. The solid line represents mean amplitude, and the coloured shaded areas represent SE. The grey area represents the tremor frequency. Arrows indicate peaks in coherence at roughly double the tremor frequency (~24Hz). C-E Ratio of amplitude at the tremor peak for C) Cerebellar cortex and D&E) cerebellar nuclei, where the violin plots show the distribution of this ratio across all epochs (pooled across rats). For E) n=8 as analyses were computed with an outlier removed. Individual grey points represent mean per rat. Fixed effects parameter estimates (± SE) representing predicted mean estimates are shown by ◆ and corresponding error bars. *** indicates p<.001, ** indicates p<.01, and * indicates p<.05.

3.3.4 Harmaline does not increase the amplitude of tremor rhythms in thalamocortical circuits

Electrophysiological studies in humans have shown that ~50% of neurons in the ventral thalamus (part of the motor region of the thalamus) exhibit rhythmic burst firing at the tremor frequency in response to postural-induced tremor in awake ET patients prior to thalamotomy (Hua & Lenz, 2005). A greater proportion of these neurons were also found in the ventral intermediate portion of the thalamus, which is the portion that receives direct inputs from the cerebellar nuclei (Hua & Lenz, 2005). Therefore, to examine whether there is a change in oscillatory activity in the thalamocortical circuits associated with harmaline tremor, the amplitude spectrum of LFP recorded from the motor region of the thalamus and subdural EEG recorded above the motor cortex were assessed. The average amplitude spectra of signals recorded from the thalamus and EEG during control and harmaline conditions across rats are shown in Figure 3-11 (A&B). Inspection of the amplitude spectra of both the thalamus and EEG indicates a peak in oscillatory activity at around 7Hz during control conditions (vertical blue dotted line in Figure 3-11 A&B). However, during harmaline conditions, this 7Hz peak disappears and is replaced by a less distinct oscillation at 5Hz (vertical red dotted line in Figure 3-11 A&B). No distinct peaks in oscillatory activity were detected at the tremor frequency range (9-15Hz, grey shaded region in Figure 3-11 A&B).

To statistically compare the change in oscillatory activity, the ratio of tremor frequency (9-15Hz) signal in the motor thalamus LFP and EEG was extracted and modelled. Inclusion of harmaline in the model significantly improved model fit compared to the simple variance model for the ratio of tremor frequency activity in the motor thalamus LFP (change in log-likelihood $\chi^2(3)$ = 1779.86, p<.001), and the ratio of tremor frequency EEG (change in log-likelihood $\chi^2(3)$ = 1191.53, p<.001). However, Wald analyses revealed that there was no significant difference in motor thalamus LFP amplitude at the tremor frequency for harmaline (b = 0.24, SE = 0.01) versus control (b = 0.23, SE = 0.01, $\chi^2(1)$ = 0.84, p=0.359). Conversely, there was a significant decrease in EEG amplitude during the harmaline tremor conditions (b = 0.25, SE = 0.01) compared to control (b = 0.26, SE = 0.01, $\chi^2(1)$ = 3.85, p=0.05). Inspection of the violin plots in Figure 3-11 (C&D), also show an increase in the upper-tail distribution of the relative tremor frequency amplitude for harmaline vs. control epochs. This indicates that some epochs recorded during harmaline tremor showed a sizable increase in relative signal amplitude at the tremor frequency compared to control.

In sum, these findings illustrate a change in the rhythmicity of thalamocortical activity during harmaline conditions vs control, where there is a shift in thalamocortical rhythms from 7Hz to 5Hz.

Furthermore, although there was no significant increase in thalamocortical activity at the tremor frequency associated with harmaline tremor, there is a shift in the upper-tailed distribution of relative amplitude at the tremor frequency during harmaline tremor, indicating a small proportion of epochs showed increased signal amplitude at the tremor frequency.
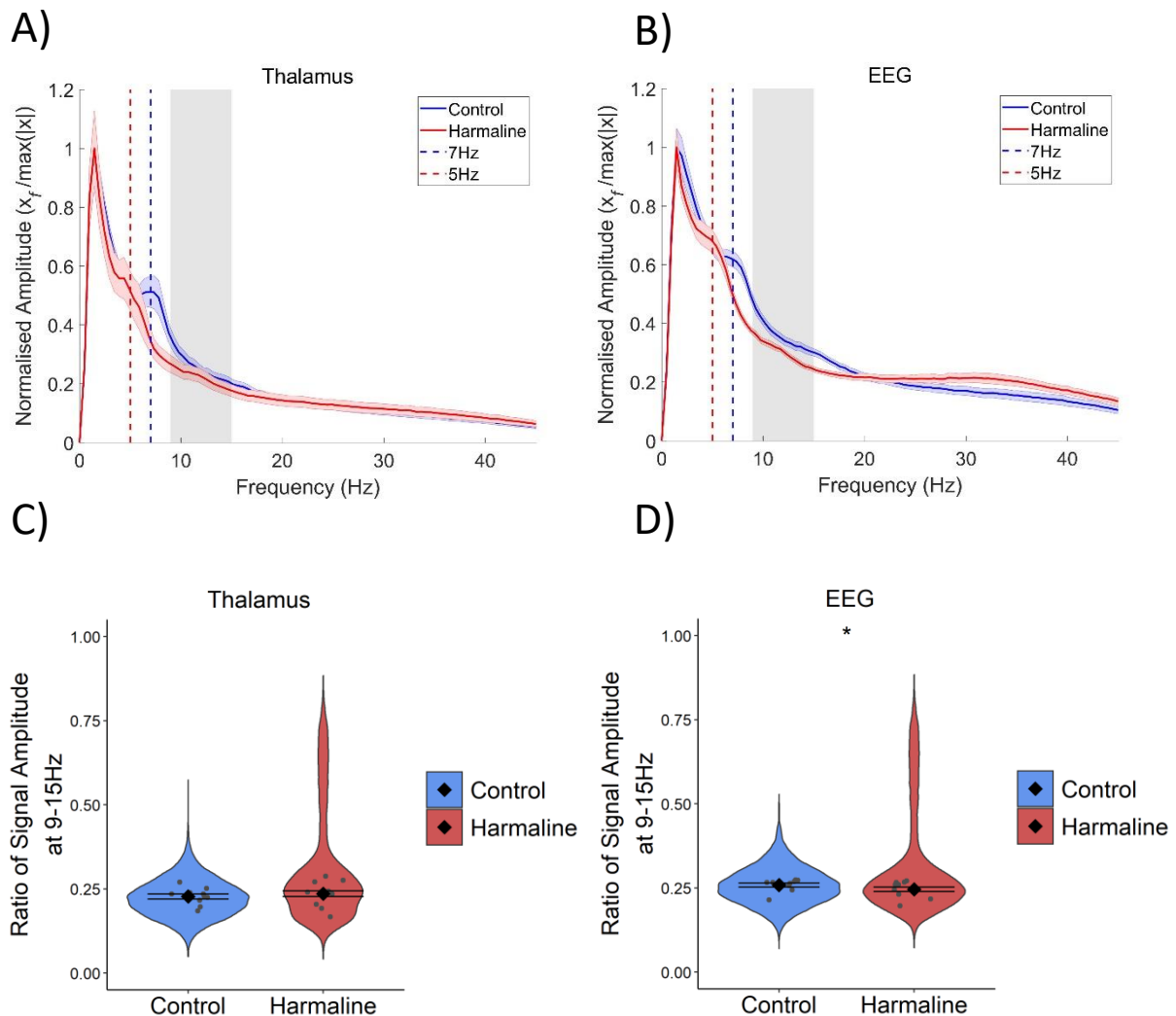
Figure 3-11. The amplitude of oscillations at the tremor frequency in the thalamocortical circuits. A&B Mean (± SE) amplitude spectrum for A) Motor thalamus (n=9) and B) EEG (n=9) during control and harmaline. The solid line represents mean amplitude, and the coloured shaded areas represent SE. The grey area represents the tremor frequency. C&D Ratio of amplitude at the tremor peak for C) Motor thalamus and D) EEG, where the violin plots show the distribution of this ratio across all epochs (pooled across rats). Individual grey points represent mean per rat. Fixed effects parameter estimates (± SE) representing predicted mean estimates are shown by ◆ and corresponding error bars. * indicates p<.05.

3.3.5 Harmaline tremor amplitude is modulated by movement

As harmaline tremor is reported to be an action tremor (Pan et al., 2018), the main aim of this research was to examine how activity and interactions within the tremor-related neural network are modulated by movement. To validate the harmaline model as a model of action tremor, the amplitude of tremor frequency activity in the EMG and accelerometer was compared for periods of resting vs. moving during harmaline tremor (Figure 3-12).

Changes in EMG and accelerometer activity were inspected by calculating total signal amplitude (Figure 3-12 A&B) and relative signal amplitude normalised to the maximum amplitude in the spectrum below 15Hz (Figure 3-12 C&D). For total amplitude, a distinct peak at the tremor frequency range (9-15Hz, grey banded section of each panel; Figure 3-12 A&B) was evident in both the EMG and accelerometer during resting and movement. Furthermore, signal amplitude was much greater during movement than resting across the spectrum (<45Hz; Figure 3-12 A&B). Total amplitude at the tremor frequency range was extracted for resting and movement (Figure 3-12 E&F), and multilevel models of EMG and accelerometer total amplitude at the tremor frequency range were examined. Inclusion of movement as a predictor provided a significantly improved fit compared to the simple variance model (EMG: change in log-likelihood $\chi^2(3)$ = 2874.30, p<.001, Accelerometer: change in log-likelihood $\chi^2(3)$ = 3155.76, p<.001). Wald analyses revealed that movement was significantly associated with increased tremor amplitude (EMG: b = 1.41, SE = 0.21, Accelerometer: b = 2.35, SE = 0.14) vs. rest (EMG: b =0.58, SE=0.05, $\chi^2(1)$ = 16.24, p<0.001, Accelerometer: b = 0.51, SE = 0.06, $\chi^2(1)$ = 166.42, p<0.001) for both the EMG and the accelerometer.

The ratio of signal amplitude at the tremor frequency was also modelled for EMG and accelerometer data (Figure 3-12 G&H). Inclusion of movement in the model significantly improved model fit (EMG: change in log-likelihood χ2(1) = 57.85, p<.001, Accelerometer: change in log-likelihood χ2(3) = 3155.76, p<.001). Wald analyses revealed that there was no difference in the ratio of EMG tremor frequency amplitude during movement (log b = -1.00, lower CI = -1.07, upper CI = -0.91, b = 0.37, lower CI = 0.36, upper CI =0.42) vs resting (log b = -1.05, lower CI = -1.20, upper CI = -0.91, b = 0.35, lower CI = 0.30, upper CI =0.40, $\chi^2(1)$ = 2.01, p=0.156, n=9). However, there was a significant increase in the ratio of accelerometer tremor frequency amplitude for resting (b = 0.57, SE = 0.02) vs movement (b = 0.46, SE = 0.02, $\chi^2(1)$ = 31.66, p<0.001, n=9). This discrepancy in findings when examining total versus the ratio of signal amplitude, is due to the broadband increase in the *total* amplitude of rhythmic movements. This is because when the rats are immobile, EMG and accelerometer activity is very minimal. Therefore, movement in general is

associated with a large broadband increase in signal activity. These findings illustrate that although movement was associated with significantly increased total amplitude of rhythmic movements and muscle contractions at the tremor frequency, this increase in amplitude was not specific to the tremor frequency range. These analyses therefore suggest that harmaline induced tremor is present when rats are resting (i.e. there is a tremor frequency specific peak in the amplitude spectrum during rest), but the total amplitude of rhythms also increases significantly with movement. This corresponds with visual inspection of tremor, where a low amplitude tremor was visible during resting, but the tremor became much more pronounced when the rat moved around the cage.
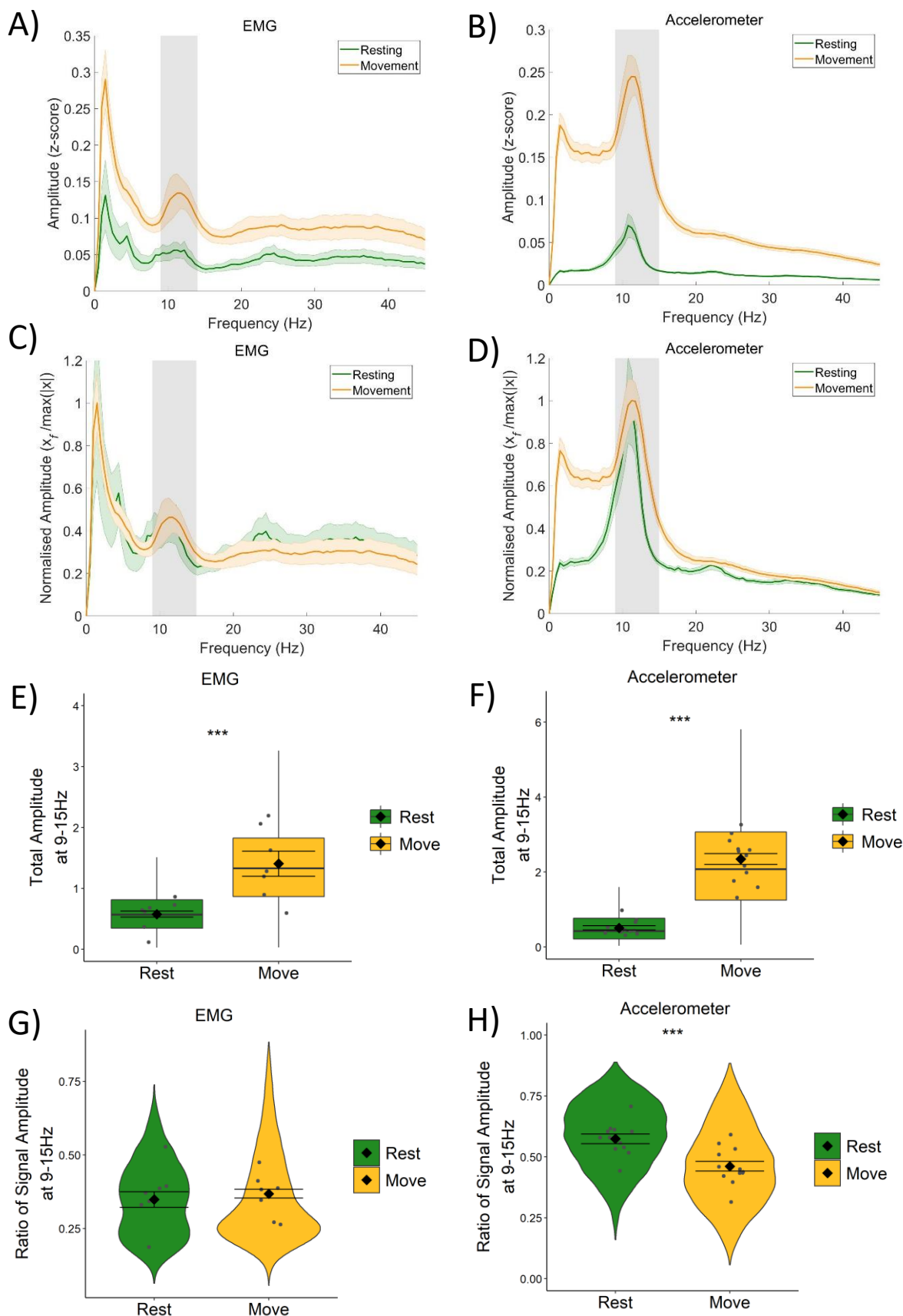
Figure 3-12. Total amplitude of harmaline-induced tremor increases with movement, but there is no relative increase in tremor frequency amplitude.

A&B) Total (± SE) and C&D) relative (± SE) amplitude spectrum for A&C) EMG (n=7) and B&D) accelerometer (n=12) during resting and movement. The solid line represents mean, and the coloured shaded areas represent SE. The grey area represents the tremor frequency. E&F) Total amplitude and G&H) ratio of amplitude at the tremor peak for E&G) EMG and F&H) accelerometer, across all epochs (pooled across rats). Individual grey points represent mean per rat. Fixed effects parameter estimates (± SE) representing predicted mean estimates are shown by ◆ and corresponding error bars. *** indicates p<.001.

3.3.6   Harmaline reduces speed of movements

In addition to harmaline producing a significant action tremor in rats, general ataxia was also qualitatively observed 5-15 minutes following the i.p. injection and lasted for up to 3 hours. This included a loss of co-ordination, an unsteady gait, also an increased spreading of the paws and foot slips during walking. There was also an absence of rearing and an increase in occurrences where the rat was lying down or leaning on the side of the cage. To examine the impact of these motor changes on spontaneous motor activity, the percentage of time rats were classified to be actively moving versus quietly resting were compared. A related-samples Wilcoxon signed rank test revealed no differences in the percentage of time spent actively moving around the cage during control conditions (median=61.96%) compared to the 2.5-hour period following harmaline administration (median=59.61, z=-0.408, p=0.683, r=-0.109, n=14 rats), suggesting harmaline had no effect on overall activity levels of the rats (Figure 3-13). However, a paired samples t-test revealed that rats' movements were significantly slower when they had been acutely treated with harmaline (mean=2.786m/s^2, SD=0.282) in comparison to control conditions (mean=3.867m/s^2, SD=0.383, t(13)=9.883, p<.001, n=14 rats; Figure 3-13). Therefore, even though there was no statistically significant difference found in overall activity levels of the rats, their movements were 27.95% slower.
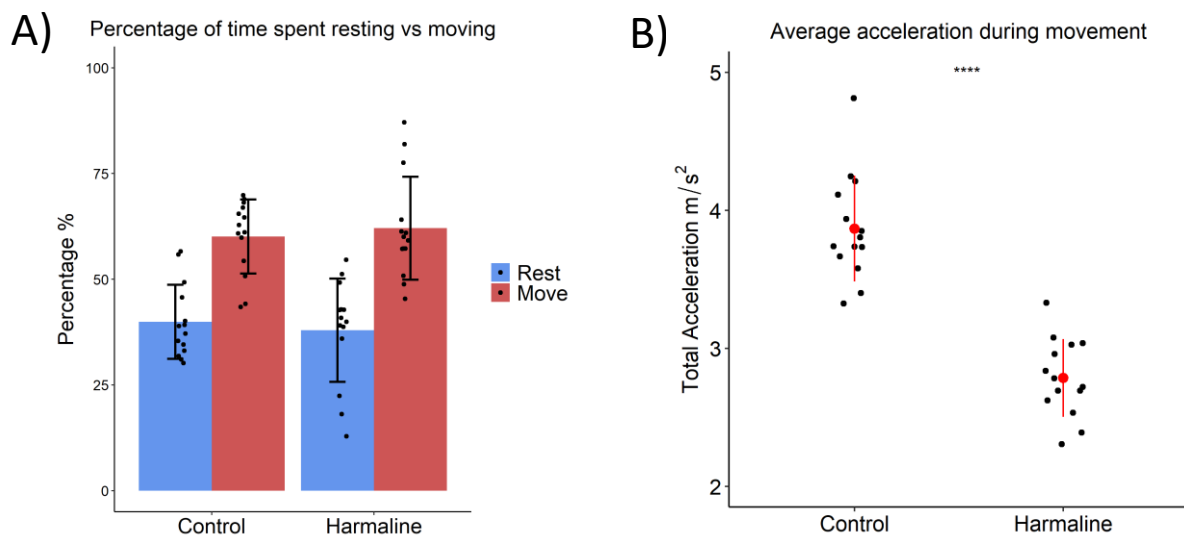
Figure 3-13. Harmaline reduces the speed of motor activity.
A) Percentage of time spent resting and moving during control and harmaline conditions. B) The average total acceleration of rats during movement for control and harmaline conditions. *** indicates p<.001.

3.3.7 Harmaline-induced neural oscillations in the cerebellum during movement and rest

Vermal cerebellar cortex and medial cerebellar nuclei LFP during rest versus movement after harmaline were also inspected by examining relative signal amplitude normalised to the maximum amplitude in the LFP spectrum. Figure 3-14 A&B illustrates a distinct peak in LFP amplitude at the tremor frequency (9-15Hz, grey banded area) in cerebellar cortex and cerebellar nuclei LFP. The ratio of LFP signal amplitude at the tremor frequency was modelled for the vermis of cerebellar cortex and medial cerebellar nucleus LFP during harmaline conditions (Figure 3-14 C&D). Inclusion of movement in the model significantly improved model fit (Cerebellar cortex: change in log-likelihood $\chi 2(3)$ = 1342.11, p<.0011, Cerebellar nuclei: change in log-likelihood $\chi 2(3)$ = 1645.06, p<.001). However, Wald analyses revealed no difference in the ratio of tremor frequency LFP amplitude for movement versus resting in the vermis of the cerebellar cortex (Resting: b = 0.36, SE = 0.3, Movement: b = 0.33, SE = 0.02, $\chi^2(1)$ = 0.35, p=0.553, n=9) or the medial cerebellar nucleus (Resting: b = 0.31, SE = 0.04, Movement: b = 0.28, SE = 0.02, $\chi^2(1)$ = 2.66, p=0.103, n=9). This suggests that although harmaline was shown to induce tremor frequency (9-15Hz) oscillations in the vermis of the cerebellar cortex and medial cerebellar nuclei compared to control conditions (see 3.3.3), the amplitude of harmaline-induced tremor frequency neural oscillations was not modulated by movement. This suggests these neural oscillations within the cerebellar cortex and medial cerebellar nuclei were equally as strong during rest and movement.
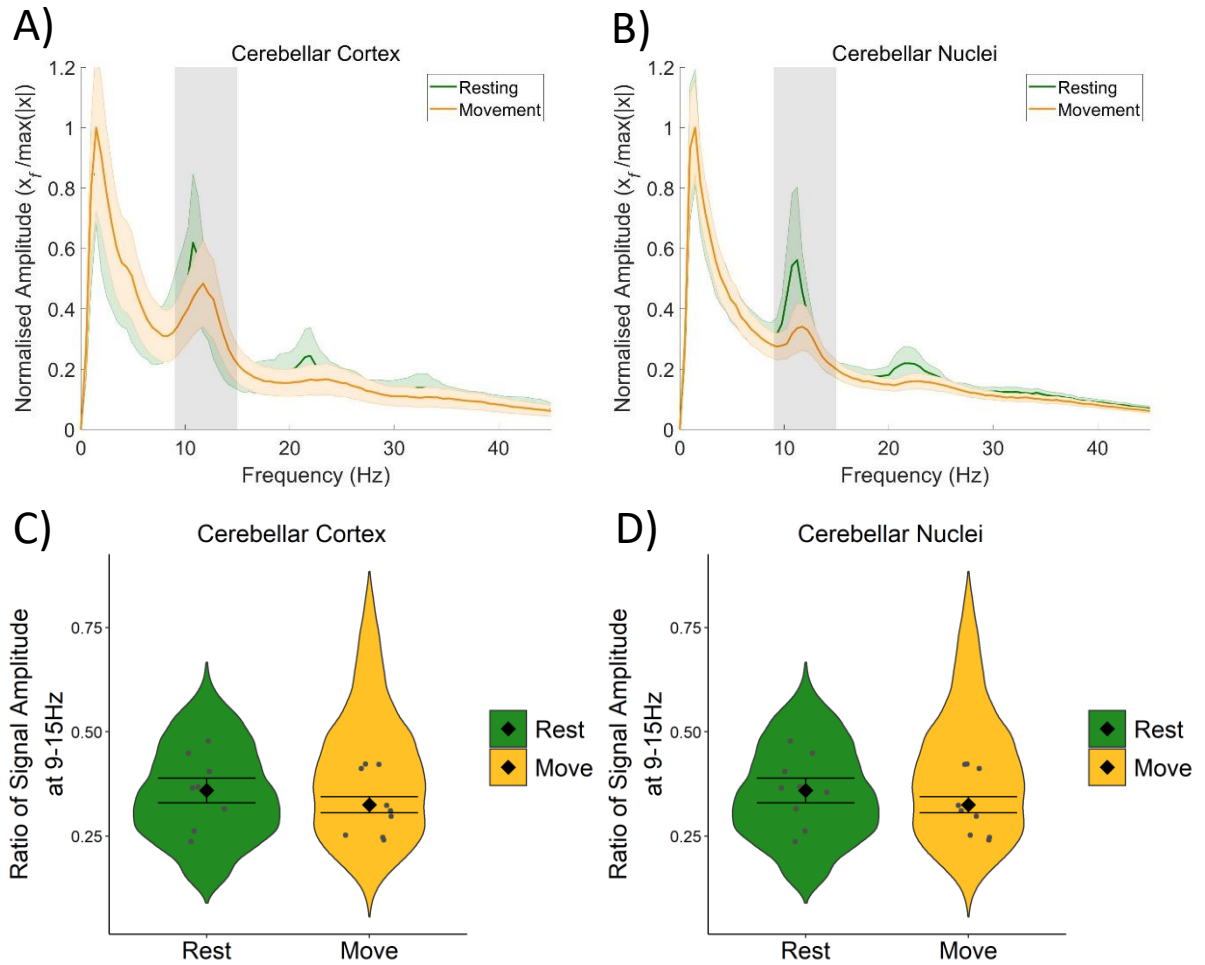
Figure 3-14. No significance differences in harmaline-induced oscillations in cerebellum for movement versus resting.
A&B) Relative (± SE) amplitude spectrum for A) Cerebellar cortex (n=9) and B) Medial Cerebellar nuclei (n=9) during resting and movement. The solid line represents mean, and the coloured shaded areas represent SE. The grey area represents the tremor frequency. C&D) Ratio of amplitude at the tremor peak for C) cerebellar cortex and D) cerebellar nucleus, across all epochs (pooled across rats). Individual grey points represent mean per rat. Fixed effects parameter estimates (± SE) representing predicted mean estimates are shown by ◆ and corresponding error bars.

3.3.8 Increased coherence between cerebellum and tremor during both resting and moving

To examine the degree to which oscillations in the cerebellum correlate with harmaline-induced behavioural tremor, coherence between cerebellar cortex and medial cerebellar nuclei LFP with accelerometer (kinematic) recordings of tremor were assessed during periods of resting and movement. Due to the greater SNR of tremor rhythms recorded from the accelerometer (see section 3.3.2 above), coherence analyses reported in the current and following results sections focus solely on coherent neural oscillations with the accelerometer rather than EMG. Accelerometer recordings were also available for a greater number of rats than artefact free EMG recordings.

As reported in the Methods section 3.2.10, surrogate analysis was applied to examine statistical significance of coherence. Spurious peaks in coherence can occur when low frequency components dominate the power spectrum, or when there are independent narrow-band oscillations in the spectral content of both signals (Faes et al., 2004; Lee et al., 2012). Surrogate analysis provides a threshold measure for determining the significance of coherence values using a parameter generated from random data sets with the same sampling distribution. Non spurious peaks in coherence are defined as coherence values greater than those obtained from randomly generated surrogate data sets with the same spectral content.

Average cerebellar-kinematic coherence spectra for real and surrogate data sets, across resting and movement epochs are presented in Figure 3-15. These figures demonstrate a dominant peak in coherence between the accelerometer and the cerebellar cortex LFP (Figure 3-15 A), and the accelerometer and cerebellar nuclear LFP (Figure 3-15 B) at the tremor frequency (9-15Hz, grey shaded area) during rest and movement. Furthermore, a peak in coherence at double the tremor frequency (~23Hz; indicated by the arrows Figure 3-15 A&B) is evident, which may be due to the non-sinosidal neural oscillation at the tremor rhythm (see 3.3.3). There was also a small shift in the frequency of peak coherence at 9-15Hz range during resting versus movement, where peak coherence was at ~11Hz during rest, and ~12Hz during movement.

Importantly, these figures demonstrate that average coherence values at the tremor frequency were greater for the real data sets compared to average values generated from surrogate data sets, indicating significant coherence at the tremor frequency (Figure 3-15 A&B). Surrogate analysis revealed that 76.58% of epochs showed significant cerebellar cortex-kinematic coherence at 9-15Hz in comparison to the surrogate dataset (n=8142 out of 10632 epochs, which included 76.22% of epochs classified as 'resting', and 77.02% of epochs classified as 'moving'), and 65.02%

of epochs showed significant cerebellar nuclear-kinematic coherence at 9-15Hz (n=6478 out of 9963, this included 64.73% of epochs classified as 'resting', and 65.02% of epochs classified as 'moving'). To quantify differences in the strength of cerebellar-kinematic coherence for resting vs. movement, surrogate-corrected mean coherence at the tremor frequency was extracted across epochs, and modelled with movement included as a predictor variable. The distribution of surrogate-corrected mean coherence across resting and movement are displayed in the violin plots in Figure 3-15 (C&D). Inclusion of movement in the model significantly improved model fit for cerebellar cortex-kinematic coherence (change in log-likelihood χ2(3) = 521.39, p<.001) and cerebellar nuclear-kinematic coherence at the tremor frequency (change in log-likelihood χ2(3) = 62.10, p<.001). However, Wald analyses revealed no difference in surrogate-corrected mean coherence at the tremor frequency across resting and movement, for either cerebellar cortex-kinematic coherence (Resting b = 0.20, SE = 0.03, Movement b = 0.22, SE = 0.04, χ^2(1) = 0.28, p=0.599, n=8) nor cerebellar-nuclei-kinematic coherence (Resting log b = -1.93, lower CI = -1.19, upper CI = -1.68, b = 0.14, lower CI = 0.11, upper CI = 0.19, Movement log b = -1.84, lower CI=-1.91, upper CI = -1.58, b = 0.16, lower CI = 0.15, upper CI = 0.21, χ^2(1) =0.16, p=0.684, n=7).

Together, the surrogate analysis revealed that tremor-frequency oscillations in the cerebellar cortex and cerebellar nuclei were significantly correlated with kinematic measures of tremor in harmaline-treated rats for the majority of epochs (76.22% for the cerebellar cortex, 65.02% for the cerebellar nuclei). Furthermore, epochs showing statistically significant coherence were equally distribtued across resting and movement epochs, and analyses revealed the strength of coherence was not modulated by movement.
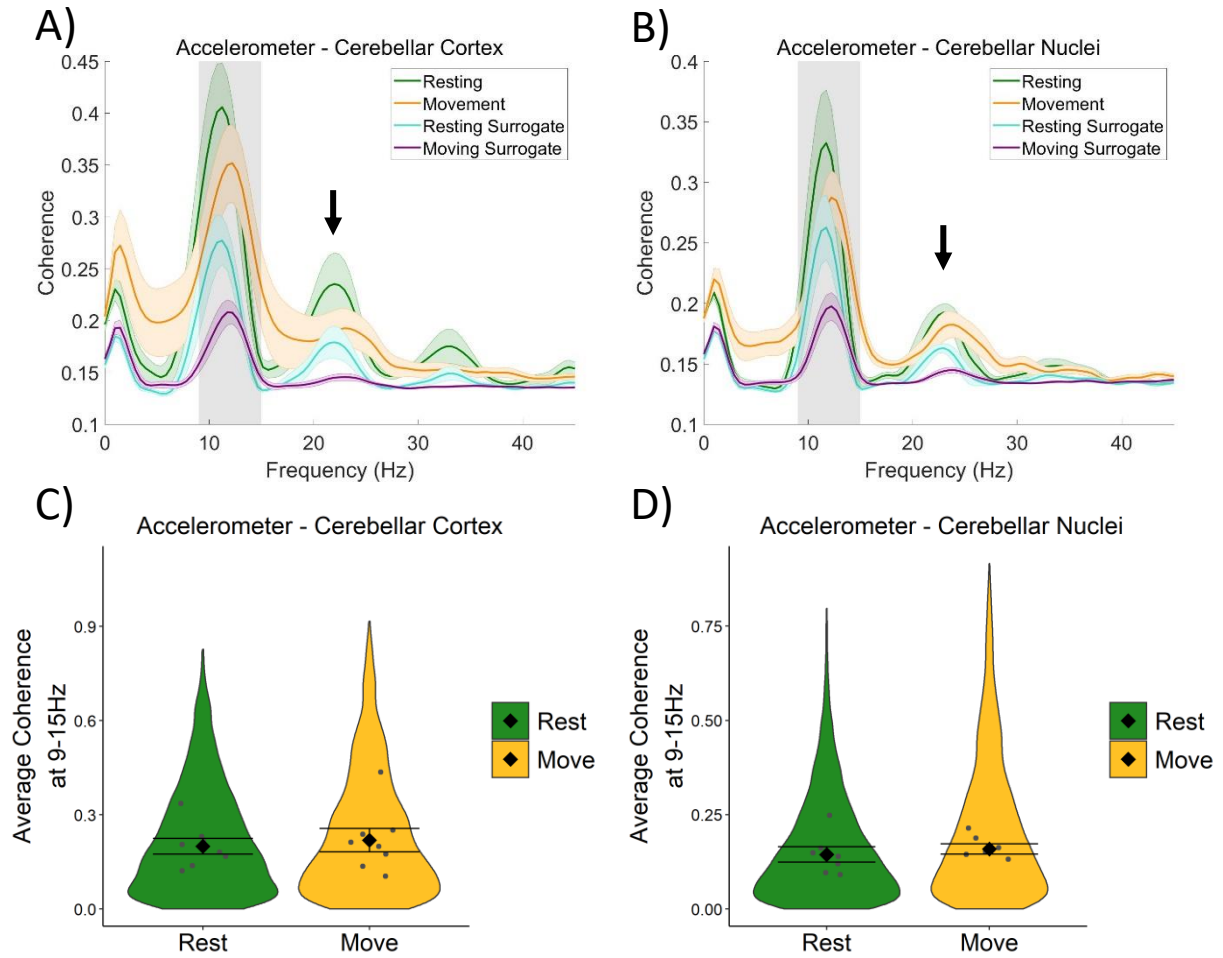
Figure 3-15. Cerebellar oscillations correlate with tremor activity during both resing and movement. A&B Mean (± SE) A) cerebellar cortex-kinematic (n=8) and B) cerebellar nuclei-kinematic (n=7) coherence during resting and movement for real and surrogate data sets. The solid line represents mean coherence, and the coloured shaded areas represent SE. The grey area represents the tremor frequency. Arrows indicate peaks in coherence at roughly double the tremor frequency (~24Hz). C&D Average surrogate-corrected C) cerebellar cortex-kinematic and D) cerebellar nuclei-kinematic coherence at the tremor peak across all epochs with significant coherence (pooled across rats). This analysis considers the difference in coherence between real and surrogate data sets. Individual grey points represent mean per rat. Fixed effects parameter estimates (± SE) representing predicted mean estimates are shown by ◆ and corresponding error bars.

3.3.9 Motor activity modulates thalamic involvement in tremor oscillations

The analyses reported in section 3.3.4 revealed that there was no significant increase in relative amplitude of thalamic or cortical oscillations at the tremor frequency associated with harmaline-induced tremor. However, there was a clear shift in the upper tail of the relative tremor frequency amplitude distribution for harmaline tremor compared to control, indicating a small proportion of epochs showed increased signal amplitude at the tremor frequency (see Figure 3-11). With ET patients, previous research has shown that ventral thalamic neurons fire at rates that correlate with behavioural tremor and that thalamo-muscular coherence is associated with the onset of postural or action-induced tremor (Hua & Lenz, 2005; Pedrosa et al., 2014). Therefore, the next step was to examine whether thalamo-kinematic coherence is modulated by movement. Furthermore, as the cerebellar nuclei send direct excitatory projections to the motor thalamus (Hintzen et al., 2018; Nakamura et al., 2014), cerebellar nuclei-thalamic coherence was also examined.

Average thalamo-kinematic and cerebellar nucleo-thalamo coherence spectra for real and surrogate data sets, across resting and movement epochs are presented in Figure 3-16 (A&B). These figures demonstrate a dominant peak in coherence between the accelerometer and the thalamus LFP (Figure 3-16A), and the cerebellar nuclear and thalamus LFP (Figure 3-16 B) at the tremor frequency (grey area, 9-15Hz) during rest and movement, with broader peaks in coherent activity at double the tremor frequency (~24Hz; indicated by the arrows in Figure 3-16). Again, there was also a small shift in frequency for peak coherence during resting versus movement, where peak coherence was at ~11Hz during resting, and ~12Hz during movement.

Figure 3-16 A indicates that average thalamo-kinematic coherence was greater for the real data sets compared to average values generated from surrogate data sets, whereby a much larger increase in coherence was evident for movement epochs compared to resting. Analysis revealed that 54.51% of epochs showed significant thalamo-kinematic coherence at 9-15Hz in comparison to the surrogate dataset (n=5597 out of 10267 epochs, 48.97% of 'resting' epochs, 61.79% of 'moving' epochs). Surrogate-corrected thalamo-kinematic coherence at the tremor frequency was modelled with movement included as a predictor variable. Inclusion of movement in the model significantly improved model fit (change in log-likelihood χ2(3) = 531.00, p<.001). Wald analyses revealed a significant increase in the strength of tremor frequency coherence for movement (log b = -1.93, lower CI = -2.25, upper CI = -1.29, b = 0.15, lower CI = 0.11, upper CI = 0.28) versus resting epochs (log b = -2.41, lower CI = -2.53, upper CI = -2.30, b = 0.09, lower CI = 0.08, upper CI = 0.10, $\chi^2(1)$ = 28.07, p<0.001, n=8), as displayed in Figure 3-16 C.

A similar pattern was shown when examining average coherence values at the tremor frequency for cerebellar nucleo-thalamic coherence. The average coherence spectra shown in Figure 3-16 B demonstrate a large difference in mean cerebellar nucleo-thalamic coherence between real and surrogate epochs for movement but not for rest. Analysis revealed that 47.32% of epochs showed significant cerebellar nucleo-thalamic coherence at 9-15Hz in comparison to the surrogate dataset (n=3635 out of 7681 epochs, 44.70% of 'resting' epochs, 49.19% of 'moving' epochs). To statistically compare the strength of cerebellar nucleo-thalamic coherence between periods of rest vs. movement, surrogate-corrected thalamo-kinematic coherence at tremor frequency was modelled with movement included as a predictor variable. Inclusion of movement in the model significantly improved model fit (change in log-likelihood $\chi2(3) = 212.68$, p<.001), whereby analyses revealed a significant increase in the strength of tremor frequency coherence for movement (log b = -2.31, lower CI = -2.36, upper CI = -1.74, b = 0.10, lower CI = 0.09, upper CI = 0.18) versus resting epochs (log b = -2.58, lower CI = -2.77, upper CI = -2.39, b = 0.08, lower CI = 0.06, upper CI =0.09, $\chi^2(1)$ = 5.79, p=0.016, n=6).

These findings therefore illustrate significant thalamo-kinematic coherence at tremor frequency for 54.51% of epochs. This is despite analyses presented in section 3.3.4 (Figure 3-11 D) showing no peak in oscillatory LFP activity at the tremor frequency during harmaline conditions compared to control. In addition, the strength of thalamo-kinematic coherence was significantly modulated by movement. Furthermore, the strength of cerebello-thalamic coupling was significantly modulated by movement, even though the strength of cerebello-kinematic coupling at the tremor frequency was not modulated by movement (see section 3.3.8). Together these findings suggest a role for thalamic involvement in harmaline-tremor rhythms during motor activity.
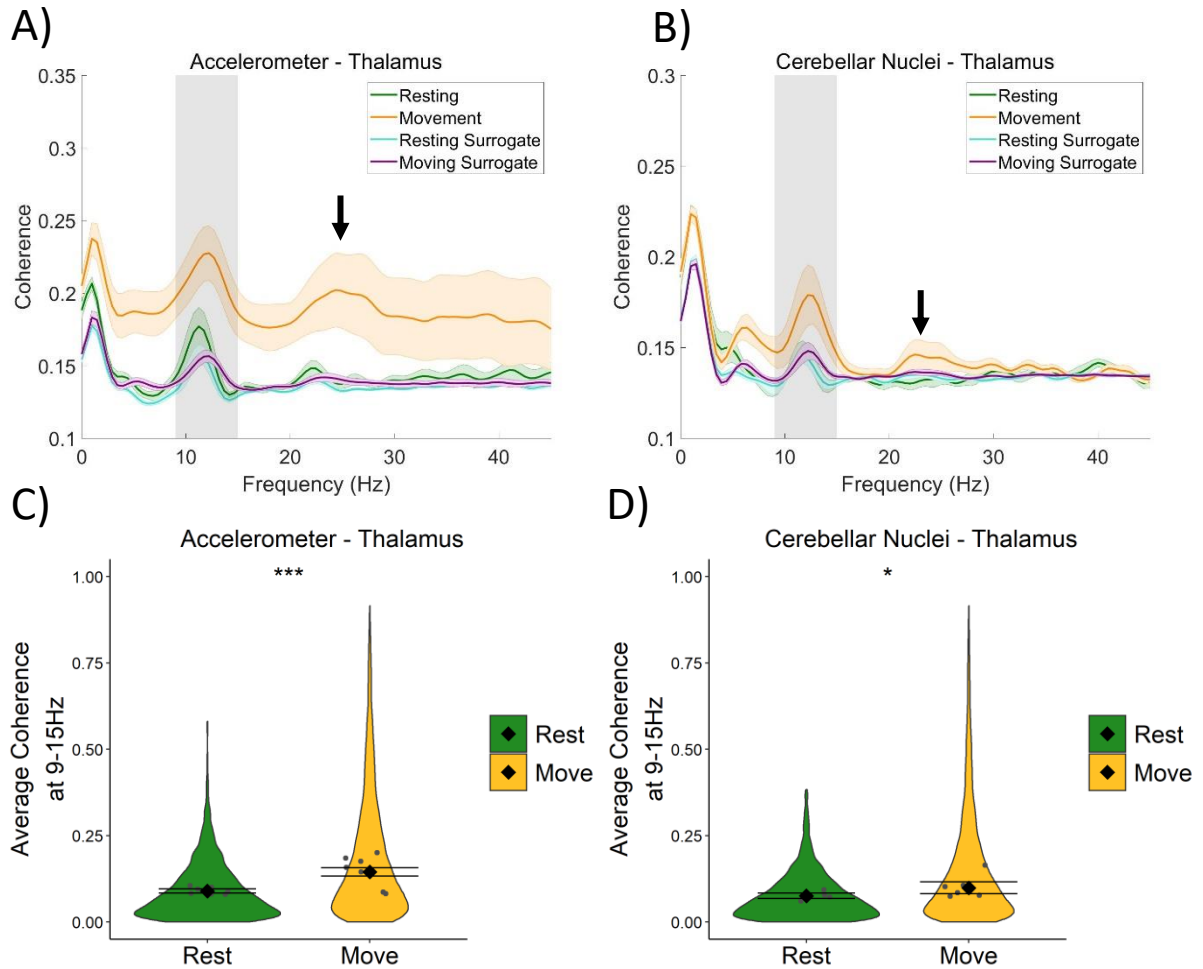
Figure 3-16 Increased thalamo-kinematic coherence for movement vs rest.
A&B Mean (± SE) A) thalamo-kinematic (n=8) and B) thalamo-cerebellar nuclear (n=6) coherence during resting and movement for real and surrogate data sets. The solid line represents mean coherence, and the coloured shaded areas represent SE. The grey area represents the tremor frequency. Arrows indicate peaks in coherence at roughly double the tremor frequency (~24Hz). C&D Average surrogate-corrected C) thalamo-kinematic and D) thalamo-cerebellar nuclear coherence at the tremor peak across all epochs with significant coherence (pooled across rats). This analysis considers the difference in coherence between real and surrogate data sets. Individual grey points represent mean per rat. Fixed effects parameter estimates (± SE) representing predicted mean estimates are shown by ◆ and corresponding error bars. *** indicates p<.001 and * indicates p<.05.

3.3.10 Thalamocortical coherence

To examine whether motor cortical EEG oscillations are correlated with harmaline-induced tremor, EEG-kinematic and thalamocortical coherence was examined during harmaline-induced tremor. Average EEG-kinematic and thalamocortical coherence (thalamus LFP-EEG) spectra for real and surrogate data sets, across resting and movement epochs are presented in Figure 3-17 (A&B).

The coherence spectra in Figure 3-17A show a peak in coherence at the tremor frequency in EEG-kinematic coherence during both rest and movement, where there is a small shift in the frequency for peak coherence during rest (~11.5Hz) versus movement (~12hz). There was also a much larger separation between real and surrogate coherence values for movement epochs (yellow versus purple lines; Figure 3-17 A) compared to resting epochs (green versus blue lines; Figure 3-17 A). Analysis revealed that 52.27% of epochs showed significant EEG-kinematic coherence at 9-15Hz in comparison to the surrogate dataset (n=6402 out of 12249 epochs, 50.82% of 'resting' epochs, 53.99% of 'moving' epochs). Surrogate-corrected EEG-kinematic coherence at the tremor frequency was modelled with movement included as a predictor variable. Inclusion of movement in the model significantly improved model fit (change in log-likelihood $\chi2(3) = 46.73$, p<.001). Analyses revealed no significant difference in EEG-kinematic coherence for movement (log b = -2.26, lower CI = -2.29, upper CI = -1.97, b = 0.10, lower CI = 0.10, upper CI = 0.14) vs. resting epochs (log b =-2.382, lower CI = -2.52, upper CI = -2.24, b = 0.09, lower CI = 0.08, upper CI = 0.11), $\chi^2(1)$ = 2.47, p=0.116, n=9; Figure 3-17 C).

When examining thalamocortical (i.e. thalamus LFP-EEG) coherence, a small peak in coherence was found at the tremor frequency range (9-15Hz; Figure 3-17 B), where mean coherence values for the real data set were greater than the average surrogate for both resting and movement epochs. However, a much larger peak in coherence is evident at 4.5-6Hz than the peak at the tremor frequency (9-15Hz). This 4.5-6Hz oscillation could be an intrinsic thalamocortical oscillation or reflect a sub-harmonic of the tremor frequency. Figure 3-18 (A&B) displays the average thalamocortical coherence spectra separately for resting and movement epochs during harmaline-tremor. Inspection of these graphs further highlight a shift in the frequency of peak coherence, where during rest, a peak in coherence is evident at 5Hz (green vertical dotted line), with a smaller peak at 11Hz (grey vertical dotted line). During movement, however, the initial peak is evident at 6Hz, with a smaller peak at 12Hz. Analysis revealed that 52.63% of epochs showed significant cortico-thalamic coherence at 9-15Hz in comparison to the surrogate dataset (n=5685 out of 10802 epochs, 52.10% of 'resting' epochs, 53.07% of 'moving' epochs). Surrogate-corrected

cortico-kinematic coherence at the tremor frequency was modelled with movement included as a predictor variable. Inclusion of movement significantly improved model fit (change in log-likelihood $\chi2(1)$ = 8.26, p=.004), however, analayses revealed that there was no significant difference in coherence at the tremor frequency for movement (log b = -2.36, lower CI = -2.62, upper CI =-2.26, b = 0.09, lower CI = 0.07, upper CI = 0.10) vs. resting (log b = -2.28, lower CI = -2.46, upper CI = -2.10, b = 0.10, lower CI =0.09, upper CI = 0.12, $\chi^2(1)$ = 0.21, p=0.646, n=8; Figure 3-17).

To examine whether the 4.5-6Hz oscillation is related to harmaline-induced tremor, or an intrinsic thalamocortical oscillation, average thalamocortical coherence during control (no harmaline) conditions for both movement and resting were also inspected (Figure 3-18 C&D). These figures illustrate a peak in coherence at 7.5-8Hz during the no harmaline control, where coherence at this frequency is greater during movement (green vertical dotted line; Figure 3-18 D) than resting (green vertical dotted line; Figure 3-18 C). This suggests the presence of an intrinsic thalamo-cortical oscillation at ~7-8Hz presence during control (no harmaline) conditions, which is modulated by motor activity. During harmaline tremor, the frequency of this oscillation shifts to ~5-6Hz (Figure 3-18 A&B; green vertical dotted line). These findings also correspond with a shift in neural oscillation frequencies identified within the motor thalamus LFP and EEG amplitude spectra in Section 3.3.4, where oscillations at ~7Hz in the thalamus and EEG during control (no harmaline) conditions are shifted to oscillations at around ~5Hz during harmaline tremor. This shift in the frequency of neural oscillations in the thalamus and motor cortex in response to harmaline could be due to entrainment of intrinsic ~7-8Hz rhythms to a sub-harmonic of the tremor frequency, as 5-6Hz is approximately half the tremor frequency.

In sum, these findings illustrate significant sensorimotor EEG-kinematic coherence and thalamocortical coherence at tremor frequency, but this was not significantly modulated by movement. Furthermore, evidence suggests harmaline can induce a change in the frequency of intrinsic thalamocortical rhythms, whereby a 7-8Hz rhythm is shifted to 5-6Hz rhythm.
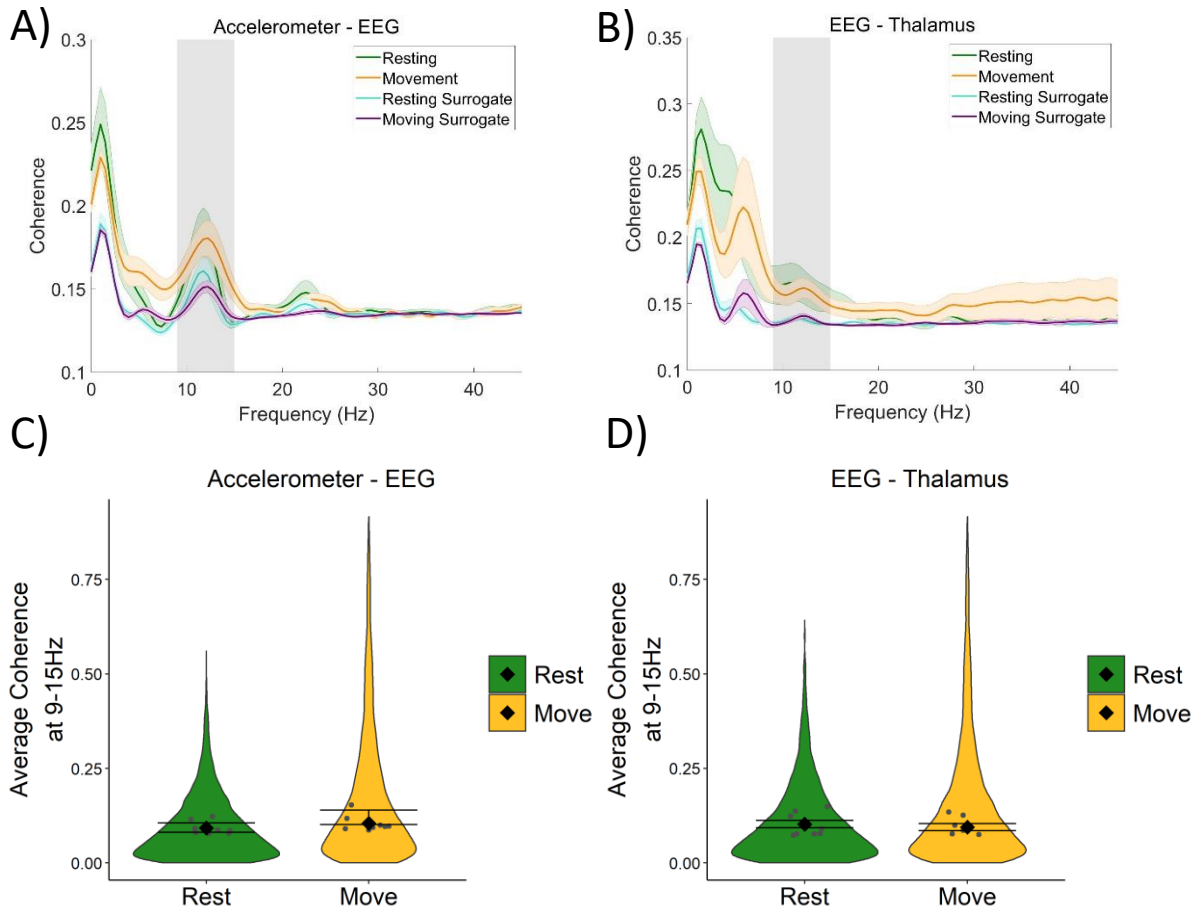
Figure 3-17. No changes in cortico-kinematic and thalamocortical tremor frequency coherence with movement.

A&B Mean (± SE) A) cortico-kinematic (n=9) and B) thalamocortical (n=8) coherence during resting and movement for real and surrogate data sets. The solid line represents mean coherence, and the coloured shaded areas represent SE. The grey area represents the tremor frequency. C&D Average surrogate-corrected C) cortico-kinematic and D) thalamocortical coherence at the tremor peak across all epochs with significant coherence (pooled across rats). This analysis considers the difference in coherence between real and surrogate data sets. Individual grey points represent mean per rat. Fixed effects parameter estimates (± SE) representing predicted mean estimates are shown by ◆ and corresponding error bars.
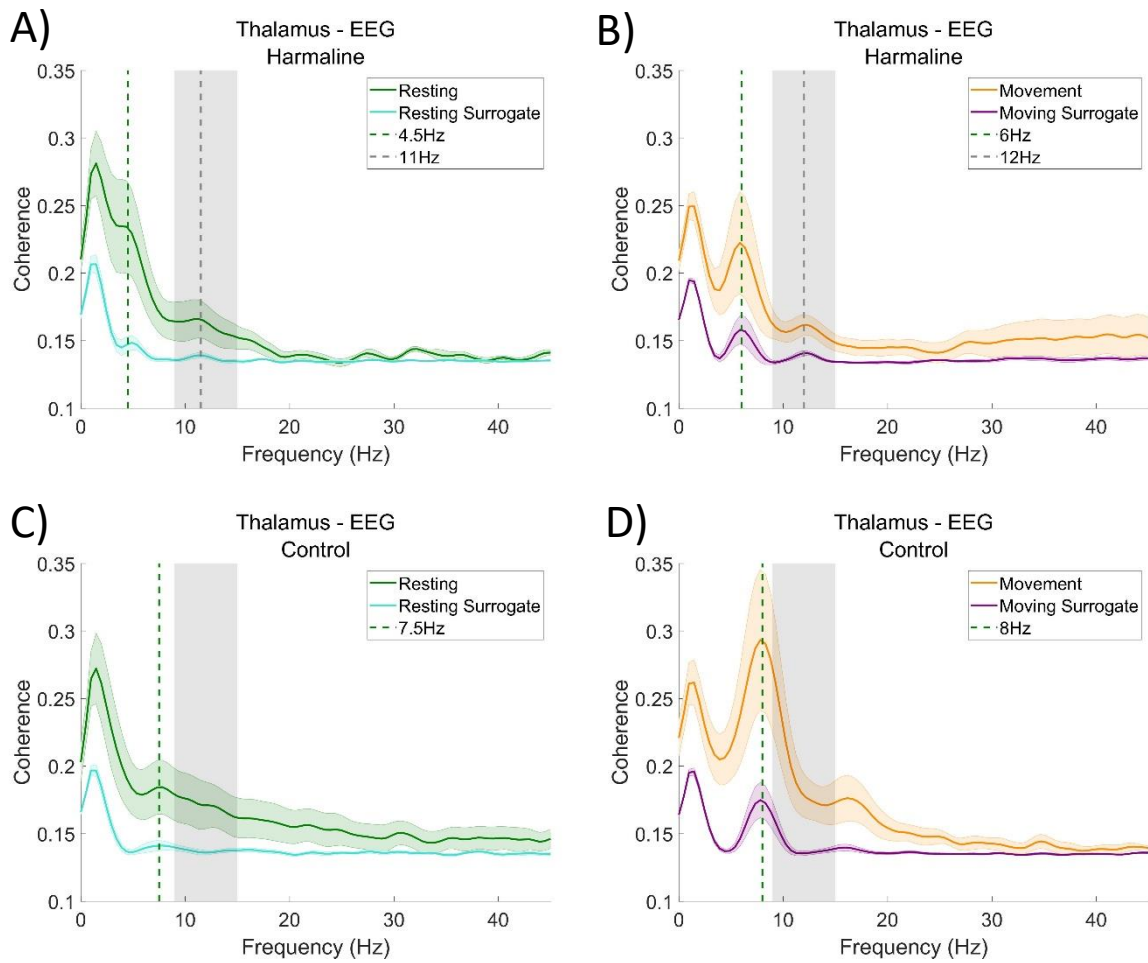
Figure 3-18. Oscillatory changes in thalamocortical coherence in response to harmaline and movement.
A-D Mean (± SE) thalamocortical coherence during A) harmaline conditions at rest, B) harmaline conditions during movement, C) control conditions at rest, and D) control conditions during movement. The solid line represents mean coherence, and the coloured shaded areas represent SE. The grey area represents the tremor frequency.

3.3.11 Changes in coherence at a network level

To examine and summarise differences in the mean magnitude of coherence at the tremor frequency at a network level, statistical analyses were applied to compare the mean area under the coherence curve at 9-15Hz for real and surrogate data sets. One-tailed paired t-tests were employed, to test the assumption that mean area under the coherence curve for the recorded data was greater than the mean area under the coherence curve for surrogate counterparts, using Holm-Bonferroni adjusted p-values to account for multiple comparisons within each condition. The results of these analyses are summarised in Table 3-1 and graphically in Figure 3-19. In Figure 3-19, the red lines indicate statistical significance in increased coherence at 9-15Hz for the recorded data (black lines indicate no statistical significance), and the thickness of red line represents the t-statistic, where the thicker the line the higher the t-statistic. The size of t-statistic reflects the difference in coherence values between the recorded data and data obtained from randomly generated surrogate data sets with the same spectral content (i.e. the null hypothesis). As reported in section 3.3.8, this comparison of coherence to values obtained from surrogate data sets corrects for spurious (not genuine) coherence values.

Figure 3-19 illustrates that during control (i.e. no harmaline) conditions, there was no statistically significant coherence in the motor network at the tremor frequency range when the rats were quietly resting. However, motor activity under control conditions (without tremor) was associated with significant 9-15Hz coherence between the kinematic measure and (1) the sensorimotor cortex (2) the cerebellar nuclei and (3) the thalamus, as well as thalamocortical coherence at 9-15Hz. Coherence at this frequency range in the absence of tremor suggests the presence of an intrinsic movement-related neural oscillation in the motor network that occurs within a similar frequency range as harmaline-induced tremor. This corresponds with data presented in section 3.3.11 (Figure 3-18 D), which identified a thalamocortical oscillation occurring within the theta frequency range (~8Hz) during movement for control (non-tremor) conditions.

Following administration of harmaline, statistically significant coherence at the tremor frequency (9-15Hz) was evident at rest between all brain regions and the kinematic measure of tremor. But no statistically significant tremor-related activity was present within the cerebello-thalamocortical pathway. By comparison, during motor activity statistically significant tremor-related coherence was found across the entire network. In sum, Figure 3-19 illustrates that both motor activity and harmaline-induced tremor are associated with increased coherence at 9-15Hz, but coherence across the cerebello-thalamocortical pathway is dependent on the presence of tremor during active movement.

Table 3-1. Surrogate analysis of coherence at tremor frequency (9-15Hz).

Paired one-tailed t-tests were applied to statistically examine whether the area under the mean coherence curve at the tremor frequency was greater than the area under the mean coherence curve at the tremor frequency from surrogate data sets. N = number of rats included in analysis.

	Control				Harmaline				
Paired Connection	During resting		During movement		During resting		During movement		
	t	p	t	P	t	p	t	p	N
Cb - Acc	2.73	0.015	2.28	0.028	5.45	<0.001*	3.86	0.003*	8
CN- Acc	1.29	0.122	3.29	0.008*	3.38	0.007*	7.80	<0.001*	7
Thal - Acc	-1.23	0.871	3.50	0.005*	2.71	0.015*	4.41	0.002*	8
EEG - Acc	0.83	0.215	7.01	<0.001*	3.37	0.005*	4.18	0.002*	9
CN – Thal	1.23	0.136	1.84	0.062	0.53	0.308	2.31	0.034*	6
Thal - EEG	2.20	0.032	3.29	0.012*	3.38	0.034	3.18	<0.001*	8
Acc = Accelerometer, Cb = Cerebellar cortex, CN = Medial Cerebellar nuclei, Thal = Thalamus.									
* significant following Holm-Bonferroni-adjusted p-values to control for family wise error rate.									
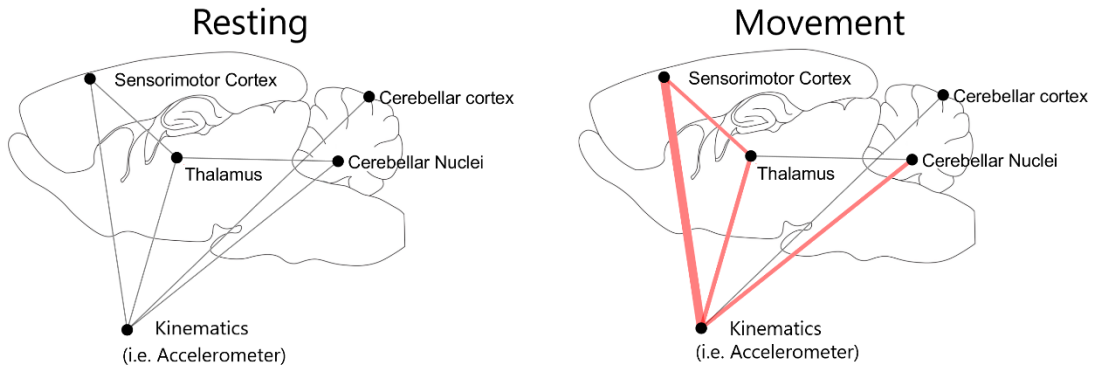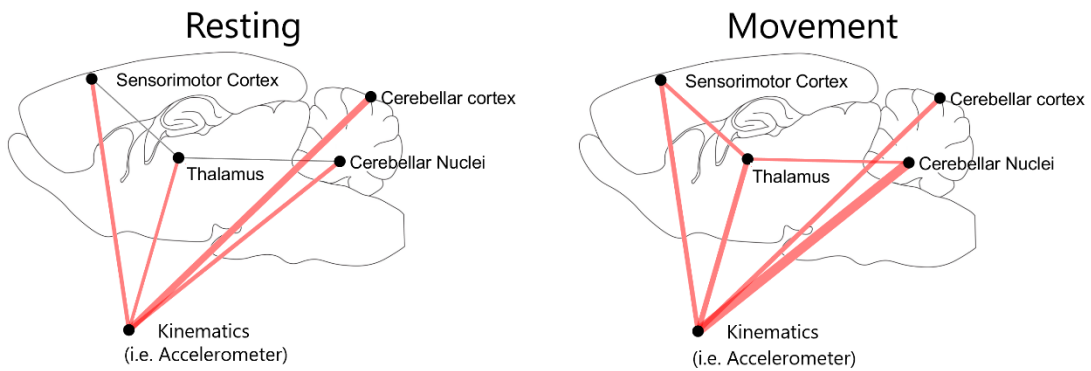
Figure 3-19. Surrogate analysis of coherence at the tremor frequency (9-15Hz) during control (rest and move) and harmaline (rest and move).

Red lines indicate significantly greater coherence at 9-15Hz for the recorded neural data compared to the mean from 99 surrogate data sets generated using IAAFT with Holm-Bonferroni adjusted significance levels for multiple comparisons. The width of the red line corresponds with the size of the t-statistic of the one-tailed paired t-tests comparing surrogate and original data sets.

3.3.12 Preliminary data on time-delays of tremor oscillations across the tremor network

The analyses presented 3.3.11 suggest there is a phase-dependant relationship of tremor frequency oscillations across the motor network during active movement, as mean coherence was significantly greater than surrogate data sets which had the same amplitude and power distribution as the original data, but shuffled (i.e. random) phase-relationships. This suggests a consistent time delay *within* epochs between tremor oscillations recorded across two brain sites or brain site and kinematics at the tremor frequency. To further examine the consistency of time-delays *across* epochs within the tremor network, histograms of the time-delays of tremor oscillations recorded across each connection within the network were assessed (e.g. LFP-LFP activity between different brain sites and EMG-LFP activity). This analysis included only epochs recorded during harmaline tremor when rats were moving (i.e. when there was maximal coherence across the network). Data was band-pass filtered at the tremor frequency range (9-15Hz), and time-delays were identified using cross-correlations, which examine the similarity between two signals at shifted time-lags, where one signal is shifted across the time axis (x-axis) relative to the other signal (see Figure 3-20). Using this method, the time-lag with absolute max cross-correlation for each epoch was identified out of 100 shifted iterations (± 100ms time-lags at 2ms bins). Normalised probability histograms were created showing time-lags with max cross-correlation. Figure 3-21 displays example normalised probability histograms of time-lags for different network connections in four different rats. Importantly, these histograms show clear peaks in probability of max correlation at certain time-lags, illustrating the presence of stable time-lagged relationships (i.e. max correlation was typically found at roughly the same time-lag).

Time-delays can also provide information of the directionality of oscillations across different regions of the network. For example, max correlation within the ±100ms window may be found when shifting one signal either forwards or backwards relative to the other signal, giving a positive or negative time-delay, respectively. For each rat, network connections were first examined to see if the peak probability of max correlation surpassed a threshold probability value (see Methods section 3.2.11). Mean (±SD) time-delays of connections surpassing this threshold were then examined across rats, where means for positive and negative time-delays were considered separately (Table 3-2

Table 3-2). When examining mean time-delays, the recording channels with greatest peak probability of max correlation was selected per rat (e.g. the tetrode-pair, such as one tetrode in the cerebellum and one tetrode in the thalamus, that showed greatest peak probability was

selected), and tetrodes within the vermal cerebellar cortex and medial cerebellar nuclei were grouped as a single brain site, due to the very small distance between these brain structures (100-1000μm).

In seven out of nine rats, estimated time-lags of simultaneous cerebellar LFP-EMG recordings suggest tremor oscillations travelled in an efferent direction from the cerebellum to the muscle (i.e. positive time-lags suggest forward connection; Table 3-2). Five out of seven rats showed positive time-lags between tremor oscillations simultaneously recorded across the cerebellum and thalamus LFP, and five out of seven rats also showed positive time-lags between tremor oscillations recorded across the thalamus LFP and EEG. This may suggest that the direction of tremor oscillations largely followed the direction of the cerebellar-thalamocortical pathway. However, estimated time-lags of oscillations simultaneously recorded across the thalamus LFP-EMG and EEG-EMG, suggest a more a complex combination of efferent and afferent inputs of tremor oscillations, as around of 50% of these connections showed a positive time-delay, and 50% showed a negative time-delay.

Importantly, the mean time-delays identified by this analysis also suggest that coherence recorded across the tremor network was not an artefact of volume conduction. Volume conduction can occur due to the instantaneous propagation of an oscillation from the source generating that oscillation to the recording electrodes (Brunner et al., 2016; Elsegai et al., 2015). The presence of volume conduction can therefore be inferred if max cross-correlation is found at a zero time-lag (i.e. peak probability of max correlation at zero). However, none of the connections included within the summary statistics showed peak probability of max cross-correlation at a zero time-lag (Table 3-2).
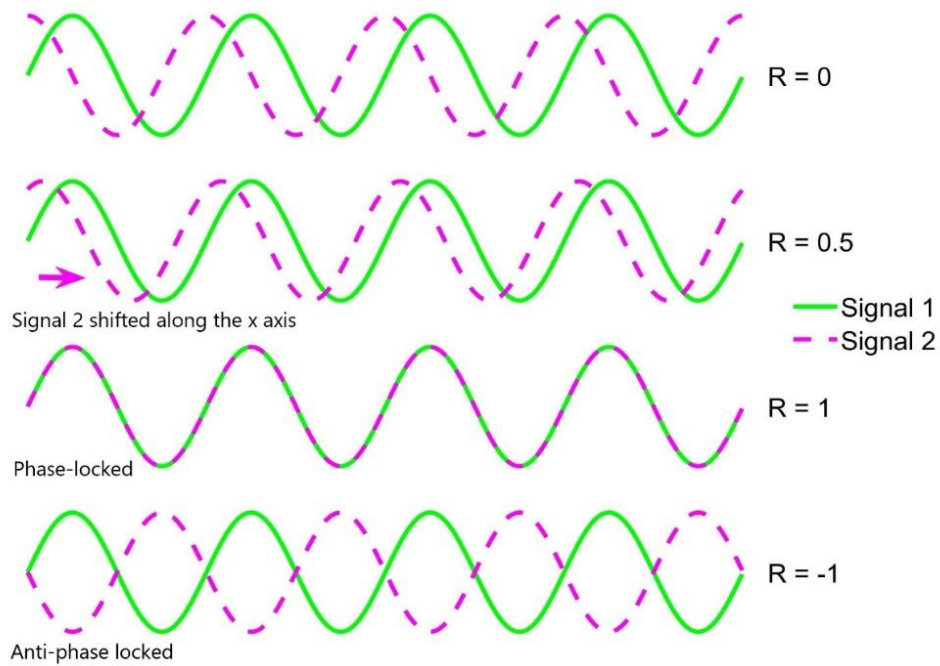
Figure 3-20. Cross-correlation at different time lags.
The diagram illustrates two perfect sine wave signals at the same frequency: signal 1 (in green) and signal 2 (in purple). Shifting one signal (e.g. signal 2) relative to the other (e.g. signal 1) influences the correlation coefficient (R), which varies between -1 (negative correlation) and 1 (positive correlation). Perfect positive correlation is found when the signals are perfectly phase-locked, (i.e. perfect alignment of the two sine waves). Perfect negative correlation between these two signals is found when signals are perfectly locked in an anti-phase direction (i.e. the peaks of signal 1 aligning with troughs of signal 2, and vice versa).

Table 3-2. Mean time delays of tremor frequency oscillations across tremor-network connections.
N corresponds to the number of rats included in the summary statistics. Positive time-delays correspond to forward connection and negative lags correspond to a backward connection.

Connections	Time-delays in a forward connection (mean in ms ± SD)	N	Time-delays in a backward connection (mean in ms ± SD)	N
Cerebellar LFP-EMG	7.0 ± 6.1	7	9.0 ± 5.7	2
Cerebellar LFP-Thalamus LFP	13.8 ± 20.5	5	18.0 ± 15.6	2
Thalamus LFP-EEG	8.2 ± 5.8	5	5.0 ± 2.8	2
Thalamus LFP-EMG	11.7 ± 12.2	3	4.0 ± 1.4	2
EEG-EMG	6.0 ± 1.4	2	4.0 ±1.4	2
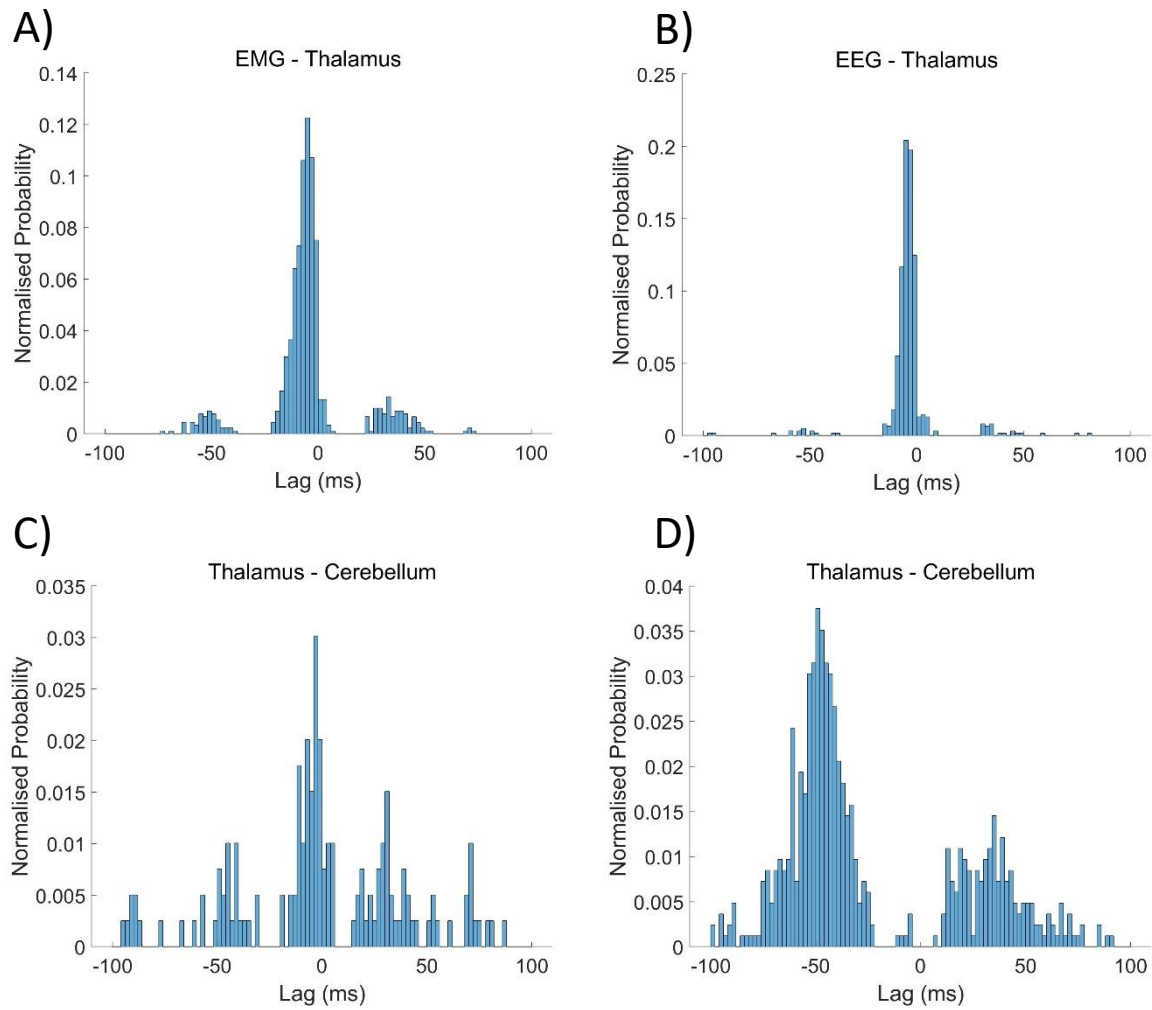
Figure 3-21. Example histograms of time-lags with maximal cross-correlation.
Cross-correlations were calculated for ± 100ms lags with a 2ms bin width. Each histogram displays the probability of time-lags with max cross-correlation across 2-second epochs taken during motor activity after harmaline administration for a single rat. Examples are from four different rats. Negative lags correspond to a backward connection between the name-pairs. A) EMG-Thalamus maximal cross-correlations with a peak time-lag at -5ms, B) EEG-thalamus maximal cross correlation with a peak time-lag at -5ms, C) Thalamus-cerebellum maximal cross-correlation with a peak time-lag at -3ms, D) Thalamus-cerebellum maximal cross-correlation with a peak time-lag at 49ms.

3.4 Discussion

The results in this Chapter are the first to provide electrophysiological evidence on changes in thalamus LFP and EEG oscillatory activity associated with harmaline-induced tremor. Specifically, these results show that harmaline-tremor was associated with increased coherence across the cerebello-thalamocortical network at the tremor frequency. This corresponds with electrophysiological findings from ET patients, which demonstrated that neural oscillations in the thalamus and EEG correlate with behavioural tremor (Hua et al., 1998; Schnitzler et al., 2009). Furthermore, these experiments demonstrate that movement significantly modulates coherence of thalamic neural oscillations with harmaline-induced behavioural tremor. Conversely, cerebellar neural tremor oscillations were not modulated by movement or increased tremor amplitude, suggesting that an extra-cerebellar source is involved in the modulation of tremor amplitude and thalamic involvement in tremor. The findings reported in this Chapter also lend support to the IO hypothesis of ET, as harmaline is known to increase oscillatory activation of the olivo-cerebellar pathway. Therefore, increased oscillatory activation of this pathway in rats is associated with similar electrophysiological correlates of tremor in ET.

3.4.1 Harmaline as a model for Essential Tremor (ET)

ET is diagnosed as an action tremor, which occurs during posture and voluntary movement and generally affects the upper limbs (Bhatia et al., 2018). Previous research has only qualitatively described that harmaline produces a tremor that increases in amplitude with movement (Handforth, 2012; Placantonakis et al., 2004). The analyses reported in this Chapter extend on previous research by quantitatively validating that harmaline produces a tremor that is significantly greater in amplitude during movement compared to resting. Although, a significant harmaline-induced behavioural tremor was also measured during rest/immobility, which could be attributed to either a resting tremor (i.e. a tremor occurring when muscles are completely relaxed), or to a postural tremor. However, the threshold used to distinguish rest vs movement in the present experiments, could not differentiate between rest with and without postural muscle control/activation of the head, body, or limbs.

Harmaline's effect on the olivo-cerebellar circuit is well-documented (for a review, see Handforth, 2012). However, little research has examined harmaline's effect on the cerebello-thalamocortical circuit. The present experiments have shown that harmaline induces significant coherence of tremor frequency oscillations across the recorded motor network. Previous research examining cerebral cortico-muscular coupling in ET patients using simultaneous EEG or MEG alongside EMG, as well as direct thalamic electrophysiological recordings, suggest that ET is a disorder involving

hyper-synchronous activity across the cerebellar-thalamocortical circuit (Muthuraman et al., 2012; Schnitzler et al., 2006). Therefore, the findings from this Chapter highlight that harmaline-induced tremor can also be characterised by increased coupling across the cerebello-thalamocortical network at the tremor frequency, suggesting propagation of neural tremor oscillations.

The IO theory of ET posits that tremor is caused by hyper-oscillatory activity of the IO (Lamarre, 1984). It is unknown whether hyper-oscillatory olivo-cerebellar activity is involved in ET. However, accumulating evidence has illustrated heterogeneous Purkinje cell-related pathologies in ET (see General introduction Section 1.3.1.3 for brief review). There is also some neuroimaging evidence indicating overactivity of portions of the brainstem, possibly reflecting the IO (Boecker et al., 1996; Hallett & Dubinsky, 1993), but this was not replicated (Wills et al., 1994). A post-mortem analysis also revealed no differences in IO density or evidence of IO neuronal damage in ET compared to controls (Louis et al., 2013). However, tremor caused by hyperactivity of the IO would presumably require an intact IO. Chronic administration of harmaline has also been associated with damage to and loss of Purkinje cells and IO neurons, which is thought to be due to excitotoxicity (Iseri et al., 2011; Miwa et al., 2006). However, chronic administration of harmaline is also associated with a reduced tremor response over time (Lorden et al., 1988). Therefore, chronic harmaline administration is not a reliable model of long-term tremor, but this does emphasise the importance of an intact olivo-cerebellar pathway if tremor is due to hyperactivation of the IO.

Different theories of ET pathophysiology suggest tremor occurs as a result of one or more cerebellar-related abnormalities (e.g. Purkinje cell degeneration, abnormal cerebellar GABAergic transmission, alterations to Glurδ2 expression; see General introduction Section 1.6 for brief discussion). However, a shared assumption of these theories is that abnormal changes within cerebellar circuits leads to dysregulation and/or increased oscillatory cerebellar nuclear output. Importantly, the findings in this Chapter provide evidence to support this assumption, by showing that increased oscillatory cerebellar nuclear output is associated with behavioural tremor and tremor-correlated neural oscillations in the thalamocortical network. Therefore, despite the likelihood that ET develops due to a complex range of degenerative and compensatory changes in cerebellar circuits, the harmaline model still provides sufficient construct validity in terms of its alterations to rhythmic cerebellar output. The construct validity of an animal model is defined by whether the model shares the same mechanism producing the disorder phenotype. The findings in this Chapter also provides evidence that the harmaline model of ET has good face validity (i.e. replication of disorder phenotype), as harmaline induces an action tremor that is associated with

significant coherent activity across the cerebellar-thalamocortical network at the tremor frequency, comparable to electrophysiological correlates reported in ET (Muthuraman et al., 2012; Schnitzler et al., 2006).

3.4.2   Thalamic involvement in harmaline tremor

The largest ascending pathway from the cerebellum to the motor cortex is via the lateral and interposed nuclei, which relay information to the VL portion of the thalamus. The medial cerebellar nuclei also projects to parts of the thalamus (VL and VM nuclei) which relays information for motor control (Klockgether et al., 1986; Teune et al., 2000). Previous research has largely overlooked the involvement of the thalamocortical network in the harmaline rodent model (Lamarre et al., 1975), instead focusing on the involvement of descending spinal pathways in harmaline tremor. Descending cerebellar motor pathways which include the reticulospinal, rubrospinal and vestibulospinal, are largely associated with gross motor function including locomotion, reaching (i.e. distal limb control), balance and postural control (Baker, 2011; Brownstone & Chopek, 2018; Juvin et al., 2016; Martinez-Lopez et al., 2015; McCall et al., 2017; Ruigrok, 2013). Alternatively, ascending cerebellar nuclear projections to motor cortex, via the thalamus, have been associated with motor adaption, timing of on-going movements, somatosensory integration and updating motor plans (Aumann, 2002; Bonnefoi-Kyriacou et al., 1998; Butler et al., 2000; Horne & Butler, 1995; Manzoni, 2007; Nashef et al., 2018).

Previous research that has examined thalamic involvement in harmaline-tremor pathways has shown that electrical stimulation of the VA/VL nuclei of the thalamus in harmaline-treated mice and rats significantly reduces the amplitude of harmaline-induced tremor, akin to the effects of deep brain stimulation observed in ET patients (Bekar et al., 2008; Lee & Chang, 2019). Harmaline tremor amplitude was also significantly reduced by intra-thalamic infusion of muscimol (GABA receptor agonist), suggesting inhibition of thalamic activity reduces tremor (Bekar et al., 2008). Furthermore, inactivation of adenosine A1 receptors blocked the therapeutic effect of thalamic stimulation on harmaline-treated mice, suggesting that release of ATP and activation of adenosine A1 receptors may be key to the depression of excitatory transmission in the thalamus and reduction of tremor in response to thalamic stimulation (Bekar et al., 2008). A selective adenosine A1 receptor agonist has been shown to significantly reduce extracellular levels of glutamate in VA/VL thalamic nuclei in rats, as well as significantly reducing the amplitude of harmaline-induced tremor (Kosmowska et al., 2020). This suggests that excitatory glutamatergic activation of the thalamus plays an important role in modulating the amplitude of harmaline-induced tremor in rats. The findings reported in this Chapter expand on this research by showing electrophysiological

oscillations in motor regions of the thalamus (i.e. portions of the VA/VL complex) cohere with harmaline-induced tremor.

The results reported in this Chapter also show that thalamo-kinematic coherence was significantly modulated by movement or increased tremor amplitude in response to movement. These results correspond with findings in ET patients (Hua & Lenz, 2005). For example, in an experimental paradigm whereby patients moved their arms from a resting position to an outstretched position, tremor onset emerged immediately upon arm elevation, and thalamo-muscular coherence occurred 220-460ms after tremor onset (Pedrosa et al., 2014). Hua & Lenz (2005) also showed that tremor-related rhythmic activity of neurons recorded from the ventral thalamus was only present during tremor induced by sustained posture and not resting. This suggests tremor-related oscillations within the thalamus occur after the onset of action tremor, and that thalamo-muscular coherence may be a consequence of tremor rather than a driver. This also suggests that tremor oscillations in the thalamus are partly a result of sensory feedback of behavioural tremor, rather than solely a result of direct cerebellar nuclear excitatory projections. Functional mapping of the ventral thalamus in ET patients also revealed that the type of thalamic neurons which exhibited tremor-related bursting included neurons that responded to sensory input as well as neurons responding to voluntary movements (Hua & Lenz, 2005). This further indicates that peripheral sensory inputs may be involved in modulating or amplifying tremor-related activity in the thalamus. Therefore, increased thalamo-kinematic coherence during movement compared to resting may be at least partly related to sensory feedback of behavioural tremor.

3.4.3   Cerebral motor cortex involvement in harmaline tremor

Whilst early research showed motor cortical lesions do not affect harmaline-induced tremor in cats and monkeys (Battista et al., 1970; Lamarre et al., 1975), there has since been very little research examining motor cortex involvement in harmaline-induced tremor. Work by Park et al., (2015) examined the presence of tremor-related cortical potentials in the awake harmaline-treated mouse as well as the awake GABA$_A$ α-1 subunit knockout mouse (see Section 1.5.2 in the General introduction for short review of this model). In the GABA$_A$ α-1 subunit knockout model, tremor-burst related cortical (EEG) potentials were found 3ms prior to the EMG tremor burst, however, tremor-burst related potentials were not found in the harmaline model (Park et al., 2015). This contrasts with the findings reported in the present Chapter, which revealed that 52.27% of epochs showed significant EEG-kinematic coherence at the tremor frequency. This difference in experimental findings may be related to differences in the localisation of the EEG recording. For example, the research by Park et al., (2015) utilised a transcranial EEG-grid array

(i.e. placed on top of the skull), and cortical potentials were calculated by taking an average EEG potential recorded across the entire scalp. Conversely, the experiment presented in this Chapter utilised an EEG skull screw which provided a localised EEG signal to the sensorimotor cortex (i.e. the base of the skull screw was positioned on the surface of M1). Clinical studies examining cortico-muscular coherence in ET have shown that EEG coherence with tremor is intermittent rather than constant, even when the tremor remains constant, suggesting that the motor cortex may not be involved in generating/driving the tremor (Raethjen et al., 2007). The findings reported in this Chapter extend on these clinical correlates by also highlighting the intermittent nature of sensorimotor EEG coherence with harmaline-induced tremor, as only around half of the total number of epochs analysed showed significant EEG-kinematic coherence at the tremor frequency.

A recent experimental study which recorded single unit activity in M1 and the VL nuclei of the thalamus in a harmaline-treated rat illustrated that harmaline increased the average firing rate of neurons in both brain regions (Lee & Chang, 2019). Furthermore, neurons which showed significantly increased firing rates were also neurons that tended to have oscillatory firing patterns (Lee & Chang, 2019). This suggests that at a single cell level, harmaline alters the firing rate of oscillatory neurons in M1 and VL nuclei of the thalamus. In relation to the findings reported in this Chapter, this may suggest that single neurons within M1 and the VL of the thalamus fire at different cycles of the tremor oscillation. This would account for the observed changes in population activity as measured by LFP and EEG (e.g. neural coherence with tremor) in this Chapter, but the varied firing rates and patterns reported on a single cell level (Lee & Chang, 2019).

The findings in this Chapter also revealed significant thalamocortical (i.e. thalamus and EEG) coherence at the tremor frequency. However, a discrepancy in findings was revealed when comparing the significance of the area under the mean thalamocortical coherence curve (reported in section 3.3.11) versus surrogate-corrected thalamocortical coherence across epochs (reported in section 3.3.10). Specifically, the former analysis revealed significantly increased thalamocortical coherence during movement but not rest, and the latter showed thalamocortical coherence was not modulated by movement. The reason for this discrepancy is that surrogate-corrected coherence takes into account the magnitude of raw coherence values in addition to the difference in coherence between the recorded and surrogate data sets. Overall the magnitude of tremor-frequency coherence with the EEG, including thalamocortical and EEG-kinematic coherence, were lower than kinetmatic coherence measures with the cerebellum and thalamus, suggesting tremor-related oscillations within the motor cortex were weaker than the other two brain regions. This

could be due to the nature of tremor oscillations within the network or related to differences in the electrode (e.g. EEG skull screw compared to tetrode LFP).

Inspection of the thalamocortical coherence spectra also indicates that harmaline induces a change in intrinsic (non-tremor frequency) thalamocortical oscillations, whereby a 7-8Hz oscillation present prior to harmaline shifted to a 5-6Hz oscillation after harmaline administration. Previous research has suggested that EEG theta oscillations (7-9Hz) in rats are associated with movement, where the amplitude of these oscillations increases with movement (Bellesi et al., 2012; Oddie & Bland, 1998). The findings reported in this Chapter extend on previous research by illustrating that a 7-8Hz thalamocortical oscillation is modulated by movement in non-tremor control conditions. Furthermore, harmaline reduces the frequency of this oscillation to 5-6Hz, which may reflect entrainment of this oscillation to a sub-harmonic frequency of the behavioural tremor. Overall, the findings reported in this Chapter illustrate that harmaline-tremor is associated with significant EEG-kinematic and thalamocortical coherence at the tremor frequency, although the magnitude of coherence was lower than cerebellar-kinematic and thalamic-kinematic coherence at the tremor frequency, indicating weaker EEG coupling with the tremor. However, harmaline was also shown to induce a change in the frequency of intrinsic thalamocortical oscillations, whereby intrinsic EEG oscillations may be entrained by a sub-harmonic of the tremor.

3.4.4   Mechanisms underlying the modulation of tremor oscillations with movement

Retrograde and anterograde tracing has shown cerebellar nuclei (including medial, interpositus and lateral cerebellar nuclei), project to regions of the VA/VL complex and VM nuclei of the contralateral thalamus in rats and mice (Bohne et al., 2019; Teune et al., 2000). Furthermore, stimulation of the cerebellar nuclei has been shown to increase action potential firing in the VA/VL complex and VM nuclei of the thalamus in mice and cats (Bava et al., 1967; Gornati et al., 2018; Steriade, 1995). Therefore, it is reasonable to assume that tremor oscillations in the cerebellar nuclei would be propagated to the contralateral thalamus. However, the results in this Chapter showed thalamo-kinematic coherence was modulated by movement but neural cerebellar-kinematic coherence was not. Furthermore, the amplitude of cerebellar LFP oscillations were not modulated by movement. As harmaline significantly induced tremor frequency oscillations in the cerebellum compared to control conditions, this shows that pathological cerebellar oscillations induced by harmaline were equal in amplitude during resting and movement. As total tremor amplitude significantly increased during movement, this points to an extra-cerebellar source involved in the modulation of tremor amplitude and thalamic tremor-oscillations with movement.

In addition to ascending projections (e.g. to the thalamus), the cerebellar nuclei have descending projections the spinal cord via the vestibular nuclei, red nucleus and reticular formation. Previous research has shown that harmaline induces rhythmic firing in parts of the red nucleus, vestibular nuclei, gigantocellular reticular nuclei, and motoneurons in the ventral efferent motor root of the spinal cord in anaesthetised cats (Batini, Bernard, et al., 1981; De Montigny & Lamarre, 1973; Llinás & Volkind, 1973). This suggests the rubrospinal and vestibulospinal tracts are central efferent pathways involved in harmaline-tremor, and harmaline-induced oscillations in this pathway occur in the absence of motor activity (i.e when anaesthetised).

The results from this Chapter show that thalamic tremor-oscillations are coupled with increased tremor amplitude during movement. This may suggest that afferent feedback of behavioural tremor amplifies thalamic tremor-oscillations. Mechanoreceptors in the skin, muscle and joints receive information on touch, vibration and proprioception, and these receptors project via the dorsal column medial-lemniscal pathway to the dorsal column nuclei complex (DCN), which comprises the gracile and cuneate nuclei (Loutit et al., 2021). The DCN complex in turn has excitatory projections to the ventral posterior lateral and ventral posterior medial (i.e. somatosensory) nuclei of the thalamus (Kramer et al., 2017; Uemura et al., 2020), as well as projections to the zona incerta, red nucleus, cerebellar cortex and IO (Boivie, 1971; McCurdy et al., 1998; Quy et al., 2011; Robinson et al., 1987). Therefore, the combination of somatosensory feedback of tremor and direct cerebellar-thalamic projections may contribute to the amplification or spread of tremor oscillations in the thalamus during movement. Conversely, evidence has shown that regions of the DCN also send bilateral inhibitory inputs to the IO (Geborek et al., 2013), which could be responsible for partially dampening somatosensory feedback of tremor oscillations to the cerebellum.

3.4.5 Theory on the roles of the cerebellum and thalamocortical loop in modulating tremor

The findings presented in this Chapter show that thalamic but not cerebellar oscillations are correlated with tremor amplitude, which is indicative that different parts of the cerebellar-thalamocortical loop have different roles in modulating tremor. Evidence from brain stimulation studies suggest that the cerebellum may be responsible for maintaining the pace/frequency of tremor in ET. For example, transcranial alternating currents applied over the cerebellum at the same frequency as the patients tremor did not affect the amplitude of the tremor, but could entrain the tremor frequency, i.e. influence the phase and instantaneous frequency of the tremor (Brittain et al., 2015). Research has also shown that tremor frequency in ET is more tuned to a

central frequency compared to PD, where tremor frequency can vary over a broader range (di Biase et al., 2017). In the harmaline model, the frequency of the tremor is also very tightly centred on a single frequency, and *in vivo* electrophysiological studies have shown that this frequency is paced by olivo-cerebellar rhythms (De Montigny & Lamarre, 1973; Llinás & Volkind, 1973). The results presented in this Chapter, also show that harmaline-induced cerebellar oscillations are independent of changes in tremor amplitude associated with movement. Taken together, this suggests that abnormalities occurring within olivo-cerebellar circuits can produce very regular pathological rhythmic oscillations that are tightly coupled with tremor frequency but are independent of behavioural state.

Evidence from Brittain et al., (2015) also showed that tremor amplitude in ET experiences a drop-off in power as the instantaneous tremor frequency is shifted away from its central point. This may suggest that disruptions to the tremor frequency, governed by the cerebellum, may influence tremor amplitude. This is supported by evidence that repetitive low-frequency (1Hz) TMS applied to the cerebellum transiently reduces tremor in ET (Gironell et al., 2002; Popa et al., 2013). Repetitive TMS stimulation of the cerebral cortex has been shown to increase the mean concentration of GABA in the stimulated region of the cortex (Gröhn et al., 2019). Therefore, repetitive TMS applied to the cerebellum may have a similar effect of increasing GABA in the cerebellar cortex to suppress cerebellar activity through increased cerebellar nuclear inhibition. This suggests suppression of cerebellar activity or disruption of tremor frequency oscillations at the level of the cerebellum reduces the amplitude of tremor in ET.

The findings from the current Chapter also show that thalamic oscillations are coupled with changes in tremor amplitude associated with movement. This is comparative with clinical research which showed a disruption or enhancement of neural oscillations in the thalamus modifies behavioural tremor. For example, the amplitude of tremor was amplified or suppressed dependant on the phase of thalamic stimulation at frequencies near to the tremor frequency (Cagnan et al., 2013). Furthermore, DBS applied to the thalamus is used as a chronic treatment for ET, where high frequency (e.g. 150Hz) stimulation is applied to disrupt or mask tremor oscillations in the thalamus (Karas et al., 2013; Kiss et al., 2002). Clinical research has also indicated that disruption of tremor oscillations in the motor cortex affect tremor amplitude. For example, continuous 50Hz theta-burst stimulation (cTBS) of the motor cortex has also been shown to reduce tremor amplitude (Hellriegel et al., 2012). However, cTBS did not affect motor-evoked potentials in ET, suggesting stimulation did not reduce cortico-spinal excitability, but likely caused a disruption to cortical oscillations.

Taken together this evidence may suggest abnormal tremor-related neural oscillations in the cerebellum and possibly descending pathways from the brainstem that receive cerebellar input (e.g., rubrospinal, vestibulospinal, reticulospinal) may play an important role in the timing or pacing of tremor rhythms. However, changes in the synchronisation of thalamocortical oscillations to the behavioural tremor rhythm may be important for modulating the amplitude of behavioural tremor, where increased synchronisation at the tremor frequency exacerbates tremor. Previous evidence has shown that thalamic neurons may be responding to sensory feedback of behavioural tremor which may contribute to increased synchronisation or spread of tremor rhythms in the thalamus (Hua & Lenz, 2005; Pedrosa et al., 2014). This is counter to traditional models of ET neural networks, which suggest that the cerebello-thalamocortical pathway is key to driving tremor in the periphery. However, the findings reported in this Chapter reveal that tremor-related neural oscillations in the cerebellum are equally as strong during movement and rest, even though the amplitude of tremor was greatly reduced during rest. Rhythmic activity in the motor thalamus, however, was modulated by movement. Therefore, abnormal cerebellar neural oscillations may play a role in governing the pace of tremor, whereas coupling of thalamic neural oscillations is related to the amplitude of tremor.

3.4.6 Limitations and challenges

One of the major limitations of the harmaline model is the non-specific or targeted effects of harmaline on the central and peripheral nervous system. Although harmaline is thought to generate tremor solely by its action on the IO (Handforth, 2012), less is known about harmaline's influence on the wider nervous system. Harmaline is a mono-amine-oxidase inhibitor for group A amine's, and therefore inhibits the breakdown down of mono-amine neurotransmitters (e.g. norepinephrine, epinephrine and serotonin), which can affect multiple and distributed neural systems (Chen & Shih, 1997; Herraiz et al., 2010). Harmaline has also been shown to be an acetylcholinesterase inhibitor (Udenfriend et al., 1958). Acetylcholine is released by the parasympathetic nervous system to slow down heart rate and is also widespread in the cerebellum, and some motor dysfunctions have been related to cerebellar cholinergic dysfunctions (Zhang et al., 2016). Therefore, in addition to inducing tremor via its effects on the olivo-cerebellar circuit, harmaline may be inducing unknown effects on the wider nervous system.

This research aimed to simultaneously record neural oscillations using multi-site LFP recordings across the cerebellum and thalamus, as well as M1 EEG, and monitor tremor rhythms using neck and limb EMG and an accelerometer. The complexities associated with these experimental techniques meant that electrophysiological data across every recording site within a rat were not

always included within the final analyses. One reason for this is that the final recording site of the tetrodes within the thalamus or cerebellum were not always located within the target structure. For some EEG and EMG recordings, ECG artefacts were found to contaminate recordings, and some connections were damaged post-surgery. To avoid excluding all data collected from a single rat, the analyses reported within this Chapter included all available and artefact-free data per brain site or pair of brain sites when examining coherence. This resulted in different numbers of rats included in each analysis. Due to the nature in which recorded epochs of data were segmented into artefact-free 'rest' or 'movement' epochs, different numbers of epochs were also available for each condition per rat (average number of epochs = 642.18±330.52). To address the unbalanced number of epochs, multi-level models were applied to examine the variation in the dependant variable (e.g. LFP amplitude or coherence) across repeated measures groups (e.g. control vs. harmaline, or resting vs. movement). An advantage of this statistical method is that dependant variable measures do not need to be averaged over epochs, which is particularly important in datasets where the number and timing of sampled observations (i.e. epochs) vary across conditions and between rats. Therefore, every epoch collected during this experiment could be included within the final analyses examining the relationship between the categorical predictor variable and the underlying distributions of the dependant variable (Hoffman & Rovine, 2007; Ma et al., 2012).

3.5 Chapter summary

The findings reported in this Chapter reveal that harmaline-induced tremor can be characterised as an action tremor associated with coherent tremor frequency oscillations across the cerebello-thalamocortical network, suggesting propagation of tremor oscillations across the cerebello-thalamocortical pathway. Furthermore, these experiments revealed that harmaline induces prominent pathological oscillations in the cerebellum that are present during resting and moving and are independent of changes in behavioural tremor amplitude associated with movement. Conversely, tremor-related neural oscillations recorded from the thalamus are modulated by movement, which could be related to somatosensory feedback of tremor. The theory presented in this discussion, is that pathological cerebellar rhythms in ET may be constant and govern the pace of the tremor. However, synchronisation of thalamocortical rhythms may be involved modulating the amplitude of these tremors. An abundance of research has shown that modulating thalamic synchronisation with the tremor rhythms can modify behavioural tremor. However, there is still uncertainty regarding the role of the sensorimotor cortex in ET. The following Chapter aims to further examine the role of the cerebral cortex in ET, and the relationship between cerebral coupling with the tremor frequency and tremor amplitude.

Chapter 4. **The impact of posture and visual feedback of tremor on cerebral cortical oscillations and tremor amplitude in Essential Tremor**

4.1   Introduction

The role of the sensorimotor cortex in the pathophysiology of ET is uncertain (Sharifi et al., 2017). Theories of ET pathophysiology suggest that peripheral tremor is driven by abnormalities occurring within the cerebellum, which may result in the relay of pathological rhythms to the motor cortex via the thalamus (Helmich et al., 2013). However, research has suggested that tremor-related activity in the thalamus and sensorimotor cortex, may be at least partly related to sensory feedback of tremor. For example, tremor onset recorded at the muscle precedes the onset of tremor-related activity within the thalamus (Pedrosa et al., 2014), and cortico-muscular coherence is reported to be intermittent even when peripheral tremor is constantly present (Raethjen et al., 2007). Furthermore, significant cortico-muscular coherence was more likely when tremor amplitude increased above a certain level (Hellwig et al., 2003; Raethjen et al., 2007), suggesting that communication between the cerebral cortex and the muscle is influenced by tremor amplitude. It also highlights that detectable sensorimotor cortex neural oscillations at the tremor frequency is not necessary for tremor symptoms in ET, suggesting tremor in ET may not have a cortical drive (Raethjen et al., 2007). One explanation is that this coupling is affected by somatosensory feedback of the tremor.

Recent research has also suggested that other forms of perception can influence tremors. For example, cortico-muscular coherence is significantly increased when ET patients performed a simple mental arithmetic task (Sharifi et al., 2017). This may be related to increased cognitive load, altered awareness of tremor, or related to increased anxiety associated with performing a mental arithmetic task. Although Sharifi et al., (2017) did not report the relationship between performance of a mental arithmetic task and tremor amplitude in ET, the performance of a stressful cognitive task has been shown to increase tremor amplitude in PD (Dirkx et al., 2020). Furthermore, visual feedback of tremor has been shown to exacerbate tremor amplitude in ET, and fMRI research has suggested abnormal processing in visual areas of the brain may be involved in tremor networks (Archer et al., 2018; Gironell et al., 2012; Grimaldi et al., 2013; Neely et al., 2015).

4.1.1   The effect of visual feedback on tremor in Essential Tremor

As noted above, research has revealed that visual feedback of tremor can exacerbate tremor in ET. This has been shown to occur when ET patients are asked to watch the tremor in their affected limbs compared to when no visual attention is paid to the tremor (Gironell et al., 2012). The same

observation has been also been found in healthy subjects who have a normal physiological tremor (Carignan et al., 2009). Furthermore, this effect has also been shown for 'extrinsic' forms of visual feedback, where instead of participants watching their hand, visual feedback of the tremor is provided from an external source. For example, 'extrinsic' visual feedback of tremor has been achieved by fixing a laser pointer fixed to the palm of healthy participants. In this paradigm, participants were asked to observe the light from the laser pointer and to maintain the light within a circular target region. When visual attention was paid to the augmented visual feedback, tremor amplitude was significantly increased compared to tremor amplitude during 'intrinsic' visual feedback, where participants observed their hand with the laser light switched off (Keogh et al., 2004). This suggests that augmented visual feedback has a larger effect at exacerbating tremor.

Visual feedback has also been shown to counteract the beneficial effects of surface muscular functional electrical stimulation (FES) on physiological tremor (Grimaldi et al., 2013). Surface FES is an alternative approach to pharmacological or surgical interventions for neurological tremors. This works by applying out of phase stimulation to the extensor and flexor muscles of the limb, to counteract the tremor movement and to reduce pathological as well as physiological tremor amplitude (Grimaldi et al., 2013; Maneski et al., 2011). When healthy controls were asked to observe their physiological tremor via a laser pointer fixed to the hand, the reduction of tremor amplitude in response to FES was abolished (Grimaldi et al., 2013). This suggests that increased awareness of tremor, facilitated by augmented visual feedback, significantly increased the excitability of the cortico-spinal pathways.

Evidence from fMRI has also suggested that activity in visual regions of the brain may be modulated by visual feedback in ET (Archer et al., 2018). This study provided extrinsic visual feedback of the amount of force applied to a force transducer, where applied force functioned to move a bar on a visual display in real-time. During the experiment, participants were asked to hold the moving bar at a target point by applying a constant force. Using this method, tremors that occur during sustained muscle contraction can be measured via rhythmic fluctuations in force at the tremor frequency. Tremor amplitude was examined during high and low gain visual feedback conditions. In the high visual feedback condition, the bar would move up/down to a greater degree than in the low visual feedback condition. Findings illustrated that increased visual feedback, led to increased tremor amplitude, accompanied by abnormal changes in blood-oxygen-level-dependent (BOLD) signals in the primary visual cortex, as well as areas of the motor cortex. Furthermore, changes in BOLD activity were not predicted by the overall error in applied force.

This suggests that activity in the visual system can be directly influenced by the amount of visual feedback and that these changes were not related to the error in the accuracy of applied force.

To date, the effect of visual feedback on the coupling between the EEG activity and tremor has not been examined. One potential mechanism by which visual feedback exacerbates tremor is via increasing synchronous oscillatory activity within cortical networks at the tremor frequency. Research has shown that attending to a rhythmic visual stimulus, can induce neural entrainment of the visual cortices at the rhythm being viewed. For example, the presentation of objects or pictures that flash on/off a computer screen at a rhythmic rate generates cortical brain rhythms at the same frequency as the flickering visual stimulus (Herrmann, 2001; Spaak et al., 2014). This is referred to as a visually evoked steady-state potential and can be measured within EEG recordings at a high signal to noise ratio. Visually evoked steady-state potentials can also be induced via observation of rhythmically moving stimuli (Heinrich & Bach, 2003). Therefore, it is viable that augmented visual feedback of tremor could induce neural entrainment of visual regions at the same frequency, and increased visuomotor synchronisation may contribute to exacerbated tremor.

Research has also illustrated that the human sensorimotor system tends to naturally synchronise to environmental rhythms through different sensory modalities, including the auditory and visual system (Ross & Balasubramaniam, 2014). Performance of rhythmic movements in time to a beat improves the accuracy and rhythmic timing of movements (Comstock et al., 2018), and auditory tones have been used to improve gait in patients with Parkinson's Disease (Bella et al., 2017). The presentation of rhythmic sounds can also induce auditory evoked potentials which are measurable EEG rhythms at the frequency of the rhythmic sound. When rhythmic movements are synchronised to a rhythmic beat, the amplitude of the steady-state response increases, indicating stronger neural entrainment to the external rhythm (Nozaradan et al., 2016). Furthermore, synchronisation of rhythmic movements (e.g. finger tapping) to visual stimuli is more successful if the stimulus is a moving visual target than flashing on/off stimulus (Hove et al., 2010, 2013; Hove & Keller, 2010; Iversen et al., 2015). This evidence suggests that the occurrence of cross-modal rhythms at the same frequency tend to synchronise, and at times can amplify the oscillatory rhythm.

Conversely, studies have revealed that the presentation of cross-modal rhythmic stimuli at different frequencies, can have a desynchronising or disruptive effect on behavioural and cortical rhythms. For example, when simultaneously presenting a visual and auditory repetitive stimulus at different frequencies (40Hz and 7.5Hz respectively), the amplitude of the auditory or visual

evoked steady-state potential is modulated depending on the modality to which participants are asked to pay attention (Saupe et al., 2009). The synchronisation of movement to a visual or auditory stimulus is also impaired if a competing stimulus at a different frequency is presented via a different modality (Hove et al., 2013).

4.1.2 Aims

The experiment reported in this Chapter aimed to examine the relationship between tremor and neural oscillations in patients diagnosed with ET. Neural activity was recorded using a 64-channel EGI EEG recording system. All participants had an active upper limb tremor, and tremor activity was simultaneously recorded using a tri-axial accelerometer fixed to the middle finger of their tremor dominant hand.

This experiment has three aims. Firstly, the experiment aimed to examine whether EEG recordings reveal changes in tremor-related EEG activity during sustained posture of the upper limb compared to resting, which corresponds to cortico-kinematic changes observed with the harmaline model in Chapter 3. Secondly, the study also aimed to examine whether passive visual feedback of tremor can influence tremor amplitude and coherence between visual and motor regions of the cerebral cortex at the tremor frequency. To examine this, two types of visual feedback were employed, which included natural visual feedback (e.g. watching tremor in participants own hands) and artificial augmented visual feedback (e.g. watching a bar on a visual display, that moves up and down at the same rate as the tremor). Thirdly, the experiment aimed to examine the impact of neural entrainment of tremor rhythms on tremor amplitude. This is investigated by inducing visually evoked steady-state potentials at tremor and non-tremor frequencies, by presenting rhythmic visual stimuli, and examining whether induced rhythms influence (amplify or suppress) tremor amplitude.

4.2 Materials and methods

4.2.1 Ethical statement

This research study was approved by the HRA and the South West – Central Bristol NHS REC and the University of Bath psychology research ethics committee. All participants received and read a participant information sheet about the study before attendance and gave written informed consent to participate.

4.2.2 Participants

A priori power calculations were conducted before testing using G*power, to calculate the sample size required to compare four within-subject measurements for one participant group. Using a

partial eta-squared effect size $\eta^2 = 0.09$ (Sharifi et al., 2017), power =0.90, alpha = 0.05, a required sample size of 20 participants was identified. However, data collection for this study was cut short due to the outbreak of COVID-19 and subsequent lockdown and social distancing measures that were brought into place.

Fourteen participants with ET participated in the study (8 male and 6 females; mean age (±SE) = 54.26 (20.1) years). Clinical assessment of tremor was completed with all participants using the Fahn-Tolosa-Marin (FTM) Clinical Rating Scale, before taking part in EEG experimental procedures at the University of Bath. Participant demographics are displayed in Table 4-1. All participants were either taking no medication or on stable medication for one month before participation. Exclusion criteria included participants with a severe head tremor, as well a history of epilepsy. Partial tremor and/or EEG data was missing for three participants.

Table 4-1. Participant demographics

Participant	Estimated Disease duration (years)	Familial ET	Tremor reduced by alcohol	FTM total score*	Tremor frequency (±SD) in Hz
1	72	Yes	Yes	66	5.79 (0.32)
2	23	Yes	Unsure	24	5.10 (1.13)
3	1	No	Unsure	14	7.12 (0.60)
4	13	No	Unsure	40	9.87 (0.58)
5	3	No	yes	36	5.64 (0.67)
6	22	Yes	Yes	75	5.20 (1.16)
7	9	Yes	No	35	8.33 (0.34)
8	47	Yes	Yes	32	6.02 (0.17)
9	19	Yes	Yes	24	8.57 (0.19)
10	10	No	Yes	13	10.19 (3.03)
11	0.5	No	Yes	39	8.59 (1.88)
12	51	Yes	Yes	35	6.84 (0.27)
13	49	No	Yes	41	6.67 (0.39)
14	61	Yes	Yes	54	5.89 (0.42)
Mean (±SE)	27.18 (24.03)			37.71 (4.73)	7.13

* Higher FTM scores reflect more severe tremor

4.2.3 EEG data acquisition

EEG signals were captured using a HydroCel Geodesic Sensor Net (GSN) 64 Channel EEG system (Philips Neuro Electrical Geodesic Inc, EGI, USA). The channel map configuration for the electrode cap is displayed in Figure 4-1. On arrival to the EEG experiment, participants head size was measured around the widest part of the head, to identify the correct HydroCel GSN size to use. Measurements were then taken across the head, from front to back (Nasion to the Inion) and from ear to ear, to mark the midline sagittal plane of the scalp (Cz) using a crayon. After soaking the HydroCel GSN in a saline solution for 5 minutes (according to manufacturer's instructions), the net was fitted onto the participants head so that the central reference electrode (Cz) lined up with the central point marked on the scalp.

Once the HydroCel GSN was fitted, participants were taken into the purpose-built Faraday cage and were sat on a chair in front of a metal frame, which will later be used to hide arm movements. Positioned on the table behind the metal frame were two screens, a centrally positioned LED screen, and a computer monitor positioned behind the LED screen and to the left-hand side. The distance from the participant's eyes to the LED screen was adjusted to be ~70cm apart. The GSN was then connected to the amplifier (Net Amps 400 series, Philips Neuro EGI, USA), and data were acquired using NetStation Acquisition software, and EEG signals were sampled at 1KHz
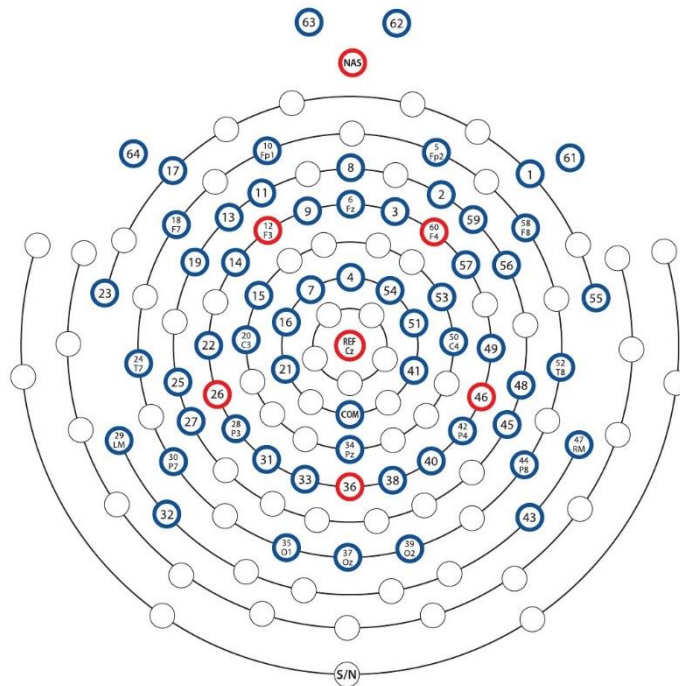
Figure 4-1. EEG channel scalp configuration.
Layout of the 64 channel GSN, taken from the GSE hardware technical manual, where all numbered circles represent electrodes. Electrodes at the top of the figure (electrode 63 and 62) sit on the cheekbones of the subject and electrodes at the bottom of the figure sit at the back of the subjects' head.

4.2.4 Visual feedback via LED screen

A custom-made LED screen was used for experimental tasks involving augmented visual feedback and presentation of rhythmic visual stimuli. This LED screen consisted of 25 horizontal strips of LEDs (20 LEDs on each row) secured in a Perspex case. The LED display was connected to an Arduino Mega, and each of the 25 LED rows could be independently turned on/off via instructions sent to the Arduino via Processing 3 open-source software. A white frosted plastic sheet was secured in front of the LEDs, to diffuse the light and to give the perception of a continuous row of light when one of the LED rows were turned on.

An apparatus was constructed to hide participants hands from view. This consisted of a metal frame on wheels, that could be adjusted in height. Cardboard was secured on top of the frame using Velcro strips, which was additionally covered by a hairdresser gown, that was fastened behind the participant's neck. This functioned to hide the full length of the arm and hand, without obstructing movement and allowing participants to elevate their arm in front of them.

4.2.5 Simultaneous tremor recording

A tremor sensor was custom-built using an MPU-6050 tri-axial accelerometer and gyroscope chip and breakout board (Sparkfun, USA), which supports the I2C serial interface. This sensor is designed for real-time motion processing. Using the I2cDev and MPU6050 Arduino libraries, the acceleration across 3 axes were digitalised with 16-bit ADC, where output acceleration was converted to a +/- 16g scale. The accelerometer was then fitted into a rubber case.

Once participants were sitting comfortably in front on the LED screen, and the GSN was connected to the amplifier, the tri-axial accelerometer was fitted to the distal region of the middle finger on the tremor dominant hand using Velcro. If tremor was equally severe in both arms, the participant's motor dominant hand was used. Real-time accelerometer output was sent from the Arduino Mega to the computer over the serial port using Processing 3, where a sampling rate of 784Hz was achieved and data was stored as a text file.

4.2.6 Experimental paradigm

Participants completed experimental tasks in a counterbalanced order, using a Latin Square counterbalance design. To maximise SNR of recorded EEG signals, at the beginning of each of the experimental tasks, all EEG sensor impedances were measured and re-calibrated so that sensor impedances were below 50kΩ. Impedances were adjusted by re-hydrating sensors with a saline solution using pipettes.

After checking EEG sensor impedances, sixty seconds of resting-state EEG data were collected, whilst participants sat in the chair, with their forearms/hands supported on their lap (palms down). Participants were instructed to focus on the white LED screen in front of them. During this time, hands were hidden from view and the LED screen was switched off. Participants were then given verbal and written instructions about the experiment task before commencing, where written instructions were presented in a large white font on a black background on the computer monitor behind the LED screen.

Each task took between 9-16 minutes, including breaks. All tasks consisted of 30-second trials, with a 20-second minimum break between trials. Task instructions were presented at the start and end of each trial, displayed on the computer monitor behind the LED screen. During the trial, the computer monitor displayed a blank black background. At the start of each trial, participants were instructed to outstretch their arm/hand that was fitted with the sensor and to hold their hand outstretched in front of them for the length of the trial. The experimenter remained in the room to monitor arm elevation during testing. Trial onset/offset timestamps were sent to

NetStation EEG acquisition software and simultaneous accelerometer data files, to enable off-line alignment of EEG and accelerometer data. A schematic diagram illustrating the experimental tasks is shown in Figure 4-2, and a description of each task is provided below.

4.2.6.1 Tremor reduction Instructions

In the three of the experimental tasks described below (A) no visual feedback, B) natural visual feedback, and C) augmented visual feedback, but not D) rhythmic stimulation) participants were given alternative instructions for 50% of the trials. For half the trials participants were instructed to try and minimise their tremor and hold their hands as still as possible. In the other half, participants were instructed to exert no control over the tremor or attempt to minimise their tremor in any way. The order of these instructions was counterbalanced across participants.
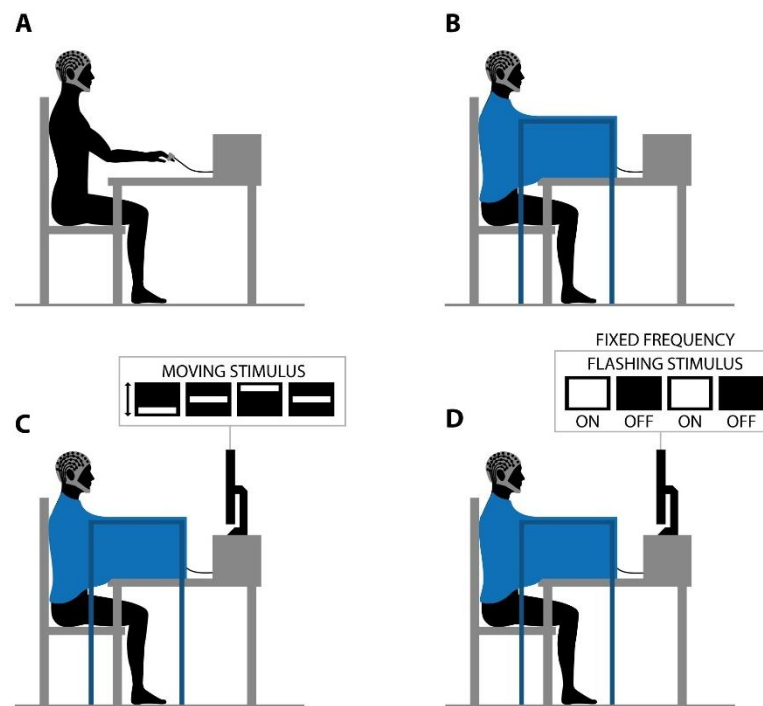
Figure 4-2. Schematic of the 4 experimental conditions and set up.
The tri-axial accelerometer was placed on the middle finger of the tremor dominant hand, and simultaneous EEG and accelerometer data were collected during the experiment. A) Natural visual feedback: Participants watched the tremor in their outstretched hand. In B-E, participant's hand was hidden from view. B) No visual feedback: Participants focused on a blank screen. C) Augmented artificial visual feedback: Participants observed a bar of LEDs moving up/down at the same rate as their tremor. D) Rhythmic visual stimulation across fixed frequencies: Participants observed flashing on/off LEDs across 16 difference fixed frequencies.

4.2.6.2　Natural visual feedback

This task included 10 30-second trials, where participants were instructed to watch the tremor in their outstretched hand during the length of the trial (Figure 4-2 A).

4.2.6.3　No visual feedback

Participants performed 10 30-seconds trials in which they were instructed to focus on a blank white screen in front of them, whilst their outstretched hands were hidden from view (Figure 4-2 B).

4.2.6.4　Augmented artificial visual feedback

In this task, visual feedback of tremor was provided through an external source, where up/down movement of the hand functioned to move a bar of LEDs on the screen in real-time. This was computed by taking the real-time acceleration in the up and down axis of the accelerometer and re-scaling the value (g-force units) to an integer value ranging from 1-25, mapping to each LED row in the display. In real-time this governed which row of LEDs should be on, whilst all other rows were turned off. Therefore, a g-force value of around zero would centre the bar of LEDs in the middle of the display. Positive g-forces indicate an acceleration in the upward direction and would move the bar of LEDs upwards, and negative g-forces indicate an acceleration in the downward direction and would move the bar of LEDs down. This produced a moving bar of LEDs (in the up/down direction) which reflected the real-time acceleration of the hand (also in the up/down axis).

During this task, the participant's arms/hands were hidden from them using the methods described above, so that the only visual feedback regarding tremor amplitude was provided through the external LED display. Participants were informed that the bar of LEDs would move with the amplitude of their tremor. This task also involved 10 30-second trials, and participants were instructed to watch the external LED display for the length of the trial (Figure 4-2 C).

4.2.6.5　Rhythmic visual stimulation across a range of fixed frequencies

To examine whether neural rhythms in visual areas of the brain can influence tremor amplitude, this task aimed to induce steady-state visual evoked potentials at tremor and non-tremor frequencies using the presentation of rhythmic visual stimuli and to observe the effect on tremor activity.

To induce visually evoked steady-state potentials at tremor and non-tremor frequencies, this task included 16 30-second trials, where for each trial participants were instructed to watch rhythmically flashing LED stimuli and to outstretch their hand for the length of the trial (Figure 4-2

D). During this task, the participant's arms/hands were hidden from them using the methods described above.

Each trial involved the presentation of one of 16 flashing frequencies, presented in a pseudo-randomised order, whereby neighbouring frequencies were not allowed to precede or follow one another. For example, a stimulus at 6Hz would not be presented before or after stimulus at 5 or 7Hz. The frequencies delivered are listed below:

$2 - 4 - 5 - 6 - 7 - 8 - 9 - 10 - 11 - 12 - 13 - 15 - 18 - 20 - 25 - 30Hz$

4.2.7 Subjective ratings of tremor severity

At the end of each trial, participants were asked to verbally rate the severity of their tremor during the trial, providing a rating on a scale of 0-10. A score of zero represents no tremor at all, and a score of 10 would represent a severe tremor.

4.2.8 Data pre-processing

4.2.8.1 Accelerometer data

The tri-axial accelerometer data were subjected to a principal component analysis to extract the dominant axis of the tremor movement, which was taken as the first principal component. Data were then up sampled to 1kHz to match the sampling rate of the EEG for coherence analysis, using the MATLAB "resample" function. An example of the first principal component of the accelerometer recording, and the up-sampled accelerometer data is shown in Figure 4-3. This figure illustrates that both time-series were perfectly aligned, indicated by the hidden time series for the unprocessed data, after the up-sampled data is overlaid. This shows that up-sampling did not introduce any distortion of the low frequency tremor data.
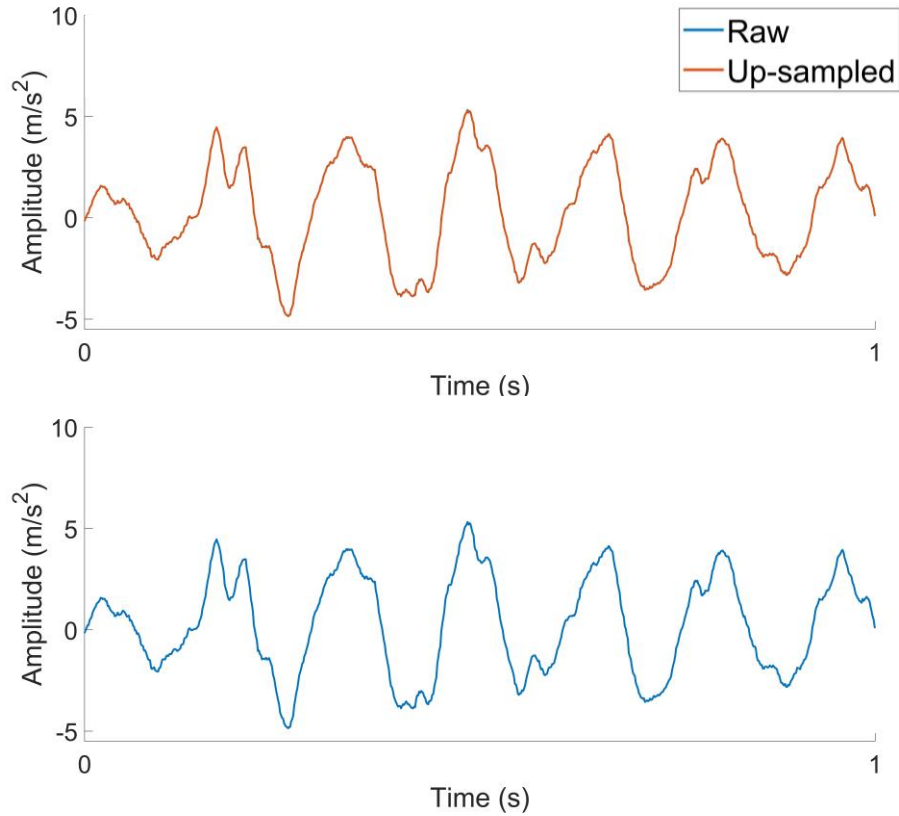
Figure 4-3. Comparison of raw and up-sampled accelerometer data.
Accelerometer data were sampled at 784Hz and up sampled to 1KHz**.** This figure provides an example of the accelerometer data before (blue) and after up-sampling (orange).

4.2.8.2 Spectral analysis of tremor recordings

To quantity tremor amplitude, each accelerometer recording was segmented into 2-second epochs, and FFTs were performed on each epoch. For each epoch, tremor frequency was identified as the frequency with peak amplitude in the low-frequency spectrum ranging from 1-20Hz, and tremor amplitude was identified as the peak amplitude at this frequency.

To examine changes in tremor amplitude, percentage change in tremor amplitude during an experimental condition, $Tremor_{exp}$, compared to the control condition, $Tremor_{control}$, was calculated using the following equation:

$$\% \ change = \frac{Tremor_{exp} - Tremor_{control}}{Tremor_{exp}} \times 100 \qquad \text{Equation 4.1}$$

4.2.8.3 Channel level cortical-kinematic coherence

Cortico-kinematic coherence was examined at the channel level, focusing on accelerometer coherence with EEG electrodes over the central regions of the scalp. Central electrodes C3 and C4 are approximately situated over the sensorimotor cortex. Previous studies have reported that maximal EEG-EMG coherence at the tremor frequency may be found on electrodes C3 and C4, or with neighbouring electrodes (Hellwig et al., 2001, 2003). The same method reported in these studies was employed here. For each epoch, coherence between the accelerometer and EEG electrodes was calculated separately for C3, C4, and the five electrodes surrounding C3 and C4. The electrode showing highest and significant coherence with the tremor, on each side of the hemisphere, was selected for further analysis.

Recordings were segmented into 5-second epochs and signal frequency coherence was computed by examining the MATLAB magnitude-squared coherence function, and the significance of coherence was assessed using surrogate analysis as reported in Chapter 3. Briefly, 99 surrogates were generated for each epoch using the iAAFFT method, and statistical significance was then examined by calculating surrogate-corrected coherence using Equation 4.2 (Rummel et al., 2015).

$$C = \frac{P - P(surr)}{1 - P(surr)} \, S \qquad\qquad \text{Equation 4.2}$$

Here P represents the coherence coefficient of the recorded data, and P(surr) represents the mean coherence across 99 surrogate epochs. If P is greater than P(surr), then the null hypothesis that the two signals are independent is rejected, and S takes a value of 1. Else, the null if not rejected and S takes on the value of 0.

To examine the topographical distribution of cortico-kinematic coherence at the tremor frequency (±1.5Hz) across the scalp, topographic maps of cortico-kinematic coherence were created using the Fieldtrip MATLAB toolbox.

4.2.8.4 Assessment of steady-state potential evoked by visual stimulation

To examine whether significant steady-state potentials were induced by rhythmic visual stimulation, a FFT was computed for the high-pass filtered (0.1Hz) EEG data recorded across 30-second blocks, and for each channel SNR was calculated by dividing the amplitude at each frequency bin, by the mean amplitude of frequencies within a +/-0.5Hz range (i.e. mean across 30 bins). Any SNR greater than 1 would indicate greater signal at that frequency compared to the

background level of noise. A scalp average SNR was calculated by taking the mean SNR across all electrodes.

4.2.8.5 *Dynamic imaging of coherent sources*

A high-pass filter (0.1Hz) was applied to accelerometer and EEG data, and each recording was segmented into 2-second epochs. Source-localization of spectral power at the tremor-frequency range was computed using dynamic imaging of coherent sources (DICS) via BESA software. DICs is a beamforming method which creates a 3D voxel matrix of the brain, computes a complex cross-density matrix across all channels and then applies a spatial filter to estimate spectral activity at each voxel. The cross-spectrum between each voxel (voxel size of 7mm) and the external accelerometer channel was examined, and tomographic maps of cerebral-kinematic coherence at the tremor frequency ($\pm$1.5Hz) were computed separately for each participant and each experimental condition. The Brodmann's atlas was applied over each tomographic map, and the Brodmann area and Talairach coordinates were extracted for the top ten local maxima (i.e. relative peaks in coherence). In some cases, less than 10 local maxima could be identified. Only cortical sources were extracted, as the reliability of modelling of subcortical and cerebellar sources is very limited with EEG (Barzegaran & Knyazeva, 2017).

A simulation study which investigated the impact of electrode density on source localisation accuracy indicated that a 64-channel cap with full coverage of the head has a mean localisation error of 21.31mm, with a SD of 11.57mm (Song et al., 2015). Due to this variability, cortical source co-ordinates were clustered together if they belonged to the same Brodmann area, or in a closely neighbouring Brodmann area that is often grouped functionally. For example, the M1 and S1 are often grouped into the primary sensorimotor region, given their close spatial alignment, and their collaborative involvement in motor tasks. For each source identified by DICS, an inverse rank value was assigned, such that sources which ranked top in the local maxima (i.e. most coherent source) were given a rank value of 10. If sources ranked last in the top ten local maxima, a rank value of 1 was given. A total rank score was then calculated across all clustered cortical sources, to identify the top ten coherent sources at a group level across all visual feedback conditions.

To identify sources showing significantly increased coherence for sustained posture versus resting at the tremor frequency ($\pm$1.5Hz), high pass filtered EEG data was exported from BESA to MATLAB, and DICS analysis was then performed using the Fieldtrip toolbox in MATLAB. Voxel grids were left-right flipped for all participants that completed the task with their left-hand extended. A two-tailed Monte-Carlo permutation paired *t*-test (50,000 permutations, *p*<0.01) with a cluster-

based correction method for multiple comparisons was performed using the Fieldtrip toolbox in MATLAB.

4.2.9 Regional source model

A regional source model was created by seeding the top ten sources identified by the exploratory DICS analysis, using the average coordinates for these sources, where all sources were seeded bilaterally. The regional source model was constructed using BESA software, which applies a forward model to predict the contribution of each source to reference-free voltage changes on scalp maps, using a volume conductor model of the head. A linear transform is then applied to the time-series data across all EEG channels, to reduce the data into time-series waveforms for each source (inverse model). The dynamics of each source are modelled by three dipoles that are orthogonal to the x, y, and z axes of the Talairach coordinate system. The inverse model also acts as a spatial filter to separate source activities of the regional sources included in the model (Scherg, 1990; Scherg et al., 2019).

Fitting the twenty-source model to each participant's data, reduced the data from 65 time-series for each recording channel, to twenty time-series estimations for regional sources. These methods are illustrated graphically in Figure 4-4.
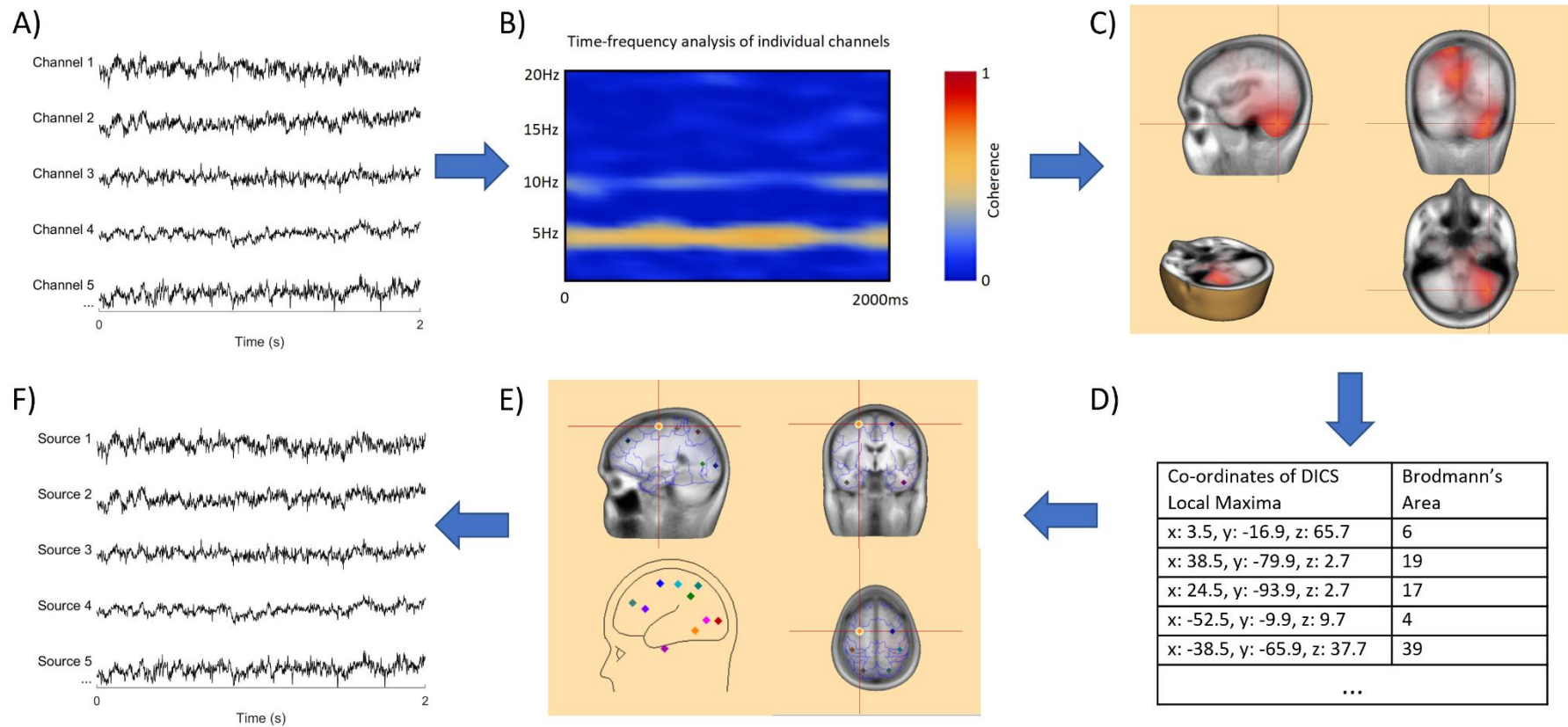
Figure 4-4. EEG data processing pipeline.
High-pass filtered (0.1Hz) accelerometer and EEG data (shown in A) were subjected to time-frequency analysis (shown in B), and mean coherence between each EEG channel and the accelerometer was computed for each condition and participant. A DICS beamformer was applied to the frequency of interest (participant individual tremor frequencies) to identify cortical source co-ordinates which showed relative peaks in coherence with the accelerometer (shown in C&D). Coherent sources which were prevalent across participants were identified, and a regional source model was constructed using the average Talairach coordinates for each source (shown in E). The regional source model was applied to each participant's data to reduce the 65 EEG channel times-series, to estimated time-series per source (shown in F).

128

4.2.9.1 Source coherence analysis

To examine visuo-motor coherence, source dipoles were exported from BESA and analysed in MATLAB. For each source, the net variation in regional source magnitude was calculated as the square root of the sum of the squares of three orthogonal dipoles. The resulting source time-series waveforms reflect local changes in the strength of the source current local to that region. Time-series were segmented into 2-second epochs, and magnitude-squared coherence analyses were performed on each epoch to examine cortico-cortical coherence between sources. Mean coherence at the tremor frequency were extracted for each participant and condition.

4.2.10 Statistics

Assumptions of statistical tests were assessed, and where data did not meet the assumptions of a parametric test, a non-parametric test was used. All statistical analyses were performed at α=0.05, and Bonferroni-adjusted p-values for multiple comparisons were applied where appropriate.

4.3 Results

4.3.1 Tremor data analysis

4.3.1.1 Essential Tremor is characterised as an action tremor

To verify that participants had a posture-induced tremor, and to verify the sensitivity of the tri-axial accelerometer to record tremor, mean tremor amplitude for resting versus sustained posture was examined. An example recording of accelerometer data recorded from a participant during resting and sustained posture is provided in Figure 4-5 A. This figure illustrates a regular tremor oscillation in the movement of the finger at 6-7Hz during sustained posture, where participants were asked to outstretch their hand. During resting, when the hand and forearm was supported on the participants lap, this oscillatory movement was absent. Tremor frequency was identified as the frequency with peak amplitude in the low-frequency amplitude spectrum (1-20Hz). In the example shown in Figure 4-5 B, a large peak is observed at 6-7Hz during sustained posture, which is absent at rest. Tremor amplitude was taken as mean peak acceleration (m/s^2) at tremor frequency. A significant correlation was shown between the accelerometer measure of tremor amplitude during sustained posture and the clinical FTM measure of tremor severity across participants (r=0.67, p=0.01, r^2=0.45, n=13; Figure 4-5 C), validating the sensitivity of the accelerometer in identifying changes in tremor amplitude.

Paired t-tests were applied to compare mean tremor amplitude as well as subjective ratings of tremor severity for rest vs. sustained posture without visual feedback. This revealed a significant increase in objective tremor amplitude during sustained posture (mean=933.34, SD = 1199.57)

versus resting (mean= 14.78, SD= 21.95; t(12)=-2.76, p=0.017, n=13; Figure 4-6 A), as well as a significant increase in subjective ratings of tremor severity for sustained posture (mean=0.59, SD=0.56) compared to rest (mean = 4.54, SD= 3.22; t(11)=4.45, p=0.001, n=12; Figure 4-6 B).
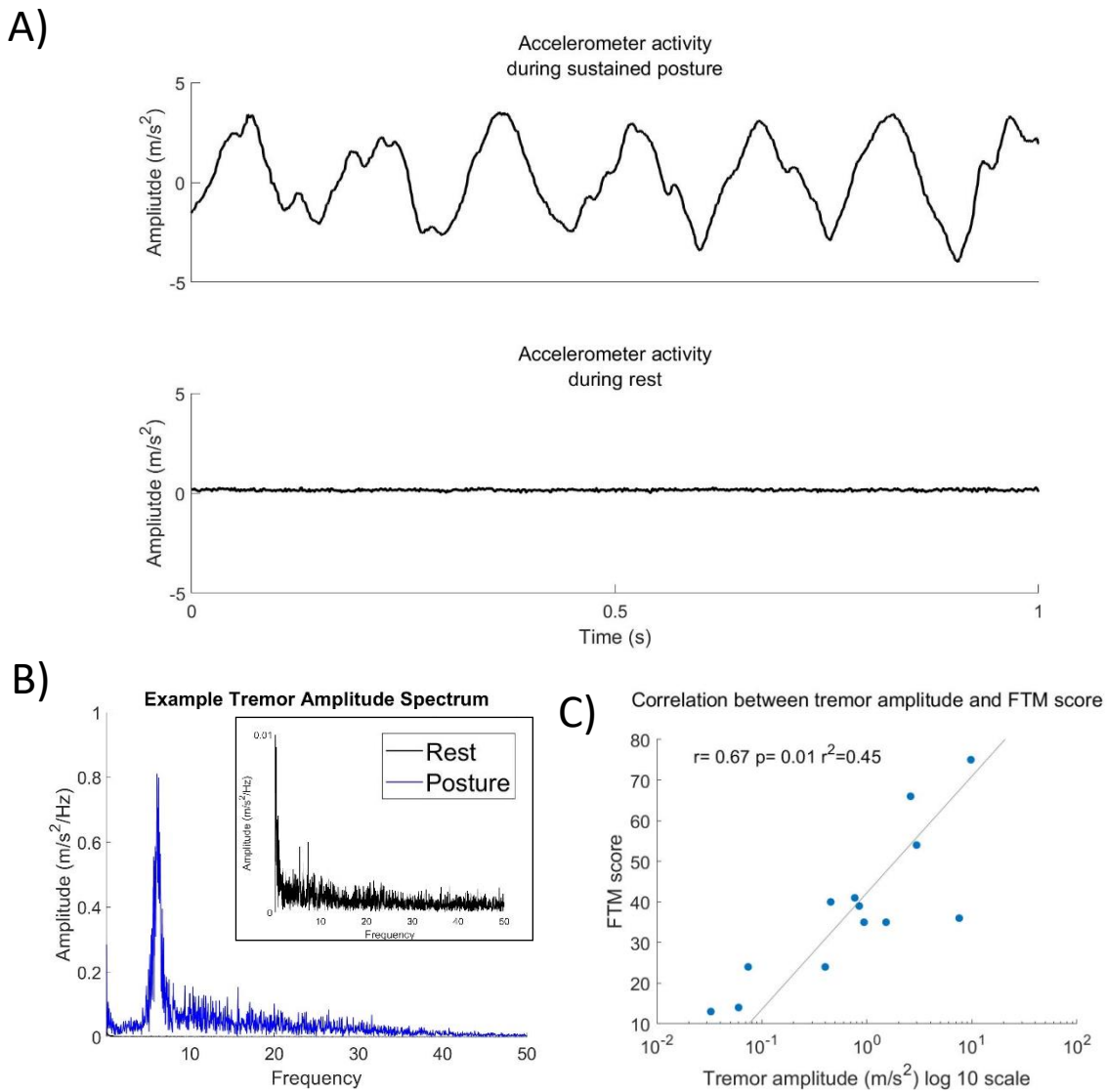
Figure 4-5. Essential Tremor activity increased with sustained posture.
Example accelerometer recording during sustained posture and rest for one individual (A) and the corresponding amplitude spectrum of these recordings (B). (B) inset shows magnification (x100) of the amplitude spectrum, to illustrate the amplitude of accelerometer recordings during rest. The correlation between accelerometer tremor amplitude and FTM scores are provided in (C), where the grey line indicates the least squares regression line.
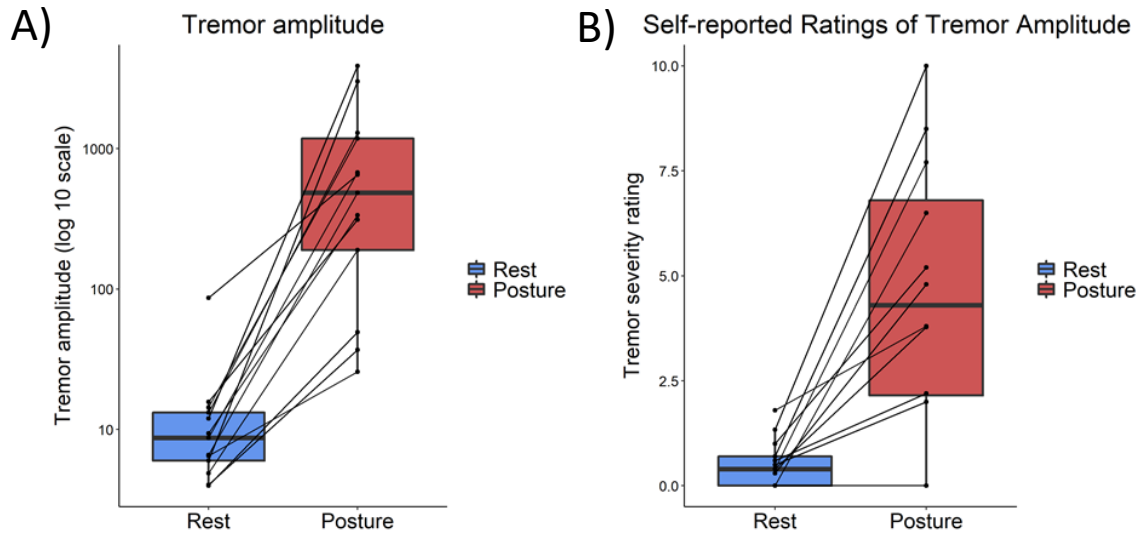
Figure 4-6. Increase in tremor amplitude during sustained posture.
Mean accelerometer tremor amplitude (A) and mean subjective ratings of tremor severity (B) across resting and sustained posture.

4.3.1.2 Essential Tremor frequency

The frequencies of tremor varied across participants, where peak tremor frequency ranged between 5-10Hz. Individual mean tremor frequencies (±SD) are presented with participant demographics reported in Table 4-1. Figure 4-7 A-C provides different examples of the variability in tremor frequency across three participants, where data were pooled across epochs from all visual feedback conditions involving extension of the hand to induce tremor. The first example of tremor frequency variability (Figure 4-7 A) is representative of the majority of participants (11/14 participants) and illustrates that tremor frequency within these participants was stable within ±1Hz. One participant showed rhythmic oscillations at two frequencies simultaneously, which is illustrated in Figure 4-7 B, where peak amplitude switched between oscillatory movements at a higher (9.87Hz) and lower (5.71Hz) frequency. The two peaks in tremor frequency may reflect harmonics of the tremor. For this participant, tremor frequency was taken as the mean frequency at the higher peak (9.87Hz) in the bimodal distribution. Finally, for two of the younger participants, the tremor frequency varied across wider range, as demonstrated by Figure 4-7 C.

To examine the relationship between tremor frequency and individual characteristics, correlations between tremor frequency, age, tremor amplitude, and clinical measures of tremor severity were examined. Analyses revealed a significant negative correlation between tremor frequency and tremor amplitude recorded via the accelerometer (r=-0.57, p=0.04, r^2=0.32, n=13; Figure 4-7 D), where patients with more severe tremor, tended to have a lower tremor frequency. There was also a negative relationship between tremor frequency and clinical FTM scores of tremor severity, but this did not reach significance (r=-0.50, p=0.08, r^2=0.25, n=13; Figure 4-7 E). Age had a stronger correlation with tremor frequency, whereby older patients had a lower tremor frequency (r=-0.78, p=0.002, r^2=0.61, n=13; Figure 4-7 F). There was also a positive relationship between age and tremor amplitude (r=0.55, p=0.05, r^2=0.31, n=13; Figure 4-7 G), such that older patients tended to have a more severe tremor. A partial correlation between tremor amplitude and frequency, which controlled for age, indicated that there was no relationship between tremor amplitude and frequency (r=-0.24, p=0.46). This suggests that age rather than tremor severity was the principal determinate of tremor frequency.
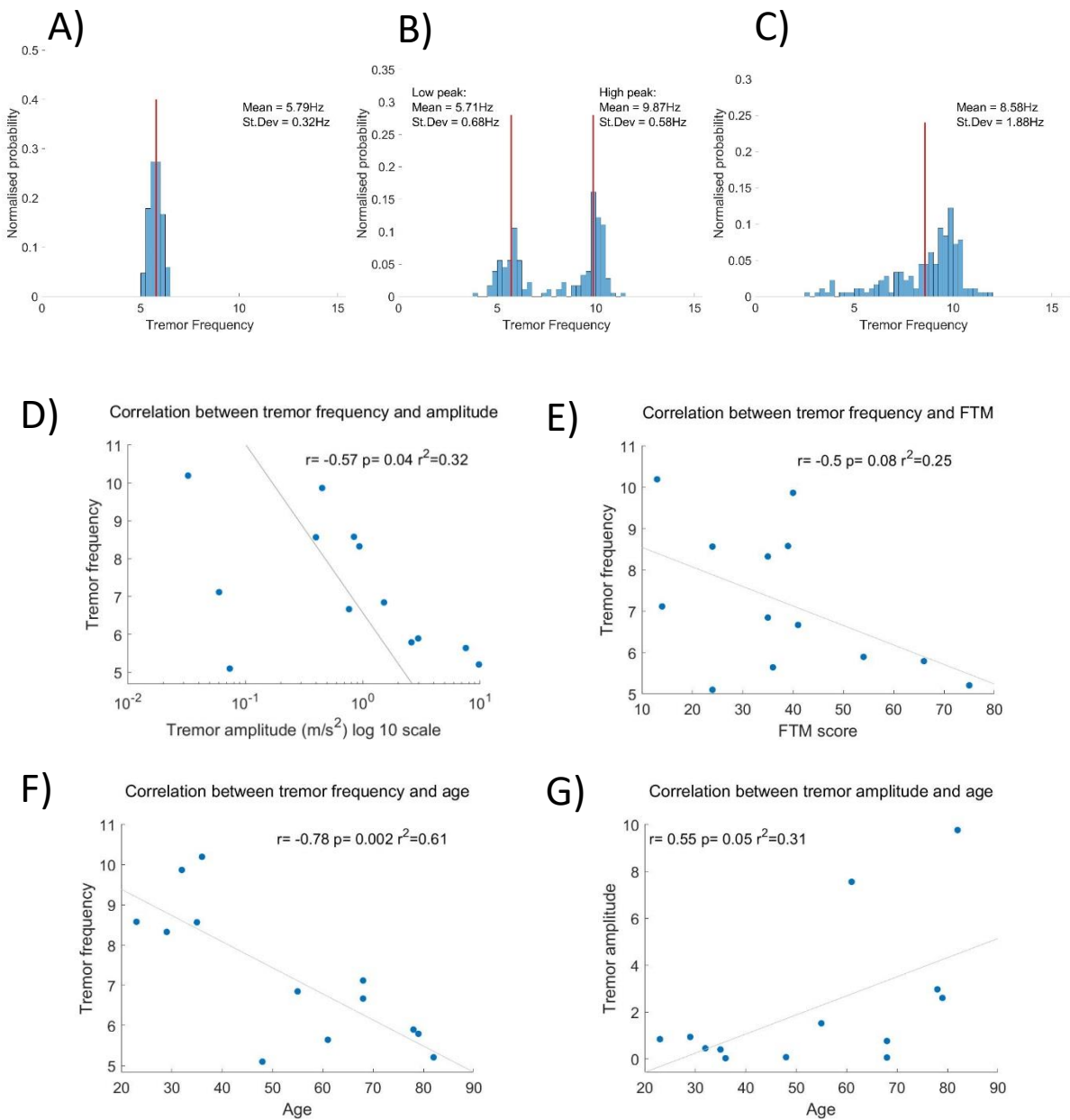
Figure 4-7. Correlations examining the relationship between participant characteristics.
(A-C) Examples of the variability in tremor frequency across three participants, where (A) shows data from a representative participant in which tremor frequency tended to be stable within ±1Hz range of the mean tremor frequency, (B) shows data from a participant whose tremor oscillated at two frequencies, and (C) shows data from a participant whose tremor frequency was not stable. (D-G) shows data from 13 participants examining the correlation between tremor frequency and (D) amplitude, (E) clinical FTM scores of tremor severity, and (F), as well as correlation between age and FTM score (G). The grey line indicates the least squares regression line.

4.3.1.3 Natural visual feedback exacerbates tremor

To examine whether natural visual feedback (i.e. watching tremor in own hands) worsens tremor, mean percentage change in tremor amplitude during natural visual feedback was compared to no visual feedback, where arms/hands were hidden from view. Percentage change in subjective ratings of tremor severity was also calculated.

A one-sample t-test revealed that mean percentage change in tremor amplitude was significantly increased in response to natural visual feedback (mean = 72.77%, SE = 23.76%, $t(11) = 3.06$, $p=0.011$, n=12; Figure 4-8 A), compared to no visual feedback. However, a one-sample Wilcoxon signed-rank test applied to subjective ratings of tremor severity revealed that natural feedback did not significantly change the subjective perception of tremor severity (median = 0%, SE = 9.81%, $Z=0.87$, $p=0.37$, n=12; Figure 4-8 B). This suggests that visual feedback of tremors can have a bigger impact on tremor amplitude than participants may be subjectively aware of. This was supported by a paired sample t-test which showed that percentage change in tremor amplitude was significantly greater for objective compared to subjective measures of tremor amplitude ($t=2.65(10)$, $p=.025$, n=11).
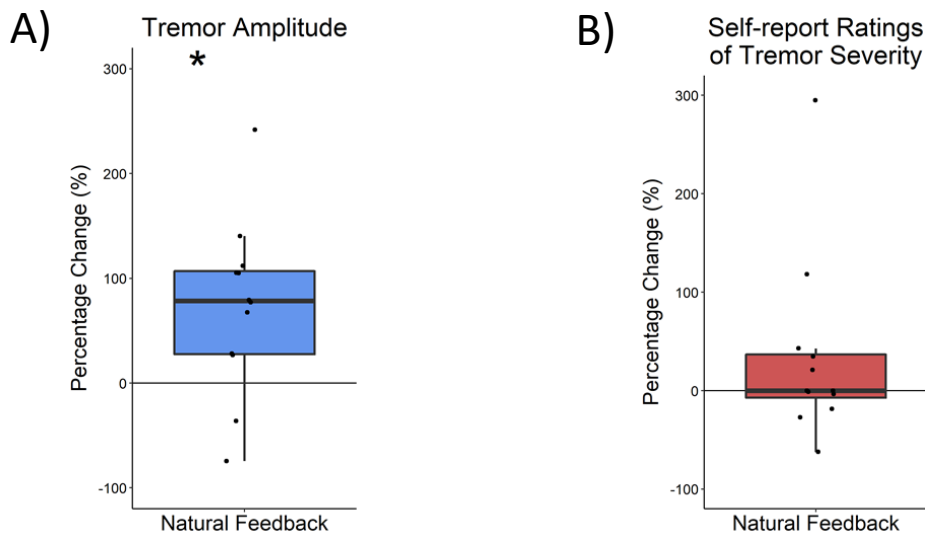
Figure 4-8. Natural visual feedback increased tremor amplitude.
Mean percentage change in accelerometer tremor amplitude (A) and subjective ratings of tremor severity (B) during natural visual feedback compared to no visual feedback. Values above zero indicate an increase in tremor, and values below zero indicate a decrease. * indicates p<0.05.

4.3.1.4 The effect of artificial augmented visual feedback on tremor amplitude

To examine whether artificial visual feedback has the same effect on tremor amplitude as natural feedback, mean percentage change in objective and subjective measures of tremor amplitude during artificial visual feedback were compared to no visual feedback. Here, artificial augmented feedback involved participants watching a moving bar on the LED screen, which oscillated up and down at the same rate as their tremor.

A one-sample Wilcoxon signed-rank test revealed that artificial visual feedback did not significantly change objective (accelerometer) measures of tremor amplitude (median = 21.60%, SE = 14.31%, Z=1.15, p=0.249, n=13; Figure 4-9 A) compared to no visual feedback. However, when examining the percentage change in tremor on an individual level, 8 out of 13 participants showed increased tremor amplitude in response to visual feedback (Figure 4-9 A). Therefore, correlation analyses were performed to examine whether any individual characteristics were associated with increased tremor amplitude in response to artificial feedback. Analyses revealed that percentage change in tremor amplitude in response to artificial feedback was not significantly correlated with participant age (r=-0.01, p=.991, n=13), FTM score (r=-0.10, p=0.742, n=13) or duration of ET (r=0.21, p=0.495, n=13). However, the percentage change in tremor amplitude in response to artificial feedback showed a significant positive correlation with the percentage change in tremor amplitude in response to natural visual feedback (r=0.71, p=0.01, n=12; Figure 4-9 C). This demonstrates that participants who showed a greater increase in tremor in response to natural visual feedback, showed a similar response to artificial visual feedback. Furthermore, those participants who did not show an increase in tremor to natural visual feedback, also showed no increase in tremor to artificial visual feedback.

A one-sample Wilcoxon signed-rank also revealed that subjective ratings of tremor severity did not significantly change during artificial feedback versus no feedback (median = -4.71%, SE = 9.81%, Z=-0.36, p=0.721, n=12; Figure 4-9 B). Furthermore, a paired sample Wilcoxon ranked signed test showed that there was no significant difference between objective and subjective measures of the percentage change in tremor (Z=-0.86, p=0.432, n=12). In contrast to previous research (Archer et al., 2018), these findings suggest that augmented visual feedback did not significantly influence tremor amplitude.
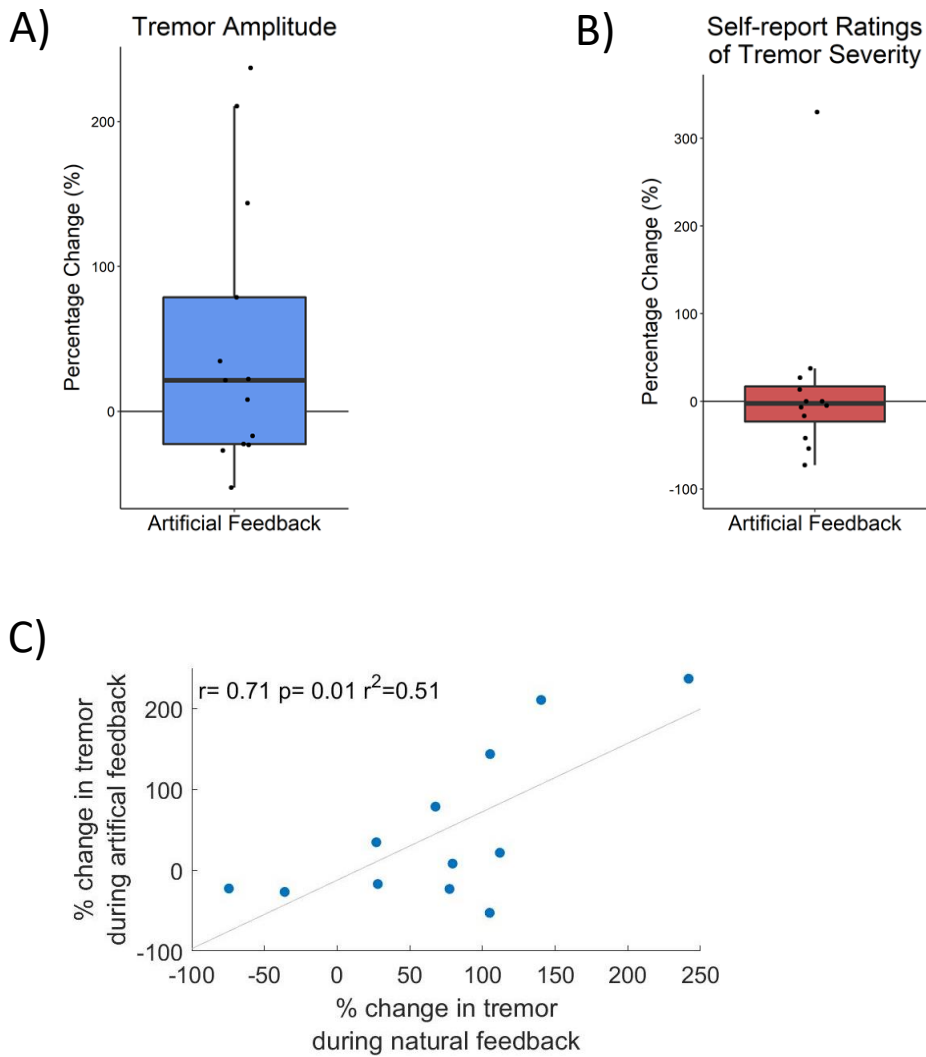
Figure 4-9. Artificial visual feedback did not significantly modulate tremor amplitude.
Mean percentage change in accelerometer tremor amplitude (A) and subjective ratings of tremor severity (B) during artificial visual feedback compared to no visual feedback. Values above zero indicate an increase in tremor, and values below zero indicate a decrease. C) shows correlation between percentage change in tremor amplitude in response to natural and artificial visual feedback.

4.3.1.5   The effectiveness of strategies to reduce tremor

Previous research has suggested that the active effort of trying to reduce tremor may be associated instead with exacerbating tremor, perhaps due to increased motoneuron activity when trying to control the hand (Morrison & Keogh, 2001). Increased tremor amplitude in response to visual feedback may, therefore, be explained by an increased awareness of tremor leading to a greater drive to control/reduce tremor. To examine the influence of internal efforts to control tremor on tremor amplitude, the percentage change in tremor during which participants tried to minimise their tremor compared to not trying to control their tremor was examined. This analysis was restricted to the no visual feedback condition.

A one-sample Wilcoxon signed-rank test revealed that trying to minimise tremors had no significant impact on tremor amplitude on a group level (median = -17.45%, SE = 12.75%, Z=-0.78, p=0.433 n=12; Figure 4-10 A). However, a one-sample t-test applied to subjective ratings of tremor, revealed that participants reported a significant reduction in tremor severity when they were asked to try and minimise their tremors (mean = -29.69%, SE = 6.03%, t(11) = -4.93, p=0.001, n=12; Figure 4-10 B).

This suggests that participants perceived that they were able to exert some control on their tremors, but that this was not measured objectively. However, when inspecting mean percentage change in tremor at an individual level, three participants reported no change in tremor amplitude when trying to reduce tremor (i.e. their percentage change values were at 0%). Out of these three participants, two showed a large increase in objective measures of tremor amplitude when trying to reduce tremor (143% and 54%). Whereas for the participants reporting a reduction in tremor, most were accurate in their judgements (6 out of 8 participants). Furthermore, a paired sample Wilcoxon rank test revealed that there was no significant difference between objective and subjective measures of the percentage change in tremor (Z=-0.26, p=0.846, n=12). Contrary to the mechanism proposed by Morrison & Keogh, (2001), this research revealed that trying to control tremor did not exacerbate tremor.
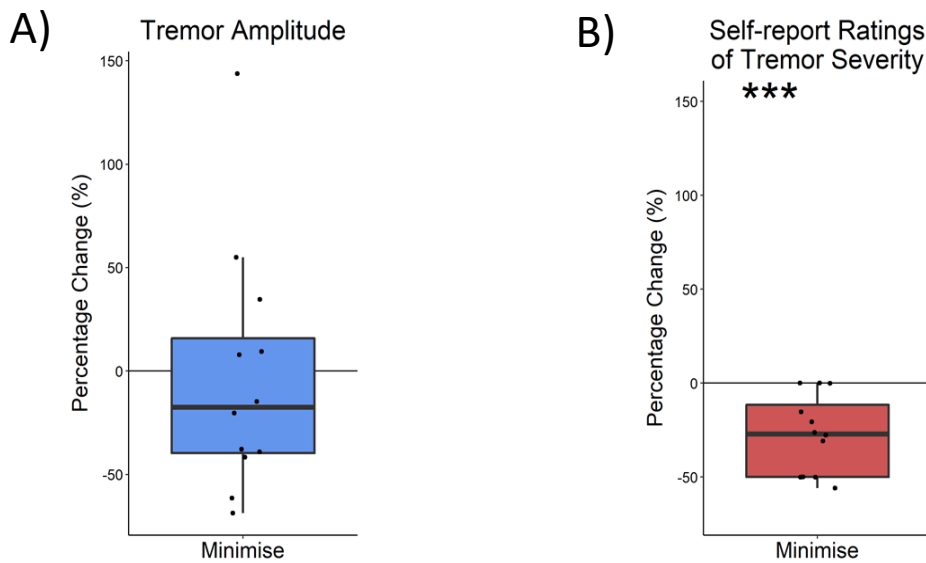
Figure 4-10. Without visual feedback, participants subjectively reported that they were able to reduce their tremors.
Mean percentage change in accelerometer tremor amplitude (A) and subjective ratings of tremor severity (B) when instructed to try and reduce the tremor compared to epochs when instructed to not try and control the tremor. Values above zero indicate an increase in tremor, and values below zero indicate a decrease. *** represents p<0.001.

4.3.1.6   Tremor data interim summary

Analysis examining factors which affect tremor amplitude in ET revealed that natural visual feedback significantly exacerbated tremor. However, augmented artificial visual feedback did not significantly exacerbate tremor. Augmented visual feedback involved visual amplification of the tremor movement, suggesting that increased visual gain of tremor feedback did not exacerbate tremor. Furthermore, this suggests that intrinsic versus extrinsic visual feedback has a greater impact on tremor amplitude. Previous research has suggested that visual feedback increases the awareness of tremor, which may drive increased attempts to reduce tremor activity. However, our findings revealed that attempts to exert control over tremor did not increase tremor amplitude. These analyses also revealed a dissociation between objective and subjective measures of tremor amplitude. Objectively, participant's tremor significantly worsened in response to natural visual feedback. However, subjective reports revealed that participants did not perceive a significant increase in tremor. Conversely, participants reported a significant reduction in tremor amplitude when instructed to minimise their tremor. However objective measures did not reveal a significant reduction in tremor.

4.3.2 EEG data analysis

4.3.2.1 Tremor coherence with central EEG electrodes

The neural correlates of tremor were first examined by cortico-kinematic coherence at a channel level, focusing on central electrodes which overlie sensorimotor regions. Significant coherence between the accelerometer and contralateral and ipsilateral central electrodes at the tremor frequency was examined separately across individual epochs. As reported in the Methods section, the central electrode showing the highest coherence with the tremor, on each side of the hemisphere, was selected for further analysis.

Figure 4-11 A-C shows three examples of cortico-kinematic coherence with contralateral and ipsilateral central electrodes for three different 5-second-long epochs taken from the same subject. For each epoch, the amplitude spectra of the accelerometer are shown on the left, illustrating the frequency of the tremor (i.e. 6Hz in these examples), and coherence between the accelerometer and the contralateral and ipsilateral central electrodes are displayed in the middle and right of the figure, respectively. The significance of coherence was examined using IAAFFT surrogate analysis, whereby coherence values above the surrogate threshold are defined as significant. In epoch 1 (Figure 4-11 A), significant cortico-kinematic coherence at the tremor frequency (6Hz) was found on the contralateral side only, whereas in epoch 2 (Figure 4-11 B), significant coherence at tremor frequency was found bilaterally. In epoch 3 (Figure 4-11 C), significant coherence at tremor frequency was found on the ipsilateral side only. This corresponds with previous research which showed significant coherence with central electrodes can switch between occurring exclusively contralaterally, ipsilaterally, or bilaterally within the same recording (Hellwig et al., 2003).

Previous research also illustrated that, overall, significant coherence was most frequently found exclusively with contralateral central electrodes, where coherence values were significantly higher for the contralateral compared to ipsilateral electrodes (Hellwig et al., 2003). The findings from the current study, however, showed that the probability of significant coherence across bilateral electrodes was greater than significant coherence occurring exclusively with the contralateral or ipsilateral electrodes, as illustrated by Figure 4-11 D. Furthermore, coherence with contralateral electrodes was not greater than with ipsilateral electrodes (Figure 4-11 E). Together, this indicates that significant coherence with electrodes that overlay the sensorimotor regions of the cortex was mostly found bilaterally.
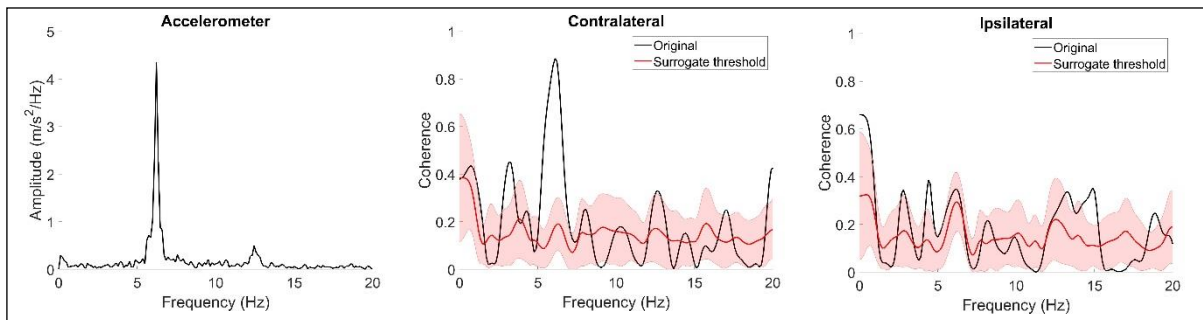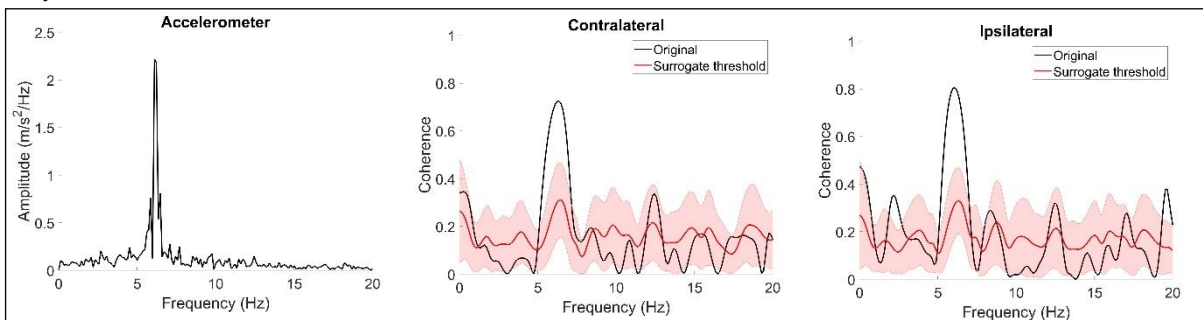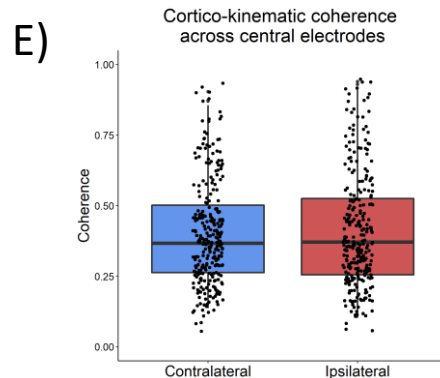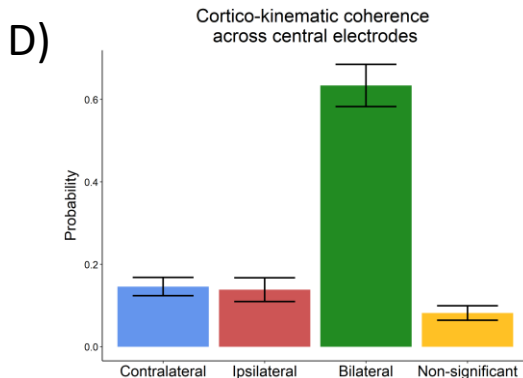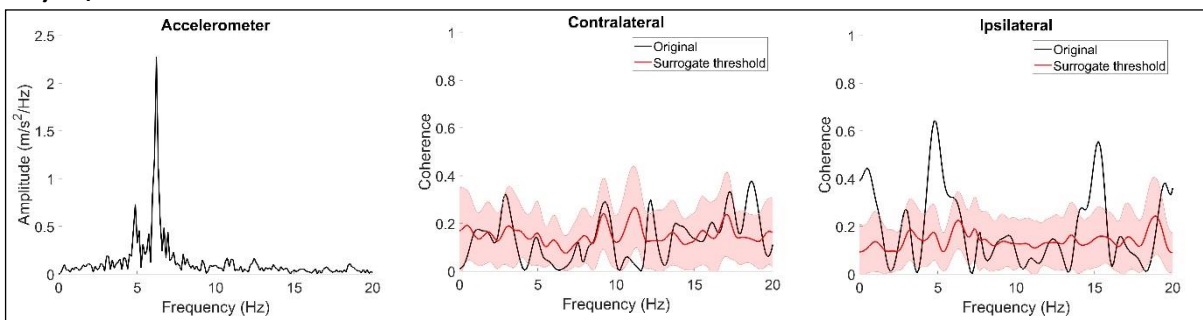
Figure 4-11. Cortico-kinematic coherence with central electrodes.
A-C show examples of accelerometer amplitude spectra and accelerometer coherence with the contralateral and ipsilateral central electrodes. Examples are from three different 5-second-long epochs taken from the same subject and recordings. Accelerometer amplitude and coherence are in black, and mean coherence across 99 surrogates is displayed by the solid red line, and the SD of coherence across the 99 surrogates is indicated by the red shaded region. D) The probability of significant coherence at the tremor frequency with the contralateral side only, ipsilateral side only and bilateral hemispheres or non-significant coherence across participants. E) Surrogate-corrected coherence values at the tremor frequency, for epochs showing significant cortico-kinematic coherence with the contralateral and ipsilateral central electrodes. Individual points reflect coherence values for individual epochs, pooled across participants.

4.3.2.2 Topographical changes in coherence

As significant cortico-kinematic coherence with central electrodes was largely found bilaterally, the next aim was to examine whether increased cortico-kinematic coherence at the tremor frequency was clustered around central electrodes or distributed equally across the scalp. If cortico-kinematic coherence showed an equal distribution across the scalp, this may indicate the presence of movement artefact or volume conduction of tremor activity biasing the data. To examine this, topographic maps of cortico-kinematic coherence at the tremor frequency were computed.

Figure 4-12 displays individual cortico-kinematic coherence maps at the participant's tremor frequency. This figure illustrates that cortico-kinematic coherence was not equally distributed across the scalp. For most participants, clusters of increased cortico-kinematic coherence were located around central rather than peripheral regions of the scalp, which are located further away from the muscles. Together this suggests that bilateral tremor coherence with central electrodes may not be explained by movement of the head or volume conduction of the tremor. However, there was also no clear pattern in the topographic distribution of coherence across participants.

4.3.2.3 Coherent sources identified by DICs

As the surface of the cerebral cortex is covered by gyri and sulci, the orientation of pyramidal cells in the cerebral cortex is not always perpendicular to the scalp, and so electrode-level EEG data analysis (i.e. in the absence of source reconstruction techniques) does not allow inferences to be made in terms of the underlying neuroanatomy. Therefore, to further assess cortico-kinematic coherence associated with tremor, exploratory source analysis was conducted to identify coherent brain sources.

Right hand extended
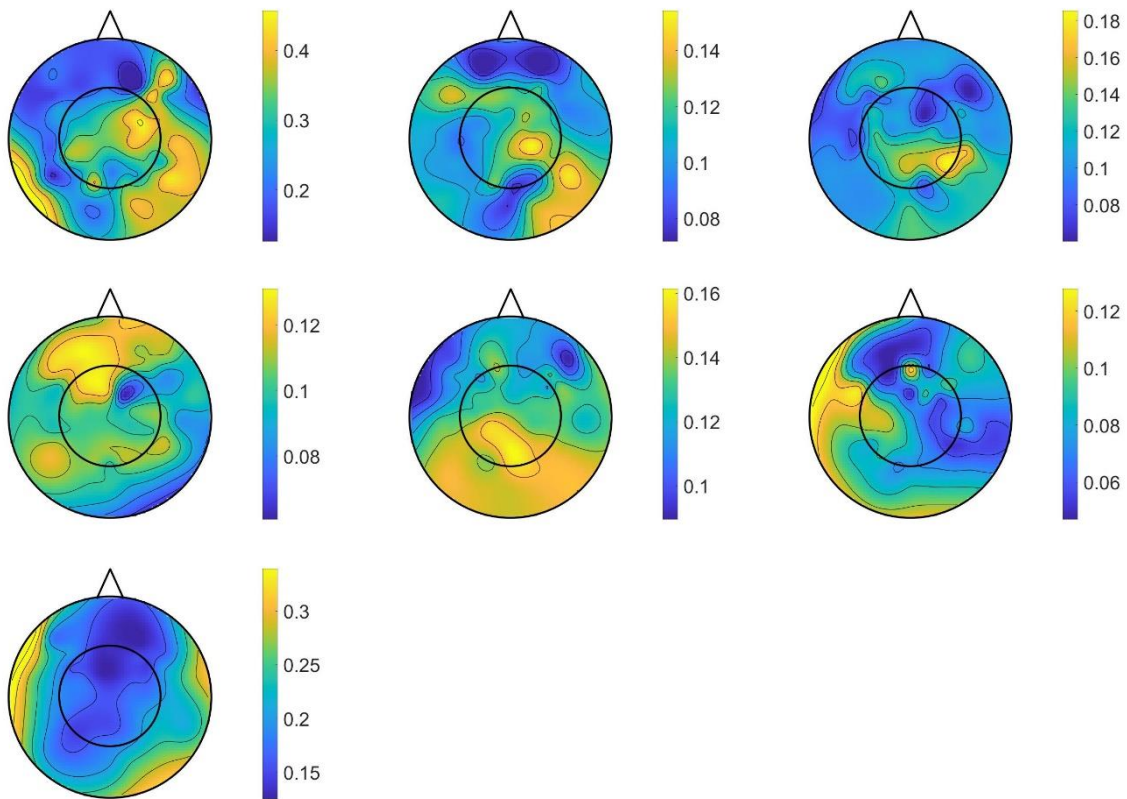
Left hand extended
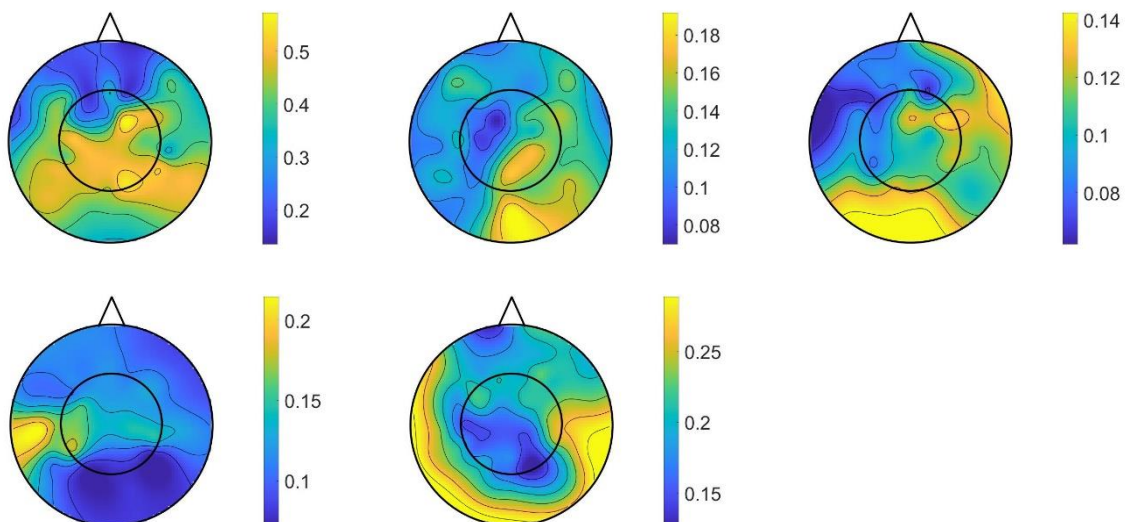
Figure 4-12. Topographic representation of cortico-kinematic coherence at the tremor frequency. Topographic maps represent cortico-kinematic coherence at the participant's own tremor frequency (±1.5Hz) across the scalp. The central circle on the maps identifies the location of the central electrodes. Topographic maps are grouped based on whether tremor was recorded from the right or left hand. The colour bar on each topographic map represents coherence values, where the scale is set to the participants minimal and maximal coherence value (the possible range is between 0&1).

142

4.3.2.4   Identification of coherent sources during posture and rest, without visual feedback

Coherence with the accelerometer at the tremor frequency were estimated across the whole brain volume, and identification of coherent sources were then restricted to the cerebral cortex as estimating coherence for deep brain sources has been shown to be unreliable with EEG (Barzegaran & Knyazeva, 2017). Figure 4-13 illustrates the areas of the brain which showed significantly increased coherence with the accelerometer during posture versus rest without visual feedback. A two-tailed paired t-test revealed a significant increase in cortico-kinematic coherence in regions of the primary sensorimotor cortex (SMC), frontal lobe, SMA, and the superior and inferior posterior parietal cortex during sustained posture compared to rest (Table 4-2 p < 0.01, cluster-corrected, n=12 participants).

4.3.2.5   Identification of coherent sources across conditions

Table 4-3 displays the top ten clustered coherent sources identified by DICS analysis pooled across all participants and visual feedback conditions. The gross locations of these cortical sources are summarised in Figure 4-14.

The top ten coherent sources identified by DICS across all conditions included the same regions showing significantly increased cortico-kinematic coherence during posture versus rest. Namely, the SMC, SMA, the inferior and superior posterior parietal cortex (IPPC & SPPC), and the dorsal lateral prefrontal cortex (PFC). In addition, analysis revealed increased coherence with the primary and associative visual areas, the inferior temporal gyrus, the occipital temporal area, and Broca's area.

These identified regions reflect a visuomotor network. For example, in addition to key cortical motor areas (i.e. the SMC and SMA), the posterior parietal cortex and dlPFC have been shown to be involved in the control of movement (Mulliken et al., 2008; Verstraelen et al., 2020). Broca's area also forms part of the motor network, owing to is connections with neighbouring supplementary and premotor areas, along with the frontal eye field, which controls the movement of the eyes (Ford et al., 2010). Key visual regions include the primary and associative visual areas. In addition, the inferior temporal gyrus and occipital-temporal region both constitute part of the ventral visual pathway, and including motion sensitive areas of the visual pathway such as the middle temporal visual area MT/V5 (Bi et al., 2016; Conway, 2018).
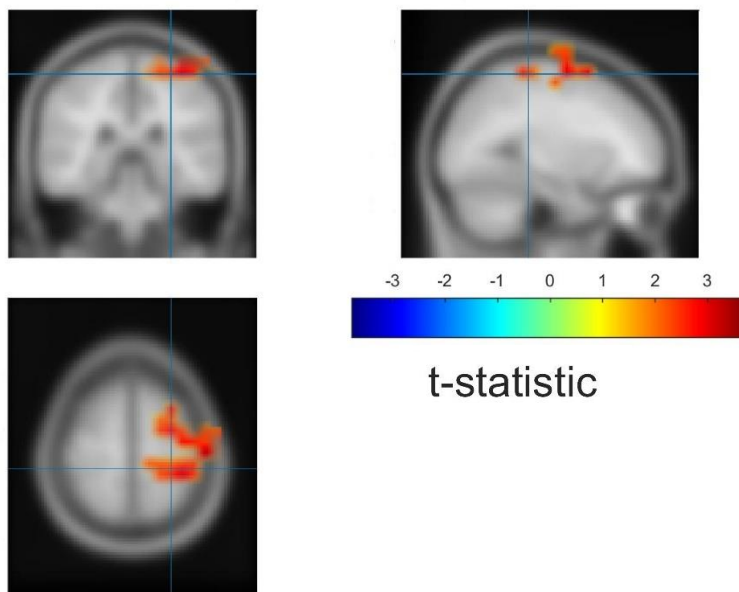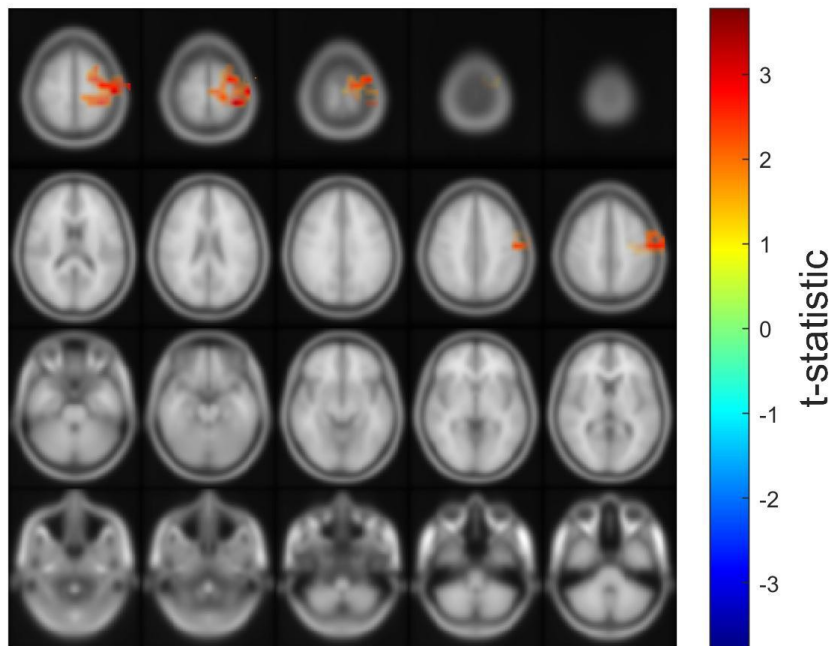
Figure 4-13. Coherent sources during posture versus rest.
Localisations of sources showing significantly increased coherence at the tremor frequency for posture versus rest (two-tailed paired t-test, *p*<0.01 cluster corrected, n=12 participants). The colour bar represents the dependant sample t-statistic.

Table 4-2. Clustered coherent sources identified DICs during sustained posture vs rest

Atlas label	Brodmann Area(S)	Region	Laterality	Cluster size*
Postcentral	1, 2, 3	Primary Sensorimotor Cortex (SMC)	Contralateral	2114
Precentral	4	SMC	Contralateral	1921
Paracentral Lobule	4, 6	SMC	Bilateral	958
Frontal Superior	9	Frontal Lobe	Contralateral	671
Frontal Mid	10	Frontal Lobe	Contralateral	285
SMA	6	Supplementary Motor Area (SMA)	Bilateral	309
Parietal Superior	5, 7	Superior Posterior Parietal Cortex (SPPC)	Contralateral	138
Precuneus	7	SPPC	Contralateral	117
Parietal Inferior	40	Inferior Posterior Parietal Cortex (IPPC)	Contralateral	128
Supra Marginal	40	IPPC	Contralateral	54
*Cluster size = number of voxels (~1.77mm) after interpolating voxel grid to MRI template. All listed regions show *p*-values significant at $p<0.01$, whole brain corrected at cluster levels. N= 12 participants.				

Table 4-3. Top-10 clustered coherent sources identified by DICs across visual feedback conditions.

Rank	Clustered coherent source	Brodmann Area(s)	Rank score*	Ave. TAL co-ordinate, and corresponding Brodmann area	
1	Pre-motor and Supplementary motor area (SMA)	6, 8	367	x: 24.4, y: -6.3, z: 57.5	BA6
2	Associative Visual Cortex	19	318	x: 31.6, y: -71. z: 2.1	BA19
3	Primary Visual cortex	17,18	311	x:17.9, y: -90.1, z: -0.7	BA18
4	Primary Sensorimotor cortex (SMC)	1,2,3,4	255	x:35.1, y: -33.4, z: 53.7	Right: BA4, Left: BA3
5	Inferior Posterior Parietal Cortex (IPPC)	39, 40	232	x: 46.6, y: -51.3, z: 36.6	BA40
6	Inferior temporal gyrus (ITG)	20	191	x: 42.1, y: -3.3, z: -28.5	BA20
7	Superior Posterior Parietal Cortex (SPPC)	5, 7	175	x: 19, y: -64, z: 49.1	Right: BA7, Left: BA5
8	Dorsal Lateral Prefrontal Cortex (dLPFC)	9, 10, 46	159	x: 23.9, y: -39.1, z:36	Right: BA46, Left: BA9
9	Occipital-temporal area	37	143	x: 49.5, y: -52.9, z: -9.5	BA37
10	Broca's area	44, 45	137	x: 49.1, y: 20.4, z: 26.5	BA45

* A rank score was created by assigning an inverse rank value to the top-ten local maxima identified across individuals and conditions. Higher rank sources reflect the greater occurrence of this source across individuals and/or greater coherence within an individual.
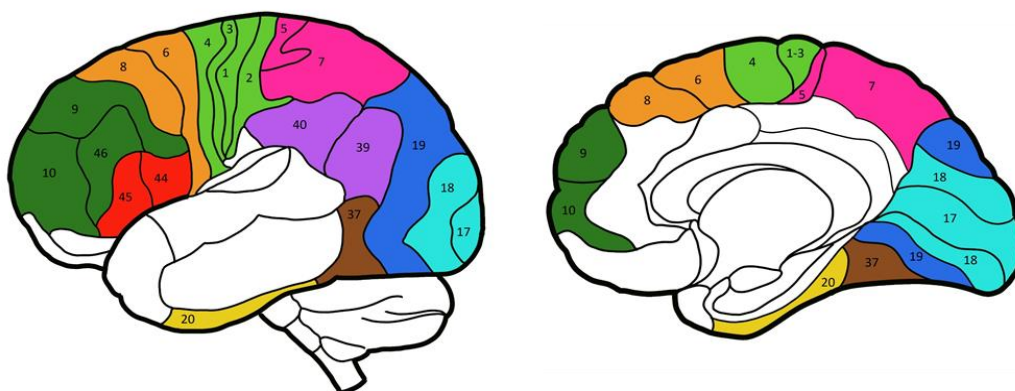
Figure 4-14. Location of clustered coherent sources.
Each coloured area represents a different cluster of cortical source co-ordinates identified by DICs, and the numbers on the brain diagram represent Brodmann areas.

Premotor and SMA =orange, Associative Visual Cortex = Dark blue, Primary Visual Cortex = Light blue, SMC = Light green, IPPC = Purple, SPPC = Pink, ITG = Yellow, dlPFC = Dark green, Occipital temporal area = Brown, Broca's area = Red.

4.3.2.6   Visuomotor coherence at the tremor frequency in response to natural visual feedback

Using the clustered coherent sources identified by DICs across all visual feedback conditions, a multiple regional source model was created by fitting regional sources to the average coordinates for each source identified in Table 4-3. Fitting a regional source model to each subject's data, enabled visuomotor cortico-cortical coherence to be examined across conditions at a group level. As analyses reported above revealed a significant increase in tremor amplitude during natural visual feedback compared to no feedback, the next aim was to examine whether natural visual feedback was associated with changes in visuomotor coupling.

The regional source model included primary and associative/supplementary visual and motor brain sources within both hemispheres of the brain. Therefore, separate three-way (2 × 2 × 2) ANOVAs were applied to examine SMC-visual coherence and SMA-visual coherence, which included visual brain source (primary visual vs associative visual area), hemisphere (contralateral vs ipsilateral) and visual feedback (natural vs. no feedback) as factors. Figure 4-15 (A&B) illustrates the location of the SMC, SMA and primary visual and associative visual cortices, on a schematic of the brain, and the location of these regional sources on the BESA head model.

The three-way ANOVA examining SMC coherence with visual brain areas revealed a main effect of visual feedback approached statistical significance, ($F_{(1,11)}=4.77$, $p=.052$). Figure 4-15 C shows that coherence between both visual areas and the SMC decreased with natural visual feedback vs no visual feedback. No significant main effects of visual brain source nor hemisphere were found, nor any significant interactions (all other p's >.393; Table 4-4). The three-way ANOVA examining SMA coherence with visual brain areas, revealed a significant main effect of visual brain source ($F_{(1,11)}=9.09$, $p=0.012$). Figure 4-15 D shows that coherence between the associative visual cortex and SMA was significantly greater than coherence between the primary visual cortex and SMA. No other significant main effects of visual feedback nor hemisphere were found, nor any significant interactions (all other p value's >.480; Table 4-4). Taken together, these findings indicate that visual feedback was not associated with significant changes in visuomotor coupling. However, there was a trend towards reduced visuomotor coupling for natural visual feedback versus no feedback.
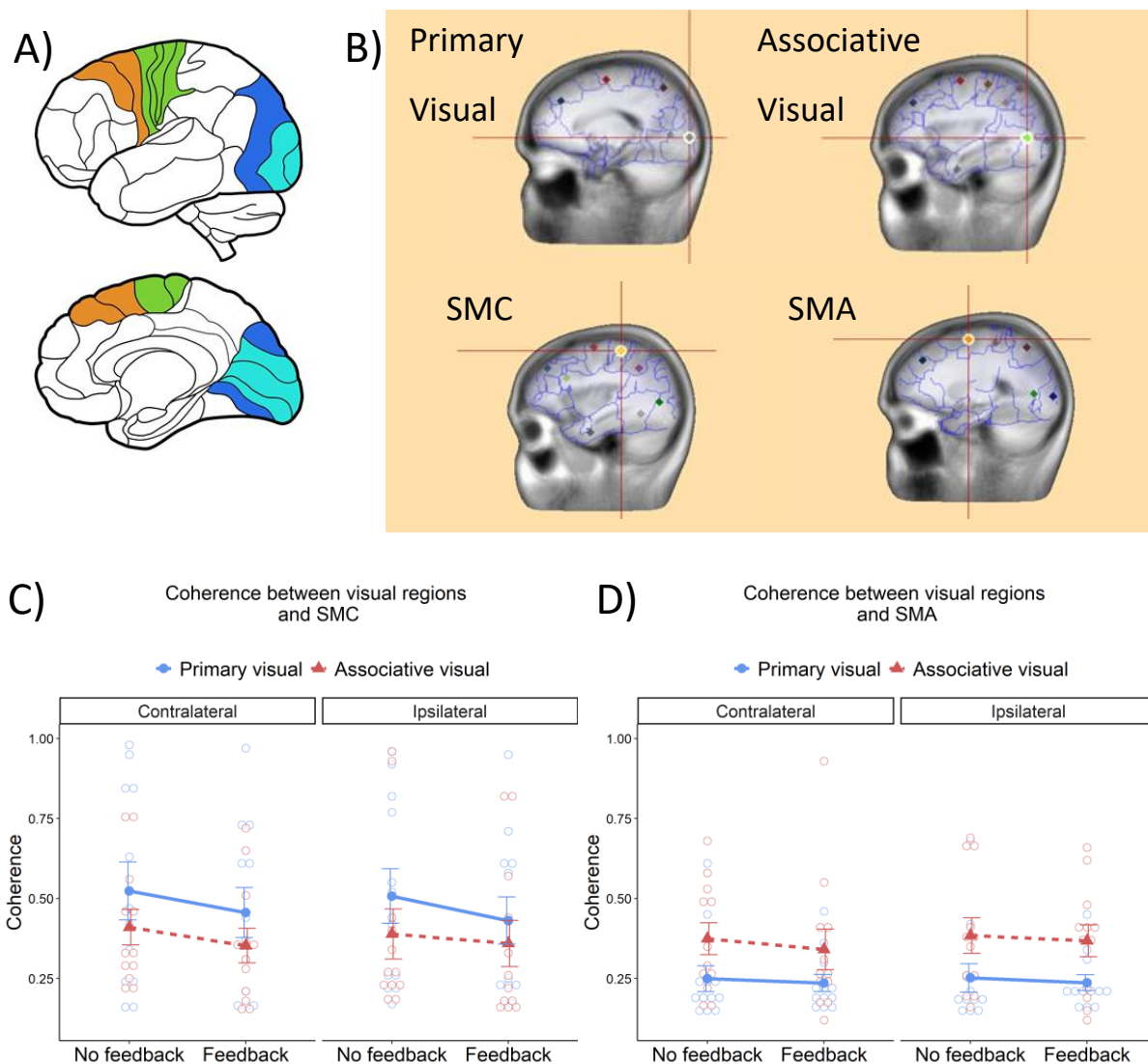
Figure 4-15. Visuo-motor coherence during no visual feedback vs. natural visual feedback.
A) displays the location of the SMC (green) and the SMA (orange) on a schematic of the brain, along with the primary visual cortex (light blue) and the associative visual area (dark blue). B) displays the location of primary visual, associative visual, SMC and SMA regional sources on the BESA brain model. C) Cortico-cortico visuomotor coherence between the SMC and primary visual cortex (blue) and associative visual cortex (red) during the no visual feedback and natural visual feedback conditions. D) Cortico-cortico visuomotor coherence between the SMA and primary visual cortex (blue) and associative visual cortex (red) during the no visual feedback and natural visual feedback conditions. In C&D coherence between brain regions on the contralateral and ipsilateral side to the extended hand are displayed separately, and coherence values for individual participants are shown by the open circles.

Table 4-4. Results from the statistical analyses applied to examine visuo-motor cortico-cortical coherence for natural visual feedback versus no visual feedback.

Variables	Coherence with SMC		Coherence with SMA	
	F	*p-value*	*F*	*p-value*
Visual feedback (A)	4.77	0.052	0.54	0.480
Visual brain source (B)	0.76	0.401	**9.09**	**0.012***
Hemisphere (C)	0.35	0.568	0.15	0.704
A × B	0.28	0.610	0.10	0.758
A × C	0.24	0.635	0.07	0.796
B × C	0.11	0.742	0.14	0.776
A × B × C	0.79	0.393	0.09	0.770

* p < 0.05

4.3.2.7 EEG data interim summary

The scalp-level EEG analysis revealed that significant cortico-kinematic coherence was most typically found bilaterally when examining tremor coherence with central electrodes, where narrow peaks in cortico-kinematic coherence around the tremor frequency were observed, rather than broad peaks across the low frequency range. In addition, the topography of cortico-kinematic coherence at the tremor frequency was not equally distributed across the scalp. This suggests that EEG coherence at the tremor frequency is not related to movement of the head, or volume conduction of the tremor.

DICS whole brain beamformer source analysis revealed that sensorimotor regions of the cerebral cortex showed a significant increase in tremor frequency coherence with the accelerometer during sustained posture versus resting. This included the SMC, SMA, frontal lobe, and the superior and inferior posterior parietal cortex. A regional source model was constructed using average source coordinates taken from DICs analysis across visual feedback conditions. This enabled group-level assessment of visuomotor coherence across visual feedback conditions. This revealed that although there were no significant changes in visuomotor coupling in response to visual feedback, there was a trend towards reduced visuomotor coherence for natural versus no feedback.

4.3.3 Can rhythmic visual stimulation entrain tremor rhythms

The next aim of the study was to examine whether inducing a visually evoked steady-state potential at tremor and non-tremor frequencies, using rhythmic visual stimuli, impacts the amplitude of tremor.

4.3.3.1 Assessment of steady-state potentials evoked by rhythmic visual stimulation

To confirm that rhythmic visual stimulation induced a steady-state potential at the frequency of the visual stimulus, the SNR of EEG oscillations at the frequency of the visual stimulus were assessed. An example of scalp average SNR of EEG rhythms across the low-frequency range is presented in Figure 4-16 A. This figure demonstrates that clear peaks in SNR were identified at the stimulation frequency (indicated by the red marker), and often peaks were also identified at harmonics of this stimulation frequency. Furthermore, for some participants, clear peaks were also observed at the participant's tremor frequency (indicated by the green marker). At each visual stimulation frequency, a one-sample t-test was applied to the scalp average SNR ratio of the stimulation frequency across participants, to examine whether the steady-state potentials were significantly greater than the noise level. Analyses revealed SNR of the steady-state potentials at each stimulation frequency were significantly greater than the noise level of 1 (all p value's <0.002; results reported in Table 4-6). Inspection of the SNRs presented in Figure 4-16 B also shows that the SNRs tended to be higher at higher frequencies. This is related to the 1/f noise, whereby the amplitude of signals is inversely proportional to the frequency of a signal, and therefore background noise at lower frequencies is proportionately higher.
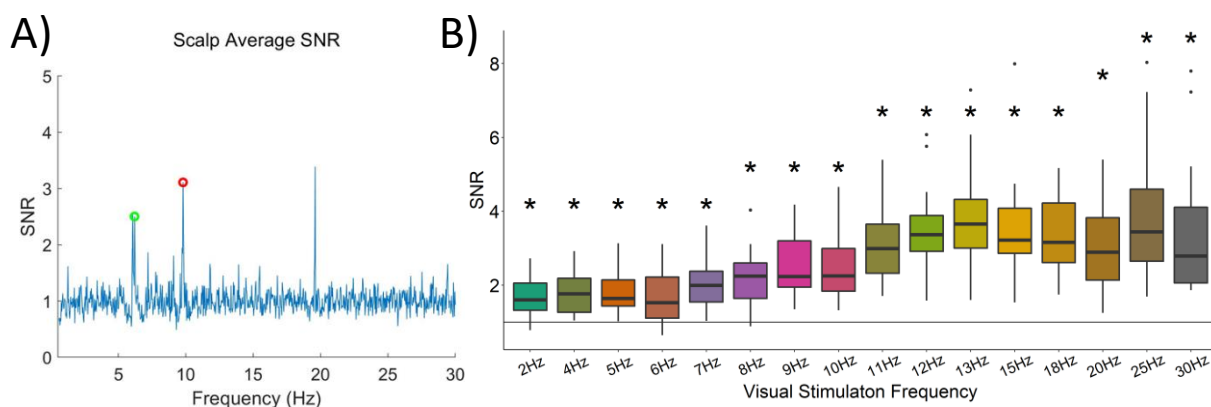
Figure 4-16. Signal to noise ratio (SNR) of steady state potentials.
A) displays an example of the scalp average SNR of EEG signals during a 10Hz flashing LED stimulus. The SNR value at the 10Hz stimulus is indicted by the red marker. The green marker indicates the frequency of the participant's tremor. B) shows the SNR across participants for each visual stimulation frequency. * indicates significant at p=.001.

4.3.3.2   The effect of rhythmic visual stimulation on tremor amplitude

The subsequent aim was to examine whether rhythmic visual stimulation at the tremor frequency or a harmonic of the tremor frequency, modulated tremor amplitude. To analyse this, percentage change in tremor amplitude during each visual stimulation frequency was calculated in comparison to no visual feedback. As rhythmic stimulation was presented at fixed frequencies, percentage change in tremor amplitude was examined for visual stimulation frequencies that were closest or 'near' to the patient's tremor frequency (condition 1) and closest to double their tremor frequency (condition 2). Mean percentage change in tremor amplitude was also calculated across conditions that involved stimulation at frequencies 'near to' the fundamental or harmonic frequencies of the tremor (termed as synchronous frequencies; condition 3), and across conditions that involved stimulation at frequencies that were not near harmonics of the tremor frequencies (termed as asynchronous frequencies; condition 4). Finally, to examine whether a flashing visual stimulus at any frequency (condition 5), or any non-tremor frequency (condition 6), modulated tremor amplitude, mean percentage change in tremor was calculated across all stimulation frequencies, or all non-tremor frequencies, respectively. An example of how these visual stimulation conditions were categorised for an individual participant is displayed in Table 4-5.

Percentage change in tremor amplitude across each of these six conditions is displayed in Figure 4-17 A. The Friedman test revealed that there were no statistically significant differences in percentage change in tremor across these conditions ($\chi^2(5) =4.245$, p=0.531, n=14). One-sample tests were also performed on each condition, to compare median percentage change in tremor amplitude from zero, which revealed no significant change in tremor amplitude (all p value's >0.331; results reported in Table 4-6).

Due to the large differences in tremor severity across the participants group, the relationship between clinical tremor severity and percentage change in tremor amplitude for each condition was also examined using bivariate correlations. Analyses revealed a trend towards a negative relationship between clinical tremor severity and percentage change in tremor in response to synchronous frequencies (r=-0.488, p=0.07, n=14), where participants with a mild tremor tended to show an increase in tremor amplitude, and participants with a severe tremor tended to show a decrease in tremor amplitude in response to visual stimulation at frequencies that were a harmonic of their tremor frequency. For all other conditions, there was no correlation between percentage change in tremor amplitude and clinical measures of tremor severity (all p value's > 0.237; Table 4-6).

Some participants showed a large increase in tremor amplitude during certain visual stimulation frequencies. Therefore, to examine whether there were any fixed frequencies which significantly modulated tremor amplitude at a group level, percentage change in tremor amplitude across each visual stimulation frequency was also assessed. A Friedman test revealed that there no were differences in percentage change in tremor across visual stimulation frequencies (χ^2(15) =16.8 p=0.331, n=14; Figure 4-17 B). One-sample tests comparing median percentage change in tremor amplitude for each visual stimulation frequency compared to zero revealed that none of the frequencies significantly changed tremor amplitude from baseline (all p value's > 0.331; results reported in Table 4-6).

4.3.3.3   Order effects

As muscle fatigue is known to impact tremor amplitude, analyses further examined whether the order of stimulation blocks significantly modulated tremor amplitude. The Friedman test revealed that there were no statistically significant differences in percentage change in tremor amplitude across blocks (χ^2(15) =17.67, p=0.281). One-sample tests applied to each block also revealed tremor amplitude did not significantly differ from baseline in any block (all p value's > 0.084; results reported in Table 4-6). However, there was a trend towards increased tremor amplitude for the final block. Inspection of the box plots displaying percentage change in tremor amplitude across blocks (Figure 4-17 C) also indicates an increased distribution of percentage change in tremor amplitude for the final three blocks. This suggests that there may have been some impact of fatigue on tremor amplitude during the final visual stimulation conditions.

4.3.3.4   Rhythmic visual stimulation interim summary

SNR analysis revealed that rhythmic visual stimulation induced a steady-state potential at the frequency of the visual stimulus with a relatively high SNR. However, rhythmic visual stimulation at the tremor frequency, or a harmonic of the tremor frequency, did not significantly modulate tremor amplitude. Nevertheless, a trend towards a negative relationship between clinical tremor severity and percentage change in tremor in response to synchronous frequencies was found. This indicated differential effects of visual stimulation at harmonic frequencies of the tremor for patients with mild vs. severe tremor, where participants with a mild tremor tended to show increased tremor amplitude in response to visual stimulation at frequencies that were a harmonic of their tremor frequency. Some participants showed very large increases in tremor amplitude (>200%) to certain stimulation frequencies. However, this was not related to the presentation block order of visual stimulation frequencies and increased fatigue.

Table 4-5. Example of visual stimulation condition categorisation

Fixed visual stimulation frequencies:

2 – 4 – 5 – 6 – 7 – 8 – 9 – 10 – 11 – 12 – 13 – 15 – 18 – 20 – 25 – 30Hz

	Condition	Categorised as mean percentage change in tremor amplitude in response to the following visual stimulation frequencies:	Example: If the participants mean tremor frequency without visual stimulation is 5.7Hz, mean percentage change in tremor amplitude at the following visual stimulation frequencies were examined:
1	**Near tremor frequency**	Mean tremor frequency rounded to nearest fixed visual stimulation frequency.	6Hz
2	**Double tremor frequency**	Double the mean tremor frequency rounded to nearest fixed visual stimulation frequency.	11Hz
3	**Synchronous tremor frequencies**	Mean across visual stimulation frequencies that are closest to the fundamental, first, and second harmonic frequencies of the mean tremor frequency.	Mean across 6Hz, 11Hz, 18Hz
4	**Asynchronous tremor frequencies**	Mean across all visual stimulation frequencies that are not closest to the harmonic frequencies of tremor	Mean across all frequencies except 6Hz, 11Hz, and 18hz
5	**All stimulation frequencies**	Mean across all stimulation frequencies	Mean across all 16 frequencies
6	**Non-tremor stimulation**	Mean across non-tremor stimulation frequencies	Mean across all frequencies except 6Hz
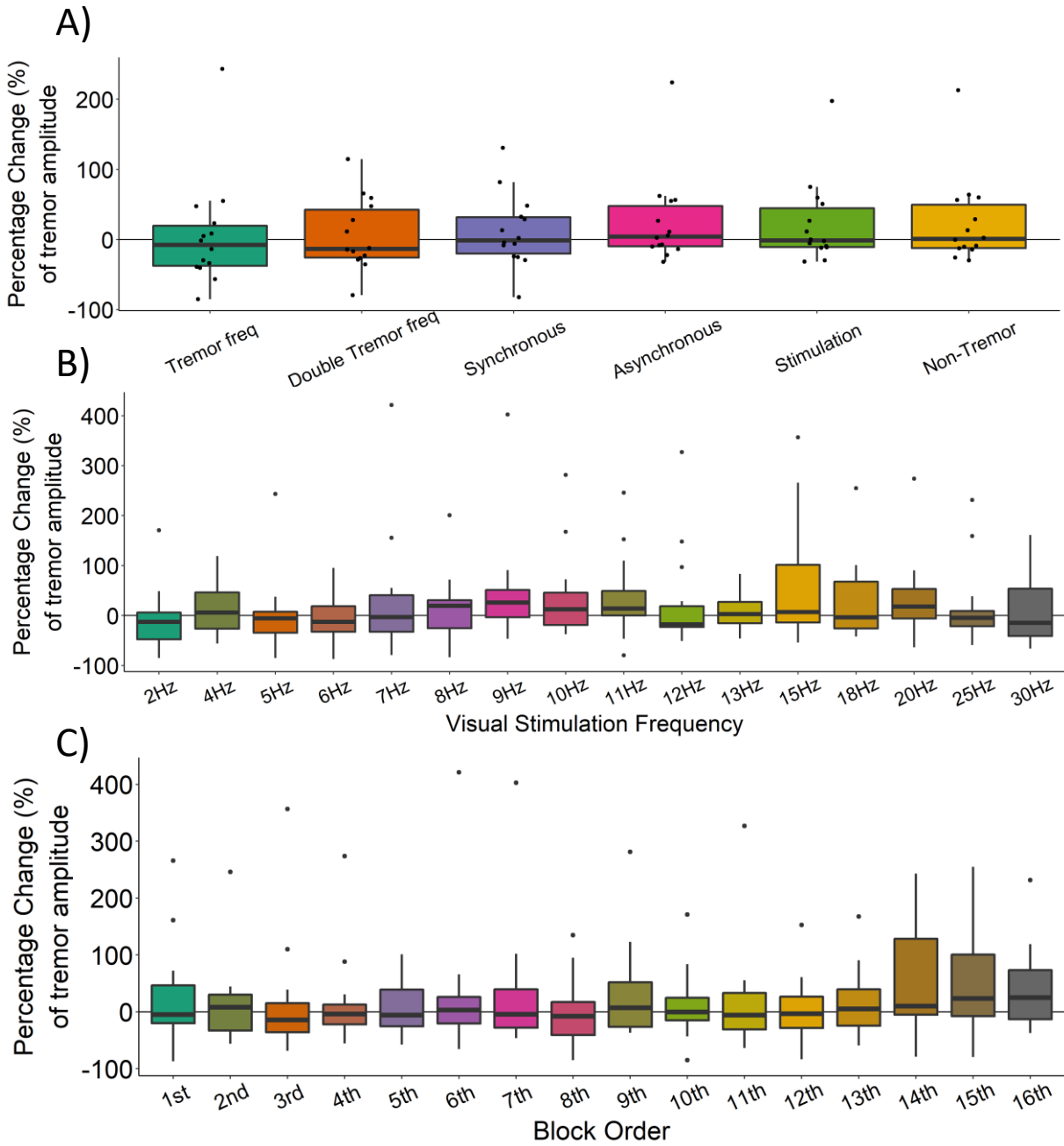
Figure 4-17. The effect of rhythmic visual stimulation on tremor amplitude.
Percentage change in tremor amplitude across six visual stimulation conditions is shown in A), where all data points across participants are displayed by individual dots. B and C) show percentage change in tremor across all visual stimulation frequencies, and all blocks, respectively. Here only outlying points are indicated by individual dots.

Table 4-6. Results from the statistical analyses applied to examine percentage change in tremor amplitude, and steady-state potential SNR, in response to visual stimulation.

Visual Stimulation Condition	One-sample Wilcoxon Signed Rank Test		Correlation between clinical tremor severity and % change in tremor amplitude	
	Z	p	r	p
Tremor frequency	-0.47	0.638	-0.33	0.248
Double tremor frequency	0.16	0.875	-0.34	0.237
Synchronous	0.53	0.594	-0.49	0.077
Asynchronous	0.97	0.331	-0.17	0.574
Stimulation (any frequency)	0.79	0.433	-0.22	0.446
Non-tremor frequencies	0.91	0.363	-0.20	0.497

One-sample Wilcoxon Signed Rank Test

SNR of EEG signal across stimulation frequencies			Tremor amplitude across stimulation frequencies			Tremor amplitude across block order		
	Z	p		Z	p		Z	p
2Hz	3.30	0.001	2Hz	-1.22	.221	1st	0.47	0.638
4Hz	3.30	0.0001	4Hz	0.85	.397	2nd	0.03	0.975
5Hz	3.30	0.001	5Hz	-0.97	.331	3rd	-0.72	0.470
6Hz	3.30	0.001	6Hz	-0.66	.510	4th	-0.16	0.875
7Hz	3.30	0.001	7Hz	0.16	.875	5th	0.28	0.778
8Hz	3.30	0.001	8Hz	0.85	.397	6th	0.28	0.778
9Hz	3.30	0.001	9Hz	1.41	.158	7th	0.22	0.826
10Hz	3.30	0.001	10Hz	0.97	.331	8th	-0.28	0.778
11Hz	3.30	0.001	11Hz	1.73	.084	9th	0.91	0.363
12Hz	3.30	0.001	12Hz	-0.28	.778	10th	0.28	0.778
13Hz	3.30	0.001	13Hz	0.53	.594	11th	-0.16	0.875
15Hz	3.30	0.001	15Hz	1.35	.177	12th	-0.16	0.875
18Hz	3.30	0.001	18Hz	0.79	.433	13th	0.60	0.551
20Hz	3.30	0.001	20Hz	1.73	.084	14th	1.41	0.158
25Hz	3.30	0.001	25Hz	-0.41	.683	15th	1.35	0.177
30Hz	3.30	0.001	30Hz	0.22	.826	16th	1.73	0.084

4.4 Discussion

The results from this Chapter revealed that ET patients show significant cortico-kinematic coherence with central electrodes overlying sensorimotor brain regions, where coherence was most frequently found bilaterally. Source analysis revealed significantly increased cortico-kinematic coherence with sensorimotor regions of the cerebral cortex, including the SMC, SMA, frontal lobe, and the superior and inferior posterior parietal cortex. When examining the effect of visual feedback on tremor amplitude, analyses showed that natural visual feedback can exacerbate tremor in ET. However, artificial visual feedback did not significantly exacerbate tremor at the group level. This suggests that intrinsic rather than extrinsic visual feedback has a greater impact on tremor amplitude, in tasks that involve passive visual feedback rather than goal-directed actions. Furthermore, findings revealed that attempts to exert control over tremor did not increase tremor amplitude. Therefore, increased cortico-spinal control over tremor may not explain the effect of exacerbated tremor amplitude in response to visual feedback. A trend towards a reduction in visuomotor coherence in response to natural visual feedback also suggests that exacerbation of tremor is not explained by increased visuomotor coupling. Furthermore, inducing steady-state potentials at frequencies 'near' to the tremor frequency, or harmonics of the tremor frequency, did not impact tremor amplitude.

4.4.1 Bilateral cortico-kinematic coherence with central electrodes

In line with previous research (Hellwig et al., 2001, 2003), narrow-band peaks in coherence at the tremor frequencies were found between the accelerometer and central electrodes. However, in contrast to this research, the current study revealed that significant coherence was typically found bilaterally rather than contralaterally, and coherence was not stronger on the contralateral side. One possibility is that coherence between unilaterally stimulated postural tremor and bilateral central electrodes could be an artefact of head movement or volume conduction of the tremor. However, inspection of topographic changes in coherence across the scalp revealed that cortico-kinematic coherence was not equally distributed across the scalp, which may be expected if coherence was related to head movement or volume conduction. Instead, bilateral, or ipsilateral coherence may be related to increased resting tremor on the non-recorded hand or bilateral synchronisation of the motor cortex.

Previous research has shown that M1 can be activated bilaterally during unilateral movements (Brus-Ramer et al., 2009; Cisek et al., 2003; Donchin et al., 2002). For example, healthy controls performing unilateral voluntary movements of their index finger showed bilaterally coherent alpha rhythms across central electrodes (Florian et al., 1998). Anatomical evidence shows cortico-

spinal tracts predominately cross over to the contralateral side of the body, although evidence also points to a minority of ipsilaterally descending cortico-spinal connections (Jankowska & Edgley, 2006), as well as interhemispheric connections (Brus-Ramer et al., 2009). As ET is associated with abnormal functioning of sensorimotor regions, it may be ET patients develop a greater reliance on ipsilateral or interhemispheric sensorimotor connections.

Research has also shown that increased SNR of tremor activity recorded via EMG was associated with significant bilateral EEG-EMG coherence (Hellwig et al., 2003), whereby the authors suggest that bilateral coherence may be a clinical correlate for more severe cases of tremor. However, in the current study there was a wide range in tremor severity across participants, and bilateral EEG-accelerometer coherence was found across the pooled sample. Therefore, bilateral coherence observed in this study may also be due to the greater SNR of tremor recorded via the accelerometer compared to EMG.

4.4.2 The involvement of sensorimotor regions of the cerebral cortex in tremor activity

This study was the first to examine cortico-kinematic coherence with tremor activity, as opposed to cortico-muscular coherence, where EEG coherence with tremor was examined using accelerometer rather than EMG measures of tremor activity. In accordance with previous research, this study revealed significant postural tremor cortico-kinematic coherence with sensorimotor regions of the cerebral cortex (Muthuraman et al., 2012, 2018; Pedrosa et al., 2017). Previous studies have applied a region of interest approach to identifying coherent sources using DICS, whereby analysis was restricted to motor cortical and cerebellar regions (Pedrosa et al., 2017), or focused only on time-intervals where coherence was greatest (Muthuraman et al., 2012, 2018). The results reported in this Chapter expand on this research by identifying significantly coherent sensorimotor cortical brain sources following a whole-brain exploratory analysis. Furthermore, this study revealed that coherent cortical sources extend to frontal and posterior parietal regions of the cerebral cortex, which also play a role in motor control (Mulliken et al., 2008; Verstraelen et al., 2020). Consequently, these findings provide further support that sensorimotor regions of the cerebral cortex play a role in propagating tremor oscillations in ET.

4.4.3 Natural visual feedback has a greater impact on postural tremor than augmented visual feedback

This study revealed that natural visual feedback but not augmented artificial visual feedback significantly exacerbated tremor in ET during a passive visual feedback task. However, at a group level, tremor amplitude during augmented artificial visual feedback was still greater than no visual feedback. This may suggest that intrinsic (natural) feedback has a greater impact on tremor

amplitude than extrinsic (augmented) feedback in passive visual feedback tasks. Previous research which has shown that augmented visual feedback exacerbates tremor in ET have employed tasks which require contraction of hand muscles to apply a target amount of force (Archer et al., 2018; Neely et al., 2015). These tasks involve both co-ordinated control of multiple joints, and goal-directed behaviour that is visually guided. The task in the current study, however, involved a more passive motor task, that did not involve application of force or visually guided goal-directed movements. And so, participants may rely less on visual stimuli and more on somatosensory signals from hand/finger movements or positioning. Previous research has shown that congruent versus incongruent visual inputs provide a more accurate estimate of limb position/location (Christie et al., 2019; Stone et al., 2018). Therefore, directly watching the hand (congruent visual input) versus watching an exaggerated one-dimensional movement (incongruent visual input) may enhance sensorial awareness of the peripheral tremor, resulting in increased tremor amplitude in response to natural but not augmented visual feedback in the current study. Future research examining the effect of augmented visual feedback on tremor amplitude in a passive motor task may benefit from the use of a 3D virtual space or manipulated recording of the participants hand, to provide a more comparable visual input.

Natural visual feedback has previously been shown to significantly increase tremor in ET (Gironell et al., 2012), where tremor amplitude increased in 14 out of 19 ET patients. However, in the Gironell et al., (2012) study, participants were instructed to try and minimise their finger tremor during visual feedback compared to no visual feedback where eyes were closed. Therefore, this design examined natural visual feedback and attempts to minimise tremor amplitude separately. As previous research suggested that trying to reduce tremor may instead exacerbate tremor (Morrison & Keogh, 2001), instructing participant to try and minimise their tremor may have additionally contributed to exacerbated tremor in the visual feedback condition. The current study therefore included an additional manipulation contrasting tremor amplitude when participants were asked not to attempt to control their tremor versus trying to minimise their tremor. This revealed that attempts to reduce tremor did not exacerbate tremor, and most participants were able to exert some control over their tremors. Therefore, the results from this study confirm that natural visual feedback and not attempts to minimise tremor, is likely to explain the effect of exacerbated tremor during hand/finger extension in the study by Gironell et al., (2012).

4.4.3.1 Neurophysiological mechanisms underlying exacerbated tremor in response to visual feedback

One of the aims of this Chapter was to examine whether exacerbated tremor in response to visual feedback was associated with increased coupling between the visual and motor network. To examine this, a flashing stimulus at near to tremor frequencies was delivered to assess whether increasing the amplitude of EEG rhythms at the tremor frequency impacts behavioural tremor amplitude. However, this study showed that inducing an oscillation in EEG rhythms at near to tremor frequencies did not affect tremor amplitude. One limitation of this method is that the steady state potentials induced by watching flashing stimuli were at a fixed frequency, whereas the recorded tremor oscillations varied over a narrow range of frequencies (e.g. ±1Hz). Furthermore, the steady state potentials induced by flashing stimulus at fixed frequencies were not aligned with the tremor in terms of the phase of the oscillations. Previous research which applied transcranial alternating current stimulation (TACS) over the motor cortex in PD (Brittain et al., 2013), or thalamic stimulation in ET (Cagnan et al., 2013, 2017), at near to tremor frequencies, showed that the phase alignment of the applied stimulation with the tremor oscillation can significantly impact the effect of tremor frequency neural stimulation on tremor amplitude. Therefore, phase alignment of the flashing visual stimulus to the tremor would provide a more accurate assessment of whether visual synchronous inputs with the tremor influence visuomotor neural coupling and tremor amplitude.

The synchronisation of tremor frequency oscillations across visual and motor brain areas in response to visual feedback was further examined by visuomotor coherence during natural visual feedback compared to no visual feedback. This showed that despite worsening of tremor during natural visual feedback, there was a trend towards reduced visuomotor coherence at the tremor frequency during natural versus no visual feedback. This contrasts with the hypotheses of the experiment and with previous research in healthy participants, which demonstrated that synchronised visual input and motor output lead to increased visuomotor coherence (Classen et al., 1998). Instead, these findings may therefore be indicative of impaired visuomotor communication in ET. Previous research has suggested that ET patients with head tremor performed significantly worse in a predictive motor timing task that involved pressing a button to intercept a moving virtual target (Bareš et al., 2010). This task involved integrating incoming visual information with motor output and may therefore indicate that individuals with severe ET show impaired visuomotor integration. To support this, there also been evidence to suggest ET is associated with grey and white matter changes in occipital lobes (Benito-León et al., 2009, 2019; Tuleasca et al., 2017, 2018).

Exacerbated tremor during motor tasks that require goal-directed actions could also be attributed to disrupted neural processing relating to movement error. The cerebellum plays an important role in error detection and correction of movement in response to feedback, and research has identified pathological changes occurring within the cerebellum in ET (Louis, 2016). Therefore, ET may be associated with disruption of cerebellar-dependant error correction mechanisms. However, it is unlikely that increased visual feedback of movement would impact online cerebellar processing relating to error detection and correction and to influence tremor amplitude via this mechanism. For example, visual cues have long neural delays and therefore cerebellar control of routine behaviours are theorised to have a greater reliance on predictive internal models of behaviour than real-time visual cues (Cerminara et al., 2009). Furthermore, research by Archer et al., (2018) suggests that tremor amplitude is not related to movement error, as augmented visual feedback significantly increased tremor amplitude but decreased the goal-directed performance error. The cerebellar feedback error-learning model suggests the central nervous system learns and adapts movements by making predictions about the sensory consequences of an action, and calibrating movements based on sensory prediction error (Kawato, 1999; Kawato & Wolpert, 1998). Therefore, for tremor conditions in general (with or without visual feedback), sensory predictions of movements may also be perturbed by added sensory 'noise' related to involuntary muscle contractions.

Increased awareness of tremor with visual feedback may also be associated with increased excitability of the cortico-spinal pathways. For example, mental imagery of rhythmic movements has been associated with increased motor cortex excitability (Sollfrank et al., 2015), along with watching other people performing rhythmic movements (Hari et al., 2014). Therefore, increased awareness of the tremor movement may increase the excitability of the motor cortex and cortico-spinal pathways. However, the findings reported in this Chapter did not reveal any significant changes in tremor amplitude in response to augmented visual feedback, or when participants were asked to try and reduce their tremors.

Anxiety is also associated with tremor, and ET patients can often show symptoms of anxiety and depression (Huang et al., 2019). Therefore, increased anxiety when observing tremor may be another mechanism underlying the effect of exacerbated tremor in response to visual feedback. A small proportion of ET post-mortem brains show Lewy Body pathologies within the locus coeruleus, which is a key site for synthesis of noradrenaline, which mediate the bodies physiological response to stress and acute anxiety (Louis & Vonsattel, 2008). Research has shown that noradrenaline analogues can worsen tremor (Marshall & Schnieden, 1966). Beta-blocker

propranolol is also a first line drug therapy for ET, which blocks peripheral beta-adrenergic receptors to combat tremor (Abila et al., 1985). One explanation for the findings reported in this study, is that intrinsic versus extrinsic visual feedback was associated with greater anxiety due to greater somatosensorial awareness of tremor.

Taken together, the findings from the current study would support the theory that somatosensorial awareness of tremor or increased anxiety associated with this may underlie exacerbated amplitude to natural visual feedback. However, to further examine the effect of augmented visual feedback on tremor, future research could apply a virtual 3D stimulus of the limb or enhance the phase alignment of the augmented visual stimulus to the tremor rhythm. The findings reported in this Chapter also illustrate a trend towards reduced visuomotor coupling at the tremor frequency during visual feedback which may indicate altered communication between visual and motor regions. However, the interpretation of these findings is limited without a comparative healthy control group performing mimicked tremor movements.

4.4.4 Difference between subjective and objective measures of tremor severity

Generally, the findings from this study also showed weak correspondence between objective and subjective measures of tremor amplitude during the experimental tasks. Analyses revealed a significant increase in tremor amplitude in response to natural visual feedback for objective but not subjective reports, indicating that natural visual feedback had a bigger impact on tremor amplitude than participants were subjectively aware of. This may be because participants were less accurate in assessing tremor amplitude in the absence of visual feedback when relying on proprioception alone. This corresponds with previous evidence that healthy individuals are less accurate in estimating the amplitude of movements in the absence of visual feedback (Santello et al., 2001; Sheth & Shimojo, 2002). Alternatively, individuals may underestimate the severity of their tremor in response to visual feedback, as they have become accustomed to viewing their tremor. Furthermore, subjective but not objective measures revealed a significant decrease in tremor amplitude when participants were instructed to minimise their tremor. This suggests that participants erroneously perceived they were able to exert control over their tremors. However, most participants were able to reduce their tremors to some degree, despite not showing an effect at a group level. Demand characteristics may also contribute to the dissociation between objective and subjective measures of tremor in this case, as participants may have felt the need to report a reduction in tremor to show that they were trying to comply with task instructions. However, participants were encouraged to provide an accurate estimate even if trying to reduce their tremors was an "impossible task". As most participants were able to minimise their tremor

objectively, this implies that strategies such as increasing the stiffness of muscles may be effective at reducing postural tremor.

4.4.5 Limitations of the study

As testing for the experiment was cut-short due to the COVID-19 outbreak, a limitation of this study is that it is underpowered. Previous research examining EEG correlates of tremor have identified significant correlates with smaller ET sample sizes (Hellwig et al., 2001, 2003; Muthuraman et al., 2012). However, due to the large heterogeneity of ET characterises (e.g. age of onset, familial ET, alcohol-sensitive ET, response to different medications), a much larger sample size is required to accurately examine factors which may influence tremor. In addition, the recruitment of a matched control group performing a rhythmic movement would provide a valuable comparison. This would provide further understanding on the effect of passive visual feedback on visuomotor coherence during voluntary rhythmic movements. Previous research suggests synchronisation of visual input and motor output in healthy controls is associated with increased visuomotor coherence (Classen et al., 1998), but changes in visuomotor coherence in response to passive visual feedback in healthy individuals is unknown. However, a fundamental flaw in comparing EEG correlates of tremor in ET and to rhythmic movements in healthy controls, is that tremor is involuntary. A more effective control would therefore involve involuntary rhythmic movements of limbs in healthy controls. This may be achieved by stimulating peripheral muscles, or by using apparatus to manually move or vibrate the required limb.

4.5 Chapter summary

Whole-brain exploratory analysis revealed that postural tremor was associated with significant sensorimotor (SMC and SMA) cortical-kinematic coherence, and that coherent cortical sources extended to frontal and posterior parietal regions of the cerebral cortex. Furthermore, natural, or intrinsic visual feedback significantly worsened postural tremor, whereas no significant changes in tremor amplitude were observed for augmented or intrinsic visual feedback. The lack of a significant impact of augmented feedback on postural tremor may be related to the nature of the task. Worsened tremor in response to natural visual feedback was also accompanied by a trend in decreased visuomotor coherence, which may indicate altered communication between visual and motor regions. And finally, the induction of steady-state potentials in EEG activity at near to tremor or non-tremor frequencies did not significantly influence tremor amplitude.

Chapter 5.   **General discussion**

The overarching aims of the experiments reported in this thesis were to examine the neural dynamics of ET and the relationship between neural oscillations and tremor amplitude. This was achieved by examining correlates of tremor across the cerebellar-thalamocortical network in the harmaline rodent model of tremor and examining cerebral cortical correlates of tremor in ET patients using EEG.

The findings reported in this thesis revealed that in rodents, harmaline induced an action tremor which was associated with significant coherent activity across the cerebellar-thalamocortical network at the tremor frequency, implicating the propagation of tremor oscillations across this pathway. In addition, the amplitude of tremor oscillations within the cerebellum were independent of changes in tremor amplitude associated with movement, but coherence of thalamic oscillations during tremor were significantly modulated by a change in behavioural state and associated with an increase in tremor amplitude.

Analyses reported in this thesis examined the cerebral cortical correlates of postural tremor in ET patients and revealed that primary and secondary sensorimotor regions of the cerebral cortex, as well as frontal and posterior parietal regions, significantly correlate with postural tremor. Tremor amplitude was also shown to significantly increase during natural, but not augmented visual feedback of tremor in ET. Contrary to the hypothesis that increased coupling within the cerebral cortex may exacerbate tremor, analyses revealed a trend towards reduced visuomotor coherence in response to natural visual feedback. Furthermore, the induction of EEG oscillations at frequencies near to the tremor frequency, using visual stimulation, did not influence tremor amplitude, suggesting tremor amplitude is not related to oscillations within visual brain areas.

5.1   **Pathological cerebellar activity underlying harmaline-tremor and ET**

The research reported within this thesis is the first to quantitatively verify that harmaline induces an action tremor, demonstrating the face validity of using harmaline as a model of ET. As reported in the General introduction, ET is diagnosed as an action tremor (Bhidayasiri, 2005), whereby tremor is initiated or increases in amplitude during posture or movement. This is opposed to a resting tremor, which is common in PD, and occurs when the limbs are fully relaxed and disappears with increased muscle tone associated with posture and movement (Bhidayasiri, 2005). Historical research has shown that damage to the cerebellum is associated with movement-related tremor in addition to other motor disturbances such as ataxia (Fahn, 1984; Holmes, 1939), and therefore ET has been historically associated with cerebellar dysfunction (Deuschl et al., 2000).

The IO hypothesis of ET was born out of animal research which showed harmaline induced a tremor via increasing oscillatory activation of the olivo-cerebellar pathway (De Montigny & Lamarre, 1973; Lamarre et al., 1975; Lamarre & Mercier, 1971; Llinás & Volkind, 1973). The findings reported in Chapter 2 showed that harmaline induces changes in theta range (4-15Hz) LFP oscillations in the medial but not interpositus nuclei, in anaesthetised rats. This extends previous research which showed a greater proportion of neurons in the medial compared to interpositus cerebellar nucleus showed rhythmic burst firing at 4-6Hz in response to harmaline (Lorden et al., 1992). This can be explained by the topographic organisation of olivo-cerebellar projections in longitudinal zones, as previous research has also shown that harmaline-induced rhythmic firing of IO neurons occurs in mainly the medial accessory olive and caudal dorsal accessory olive which provide climbing fibre projections to the vermal A and B zones and the C2 zone in the paravermis (Batini, Bernard, et al., 1981; Buisseret-Delmas, 1988a, 1988b; De Montigny & Lamarre, 1973; Llinás & Volkind, 1973).

Previous research has shown that harmaline suppresses Purkinje cell simple spike firing and increases complex spike firing to a rate of 4-6Hz in anaesthetised rats, which was corroborated by the experiments reported in Chapter 2 (Lorden et al., 1988). A novel preliminary finding reported in Chapter 2 showed that these changes in Purkinje cell activity coincided with a reduction in the variability of medial cerebellar nuclei MUA, likely due to the suppression of Purkinje cells simple spikes that show variability in firing rates and an increase in very regular and synchronised Purkinje cell rhythmic complex spikes. Previous research suggests that the synchrony of converging Purkinje cell inputs, and pauses in inputs onto its target neurons in the cerebellar nuclei, has a significant impact on the timing of cerebellar nuclear firing (Person & Raman, 2011; Sudhakar et al., 2015; Wu & Raman, 2017). Therefore, harmaline's effect on increasing rhythmic and synchronous Purkinje cell complex spike firing (Stratton et al., 1988; Sugihara et al., 1995), is likely the determining mechanism for increased oscillations recorded from the cerebellar nuclei.

Converging theories of ET pathophysiology suggest ET emerges due to disinhibition and/or altered rhythmic output of cerebellar nuclear neurons (Boutin et al., 2015; Grimaldi & Manto, 2013; Handforth & Lang, 2020). This corresponds with experimental research which showed bilateral rhythmic optogenetic stimulation of the interpositus nucleus induces a tremor at the same frequency of the stimulation in mice (Brown et al., 2020), highlighting the importance of increased cerebellar nuclear rhythmicity in generating and propagating tremor rhythms. The experiments reported in Chapter 3 revealed that harmaline induces prominent oscillations in the vermis of the cerebellar cortex and the medial cerebellar nuclei at the tremor frequency (9-15hz), which were

equal in amplitude during periods of resting and movement, and therefore independent of behavioural tremor amplitude. Taken together, this suggests pathological cerebellar oscillations in harmaline-tremor are constant and may play a role in regulating the frequency of the tremor.

5.2 The relationship between tremor amplitude and thalamocortical oscillations

The findings reported within this thesis are the first to show harmaline-induced rhythmic cerebellar output is associated with tremor-correlated activity in thalamocortical circuits. Chapter 3 of this thesis illustrates that harmaline tremor is associated with increased coherence across the cerebello-thalamocortical circuit, corresponding with clinical correlates observed in ET (Schnitzler et al., 2009). This suggests that tremor oscillations may be propagated from the cerebellum to the motor cortex via the cerebello-thalamocortical pathway. The results reported in this thesis also showed that thalamic tremor frequency oscillations were modulated by movement and the associated increase in tremor amplitude, whereas cerebellar tremor frequency oscillations were not. This suggests that whilst the frequency of the tremor may be governed by the cerebellum, thalamic oscillations relate to the amplitude of the behavioural tremor. In ET patients, the disruption of cerebellar rhythms using TMS at a non-tremor frequency is associated with reduced tremor amplitude (Gironell et al., 2002; Popa et al., 2013), whereas cerebellar stimulation at the tremor frequency does not impact tremor amplitude but entrains the instantaneous timing of the tremor rhythm (Brittain et al., 2015). Conversely, thalamic stimulation at the tremor frequency influences the amplitude of tremor, such that tremor is amplified or suppressed depending on the phase of thalamic stimulation (Cagnan et al., 2013). This further implies that cerebellar oscillations are important for the timing of tremor, whereas the degree of synchronisation of thalamic oscillations to the tremor can influence the amplitude of the tremor.

Thalamo-muscular and motor cortical-muscular coherence have also been associated with changes in tremor amplitude in ET (Hellwig et al., 2003; Hua & Lenz, 2005; Pedrosa et al., 2014). The correlation between thalamocortical tremor oscillations and tremor amplitude may be partly related to afferent feedback of behavioural tremor amplifying tremor oscillations (Hua & Lenz, 2005; Pedrosa et al., 2014), in addition to the propagation of tremor oscillations via direct cerebello-thalamocortical projections. Visual feedback of tremor has also been associated with increased tremor amplitude and changes in BOLD signals in motor and visual areas of the cerebral cortex (Archer et al., 2018; Gironell et al., 2012; Grimaldi et al., 2013). One potential mechanism for this is that visual feedback exacerbates tremor via increasing synchronous oscillations within cortical networks at the tremor frequency. However, the findings presented in this thesis show

that despite natural visual feedback significantly worsening postural tremor, there was a trend towards decreased (rather than increased) synchronisation across visual and motor regions of the cerebral cortex. However, due to the nature of the task which involved passive postural extension of arms/hands rather than visual goal-directed movements, participants attention may have been more focused on sensorial awareness of tremor than visual feedback. The findings reported in this thesis further revealed that rhythmic visual stimulation induced significant EEG oscillations at the stimulus frequency but did not systematically influence tremor amplitude. This suggests that worsening of tremor amplitude in response to visual feedback may not be mediated by increased synchronisation of tremor oscillations within visual brain areas. However, evidence presented within this thesis also verify the presence of significant tremor-coherent oscillations within the sensorimotor regions of the cerebral cortex during sustained posture compared to rest. Therefore, cortical involvement in tremor may be confined to sensorimotor rather than visual regions of the brain.

5.3   Suggestions for future research

To further examine the role of sensory afferents in amplifying thalamic tremor oscillations, future research could assess tremor and thalamic oscillations in the awake harmaline rodent model during treatment with anti-ET drugs which suppress tremor peripherally rather than centrally. For example, propranolol is a first line treatment for ET, and is thought to reduce tremor through its effects on the peripheral nervous system via blockage of β-adrenergic receptors located within muscle spindles (Abila et al., 1985). Propranolol is effective at reducing tremor in the harmaline rodent model (Paterson et al., 2009), however propranolol's effects on reducing harmaline-induced tremor may also partly occur via central mechanisms. This is because propranolol has been shown to reduce serotonin levels (Jones & Tackett, 1988) and harmaline's mechanisms of action are thought to be partly related to increased serotonin within the IO (see General introduction section 1.5.1 for a review on harmaline's mechanisms of action). As an alternative to the harmaline model, this suggested experiment could utilise an animal model which induces tremor vias rhythmic optogenetic stimulation of the cerebellar nuclei (Brown et al., 2020). In conjunction with treatment of drugs that suppress tremor peripherally, this model could be used to assess the degree to which thalamic tremor oscillations are due to direct cerebellar projections and/or sensory afferent effects of tremor.

5.4   Conclusions

Harmaline induces a tremor by increasing olivo-cerebellar rhythmicity, whereas tremor in ET likely arises due to a range of complex degenerative and compensatory changes occurring within

cerebellar circuits to produce changes in cerebellar output. Despite possible differences in the pathological catalyst producing abnormal cerebellar oscillations, this thesis provides evidence that harmaline-induced tremor involves comparable electrophysiological correlates to those reported in ET, specifically, increased coherence across the cerebellar-thalamocortical network at the tremor frequency. In addition, these findings suggests that the neural oscillations in cerebellum and thalamus have different roles in modulating tremor, as thalamus but not cerebellar oscillations are influenced by movement and/or behavioural tremor amplitude in the harmaline model. In ET postural tremor was significantly coherent with oscillations in sensorimotor regions of the cerebral cortex. However, despite natural visual feedback increasing tremor amplitude in ET, changes in tremor amplitude associated with visual feedback do not appear to be related to entrainment of cortical rhythms via the visual system.

References

Abbruzzese, G., & Berardelli, A. (2003). Sensorimotor integration in movement disorders. In *Movement Disorders* (Vol. 18, Issue 3, pp. 231–240). Mov Disord. https://doi.org/10.1002/mds.10327

Abila, B., Wilson, J. F., Marshall, R. W., & Richens, A. (1985). The tremorolytic action of beta-adrenoceptor blockers in essential, physiological and isoprenaline-induced tremor is mediated by beta-adrenoceptors located in a deep peripheral compartment. *British Journal of Clinical Pharmacology*, *20*(4), 369–376. http://www.ncbi.nlm.nih.gov/pubmed/2866785

Allum, J. H. J., & Young, L. R. (1976). The relaxed oscillation technique for the determination of the moment of inertia of limb segments. *Journal of Biomechanics*, *9*(1). https://doi.org/10.1016/0021-9290(76)90135-4

Alvĩa, K., Walter, J. T., Kohn, A., Ellis-Davies, G., & Khodakhah, K. (2008). Questioning the role of rebound firing in the cerebellum. *Nature Neuroscience*, *11*(11), 1256–1258. https://doi.org/10.1038/nn.2195

Apps, R., & Hawkes, R. (2009). Cerebellar cortical organization: a one-map hypothesis. *Nature Reviews Neuroscience*, *10*(9), 670–681. https://doi.org/10.1038/nrn2698

Archer, D. B., Coombes, S. A., Chu, W. T., Chung, J. W., Burciu, R. G., Okun, M. S., Wagle Shukla, A., & Vaillancourt, D. E. (2018). A widespread visually-sensitive functional network relates to symptoms in essential tremor. *Brain*, *141*(2), 472–485. https://doi.org/10.1093/brain/awx338

Arkadir, D., & Louis, E. D. (2013). The balance and gait disorder of essential tremor: what does this mean for patients? *Therapeutic Advances in Neurological Disorders*, *6*(4), 229–236. https://doi.org/10.1177/1756285612471415

Armstrong, D. M., & Edgley, S. A. (1984). Discharges of nucleus interpositus neurones during locomotion in the cat. *The Journal of Physiology*, *351*(1), 411–432. https://doi.org/10.1113/jphysiol.1984.sp015253

Asanuma, C., Thach, W. T., & Jones, E. G. (1983). Distribution of cerebellar terminations and their relation to other afferent terminations in the ventral lateral thalamic region of the monkey. *Brain Research Reviews*, *5*(3), 237–265. https://doi.org/10.1016/0165-0173(83)90015-2

Aumann, T. D. (2002). Cerebello-thalamic synapses and motor adaptation. In *Cerebellum* (Vol. 1,

Issue 1, pp. 69–77). https://doi.org/10.1080/147342202753203104

Avanzino, L., Bove, M., Tacchino, A., Ruggeri, P., Giannini, A., Trompetto, C., & Abbruzzese, G. (2009). Cerebellar involvement in timing accuracy of rhythmic finger movements in essential tremor. *European Journal of Neuroscience*, *30*(10), 1971–1979. https://doi.org/10.1111/j.1460-9568.2009.06984.x

Babij, R., Lee, M., Cortés, E., Vonsattel, J. P. G., Faust, P. L., & Louis, E. D. (2013). Purkinje cell axonal anatomy: Quantifying morphometric changes in essential tremor versus control brains. *Brain*, *136*(10), 3051–3061. https://doi.org/10.1093/brain/awt238

Bain, P. G. (2002). The management of tremor. *Neurology in Practice*, *72*(1). https://doi.org/10.1136/jnnp.72.suppl_1.i3

Baker, S. N. (2011). The primate reticulospinal tract, hand function and functional recovery. In *Journal of Physiology* (Vol. 589, Issue 23, pp. 5603–5612). Wiley-Blackwell. https://doi.org/10.1113/jphysiol.2011.215160

Bareš, M., Lungu, O. V., Husárová, I., & Gescheidt, T. (2010). Predictive Motor Timing Performance Dissociates Between Early Diseases of the Cerebellum and Parkinson's Disease. *The Cerebellum*, *9*(1), 124–135. https://doi.org/10.1007/s12311-009-0133-5

Barzegaran, E., & Knyazeva, M. G. (2017). Functional connectivity analysis in EEG source space: The choice of method. *PLOS ONE*, *12*(7), e0181105. https://doi.org/10.1371/journal.pone.0181105

Batini, C., Bernard, J., Buisseret-Delmas, C., Conrath-Verrier, M., & Horcholle-Bossavit, G. (1981). Harmaline-induced tremor - II. Unit activity correlation in the interposito-rubral and oculomotor systems of cat. *Experimental Brain Research*, *42*(3–4), 383–391. https://doi.org/10.1007/BF00237503

Batini, C., Buisseret-Delmas, C., & Conrath-Verrier, M. (1981). Harmaline-induced tremor. *Experimental Brain Research*, *42–42*(3–4), 371–382. https://doi.org/10.1007/BF00237502

Battista, A. F., Nakatani, S., Goldstein, M., & Anagnoste, B. (1970). Effect of harmaline in monkeys with central nervous system lesions. *Experimental Neurology*, *28*(3), 513–524. https://doi.org/10.1016/0014-4886(70)90189-5

Bava, A., Manzoni, T., & Urbano, A. (1967). Effects of fastigial stimulation on thalamic neurones belonging to the diffuse projection system. *Brain Research*, *4*(4), 378–380.

https://doi.org/10.1016/0006-8993(67)90168-0

Bazzigaluppi, P., & de Jeu, M. T. G. (2016). Heterogeneous Expression of T-type Ca2+ Channels Defines Different Neuronal Populations in the Inferior Olive of the Mouse. *Frontiers in Cellular Neuroscience*, *10*, 192. https://doi.org/10.3389/fncel.2016.00192

Beitz, A. J., & Saxon, D. (2004). Harmaline-induced climbing fiber activation causes amino acid and peptide release in the rodent cerebellar cortex and a unique temporal pattern of Fos expression in the olivo-cerebellar pathway. *Journal of Neurocytology*, *33*(1 SPEC. ISS.), 49–74. https://doi.org/10.1023/B:NEUR.0000029648.81071.20

Bekar, L., Libionka, W., Tian, G.-F., Xu, Q., Torres, A., Wang, X., Lovatt, D., Williams, E., Takano, T., Schnermann, J., Bakos, R., & Nedergaard, M. (2008). Adenosine is crucial for deep brain stimulation-mediated attenuation of tremor. *Nature Medicine*, *14*(1), 75–80. https://doi.org/10.1038/nm1693

Bell, A., Fairbrother, M., & Jones, K. (2019). Fixed and random effects models: making an informed choice. *Quality and Quantity*, *53*(2), 1051–1074. https://doi.org/10.1007/s11135-018-0802-x

Bella, S. D., Benoit, C. E., Farrugia, N., Keller, P. E., Obrig, H., Mainka, S., & Kotz, S. A. (2017). Gait improvement via rhythmic stimulation in Parkinson's disease is linked to rhythmic skills. *Scientific Reports*, *7*. https://doi.org/10.1038/srep42005

Bellesi, M., Vyazovskiy, V. V., Tononi, G., Cirelli, C., & Conti, F. (2012). Reduction of EEG Theta Power and Changes in Motor Activity in Rats Treated with Ceftriaxone. *PLoS ONE*, *7*(3), e34139. https://doi.org/10.1371/journal.pone.0034139

Benito-León, J., Alvarez-Linera, J., Hernández-Tamames, J. A., Alonso-Navarro, H., Jiménez-Jiménez, F. J., & Louis, E. D. (2009). Brain structural changes in essential tremor: Voxel-based morphometry at 3-Tesla. *Journal of the Neurological Sciences*, *287*(1–2), 138–142. https://doi.org/10.1016/J.JNS.2009.08.037

Benito-León, J., & Labiano-Fontcuberta, A. (2016). Linking Essential Tremor to the Cerebellum: Clinical Evidence. In *Cerebellum* (Vol. 15, Issue 3, pp. 253–262). Springer New York LLC. https://doi.org/10.1007/s12311-015-0741-1

Benito-León, J., Serrano, J. I., Louis, E. D., Holobar, A., Romero, J. P., Povalej-Bržan, P., Kranjec, J., Bermejo-Pareja, F., del Castillo, M. D., Posada, I. J., & Rocon, E. (2019). Essential tremor

severity and anatomical changes in brain areas controlling movement sequencing. *Annals of Clinical and Translational Neurology*, *6*(1), 83–97. https://doi.org/10.1002/acn3.681

Bernard, J. F., Buisseret-Delmas, C., Compoint, C., & Laplante, S. (1984). Harmaline induced tremor III. A combined simple units, horseradish peroxidase, and 2-deoxyglucose study of the olivocerebellar system in the rat. *Experimental Brain Research*, *57*(1), 128–137. https://doi.org/10.1007/BF00231139

Bhatia, K. P., Bain, P., Bajaj, N., Elble, R. J., Hallett, M., Louis, E. D., Raethjen, J., Stamelou, M., Testa, C. M., & Deuschl, G. (2018). Consensus Statement on the classification of tremors. from the task force on tremor of the International Parkinson and Movement Disorder Society. *Movement Disorders*, *33*(1), 75–87. https://doi.org/10.1002/mds.27121

Bhidayasiri, R. (2005). Differential diagnosis of common tremor syndromes. *Postgraduate Medical Journal*, *81*(962), 756–762. https://doi.org/10.1136/pgmj.2005.032979

Bi, Y., Wang, X., & Caramazza, A. (2016). Object Domain and Modality in the Ventral Visual Pathway. In *Trends in Cognitive Sciences* (Vol. 20, Issue 4, pp. 282–290). Elsevier Ltd. https://doi.org/10.1016/j.tics.2016.02.002

Blair, M. A., Ma, S., Phibbs, F., Fang, J. Y., Cooper, M. K., Davis, T. L., & Hedera, P. (2008). Reappraisal of the role of the DRD3 gene in essential tremor. *Parkinsonism and Related Disorders*, *14*(6), 471–475. https://doi.org/10.1016/j.parkreldis.2007.11.002

Blenkinsop, T. A., & Lang, E. J. (2006). Block of inferior olive gap junctional coupling decreases Purkinje cell complex spike synchrony and rhythmicity. *Journal of Neuroscience*, *26*(6), 1739–1748. https://doi.org/10.1523/JNEUROSCI.3677-05.2006

Boecker, H., Weindl, A., Brooks, D. J., Ceballos-Baumann, A. O., Liedtke, C., Miederer, M., Sprenger, T., Wagner, K. J., & Miederer, I. (2010). GABAergic dysfunction in essential tremor: an 11C-flumazenil PET study. *Journal of Nuclear Medicine : Official Publication, Society of Nuclear Medicine*, *51*(7), 1030–1035. https://doi.org/10.2967/jnumed.109.074120

Boecker, H., Wills, A. J., Ceballos-Baumann, A., Samuel, M., Thompson, P. D., Findley, L. J., & Brooks, D. J. (1996). The effect of ethanol on alcohol-responsive essential tremor: A positron emission tomography study. *Annals of Neurology*, *39*(5), 650–658. https://doi.org/10.1002/ana.410390515

Bohne, P., Schwarz, M. K., Herlitze, S., & Mark, M. D. (2019). A New Projection From the Deep

Cerebellar Nuclei to the Hippocampus via the Ventrolateral and Laterodorsal Thalamus in Mice. *Frontiers in Neural Circuits*, *13*. https://doi.org/10.3389/fncir.2019.00051

Boivie, J. (1971). The termination in the thalamus and the zona incerta of fibres from the dorsal column nuclei (DCN) in the cat. An experimental study with silver impregnation methods. *Brain Research*, *28*(3), 459–490. https://doi.org/10.1016/0006-8993(71)90056-4

Bonnefoi-Kyriacou, B., Legallet, E., Lee, R. G., & Trouche, E. (1998). Spatio-temporal and kinematic analysis of pointing movements performed by cerebellar patients with limb ataxia. *Experimental Brain Research*, *119*(4), 460–466. https://doi.org/10.1007/s002210050361

Bosch-Bouju, C., Hyland, B. I., & Parr-Brownlie, L. C. (2013). Motor thalamus integration of cortical, cerebellar and basal ganglia information: implications for normal and parkinsonian conditions. *Frontiers in Computational Neuroscience*, *7*, 163. https://doi.org/10.3389/fncom.2013.00163

Bourassa, C. V, Rivière, J.-B., Dion, P. A., Bernard, G., & Diab, S. (2011). LINGO1 Variants in the French-Canadian Population. *PLoS ONE*, *6*(1), 16254. https://doi.org/10.1371/journal.pone.0016254

Boutin, E., Vaugoyeau, M., Eusebio, A., Azulay, J. P., & Witjas, T. (2015). News and controversies regarding essential tremor. *Revue Neurologique*, *171*(5), 415–425. https://doi.org/10.7916/D8SF2T9C

Brittain, J. S., Cagnan, H., Mehta, A. R., Saifee, T. A., Edwards, M. J., & Brown, P. (2015). Distinguishing the central drive to tremor in Parkinson's disease and essential tremor. *Journal of Neuroscience*, *35*(2), 795–806. https://doi.org/10.1523/JNEUROSCI.3768-14.2015

Brittain, J. S., Probert-Smith, P., Aziz, T. Z., & Brown, P. (2013). Tremor suppression by rhythmic transcranial current stimulation. *Current Biology*, *23*(5), 436–440. https://doi.org/10.1016/j.cub.2013.01.068

Britton, T. C., Thompson, P. D., Day, B. L., Rothwell, J. C., Findley, L. J., & Marsden, C. D. (1994). Rapid wrist movements in patients with essential tremor. *Brain*, *117*, 39–47. http://arch.neicon.ru/xmlui/bitstream/handle/123456789/1491217/brain_brain_117_1.117-1-39.pdf?sequence=1

Brodal, P., & Bjaalie, J. G. (1997). Chapter 13 Salient anatomic features of the cortico-ponto-cerebellar pathway. *Progress in Brain Research*, *114*, 227–249.

https://doi.org/10.1016/S0079-6123(08)63367-1

Brown, A. M., White, J. J., van der Heijden, M. E., Zhou, J., Lin, T., & Sillitoe, R. V. (2020). Purkinje cell misfiring generates high-amplitude action tremors that are corrected by cerebellar deep brain stimulation. *ELife*, *9*. https://doi.org/10.7554/eLife.51928

Brownstone, R. M., & Chopek, J. W. (2018). Reticulospinal systems for tuning motor commands. In *Frontiers in Neural Circuits* (Vol. 12, pp. 1–10). Frontiers Media S.A. https://doi.org/10.3389/fncir.2018.00030

Brunner, C., Billinger, M., Seeber, M., Mullen, T. R., & Makeig, S. (2016). Volume Conduction Influences Scalp-Based Connectivity Estimates. *Frontiers in Computational Neuroscience*, *10*(NOV), 121. https://doi.org/10.3389/fncom.2016.00121

Brus-Ramer, M., Carmel, J. B., & Martin, J. H. (2009). Motor cortex bilateral motor representation depends on subcortical and interhemispheric interactions. *Journal of Neuroscience*, *29*(19), 6196–6206. https://doi.org/10.1523/JNEUROSCI.5852-08.2009

Bucher, S. F., Seelos, K. C., Dodel, R. C., Reiser, M., & Oertel, W. H. (1997). Activation mapping in essential tremor with functional magnetic resonance imaging. *Annals of Neurology*, *41*(1), 32–40. https://doi.org/10.1002/ana.410410108

Buijink, A. W. G., Broersma, M., van der Stouwe, A. M. M., van Wingen, G. A., Groot, P. F. C., Speelman, J. D., Maurits, N. M., & van Rootselaar, A. F. (2015). Rhythmic finger tapping reveals cerebellar dysfunction in essential tremor. *Parkinsonism and Related Disorders*, *21*(4), 383–388. https://doi.org/10.1016/j.parkreldis.2015.02.003

Buijink, A. W. G., van der Stouwe, A. M. M., Broersma, M., Sharifi, S., Groot, P. F. C., Speelman, J. D., Maurits, N. M., & Van Rootselaar, A. F. (2015). Motor network disruption in essential tremor: A functional and effective connectivity study. *Brain*, *138*(10), 2934–2947. https://doi.org/10.1093/brain/awv225

Buisseret-Delmas, C. (1988a). Sagittal organization of the olivocerebellonuclear pathway in the rat. I. Connections with the nucleus fastigii and the nucleus vestibularis lateralis. *Neuroscience Research*, *5*(6), 475–493. https://doi.org/10.1016/0168-0102(88)90038-7

Buisseret-Delmas, C. (1988b). Sagittal organization of the olivocerebellonuclear pathway in the rat. I. Connections with the nucleus fastigii and the nucleus vestibularis lateralis. *Neuroscience Research*, *5*(6), 475–493. https://doi.org/10.1016/0168-0102(88)90038-7

Butler, E. G., Bourke, D. W., & Horne, M. K. (2000). The activity of primate ventrolateral thalamic neurones during motor adaptation. *Experimental Brain Research*, *133*(4), 514–531. https://doi.org/10.1007/s002210000355

Cagnan, H., Brittain, J.-S., Little, S., Foltynie, T., Limousin, P., Zrinzo, L., Hariz, M., Joint, C., Fitzgerald, J., Green, A. L., Aziz, T., & Brown, P. (2013). Phase dependent modulation of tremor amplitude in essential tremor through thalamic stimulation. *Brain : A Journal of Neurology*, *136*(Pt 10), 3062–3075. https://doi.org/10.1093/brain/awt239

Cagnan, H., Pedrosa, D., Little, S., Pogosyan, A., Cheeran, B., Aziz, T., Green, A., Fitzgerald, J., Foltynie, T., Limousin, P., Zrinzo, L., Hariz, M., Friston, K. J., Denison, T., & Brown, P. (2017). Stimulating at the right time: phase-specific deep brain stimulation. *Brain : A Journal of Neurology*, *140*(Pt 1), 132–145. https://doi.org/10.1093/brain/aww286

Carignan, B., Daneault, J. F., & Duval, C. (2009). The amplitude of physiological tremor can be voluntarily modulated. *Experimental Brain Research*, *194*(2), 309–316. https://doi.org/10.1007/s00221-008-1694-0

Carvajal, S. C., Baumler, E., Harrist, R. B., & Parcel, G. S. (2001). Multilevel models and unbiased tests for group based interventions: Examples from the safer choices study. *Multivariate Behavioral Research*, *36*(2), 185–205. https://doi.org/10.1207/S15327906MBR3602_03

Cerminara, N. L., Apps, R., & Marple-Horvat, D. E. (2009). An internal model of a moving visual target in the lateral cerebellum. *The Journal of Physiology*, *587*(2), 429–442. https://doi.org/10.1113/jphysiol.2008.163337

Chapin, J. K., & Lin, C. -S. (1984). Mapping the body representation in the SI cortex of anesthetized and awake rats. *Journal of Comparative Neurology*, *229*(2), 199–213. https://doi.org/10.1002/cne.902290206

Chen, K., & Shih, J. C. (1997). Monoamine Oxidase A and B: Structure, Function, and Behavior. *Advances in Pharmacology*, *42*(C), 292–296. https://doi.org/10.1016/S1054-3589(08)60747-4

Cheng, M. M., Tang, G., & Kuo, S.-H. (2013). Harmaline-induced tremor in mice: videotape documentation and open questions about the model. *Tremor and Other Hyperkinetic Movements (New York, N.Y.)*, *3*. https://doi.org/10.7916/D8H993W3

Cheron, G., Márquez-Ruiz, J., Cheron, J., Prigogine, C., Ammann, C., Lukowski, R., Ruth, P., & Dan,

B. (2018). Purkinje cell BKchannel ablation induces abnormal rhythm in deep cerebellar nuclei and prevents LTD. *Scientific Reports*, *8*(1), 1–17. https://doi.org/10.1038/s41598-018-22654-6

Choi, S., Yu, E., Kim, D., Urbano, F. J., Makarenko, V., Shin, H. S., & Llinás, R. (2010). Subthreshold membrane potential oscillations in inferior olive neurons are dynamically regulated by P/Q- and T-type calcium channels: A study in mutant mice. *Journal of Physiology*, *588*(16), 3031–3043. https://doi.org/10.1113/jphysiol.2009.184705

Chorev, E., Yarom, Y., & Lampl, I. (2007). Rhythmic episodes of subthreshold membrane potential oscillations in the rat inferior olive nuclei in vivo. *Journal of Neuroscience*, *27*(19), 5043–5052. https://doi.org/10.1523/JNEUROSCI.5187-06.2007

Christakos, C. N. (2005). Parallel Neuronal Mechanisms Underlying Physiological Force Tremor in Steady Muscle Contractions of Humans. *Journal of Neurophysiology*, *95*(1), 53–66. https://doi.org/10.1152/jn.00051.2005

Christie, B. P., Charkhkar, H., Shell, C. E., Marasco, P. D., Tyler, D. J., & Triolo, R. J. (2019). Visual inputs and postural manipulations affect the location of somatosensory percepts elicited by electrical stimulation. *Scientific Reports*, *9*(1), 1–14. https://doi.org/10.1038/s41598-019-47867-1

Chuang, W.-L., Huang, Y.-Z., Lu, C.-S., & Chen, R.-S. (2014). Reduced cortical plasticity and GABAergic modulation in essential tremor. *Movement Disorders*, *29*(4), 501–507. https://doi.org/10.1002/mds.25809

Cisek, P., Crammond, D. J., & Kalaska, J. F. (2003). Neural activity in primary motor and dorsal premotor cortex in reaching tasks with the contralateral versus ipsilateral arm. *Journal of Neurophysiology*, *89*(2), 922–942. https://doi.org/10.1152/jn.00607.2002

Clark, G. A., McCormick, D. A., Lavond, D. G., & Thompson, R. F. (1984). Effects of lesions of cerebellar nuclei on conditioned behavioral and hippocampal neuronal responses. *Brain Research*, *291*(1), 125–136. https://doi.org/10.1016/0006-8993(84)90658-9

Clark, L. N., Park, N., Kisselev, S., Rios, E., Lee, J. H., & Louis, E. D. (2010). Replication of the LINGO1 gene association with essential tremor in a North American population. *European Journal of Human Genetics*, *18*(7), 838–843. https://doi.org/10.1038/ejhg.2010.27

Classen, J., Gerloff, C., Honda, M., & Hallett, M. (1998). Integrative Visuomotor Behavior Is

Associated With Interregionally Coherent Oscillations in the Human Brain. *Journal of Neurophysiology*, *79*(3), 1567–1573. https://doi.org/10.1152/jn.1998.79.3.1567

Clement, E. A., Richard, A., Thwaites, M., Ailon, J., Peters, S., & Dickson, C. T. (2008). Cyclic and Sleep-Like Spontaneous Alternations of Brain State Under Urethane Anaesthesia. *PLOS ONE*, *3*(4), e2004. https://doi.org/10.1371/JOURNAL.PONE.0002004

Comstock, D. C., Hove, M. J., & Balasubramaniam, R. (2018). Sensorimotor synchronization with auditory and visual modalities: Behavioral and neural differences. In *Frontiers in Computational Neuroscience* (Vol. 12, p. 53). Frontiers Media S.A. https://doi.org/10.3389/fncom.2018.00053

Constantinou, M., Elijah, D. H., Squirrell, D., Gigg, J., & Montemurro, M. A. (2015). Phase-locking of bursting neuronal firing to dominant LFP frequency components. *BioSystems*, *136*, 73–79. https://doi.org/10.1016/j.biosystems.2015.08.004

Conway, B. R. (2018). The Organization and Operation of Inferior Temporal Cortex. *Annual Review of Vision Science*, *4*(1), 381–402. https://doi.org/10.1146/annurev-vision-091517-034202

Courtemanche, R., Robinson, J. C., & Aponte, D. I. (2013). Linking oscillations in cerebellar circuits. *Frontiers in Neural Circuits*, *7*, 125. https://doi.org/10.3389/fncir.2013.00125

Cowper-Smith, C. D., Lau, E. Y. Y., Helmick, C. A., Eskes, G. A., & Westwood, D. A. (2010). Neural coding of movement direction in the healthy human brain. *PLoS ONE*, *5*(10), 13330. https://doi.org/10.1371/journal.pone.0013330

Critchley, E. (1972). Clinical manifestations of essential tremor. In *Journal of neurology, neurosurgery, and psychiatry* (Vol. 35, Issue 3). https://doi.org/10.1136/jnnp.35.3.365

Danos, P., Baumann, B., Krämer, A., Bernstein, H. G., Stauch, R., Krell, D., Falkai, P., & Bogerts, B. (2003). Volumes of association thalamic nuclei in schizophrenia: A postmortem study. *Schizophrenia Research*, *60*(2–3), 141–155. https://doi.org/10.1016/S0920-9964(02)00307-9

De Groote, F., Blum, K. P., Horslen, B. C., & Ting, L. H. (2018). Interaction between muscle tone, short-range stiffness and increased sensory feedback gains explains key kinematic features of the pendulum test in spastic cerebral palsy: A simulation study. *PLoS ONE*, *13*(10). https://doi.org/10.1371/journal.pone.0205763

De Gruijl, J. R., Bosman, L. W. J., De Zeeuw, C. I., & De Jeu, M. T. G. (2013). Inferior olive: All ins

and outs. In *Handbook of the Cerebellum and Cerebellar Disorders* (pp. 1013–1058). Springer Netherlands. https://doi.org/10.1007/978-94-007-1333-8_43

De Gruijl, J. R., Sokó, P. A., Negrello, M., & De Zeeuw, C. I. (2014). Previews Modulation of Electrotonic Coupling in the Inferior Olive by Inhibitory and Excitatory Inputs: Integration in the Glomerulus. *NEURON*, *81*, 1215–1217. https://doi.org/10.1016/j.neuron.2014.03.009

De Montigny, C., & Lamarre, Y. (1973). Rhythmic activity induced by harmaline in the olivo-cerebello-bulbar system of the cat. *Brain Research*, *53*(1), 81–95. https://doi.org/10.1016/0006-8993(73)90768-3

De Montigny, C., & Lamarre, Y. (1975). Effects Produced by Local Applications of Harmaline in the Inferior Olive. *Canadian Journal of Physiology and Pharmacology*, *53*(5), 845–849. https://doi.org/10.1139/y75-116

De Zeeuw, C. I., Chorev, E., Devor, A., Manor, Y., Van Der Giessen, R. S., De Jeu, M. T., Hoogenraad, C. C., Bijman, J., Ruigrok, T. J. H., French, P., Jaarsma, D., Kistler, W. M., Meier, C., Petrasch-Parwez, E., Dermietzel, R., Sohl, G., Gueldenagel, M., Willecke, K., & Yarom, Y. (2003). Deformation of network connectivity in the inferior olive of connexin 36-deficient mice is compensated by morphological and electrophysiological changes at the single neuron level. *Journal of Neuroscience*, *23*(11), 4700–4711. https://doi.org/10.1523/jneurosci.23-11-04700.2003

Deecher, D. C., Teitler, M., Soderlund, D. M., Bornmann, W. G., Kuehne, M. E., & Glick, S. D. (1992). Mechanisms of action of ibogaine and harmaline congeners based on radioligand binding studies. *Brain Research*, *571*(2), 242–247. https://doi.org/10.1016/0006-8993(92)90661-R

DeGruijl, J. R., Sokół, P. A., Negrello, M., & DeZeeuw, C. I. (2014). Modulation of electrotonic coupling in the inferior olive by inhibitory and excitatory inputs: Integration in the glomerulus. In *Neuron* (Vol. 81, Issue 6, pp. 1215–1217). Cell Press. https://doi.org/10.1016/j.neuron.2014.03.009

Delay, C., Tremblay, C., Brochu, E., Paris-Robidas, S., Emond, V., Rajput, A. H., Rajput, A., & Calon, F. (2014). Increased LINGO1 in the cerebellum of essential tremor patients. *Movement Disorders*, *29*(13), 1637–1647. https://doi.org/10.1002/mds.25819

Deng, H., Le, W. D., Guo, Y., Huang, M. S., Xie, W. J., & Jankovic, J. (2005). Extended study of A265G variant of HS1BP3 in essential tremor and Parkinson disease. *Neurology*, *65*(4), 651–652. https://doi.org/10.1212/01.wnl.0000173033.32535.23

Deuschl, G., Raethjen, J., Hellriegel, H., & Elble, R. (2011). Treatment of patients with essential tremor. *The Lancet Neurology*, *10*(2), 148–161. https://doi.org/10.1016/S1474-4422(10)70322-7

Deuschl, G., Raethjen, J., Lindemann, M., & Krack, P. (2001). The pathophysiology of tremor. *Muscle and Nerve*, *24*(6), 716–735. https://doi.org/10.1002/mus.1063

Deuschl, G., Wenzelburger, R., Löffler, K., Raethjen, J., & Stolze, H. (2000). Essential tremor and cerebellar dysfunction Clinical and kinematic analysis of intention tremor. *Brain*, *123*(8), 1568–1580. https://doi.org/10.1093/brain/123.8.1568

di Biase, L., Brittain, J.-S., Shah, S. A., Pedrosa, D. J., Cagnan, H., Mathy, A., Chen, C. C., Martín-Rodríguez, J. F., Mir, P., Timmerman, L., Schwingenschuh, P., Bhatia, K., Di Lazzaro, V., & Brown, P. (2017). Tremor stability index: a new tool for differential diagnosis in tremor syndromes. *Brain : A Journal of Neurology*, *140*(7), 1977–1986. https://doi.org/10.1093/brain/awx104

Diamond, M. E., Armstrong-James, M., & Ebner, F. F. (1992). Somatic sensory responses in the rostral sector of the posterior group (POm) and in the ventral posterior medial nucleus (VPM) of the rat thalamus. *Journal of Comparative Neurology*, *318*(4), 462–476. https://doi.org/10.1002/cne.903180410

Diener, H. -C, & Dichgans, J. (1992). Pathophysiology of cerebellar ataxia. *Movement Disorders*, *7*(2), 95–109. https://doi.org/10.1002/mds.870070202

Dirkx, M. F., Zach, H., van Nuland, A. J., Bloem, B. R., Toni, I., & Helmich, R. C. (2020). Cognitive load amplifies Parkinson's tremor through excitatory network influences onto the thalamus. *Brain : A Journal of Neurology*, *143*(5). https://doi.org/10.1093/brain/awaa083

Donchin, O., Gribova, A., Steinberg, O., Mitz, A. R., Bergman, H., & Vaadia, E. (2002). Single-unit activity related to bimanual arm movements in the primary and supplementary motor cortices. *Journal of Neurophysiology*, *88*(6), 3498–3517. https://doi.org/10.1152/jn.00335.2001

Donoghue, J. P., & Wise, S. P. (1982). The motor cortex of the rat: Cytoarchitecture and microstimulation mapping. *Journal of Comparative Neurology*, *212*(1), 76–88. https://doi.org/10.1002/cne.902120106

Du, W., Aloyo, V. J., & Harvey, J. A. (1997). Harmaline competitively inhibits [3H]MK-801 binding

to the NMDA receptor in rabbit brain. *Brain Research*, *770*(1–2), 26–29. https://doi.org/10.1016/S0006-8993(97)00606-9

Dum, R. P., & Strick, P. L. (2005). Frontal lobe inputs to the digit representations of the motor areas on the lateral surface of the hemisphere. *Journal of Neuroscience*, *25*(6), 1375–1386. https://doi.org/10.1523/JNEUROSCI.3902-04.2005

Dupuis, M. J.-M., Evrard, F. L. A., Jacquerye, P. G., Picard, G. R., & Lermen, O. G. (2010). Disappearance of essential tremor after stroke. *Movement Disorders*, *25*(16), 2884–2887. https://doi.org/10.1002/mds.23328

Duval, C., Sadikot, A. F., & Panisset, M. (2006). Bradykinesia in patients with essential tremor. *Brain Research*, *1115*(1), 213–216. https://doi.org/10.1016/j.brainres.2006.07.066

Ebner, T. J., Hewitt, A. L., & Popa, L. S. (2011). What features of limb movements are encoded in the discharge of cerebellar neurons? *Cerebellum*, *10*(4), 683–693. https://doi.org/10.1007/s12311-010-0243-0

Ebner, T. J., Johnson, M. T. V., Roitman, A., & Fu, Q. (2002). What do complex spikes signal about limb movements? *Annals of the New York Academy of Sciences*, *978*, 205–218. https://doi.org/10.1111/j.1749-6632.2002.tb07568.x

Eccles, J. C., Llinás, R., & Sasaki, K. (1966). The excitatory synaptic action of climbing fibres on the Purkinje cells of the cerebellum. *The Journal of Physiology*, *182*(2), 268–296. https://doi.org/10.1113/jphysiol.1966.sp007824

Elsegai, H., Shiells, H., Thiel, M., & Schelter, B. (2015). Network inference in the presence of latent confounders: The role of instantaneous causalities. *Journal of Neuroscience Methods*, *245*, 91–106. https://doi.org/10.1016/j.jneumeth.2015.02.015

Erickson-Davis, C. R., Faust, P. L., Vonsattel, J. P. G., Gupta, S., Honig, L. S., & Louis, E. D. (2010). Hairy baskets associated with degenerative purkinje cell changes in essential tremor. *Journal of Neuropathology and Experimental Neurology*, *69*(3), 262–271. https://doi.org/10.1097/NEN.0b013e3181d1ad04

Erickson, R. W., Maksimović, D., Erickson, R. W., & Maksimović, D. (2001). Power and Harmonics in Nonsinusoidal Systems. In *Fundamentals of Power Electronics* (pp. 589–607). Springer US. https://doi.org/10.1007/0-306-48048-4_16

Faber, D. S., & Pereda, A. E. (2018). Two forms of electrical transmission between neurons. In

Frontiers in Molecular Neuroscience (Vol. 11, p. 427). Frontiers Media S.A. https://doi.org/10.3389/fnmol.2018.00427

Faes, L., Pinna, G. D., Porta, A., Maestri, R., & Nollo, G. (2004). Surrogate data analysis for assessing the significance of the coherence function. *IEEE Transactions on Biomedical Engineering*, *51*(7), 1156–1166. https://doi.org/10.1109/TBME.2004.827271

Fahn, S. (1984). Cerebellar tremor: clinical aspects. In *Movement Disorders: Tremor* (pp. 355–363). Palgrave Macmillan UK. https://doi.org/10.1007/978-1-349-06757-2_26

Farkas, Z., Szirmai, I., & Kamondi, A. (2006). Impaired rhythm generation in essential tremor. *Movement Disorders*, *21*(8), 1196–1199. https://doi.org/10.1002/mds.20934

Ferreira, J. J., Mestre, T. A., Lyons, K. E., Benito-León, J., Tan, E. K., Abbruzzese, G., Hallett, M., Haubenberger, D., Elble, R., & Deuschl, G. (2019). MDS evidence-based review of treatments for essential tremor. *Movement Disorders*, *34*(7), 950–958. https://doi.org/10.1002/mds.27700

Florian, G., Andrew, C., & Pfurtscheller, G. (1998). Do changes in coherence always reflect changes in functional coupling? *Electroencephalography and Clinical Neurophysiology*, *106*(1), 87–91. https://doi.org/10.1016/S0013-4694(97)00105-3

Ford, A., McGregor, K. M., Case, K., Crosson, B., & White, K. D. (2010). Structural connectivity of Broca's area and medial frontal cortex. *NeuroImage*, *52*(4), 1230–1237. https://doi.org/10.1016/j.neuroimage.2010.05.018

Gaidica, M., Hurst, A., Cyr, C., & Leventhal, D. K. (2018). Distinct Populations of Motor Thalamic Neurons Encode Action Initiation, Action Selection, and Movement Vigor. *The Journal of Neuroscience : The Official Journal of the Society for Neuroscience*, *38*(29), 6563–6573. https://doi.org/10.1523/JNEUROSCI.0463-18.2018

Garden, D. L. F., Oostland, M., Jelitai, M., Rinaldi, A., Duguid, I., & Nolan, M. F. (2018). Inferior Olive HCN1 Channels Coordinate Synaptic Integration and Complex Spike Timing. *Cell Reports*, *22*(7), 1722–1733. https://doi.org/10.1016/j.celrep.2018.01.069

Garwicz, M., & Ekerot, C. F. (1994). Topographical organization of the cerebellar cortical projection to nucleus interpositus anterior in the cat. *The Journal of Physiology*, *474*(2), 245–260. https://doi.org/10.1113/jphysiol.1994.sp020017

Geborek, P., Jörntell, H., & Bengtsson, F. (2013). Stimulation within the cuneate nucleus

suppresses synaptic activation of climbing fibers. *Frontiers in Neural Circuits*, *6*(DEC), 120. https://doi.org/10.3389/fncir.2012.00120

Gironell, A., Kulisevsky, J., Lorenzo, J., Barbanoj, M., Pascual-Sedano, B., & Otermin, P. (2002). Transcranial magnetic stimulation of the cerebellum in essential tremor: A controlled study. *Archives of Neurology*, *59*(3), 413–417. https://doi.org/10.1001/archneur.59.3.413

Gironell, A., Ribosa-Nogué, R., Gich, I., Marin-Lahoz, J., & Pascual-Sedano, B. (2015). Severity stages in essential tremor: a long-term retrospective study using the glass scale. *Tremor and Other Hyperkinetic Movements (New York, N.Y.)*, *5*, 299. https://doi.org/10.7916/D8DV1HQC

Gironell, A., Ribosa-Nogué, R., & Pagonabarraga, J. (2012). Withdrawal of visual feedback in essential tremor. *Parkinsonism and Related Disorders*, *18*(4), 402–403. https://doi.org/10.1016/j.parkreldis.2011.11.029

Giuffrida, R., Volsi, G. L., Perciavalle, V., Santangelo, F., & Urbano, A. (1981). Influences of precerebellar systems triggering movement on single cells of the interpositus nucleus of the cat. *Neuroscience*, *6*(8), 1625–1631. https://doi.org/10.1016/0306-4522(81)90228-1

Glennon, R. A., Dukat, M., Grella, B., Hong, S. S., Costantino, L., Teitler, M., Smith, C., Egan, C., Davis, K., & Mattson, M. V. (2000). Binding of β-carbolines and related agents at serotonin (5-HT2 and 5- HT(1A)), dopamine (D2) and benzodiazepine receptors. *Drug and Alcohol Dependence*, *60*(2), 121–132. https://doi.org/10.1016/S0376-8716(99)00148-9

Gornati, S. V, Schä, C. B., Rooda, O. H. J. E., Nigg, A. L., De Zeeuw, C. I., Correspondence, F. E. H., & Hoebeek, F. E. (2018). Differentiating Cerebellar Impact on Thalamic Nuclei In Brief Article Differentiating Cerebellar Impact on Thalamic Nuclei. *CellReports*, *23*, 2690–2704. https://doi.org/10.1016/j.celrep.2018.04.098

Green, J. (2020). *A tutorial on modelling health behaviour as count data with Poisson and negative binomial regression*. https://doi.org/10.31219/osf.io/ux9et

Gremel, C. M., & Costa, R. M. (2013). Premotor cortex is critical for goal-directed actions. *Frontiers in Computational Neuroscience*, *7*(AUG), 110. https://doi.org/10.3389/fncom.2013.00110

Grimaldi, G., Fernandez, A., & Manto, M. (2013). Augmented visual feedback counteracts the effects of surface muscular functional electrical stimulation on physiological tremor. *Journal of NeuroEngineering and Rehabilitation*, *10*(1), 100. https://doi.org/10.1186/1743-0003-10-100

Grimaldi, G., & Manto, M. (2013). Is essential tremor a *Purkinjopathy* ? The role of the cerebellar cortex in its pathogenesis. *Movement Disorders*, *28*(13), 1759–1761. https://doi.org/10.1002/mds.25645

Gröhn, H., Gillick, B. T., Tkáč, I., Bednařík, P., Mascali, D., Deelchand, D. K., Michaeli, S., Meekins, G. D., Leffler-McCabe, M. J., MacKinnon, C. D., Eberly, L. E., & Mangia, S. (2019). Influence of Repetitive Transcranial Magnetic Stimulation on Human Neurochemistry and Functional Connectivity: A Pilot MRI/MRS Study at 7 T. *Frontiers in Neuroscience*, *13*. https://doi.org/10.3389/fnins.2019.01260

Guillery, R. W. (1995). Anatomical evidence concerning the role of the thalamus in corticocortical communication: a brief review. *Journal of Anatomy*, *187 (Pt 3*(Pt 3), 583–592. http://www.ncbi.nlm.nih.gov/pubmed/8586557%0Ahttp://www.pubmedcentral.nih.gov/articlerender.fcgi?artid=PMC1167461

Guitchounts, G., Masís, J., Wolff, S. B. E., & Cox, D. (2020). Encoding of 3D Head Orienting Movements in the Primary Visual Cortex. *Neuron*, *108*(3), 512-525.e4. https://doi.org/10.1016/J.NEURON.2020.07.014

Gulcher, J. R., Jónsson, P., Kong, A., Kristjánsson, K., Frigge, M. L., Kárason, A., Einarsdóttir, I. E., Stefánsson, H., Einarsdóttir, A. S., Siguroardóttir, S., Baldursson, S., Bjrnsdóttir, S., Hrafhkelsdóttir, S. M., Jakobsson, F., Benedickz, J., & Stefánsson, K. (1997). Mapping of a familial essential tremor gene, FET1, to chromosome 3q13. *Nature Genetics*, *17*(1), 84–87. https://doi.org/10.1038/ng0997-84

Gutierrez, J., Park, J., Badejo, O., & Louis, E. D. (2016). Worse and Worse and Worse: Essential Tremor Patients' Longitudinal Perspectives on Their Condition. *Frontiers in Neurology*, *7*, 175. https://doi.org/10.3389/fneur.2016.00175

Habas, C., Manto, M., & Cabaraux, P. (2019). The Cerebellar Thalamus. In *Cerebellum* (Vol. 18, Issue 3, pp. 635–648). Springer New York LLC. https://doi.org/10.1007/s12311-019-01019-3

Hallett, M. (1998). Overview of human tremor physiology. *Movement Disorders : Official Journal of the Movement Disorder Society*, *13 Suppl 3*, 43–48. http://www.ncbi.nlm.nih.gov/pubmed/9827594

Hallett, M., & Dubinsky, R. M. (1993). Glucose metabolism in the brain of patients with essential tremor. In *Journal of the Neurological Sciences* (Vol. 114, Issue 1). https://doi.org/10.1016/0022-510X(93)90047-3

Halliday, D. M., Conway, B. A., Farmer, S. F., Shahani, U., Russell, A. J. C., & Rosenberg, J. R. (2000). Coherence between low-frequency activation of the motor cortex and tremor in patients with essential tremor. *Lancet*, *355*(9210), 1149–1153. https://doi.org/10.1016/S0140-6736(00)02064-X

Hamed, S. Ben, Schieber, M. H., & Pouget, A. (2007). Decoding M1 Neurons During Multiple Finger Movements. *Journal of Neurophysiology*, *98*(1), 327–333. https://doi.org/10.1152/jn.00760.2006

Hanajima, R., Tsutsumi, R., Shirota, Y., Shimizu, T., Tanaka, N., & Ugawa, Y. (2016). Cerebellar dysfunction in essential tremor. *Movement Disorders*, *31*(8), 1230–1234. https://doi.org/10.1002/mds.26629

Handforth, A. (2012). Harmaline Tremor: Underlying Mechanisms in a Potential Animal Model of Essential Tremor. *Tremor and Other Hyperkinetic Movements*, *2*(0), 02. https://doi.org/10.5334/tohm.108

Handforth, A., Homanics, G. E., Covey, D. F., Krishnan, K., Lee, J. Y., Sakimura, K., Martin, F. C., & Quesada, A. (2010). T-type calcium channel antagonists suppress tremor in two mouse models of essential tremor. *Neuropharmacology*, *59*(6), 380–387. https://doi.org/10.1016/j.neuropharm.2010.05.012

Handforth, A., & Lang, E. J. (2020). Increased Purkinje Cell Complex Spike and Deep Cerebellar Nucleus Synchrony as a Potential Basis for Syndromic Essential Tremor. A Review and Synthesis of the Literature. In *Cerebellum*. Springer. https://doi.org/10.1007/s12311-020-01197-5

Hantman, A. W., & Jessell, T. M. (2010). Clarke's Column Neurons as the Focus of a Corticospinal Corollary Circuit. *Nature Neuroscience*, *13*(10), 1233. https://doi.org/10.1038/NN.2637

Hao, X.-M., Xu, R., Chen, A.-Q., Sun, F.-J., Wang, Y., Liu, H.-X., Chen, H., Xue, Y., & Chen, L. (2019). Endogenous HCN Channels Modulate the Firing Activity of Globus Pallidus Neurons in Parkinsonian Animals. *Frontiers in Aging Neuroscience*, *11*(JUL), 190. https://doi.org/10.3389/fnagi.2019.00190

Hari, R., Bourguignon, M., Piitulainen, H., Smeds, E., De Tiège, X., & Jousmäki, V. (2014). Human primary motor cortex is both activated and stabilized during observation of other person's phasic motor actions. *Philosophical Transactions of the Royal Society B: Biological Sciences*, *369*(1644). https://doi.org/10.1098/rstb.2013.0171

Hartmann, M. J., & Bower, J. M. (1998). Oscillatory activity in the cerebellar hemispheres of unrestrained rats. *Journal of Neurophysiology*, *80*(3), 1598–1604. https://doi.org/10.1152/jn.1998.80.3.1598

Hashizume, M., Miyazaki, T., Sakimura, K., Watanabe, M., Kitamura, K., & Kano, M. (2013). Disruption of cerebellar microzonal organization in GluD2 (Glurδ2) knockout mouse. *Frontiers in Neural Circuits*, *7*(JUL). https://doi.org/10.3389/fncir.2013.00130

Haubenberger, D., Nahab, F. B., Voller, B., & Hallett, M. (2014). Treatment of essential tremor with long-chain alcohols: still experimental or ready for prime time? *Tremor and Other Hyperkinetic Movements (New York, N.Y.)*, *4*, 1–8. https://doi.org/10.7916/D8RX991R

He, F., Sarrigiannis, P. G., Billings, S. A., Wei, H., Rowe, J., Romanowski, C., Hoggard, N., Hadjivassilliou, M., Rao, D. G., Grünewald, R., Khan, A., & Yianni, J. (2016). Nonlinear interactions in the thalamocortical loop in essential tremor: A model-based frequency domain analysis. *Neuroscience*, *324*, 377–389. https://doi.org/10.1016/J.NEUROSCIENCE.2016.03.028

Headley, P. M., & Lodge, D. (1976). Studies on field potentials and on single cells in the inferior olivary complex of the rat. *Brain Research*, *101*(3), 445–459. https://doi.org/10.1016/0006-8993(76)90470-4

Hedera, P., Cibulčík, F., & Davis, T. L. (2013). Pharmacotherapy of Essential Tremor. *Journal of Central Nervous System Disease*, *5*, JCNSD.S6561. https://doi.org/10.4137/jcnsd.s6561

Heinrich, S. P., & Bach, M. (2003). Adaptation characteristics of steady-state motion visual evoked potentials. *Clinical Neurophysiology*, *114*(7), 1359–1366. https://doi.org/10.1016/S1388-2457(03)00088-9

Hellriegel, H., Schulz, E. M., Siebner, H. R., Deuschl, G., & Raethjen, J. H. (2012). Continuous theta-burst stimulation of the primary motor cortex in essential tremor. *Clinical Neurophysiology*, *123*(5), 1010–1015. https://doi.org/10.1016/J.CLINPH.2011.08.033

Hellwig, B., Häußler, S., Schelter, B., Lauk, M., Guschlbauer, B., Timmer, J., & Lücking, C. H. (2001). Tremor-correlated cortical activity in essential tremor. *Lancet*, *357*(9255), 519–523. https://doi.org/10.1016/S0140-6736(00)04044-7

Hellwig, B., Schelter, B., Guschlbauer, B., Timmer, J., & Lücking, C. H. (2003). Dynamic synchronisation of central oscillators in essential tremor. *Clinical Neurophysiology*, *114*(8),

1462–1467. https://doi.org/10.1016/S1388-2457(03)00116-0

Helmchen, C., Hagenow, A., Miesner, J., Sprenger, A., Rambold, H., Wenzelburger, R., Heide, W., & Deuschl, G. (2003). Eye movement abnormalities in essential tremor may indicate cerebellar dysfunction. *Brain*, *126*(6), 1319–1332. https://doi.org/10.1093/brain/awg132

Helmich, R. C., Toni, I., Deuschl, G., & Bloem, B. R. (2013). The pathophysiology of essential tremor and parkinson's tremor. *Current Neurology and Neuroscience Reports*, *13*(9). https://doi.org/10.1007/s11910-013-0378-8

Herraiz, T., González, D., Ancín-Azpilicueta, C., Arán, V. J., & Guillén, H. (2010). β-Carboline alkaloids in Peganum harmala and inhibition of human monoamine oxidase (MAO). *Food and Chemical Toxicology*, *48*(3), 839–845. https://doi.org/10.1016/j.fct.2009.12.019

Herrmann, C. S. (2001). Human EEG responses to 1-100 Hz flicker: Resonance phenomena in visual cortex and their potential correlation to cognitive phenomena. *Experimental Brain Research*, *137*(3–4), 346–353. https://doi.org/10.1007/s002210100682

Hewitt, A. L., Popa, L. S., & Ebner, T. J. (2015). Changes in Purkinje cell simple spike encoding of reach kinematics during adaption to a mechanical perturbation. *Journal of Neuroscience*, *35*(3), 1106–1124. https://doi.org/10.1523/JNEUROSCI.2579-14.2015

Higgins, J. J., Pho, L. T., & Nee, L. E. (1997). A gene (ETM) for essential tremor maps to chromosome 2p22-p25. In *Movement Disorders* (Vol. 12, Issue 6, pp. 859–864). https://doi.org/10.1002/mds.870120605

Hintzen, A., Pelzer, E. A., & Tittgemeyer, M. (2018). Thalamic interactions of cerebellum and basal ganglia. In *Brain Structure and Function*. https://doi.org/10.1007/s00429-017-1584-y

Hoechstetter, K., Bornfleth, H., Weckesser, D., Ille, N., Berg, P., & Scherg, M. (2004). *BESA Source Coherence: A New Method to Study Cortical Oscillatory Coupling*.

Hoffman, L., & Rovine, M. J. (2007). Multilevel models for the experimental psychologist: Foundations and illustrative examples. In *Behavior Research Methods* (Vol. 39, Issue 1). https://doi.org/10.3758/BF03192848

Holmes, G. (1939). The cerebellum of man. In *Brain* (Vol. 62, Issue 1). https://doi.org/10.1093/brain/62.1.1

Homberg, V., Hefter, H., Reiners, K., & Freund, H. J. (1987). Differential effects of changes in

mechanical limb properties on physiological and pathological tremor. *Journal of Neurology, Neurosurgery and Psychiatry*, *50*(5), 568–579. https://doi.org/10.1136/jnnp.50.5.568

Hopfner, F., Erhart, T., Knudsen, K., Lorenz, D., Schneider, S. A., Zeuner, K. E., Deuschl, G., & Kuhlenbäumer, G. (2015). Testing for alcohol sensitivity of tremor amplitude in a large cohort with essential tremor. *Parkinsonism and Related Disorders*, *21*(8), 848–851. https://doi.org/10.1016/j.parkreldis.2015.05.005

Hornabrook, R. W., & Nagurney, J. T. (1976). Essential tremor in Papua New Guinea. In *Brain* (Vol. 99, Issue 4). https://doi.org/10.1093/brain/99.4.659

Horne, M. K., & Butler, E. G. (1995). The role of the cerebello-thalamo-cortical pathway in skilled movement. In *Progress in Neurobiology*. https://doi.org/10.1016/0301-0082(95)80011-V

Hove, M. J., Iversen, J. R., Zhang, A., & Repp, B. H. (2013). Synchronization with competing visual and auditory rhythms: Bouncing ball meets metronome. *Psychological Research*, *77*(4), 388–398. https://doi.org/10.1007/s00426-012-0441-0

Hove, M. J., & Keller, P. E. (2010). Spatiotemporal Relations and Movement Trajectories in Visuomotor Synchronization. *Music Perception*, *28*(1), 15–26. https://doi.org/10.1525/mp.2010.28.1.15

Hove, M. J., Spivey, M. J., & Krumhansl, C. L. (2010). Compatibility of Motion Facilitates Visuomotor Synchronization. *Journal of Experimental Psychology: Human Perception and Performance*, *36*(6), 1525–1534. https://doi.org/10.1037/a0019059

Hua, S. E., & Lenz, F. A. (2005). Posture-related oscillations in human cerebellar thalamus in essential tremor are enabled by voluntary motor circuits. *Journal of Neurophysiology*, *93*(1), 117–127. https://doi.org/10.1152/jn.00527.2004

Hua, S. E., Lenz, F. A., Zirh, T. A., Reich, S. G., & Dougherty, P. M. (1998). Thalamic neuronal activity correlated with essential tremor. *Journal of Neurology, Neurosurgery, and Psychiatry*, *64*(2), 273–276. https://doi.org/10.1136/JNNP.64.2.273

Huang, H., Yang, X., Zhao, Q., Chen, Y., Ning, P., Shen, Q., Wang, H., An, R., & Xu, Y. (2019). Prevalence and Risk Factors of Depression and Anxiety in Essential Tremor Patients: A Cross-Sectional Study in Southwest China. *Frontiers in Neurology*, *10*, 1194. https://doi.org/10.3389/fneur.2019.01194

Ichikawa, R., Hashimoto, K., Miyazaki, T., Uchigashima, M., Yamasaki, M., Aiba, A., Kano, M., &

Watanabe, M. (2016). Territories of heterologous inputs onto purkinje cell dendrites are segregated by mglur1-dependent parallel fiber synapse elimination. *Proceedings of the National Academy of Sciences of the United States of America*, *113*(8), 2282–2287. https://doi.org/10.1073/pnas.1511513113

Indovina, I., & Sanes, J. N. (2001). On somatotopic representation centers for finger movements in human primary motor cortex and supplementary motor area. *NeuroImage*, *13*(6), 1027–1034. https://doi.org/10.1006/nimg.2001.0776

Iseri, P. K., Karson, A., Gullu, K. M., Akman, O., Kokturk, S., Yardýmoglu, M., Erturk, S., & Ates, N. (2011). The effect of memantine in harmaline-induced tremor and neurodegeneration. *Neuropharmacology*, *61*(4), 715–723. https://doi.org/10.1016/j.neuropharm.2011.05.015

Iversen, J. R., Patel, A. D., Nicodemus, B., & Emmorey, K. (2015). Synchronization to auditory and visual rhythms in hearing and deaf individuals. *Cognition*, *134*, 232–244. https://doi.org/10.1016/J.COGNITION.2014.10.018

Jankowska, E., & Edgley, S. A. (2006). How can corticospinal tract neurons contribute to ipsilateral movements? A question with implications for recovery of motor functions. In *Neuroscientist* (Vol. 12, Issue 1, pp. 67–79). NIH Public Access. https://doi.org/10.1177/1073858405283392

Jeanneteau, F., Funalot, B., Jankovic, J., Deng, H., Lagarde, J. P., Lucotte, G., & Sokoloff, P. (2006). A functional variant of the dopamine D3 receptor is associated with risk and age-at-onset of essential tremor. *Proceedings of the National Academy of Sciences of the United States of America*, *103*(28), 10753–10758. https://doi.org/10.1073/pnas.0508189103

Jiménez-Jiménez, F. J., García-Martín, E., Lorenzo-Betancor, O., Pastor, P., Alonso-Navarro, H., & Agúndez, J. A. G. (2012). LINGO1 and risk for essential tremor: Results of a meta-analysis of rs9652490 and rs11856808. *Journal of the Neurological Sciences*, *317*(1–2), 52–57. https://doi.org/10.1016/j.jns.2012.02.030

Jiménez-Jiménez, F. J., Rubio, L., Alonso-Navarro, H., Calleja, M., Pilo-de-la-Fuente, B., Plaza-Nieto, J. F., Benito-León, J., García-Ruiz, P. J., & Agúndez, J. A. G. (2010). Impairment of rapid repetitive finger movements and visual reaction time in patients with essential tremor. *European Journal of Neurology*, *17*(1), 152–159. https://doi.org/10.1111/j.1468-1331.2009.02784.x

Jones, L. F., & Tackett, R. L. (1988). Interaction of propranolol with central serotonergic neurons. *Life Sciences*, *43*(26), 2249–2255. https://doi.org/10.1016/0024-3205(88)90418-3

Juvin, L., Grätsch, S., Trillaud-Doppia, E., Gariépy, J. F., Büschges, A., & Dubuc, R. (2016). A Specific Population of Reticulospinal Neurons Controls the Termination of Locomotion. *Cell Reports*, *15*(11), 2377–2386. https://doi.org/10.1016/j.celrep.2016.05.029

Kaas, J. H., Nelson, R. J., Sur, M., Lin, C. S., & Merzenich, M. M. (1979). Multiple representations of the body within the primary somatosensory cortex of primates. *Science*, *204*(4392), 521–523. https://doi.org/10.1126/science.107591

Kantak, S. S., Stinear, J. W., Buch, E. R., & Cohen, L. G. (2012). Rewiring the brain: Potential role of the premotor cortex in motor control, learning, and recovery of function following brain injury. In *Neurorehabilitation and Neural Repair* (Vol. 26, Issue 3, pp. 282–292). SAGE PublicationsSage CA: Los Angeles, CA. https://doi.org/10.1177/1545968311420845

Karas, P. J., Mikell, C. B., Christian, E., Liker, M. A., & Sheth, S. A. (2013). Deep brain stimulation: A mechanistic and clinical update. *Neurosurgical Focus*, *35*(5), 1. https://doi.org/10.3171/2013.9.FOCUS13383

Kawato, M. (1999). Internal models for motor control and trajectory planning. In *Current Opinion in Neurobiology* (Vol. 9, Issue 6, pp. 718–727). Current Biology Ltd. https://doi.org/10.1016/S0959-4388(99)00028-8

Kawato, M., & Wolpert, D. (1998). Internal models for motor control. *Novartis Foundation Symposium*, *218*(218), 291–307. https://doi.org/10.1002/9780470515563.ch16

Keogh, J., Morrison, S., & Barrett, R. (2004). Augmented visual feedback increases finger tremor during postural pointing. *Experimental Brain Research*, *159*(4), 467–477. https://doi.org/10.1007/s00221-004-1968-0

Kiss, Z. H. T., Mooney, D. M., Renaud, L., & Hu, B. (2002). Neuronal response to local electrical stimulation in rat thalamus: Physiological implications for mechanisms of deep brain stimulation. *Neuroscience*, *113*(1), 137–143. https://doi.org/10.1016/S0306-4522(02)00122-7

Kistler, W. M., De Jeu, M. T. G., Elgersma, Y., Van Der Giessen, R. S., Hensbroek, R., Luo, C., Koekkoek, S. K. E., Hoogenraad, C. C., Hamers, F. P. T., Gueldenagel, M., Sohl, G., Willecke, K., & De Zeeuw, C. I. (2002). Analysis of Cx36 knockout does not support tenet that olivary gap junctions are required for complex spike synchronization and normal motor performance. *Annals of the New York Academy of Sciences*, *978*(1 THE CEREBELLU), 391–404. https://doi.org/10.1111/j.1749-6632.2002.tb07582.x

Klein, J. C., Lorenz, B., Kang, J.-S., Baudrexel, S., Seifried, C., van de Loo, S., Steinmetz, H., Deichmann, R., & Hilker, R. (2011). Diffusion tensor imaging of white matter involvement in essential tremor. *Human Brain Mapping*, *32*(6), 896–904. https://doi.org/10.1002/hbm.21077

Klockgether, T., Schwarz, M., Turski, L., & Sontag, K.-H. (1986). The Rat Ventromedial Thalamic Nucleus and Motor Control: Role of /V-Methyl-D-aspartate-Mediated Excitation, GABAergic Inhibition, and Muscarinic Transmission. *The Journal of Neuroscience*, *6*(6), 1702–1711. http://www.jneurosci.org/content/jneuro/6/6/1702.full.pdf

Kosmowska, B., Ossowska, K., Konieczny, J., Lenda, T., Berghauzen-Maciejewska, K., & Wardas, J. (2020). Inhibition of Excessive Glutamatergic Transmission in the Ventral Thalamic Nuclei by a Selective Adenosine A1 Receptor Agonist, 5′-Chloro-5′-Deoxy-(±)-ENBA Underlies its Tremorolytic Effect in the Harmaline-Induced Model of Essential Tremor. *Neuroscience*, *429*, 106–118. https://doi.org/10.1016/j.neuroscience.2019.12.045

Kralic, J. E., Criswell, H. E., Osterman, J. L., O'Buckley, T. K., Wilkie, M. E., Matthews, D. B., Hamre, K., Breese, G. R., Homanics, G. E., & Morrow, A. L. (2005). Genetic essential tremor in γ-aminobutyric acidA receptor α1 subunit knockout mice. *Journal of Clinical Investigation*, *115*(3), 774–779. https://doi.org/10.1172/jci23625

Kralic, J. E., Korpi, E. R., O'Buckley, T. K., Homanics, G. E., & Morrow, A. L. (2002). Molecular and pharmacological characterization of GABAA receptor α1 subunit knockout mice. *Journal of Pharmacology and Experimental Therapeutics*, *302*(3), 1037–1045. https://doi.org/10.1124/jpet.102.036665

Kramer, P. R., Strand, J., Stinson, C., Bellinger, L. L., Kinchington, P. R., Yee, M. B., Umorin, M., & Peng, Y. B. (2017). Role for the ventral posterior medial/posterior lateral thalamus and anterior cingulate cortex in affective/motivation pain induced by varicella zoster virus. *Frontiers in Integrative Neuroscience*, *11*. https://doi.org/10.3389/fnint.2017.00027

Kronenbuerger, M., Gerwig, M., Brol, B., Block, F., & Timmann, D. (2007). Eyeblink conditioning is impaired in subjects with essential tremor. *Brain*, *130*(6), 1538–1551. https://doi.org/10.1093/brain/awm081

Kronenbuerger, M., Tronnier, V. M., Gerwig, M., Fromm, C., Coenen, V. A., Reinacher, P., Kiening, K. L., Noth, J., & Timmann, D. (2008). Thalamic deep brain stimulation improves eyeblink conditioning deficits in essential tremor. *Experimental Neurology*, *211*(2), 387–396.

https://doi.org/10.1016/j.expneurol.2008.02.002

Kuo, S. H., Erickson-Davis, C., Gillman, A., Faust, P. L., Vonsattel, J. P. G., & Louis, E. D. (2011). Increased number of heterotopic Purkinje cells in essential tremor. *Journal of Neurology, Neurosurgery and Psychiatry*, *82*(9), 1038–1040. https://doi.org/10.1136/jnnp.2010.213330

Kuo, S. H., Lin, C. Y., Wang, J., Sims, P. A., Pan, M. K., Liou, J. you, Lee, D., Tate, W. J., Kelly, G. C., Louis, E. D., & Faust, P. L. (2017). Climbing fiber-Purkinje cell synaptic pathology in tremor and cerebellar degenerative diseases. *Acta Neuropathologica*, *133*(1), 121–138. https://doi.org/10.1007/s00401-016-1626-1

Kuo, S. H., Tang, G., Louis, E. D., Ma, K., Babji, R., Balatbat, M., Cortes, E., Vonsattel, J. P. G., Yamamoto, A., Sulzer, D., & Faust, P. L. (2013). Lingo-1 expression is increased in essential tremor cerebellum and is present in the basket cell pinceau. *Acta Neuropathologica*, *125*(6), 879–889. https://doi.org/10.1007/s00401-013-1108-7

Kuo, S. H., Wang, J., Tate, W. J., Pan, M. K., Kelly, G. C., Gutierrez, J., Cortes, E. P., Vonsattel, J. P. G., Louis, E. D., & Faust, P. L. (2017). Cerebellar Pathology in Early Onset and Late Onset Essential Tremor. *Cerebellum*, *16*(2), 473–482. https://doi.org/10.1007/s12311-016-0826-5

Kuramoto, E., Fujiyama, F., Nakamura, K. C., Tanaka, Y., Hioki, H., & Kaneko, T. (2011). Complementary distribution of glutamatergic cerebellar and GABAergic basal ganglia afferents to the rat motor thalamic nuclei. *European Journal of Neuroscience*, *33*(1), 95–109. https://doi.org/10.1111/j.1460-9568.2010.07481.x

Kuramoto, E., Furuta, T., Nakamura, K. C., Unzai, T., Hioki, H., & Kaneko, T. (2009a). Two types of thalamocortical projections from the motor thalamic nuclei of the rat: A single neuron-tracing study using viral vectors. *Cerebral Cortex*. https://doi.org/10.1093/cercor/bhn231

Kuramoto, E., Furuta, T., Nakamura, K. C., Unzai, T., Hioki, H., & Kaneko, T. (2009b). Two Types of Thalamocortical Projections from the Motor Thalamic Nuclei of the Rat: A Single Neuron-Tracing Study Using Viral Vectors. *Cerebral Cortex*, *19*(9), 2065–2077. https://doi.org/10.1093/cercor/bhn231

Lalla, L., Rueda Orozco, P. E., Jurado-Parras, M.-T., Brovelli, A., & Robbe, D. (2017). Local or Not Local: Investigating the Nature of Striatal Theta Oscillations in Behaving Rats. *ENeuro*, *4*(5). https://doi.org/10.1523/ENEURO.0128-17.2017

Lamarre, Y. (1984). Animal models of physiological, essential and parkinsonian-like tremors. In

Movement Disorders: Tremor (pp. 183–194). Palgrave Macmillan UK. https://doi.org/10.1007/978-1-349-06757-2_11

Lamarre, Y., Joffroy, A. J., Dumont, M., de Montigny, C., Grou, F., & Lund, J. P. (1975). Central Mechanisms of Tremor in Some Feline and Primate Models. *Canadian Journal of Neurological Sciences / Journal Canadien Des Sciences Neurologiques*, *2*(3), 227–233. https://doi.org/10.1017/S0317167100020321

Lamarre, Y., & Mercier, L. A. (1971). Neurophysiological studies of harmaline-induced tremor in the cat. *Canadian Journal of Physiology and Pharmacology*, *49*(12), 1049–1058. https://doi.org/10.1139/y71-149

Lang, E. J. (2002). GABAergic and glutamatergic modulation of spontaneous and motor-cortex-evoked complex spike activity. *Journal of Neurophysiology*, *87*(4), 1993–2008. https://doi.org/10.1152/jn.00477.2001

Lang, E. J., & Blenkinsop, T. A. (2011). Control of cerebellar nuclear cells: A direct role for complex spikes? *Cerebellum*, *10*(4), 694–701. https://doi.org/10.1007/s12311-011-0261-6

Lang, E. J., Sugihara, I., & Llinás, R. (1996). GABAergic modulation of complex spike activity by the cerebellar nucleoolivary pathway in rat. *Journal of Neurophysiology*, *76*(1), 255–275. https://doi.org/10.1152/jn.1996.76.1.255

Lang, E. J., Sugihara, I., Welsh, J. P., & Llinás, R. (1999). Patterns of spontaneous purkinje cell complex spike activity in the awake rat. *Journal of Neuroscience*, *19*(7), 2728–2739. https://doi.org/10.1523/jneurosci.19-07-02728.1999

Lauk, M., Köster, B., Timmer, J., Guschlbauer, B., Deuschl, G., & Lücking, C. H. (1999). Side-to-side correlation of muscle activity in physiological and pathological human tremors. *Clinical Neurophysiology*, *110*(10), 1774–1783. https://doi.org/10.1016/S1388-2457(99)00130-3

Laurens, J., & Angelaki, D. E. (2020). Simple spike dynamics of Purkinje cells in the macaque vestibulo-cerebellum during passive whole-body self-motion. *Proceedings of the National Academy of Sciences of the United States of America*, *117*(6), 3232–3238. https://doi.org/10.1073/pnas.1915873117

Ledoux, M. S., & Lorden, J. F. (2002). Abnormal spontaneous and harmaline-stimulated Purkinje cell activity in the awake genetically dystonic rat. *Experimental Brain Research*, *145*(4), 457–467. https://doi.org/10.1007/s00221-002-1127-4

Lee, D., Gan, S. R., Faust, P. L., Louis, E. D., & Kuo, S. H. (2018). Climbing fiber-Purkinje cell synaptic pathology across essential tremor subtypes. *Parkinsonism and Related Disorders*, *51*, 24–29. https://doi.org/10.1016/j.parkreldis.2018.02.032

Lee, J., & Chang, S. (2019). Altered Primary Motor Cortex Neuronal Activity in a Rat Model of Harmaline-Induced Tremor During Thalamic Deep Brain Stimulation. *Frontiers in Cellular Neuroscience*, *13*, 448. https://doi.org/10.3389/fncel.2019.00448

Lee, J., Kim, I., Lee, J., Knight, E., Cheng, L., Il Kang, S., Jang, D. P., & Chang, S. Y. (2018). Development of harmaline-induced tremor in a swine model. *Tremor and Other Hyperkinetic Movements*, *8*. https://doi.org/10.7916/D8J68TV7

Lee, U., Lee, H., Müller, M., Noh, G.-J., & Mashour, G. A. (2012). Genuine and Spurious Phase Synchronization Strengths during Consciousness and General Anesthesia. *PLoS ONE*, *7*(10), e46313. https://doi.org/10.1371/journal.pone.0046313

Lefler, Y., Yarom, Y., & Uusisaari, M. Y. (2014). Cerebellar inhibitory input to the inferior olive decreases electrical coupling and blocks subthreshold oscillations. *Neuron*, *81*(6), 1389–1400. https://doi.org/10.1016/j.neuron.2014.02.032

Leyland, A. H., Groenewegen, P. P., Leyland, A. H., & Groenewegen, P. P. (2020). Multilevel Linear Regression Using MLwiN: Mortality in England and Wales, 1979–1992. In *Multilevel Modelling for Public Health and Health Services Research* (pp. 173–254). Springer International Publishing. https://doi.org/10.1007/978-3-030-34801-4_11

Leznik, E., & Llinás, R. (2005). Role of gap junctions in synchronized neuronal oscillations in the inferior olive. *Journal of Neurophysiology*, *94*(4), 2447–2456. https://doi.org/10.1152/jn.00353.2005

Lierse, W. (1993). Functional Anatomy of the Thalamus. In *Basic Mechanisms of the EEG*. https://doi.org/10.1007/978-1-4612-0341-4_9

Lin, C. Y., Louis, E. D., Faust, P. L., Koeppen, A. H., Vonsattel, J. P. G., & Kuo, S. H. (2014). Abnormal climbing fibre-Purkinje cell synaptic connections in the essential tremor cerebellum. *Brain*, *137*(12), 3149–3159. https://doi.org/10.1093/brain/awu281

Llinás, R. (1988). The intrinsic electrophysiological properties of mammalian neurons: Insights into central nervous system function. In *Science* (Vol. 242, Issue 4886). https://doi.org/10.1126/science.3059497

Llinás, R. (1989). The role of the intrinsic electrophysiological properties of central neurones in oscillation and resonance. In *Cell to Cell Signalling* (pp. 3–16). https://doi.org/10.1016/b978-0-12-287960-9.50007-1

Llinás, R., & Mühlethaler, M. (1988). Electrophysiology of guinea-pig cerebellar nuclear cells in the in vitro brain stem-cerebellar preparation. *The Journal of Physiology*, *404*, 241–258. http://www.ncbi.nlm.nih.gov/pubmed/2855348

Llinás, R., & Volkind, R. A. (1973). The olivo-cerebellar system: Functional properties as revealed by harmaline-induced tremor. *Experimental Brain Research*, *18*(1), 69–87. https://doi.org/10.1007/BF00236557

Llinás, R., & Yarom, Y. (1981). Electrophisiology of mammalian inferior olivary neurons "in vitro". Different types of voltage dependent ionic conductances. *J. Physiol.*, *315*, 549–567. https://www.ncbi.nlm.nih.gov/pmc/articles/PMC1249398/pdf/jphysiol00701-0544.pdf

Long, M. A., Deans, M. R., Paul, D. L., & Connors, B. W. (2002). Rhythmicity without synchrony in the electrically uncoupled inferior olive. *Journal of Neuroscience*, *22*(24), 10898–10905. https://doi.org/10.1523/jneurosci.22-24-10898.2002

Lorden, J. F., Lutes, J., Michela, V. L., & Ervin, J. (1992). Abnormal cerebellar output in rats with an inherited movement disorder. *Experimental Neurology*, *118*(1), 95–104. https://doi.org/10.1016/0014-4886(92)90026-M

Lorden, J. F., Stratton, S. E., Mays, L. E., & Oltmans, G. A. (1988). Purkinje cell activity in rats following chronic treatment with harmaline. *Neuroscience*, *27*(2), 465–472. https://doi.org/10.1016/0306-4522(88)90281-3

Lorenzo-Betancor, O., García-Martín, E., Cervantes, S., Agúndez, J. A. G., Jiménez-Jiménez, F. J., Alonso-Navarro, H., Luengo, A., Coria, F., Lorenzo, E., Irigoyen, J., & Pastor, P. (2011). Lack of association of LINGO1 rs9652490 and rs11856808 SNPs with familial essential tremor. *European Journal of Neurology*, *18*(8), 1085–1089. https://doi.org/10.1111/j.1468-1331.2010.03251.x

Lou, J. S., & Jankovic, J. (1991). Essential tremor: Clinical correlates in 350 patients. *Neurology*, *41*(2), 234–238. https://doi.org/10.1212/wnl.41.2_part_1.234

Louis, E. D. (2014). From neurons to neuron neighborhoods: The rewiring of the cerebellar cortex in essential tremor. *Cerebellum*, *13*(4), 501–512. https://doi.org/10.1007/s12311-013-0545-

0

Louis, E. D. (2016). Linking Essential Tremor to the Cerebellum: Neuropathological Evidence. *Cerebellum*, *15*(3), 235–242. https://doi.org/10.1007/s12311-015-0692-6

Louis, E. D., Agnew, A., Gillman, A., Gerbin, M., & Viner, A. S. (2011). Estimating annual rate of decline: Prospective, longitudinal data on arm tremor severity in two groups of essential tremor cases. *Journal of Neurology, Neurosurgery and Psychiatry*, *82*(7), 761–765. https://doi.org/10.1136/jnnp.2010.229740

Louis, E. D., Babij, R., Cortés, E., Vonsattel, J. P. G., & Faust, P. L. (2013). The inferior olivary nucleus: A postmortem study of essential tremor cases versus controls. *Movement Disorders*, *28*(6), 779–786. https://doi.org/10.1002/mds.25400

Louis, E. D., Clark, L. N., & Ottman, R. (2015). Familial versus sporadic essential tremor: What patterns can one decipher in age of onset? *Neuroepidemiology*, *44*(3), 166–172. https://doi.org/10.1159/000381807

Louis, E. D., & Dogu, O. (2008). Does age of onset in essential tremor have a bimodal distribution? Data from a tertiary referral setting and a population-based study. *Neuroepidemiology*, *29*(3–4), 208–212. https://doi.org/10.1159/000111584

Louis, E. D., & Ferreira, J. J. (2010). How common is the most common adult movement disorder? Update on the worldwide prevalence of essential tremor. *Movement Disorders*, *25*(5), 534–541. https://doi.org/10.1002/mds.22838

Louis, E. D., Frucht, S. J., & Rios, E. (2009). Intention tremor in essential tremor: Prevalence and association with disease duration. *Movement Disorders*, *24*(4), 626–627. https://doi.org/10.1002/mds.22370

Louis, E. D., Lee, M., Babij, R., Ma, K., Cort??s, E., Vonsattel, J. P. G., & Faust, P. L. (2014). Reduced Purkinje cell dendritic arborization and loss of dendritic spines in essential tremor. *Brain*, *137*(12), 3142–3148. https://doi.org/10.1093/brain/awu314

Louis, E. D., & Ottman, R. (2006). Study of possible factors associated with age of onset in essential tremor. *Movement Disorders*, *21Louis, E*(11), 1980–1986. https://doi.org/10.1002/mds.21102

Louis, E. D., & Vonsattel, J. P. G. (2008). The emerging neuropathology of essential tremor. In *Movement Disorders* (Vol. 23, Issue 2, pp. 174–182). NIH Public Access.

https://doi.org/10.1002/mds.21731

Loutit, A. J., Vickery, R. M., & Potas, J. R. (2021). Functional organization and connectivity of the dorsal column nuclei complex reveals a sensorimotor integration and distribution hub. *Journal of Comparative Neurology*, *529*(1), 187–220. https://doi.org/10.1002/cne.24942

Low, A. Y. T., Thanawalla, A. R., Yip, A. K. K., Kim, J., Wong, K. L. L., Tantra, M., Augustine, G. J., & Chen, A. I. (2018). Precision of Discrete and Rhythmic Forelimb Movements Requires a Distinct Neuronal Subpopulation in the Interposed Anterior Nucleus. *Cell Reports*, *22*(9), 2322–2333. https://doi.org/10.1016/j.celrep.2018.02.017

Lu, M. K., Chiou, S. M., Ziemann, U., Huang, H. C., Yang, Y. W., & Tsai, C. H. (2015). Resetting tremor by single and paired transcranial magnetic stimulation in Parkinson's disease and essential tremor. *Clinical Neurophysiology*, *126*(12), 2330–2336. https://doi.org/10.1016/j.clinph.2015.02.010

Ludwig, K. A., Miriani, R. M., Langhals, N. B., Joseph, M. D., Anderson, D. J., & Kipke, D. R. (2009). Using a common average reference to improve cortical neuron recordings from microelectrode arrays. *Journal of Neurophysiology*, *101*(3), 1679–1689. https://doi.org/10.1152/jn.90989.2008

Luo, J. (2015). Effects of ethanol on the cerebellum: Advances and prospects. In *Cerebellum* (Vol. 14, Issue 4, pp. 383–385). Springer New York LLC. https://doi.org/10.1007/s12311-015-0674-8

Ma, Y., Mazumdar, M., & Memtsoudis, S. G. (2012). Beyond repeated-measures analysis of variance: Advanced statistical methods for the analysis of longitudinal data in anesthesia research. *Regional Anesthesia and Pain Medicine*, *37*(1), 99–105. https://doi.org/10.1097/AAP.0b013e31823ebc74

Makoshi, Z., Kroliczak, G., & Van Donkelaar, P. (2011). Human supplementary motor area contribution to predictive motor planning. *Journal of Motor Behavior*, *43*(4), 303–309. https://doi.org/10.1080/00222895.2011.584085

Málly, J., Baranyi, M., & Vizi, E. S. (1996). Change in the concentrations of amino acids in CSF and serum of patients with essential tremor. *Journal of Neural Transmission*, *103*(5), 555–560. https://doi.org/10.1007/BF01273153

Maneski, L. P., Jorgovanović, N., Ilić, V., Došen, S., Keller, T., Popović, M. B., & Popovic, D. B. (2011).

Electrical stimulation for the suppression of pathological tremor. *Medical and Biological Engineering and Computing*, *49*(10), 1187–1193. https://doi.org/10.1007/s11517-011-0803-6

Manzoni, D. (2007). The cerebellum and sensorimotor coupling: Looking at the problem from the perspective of vestibular reflexes. *Cerebellum*, *6*(1), 24–37. https://doi.org/10.1080/14734220601132135

Marek, M., Paus, S., Allert, N., Mädler, B., Klockgether, T., Urbach, H., & Coenen, V. A. (2015). Ataxia and tremor due to lesions involving cerebellar projection pathways: A DTI tractographic study in six patients. *Journal of Neurology*, *262*(1), 54–58. https://doi.org/10.1007/s00415-014-7503-8

Marsden, C. D. (1984). Origins of normal and pathological tremor. *Movement Disorders: Tremor*, 37–84. https://doi.org/10.1007/978-1-349-06757-2_4

Marshall, J., & Schnieden, H. (1966). Effect of adrenaline, noradrenaline, atropine, and nicotine on some types of human tremor. *Journal of Neurology, Neurosurgery, and Psychiatry*, *29*(3), 214–218. https://doi.org/10.1136/jnnp.29.3.214

Martin, F. C., & Handforth, A. (2006). Carbenoxolone and mefloquine suppress tremor in the harmaline mouse model of essential tremor. *Movement Disorders*, *21*(10), 1641–1649. https://doi.org/10.1002/mds.20940

Martin, F. C., Thu Le, A., & Handforth, A. (2005). Harmaline-induced tremor as a potential preclinical screening method for essential tremor medications. *Movement Disorders*, *20*(3), 298–305. https://doi.org/10.1002/mds.20331

Martinez-Lopez, J. E., Moreno-Bravo, J. A., Madrigal, M. P., Martinez, S., & Puelles, E. (2015). Red nucleus and rubrospinal tract disorganization in the absence of Pou4f1. *Frontiers in Neuroanatomy*, *9*(FEB), 1–8. https://doi.org/10.3389/fnana.2015.00008

Matelli, M., Camarda, R., Glickstein, M., & Rizzolatti, G. (1986). Afferent and efferent projections of the inferior area 6 in the macaque monkey. *Journal of Comparative Neurology*, *251*(3), 281–298. https://doi.org/10.1002/cne.902510302

Mathy, A., Clark, B. A., & Häusser, M. (2014). Synaptically induced long-term modulation of electrical coupling in the inferior olive. *Neuron*, *81*(6), 1290–1296. https://doi.org/10.1016/j.neuron.2014.01.005

McCall, A. A., Miller, D. M., & Yates, B. J. (2017). Descending influences on vestibulospinal and vestibulosympathetic reflexes. In *Frontiers in Neurology* (Vol. 8, Issue MAR). Frontiers Research Foundation. https://doi.org/10.3389/fneur.2017.00112

McCormick, D. A., Clark, G. A., Lavond, D. G., & Thompson, R. F. (1982). Initial localization of the memory trace for a basic form of learning. *Proceedings of the National Academy of Sciences of the United States of America*, *79*(8 I), 2731–2735. https://doi.org/10.1073/pnas.79.8.2731

McCurdy, M. L., Houk, J. C., & Gibson, A. R. (1998). Organization of ascending pathways to the forelimb area of the dorsal accessory olive in the cat. *Journal of Comparative Neurology*, *392*(1), 115–133. https://doi.org/10.1002/(SICI)1096-9861(19980302)392:1<115::AID-CNE8>3.0.CO;2-5

Mehta, H., Saravanan, K. S., & Mohanakumar, K. P. (2003). Serotonin synthesis inhibition in olivo-cerebellar system attenuates harmaline-induced tremor in Swiss albino mice. *Behavioural Brain Research*, *145*(1–2), 31–36. https://doi.org/10.1016/S0166-4328(03)00094-9

Mengano, A., Di Maio, L., Maggio, M. A., Squitieri, F., Di Donato, M., Barbieri, F., & Campanella, G. (1989). Benign essential tremor. A clinical survey of 82 patients from Campania, a region of southern Italy. *Acta Neurologica*, *11*(4), 239–246. http://www.ncbi.nlm.nih.gov/pubmed/2801257

Meyer, A. F., Poort, J., O'Keefe, J., Sahani, M., & Linden, J. F. (2018). A Head-Mounted Camera System Integrates Detailed Behavioral Monitoring with Multichannel Electrophysiology in Freely Moving Mice. *Neuron*, *100*(1), 46-60.e7. https://doi.org/10.1016/j.neuron.2018.09.020

Meyer, J. H., Ginovart, N., Boovariwala, A., Sagrati, S., Hussey, D., Garcia, A., Young, T., Praschak-Rieder, N., Wilson, A. A., & Houle, S. (2006). Elevated monoamine oxidase A levels in the brain: An explanation for the monoamine imbalance of major depression. *Archives of General Psychiatry*, *63*(11), 1209–1216. https://doi.org/10.1001/archpsyc.63.11.1209

Miwa, H. (2007). Rodent models of tremor. *Cerebellum*, *6*(1), 66–72. https://doi.org/10.1080/14734220601016080

Miwa, H., Kubo, T., Suzuki, A., Kihira, T., & Kondo, T. (2006). A species-specific difference in the effects of harmaline on the rodent olivocerebellar system. *Brain Research*, *1068*(1), 94–101. https://doi.org/10.1016/J.BRAINRES.2005.11.036

Morecraft, R. J., & van Hoesen, G. W. (1992). Cingulate input to the primary and supplementary motor cortices in the rhesus monkey: Evidence for somatotopy in areas 24c and 23c. *Journal of Comparative Neurology*, *322*(4), 471–489. https://doi.org/10.1002/cne.903220403

Moro, E., Schwalb, J. M., Piboolnurak, P., Poon, Y. Y. W., Hamani, C., Hung, S. W., Arenovich, T., Lang, A. E., Chen, R., & Lozano, A. M. (2011). Unilateral subdural motor cortex stimulation improves essential tremor but not Parkinson's disease. *Brain*, *134*(7), 2096–2105. https://doi.org/10.1093/brain/awr072

Morrison, S., & Keogh, J. (2001). Changes in the dynamics of tremor during goal-directed pointing. *Human Movement Science*, *20*(4–5), 675–693. https://doi.org/10.1016/S0167-9457(01)00072-0

Mulliken, G. H., Musallam, S., & Andersen, R. A. (2008). Forward estimation of movement state in posterior parietal cortex. *Proceedings of the National Academy of Sciences of the United States of America*, *105*(24), 8170–8177. https://doi.org/10.1073/pnas.0802602105

Muthuraman, M., Heute, U., Arning, K., Anwar, A. R., Elble, R., Deuschl, G., & Raethjen, J. (2012). Oscillating central motor networks in pathological tremors and voluntary movements. What makes the difference? *NeuroImage*, *60*(2), 1331–1339. https://doi.org/10.1016/j.neuroimage.2012.01.088

Muthuraman, M., Raethjen, J., Koirala, N., Anwar, A. R., Mideksa, K. G., Elble, R., Groppa, S., & Deuschl, G. (2018). Cerebello-cortical network fingerprints differ between essential, Parkinson's and mimicked tremors. *Brain*, *141*(6), 1770–1781. https://doi.org/10.1093/brain/awy098

Nakamura, K. C., Sharott, A., & Magill, P. J. (2014). Temporal Coupling with Cortex Distinguishes Spontaneous Neuronal Activities in Identified Basal Ganglia-Recipient and Cerebellar-Recipient Zones of the Motor Thalamus. *Cerebral Cortex*, *24*(1), 81–97. https://doi.org/10.1093/cercor/bhs287

Napper, R. M. A., & Harvey, R. J. (1988). Number of parallel fiber synapses on an individual Purkinje cell in the cerebellum of the rat. In *Journal of Comparative Neurology* (Vol. 274, Issue 2). https://doi.org/10.1002/cne.902740204

Narayanan, R. T., Udvary, D., & Oberlaender, M. (2017). Cell Type-Specific Structural Organization of the Six Layers in Rat Barrel Cortex. *Frontiers in Neuroanatomy*, *11*, 91. https://doi.org/10.3389/fnana.2017.00091

Nashef, A., Cohen, O., Israel, Z., Harel, R., Correspondence, Y. P., & Prut, Y. (2018). Cerebellar Shaping of Motor Cortical Firing Is Correlated with Timing of Motor Actions Article Cerebellar Shaping of Motor Cortical Firing Is Correlated with Timing of Motor Actions. *CellReports*, *23*, 1275–1285. https://doi.org/10.1016/j.celrep.2018.04.035

Neafsey, E. J., Bold, E. L., Haas, G., Hurley-Gius, K. M., Quirk, G., Sievert, C. F., & Terreberry, R. R. (1986). The organization of the rat motor cortex: A microstimulation mapping study. In *Brain Research Reviews* (Vol. 11, Issue 1, pp. 77–96). Elsevier. https://doi.org/10.1016/0165-0173(86)90011-1

Neely, K. A., Kurani, A. S., Shukla, P., Planetta, P. J., Shukla, A. W., Goldman, J. G., Corcos, D. M., Okun, M. S., & Vaillancourt, D. E. (2015). Functional brain activity relates to 0-3 and 3-8 Hz force oscillations in essential tremor. *Cerebral Cortex*, *25*(11), 4192–4202. https://doi.org/10.1093/cercor/bhu142

Nicoletti, G., Manners, D., Novellino, F., Condino, F., Malucelli, E., Barbiroli, B., Tonon, C., Arabia, G., Salsone, M., Giofre, L., Testa, C., Lanza, P., Lodi, R., & Quattrone, A. (2010). Diffusion tensor MRI changes in cerebellar structures of patients with familial essential tremor. *Neurology*, *74*(12), 988–994. https://doi.org/10.1212/WNL.0b013e3181d5a460

Nietz, A., Krook-Magnuson, C., Gutierrez, H., Klein, J., Sauve, C., Hoff, I., Christenson Wick, Z., & Krook-Magnuson, E. (2020). Selective loss of the GABA Aα1 subunit from Purkinje cells is sufficient to induce a tremor phenotype . *Journal of Neurophysiology*, *124*(4). https://doi.org/10.1152/jn.00100.2020

Nolan, M. F., Malleret, G., Lee, K. H., Gibbs, E., Dudman, J. T., Santoro, B., Yin, D., Thompson, R. F., Siegelbaum, S. A., Kandel, E. R., & Morozov, A. (2003). The Hyperpolarization-Activated HCN1 Channel Is Important for Motor Learning and Neuronal Integration by Cerebellar Purkinje Cells. *Cell*, *115*(5), 551–564. https://doi.org/10.1016/S0092-8674(03)00884-5

Nozaradan, S., Peretz, I., & Keller, P. E. (2016). Individual differences in rhythmic cortical entrainment correlate with predictive behavior in sensorimotor synchronization. *Scientific Reports*, *6*. https://doi.org/10.1038/srep20612

Oddie, S. D., & Bland, B. H. (1998). Hippocampal formation theta activity and movement selection. *Neuroscience and Biobehavioral Reviews*, *22*(2), 221–231. https://doi.org/10.1016/S0149-7634(97)00003-1

Ohno, Y., Shimizu, S., Tatara, A., Imaoku, T., Ishii, T., Sasa, M., Serikawa, T., & Kuramoto, T. (2015).

Hcn1 is a tremorgenic genetic component in a rat model of essential tremor. *PLoS ONE*, *10*(5). https://doi.org/10.1371/journal.pone.0123529

Omlor, W., Patino, L., Mendez-Balbuena, I., Schulte-Mönting, J., & Kristeva, R. (2011). Corticospinal beta-range coherence is highly dependent on the pre-stationary motor state. *Journal of Neuroscience*, *31*(22), 8037–8045. https://doi.org/10.1523/JNEUROSCI.4153-10.2011

Omori, S., Isose, S., Otsuru, N., Nishihara, M., Kuwabara, S., Inui, K., & Kakigi, R. (2013). Somatotopic representation of pain in the primary somatosensory cortex (S1) in humans. *Clinical Neurophysiology*, *124*(7), 1422–1430. https://doi.org/10.1016/j.clinph.2013.01.006

Overduin, S. A., & Servos, P. (2004). Distributed digit somatotopy in primary somatosensory cortex. *NeuroImage*, *23*(2), 462–472. https://doi.org/10.1016/j.neuroimage.2004.06.024

Pan, M. K., Li, Y. S., Wong, S. B., Ni, C. L., Wang, Y. M., Liu, W. C., Lu, L. Y., Lee, J. C., Cortes, E. P., Vonsattel, J. P. G., Sun, Q., Louis, E. D., Faust, P. L., & Kuo, S. H. (2020). Cerebellar oscillations driven by synaptic pruning deficits of cerebellar climbing fibers contribute to tremor pathophysiology. *Science Translational Medicine*, *12*(526). https://doi.org/10.1126/scitranslmed.aay1769

Pan, M. K., Ni, C. L., Wu, Y. C., Li, Y. S., & Kuo, S. H. (2018). Animal models of tremor: Relevance to human tremor disorders. *Tremor and Other Hyperkinetic Movements*, *8*. https://doi.org/10.7916/D89S37MV

Paris-Robidas, S., Brochu, E., Sintes, M., Emond, V., Bousquet, M., Vandal, M., Pilote, M., Tremblay, C., Di Paolo, T., Rajput, A. H., Rajput, A., & Calon, F. (2012). Defective dentate nucleus GABA receptors in essential tremor. *Brain*, *135*(1), 105–116. https://doi.org/10.1093/brain/awr301

Park, Y. G., Choi, J. H., Lee, C., Kim, S., Kim, Y., Chang, K.-Y., Paek, S. H., & Kim, D. (2015). Heterogeneity of tremor mechanisms assessed by tremor-related cortical potential in mice. *Molecular Brain*, *8*(1), 1–7. https://doi.org/10.1186/s13041-015-0093-2

Park, Y. G., Park, H. Y., Lee, C. J., Choi, S., Jo, S., Choi, H., Kim, Y. H., Shin, H. S., Llinas, R. R., & Kim, D. (2010). CaV3.1 is a tremor rhythm pacemaker in the inferior olive. *Proceedings of the National Academy of Sciences of the United States of America*, *107*(23), 10731–10736. https://doi.org/10.1073/pnas.1002995107

Pasquet, M. O., Tihy, M., Gourgeon, A., Pompili, M. N., Godsil, B. P., Léna, C., & Dugué, G. P. (2016). Wireless inertial measurement of head kinematics in freely-moving rats. *Scientific Reports*, *6*(1), 1–13. https://doi.org/10.1038/srep35689

Paterson, N. E., Malekiani, S. A., Foreman, M. M., Olivier, B., & Hanania, T. (2009). Pharmacological characterization of harmaline-induced tremor activity in mice. *European Journal of Pharmacology*, *616*(1–3), 73–80. https://doi.org/10.1016/j.ejphar.2009.05.031

Paxinos, G., & Watson, C. (2005). The Rat Brain in Stereotaxic Coordinates. In *English* (6th ed.). Academic Press. https://doi.org/10.1017/CBO9781107415324.004

Pedrosa, D. J., Nelles, C., Brown, P., Volz, L. J., Pelzer, E. A., Tittgemeyer, M., Brittain, J. S., & Timmermann, L. (2017). The differentiated networks related to essential tremor onset and its amplitude modulation after alcohol intake. *Experimental Neurology*, *297*, 50–61. https://doi.org/10.1016/j.expneurol.2017.07.013

Pedrosa, D. J., Nelles, C., Maier, F., Eggers, C., Burghaus, L., Fink, G. R., Wittmann, M., & Timmermann, L. (2016). Time reproduction deficits in essential tremor patients. *Movement Disorders*, *31*(8), 1234–1240. https://doi.org/10.1002/mds.26630

Pedrosa, D. J., Quatuor, E.-L., Reck, C., Pauls, K. A. M., Huber, C. A., Visser-Vandewalle, V., & Timmermann, L. (2014). Thalamomuscular Coherence in Essential Tremor: Hen or Egg in the Emergence of Tremor? *Journal of Neuroscience*, *34*(43), 14475–14483. https://doi.org/10.1523/JNEUROSCI.0087-14.2014

Pedrosa, D. J., Reck, C., Florin, E., Pauls, K. A. M., Maarouf, M., Wojtecki, L., Dafsari, H. S., Sturm, V., Schnitzler, A., Fink, G. R., & Timmermann, L. (2012). Essential tremor and tremor in Parkinson's disease are associated with distinct "tremor clusters" in the ventral thalamus. *Experimental Neurology*, *237*(2), 435–443. https://doi.org/10.1016/j.expneurol.2012.07.002

Pellerin, J. P., & Lamarre, Y. (1997). Local field potential oscillations in primate cerebellar cortex during voluntary movement. *Journal of Neurophysiology*, *78*(6), 3502–3507. https://doi.org/10.1152/jn.1997.78.6.3502

Person, A. L., & Raman, I. M. (2011). Purkinje neuron synchrony elicits time-locked spiking in the cerebellar nuclei. *Nature*, *481*(7382), 502–505. https://doi.org/10.1038/nature10732

Picard, N. (2003). Activation of the Supplementary Motor Area (SMA) during Performance of Visually Guided Movements. *Cerebral Cortex*, *13*(9), 977–986.

https://doi.org/10.1093/cercor/13.9.977

Placantonakis, D. G., Bukovsky, A. A., Zeng, X.-H., Kiem, H.-P., & Welsh, J. P. (2004). Fundamental role of inferior olive connexin 36 in muscle coherence during tremor. *Proceedings of the National Academy of Sciences of the United States of America*, *101*(18), 7164–7169. https://doi.org/10.1073/pnas.0400322101

Popa, T., Russo, M., Vidailhet, M., Roze, E., Lehéricy, S., Bonnet, C., Apartis, E., Legrand, A. P., Marais, L., Meunier, S., & Gallea, C. (2013). Cerebellar rTMS stimulation may induce prolonged clinical benefits in essential tremor, and subjacent changes in functional connectivity: An open label trial. *Brain Stimulation*, *6*(2), 175–179. https://doi.org/10.1016/j.brs.2012.04.009

Quené, H., & Van Den Bergh, H. (2004). On multi-level modeling of data from repeated measures designs: A tutorial. *Speech Communication*, *43*(1–2), 103–121. https://doi.org/10.1016/j.specom.2004.02.004

Quy, P. N., Fujita, H., Sakamoto, Y., Na, J., & Sugihara, I. (2011). Projection patterns of single mossy fiber axons originating from the dorsal column nuclei mapped on the aldolase C compartments in the rat cerebellar cortex. *The Journal of Comparative Neurology*, *519*(5), 874–899. https://doi.org/10.1002/cne.22555

Raethjen, J., Govindan, R. B., Kopper, F., Muthuraman, M., & Deuschl, G. (2007). Cortical involvement in the generation of essential tremor. *Journal of Neurophysiology*, *97*(5), 3219–3228. https://doi.org/10.1152/jn.00477.2006

Rajalingam, R., Breen, D. P., Lang, A. E., & Fasano, A. (2018). Essential tremor plus is more common than essential tremor: Insights from the reclassification of a cohort of patients with lower limb tremor. *Parkinsonism and Related Disorders*, *56*, 109–110. https://doi.org/10.1016/j.parkreldis.2018.06.029

Rajput, A. H., Offord, K. P., Beard, C. M., & Kurland, L. T. (1984). Essential tremor in Rochester, Minnesota: a 45-year study. *Journal of Neurology, Neurosurgery, and Psychiatry*, *47*(5), 466–470. http://www.ncbi.nlm.nih.gov/pubmed/6736976

Rao, S. M., Binder, J. R., Hammeke, T. A., Bandettini, P. A., Bobholz, J. A., Frost, J. A., Myklebust, B. M., Jacobson, R. D., & Hyde, J. S. (1995). Somatotopic mapping of the human primary motor cortex with functional magnetic resonance imaging. *Neurology*, *45*(5), 919–924. https://doi.org/10.1212/WNL.45.5.919

Rappaport, M. S., Gentry, R. T., Schneider, D. R., & Dole, V. P. (1984). Ethanol effects on harmaline-induced tremor and increase of cerebellar cyclic GMP. *Life Sciences*, *34*(1), 49–56. https://doi.org/10.1016/0024-3205(84)90329-1

Reeber, S. L., White, J. J., George-Jones, N. A., & Sillitoe, R. V. (2012). Architecture and development of olivocerebellar circuit topography. In *Frontiers in Neural Circuits* (Vol. 6, Issue DEC). Frontiers Media SA. https://doi.org/10.3389/fncir.2012.00115

Ristanović, D., Milošević, N. T., Stefanović, B. D., Marić, D. L., & Rajković, K. (2010). Morphology and classification of large neurons in the adult human dentate nucleus: A qualitative and quantitative analysis of 2D images. *Neuroscience Research*, *67*(1), 1–7. https://doi.org/10.1016/j.neures.2010.01.002

Robertson, H. A. (1980). Harmaline-induced tremor: The benzodiazepine receptor as a site of action. *European Journal of Pharmacology*, *67*(1), 129–132. https://doi.org/10.1016/0014-2999(80)90020-5

Robinson, F. R., Houk, J. C., & Gibson, A. R. (1987). Limb specific connections of the cat magnocellular red nucleus. *The Journal of Comparative Neurology*, *257*(4), 553–577. https://doi.org/10.1002/cne.902570406

Ross, J. M., & Balasubramaniam, R. (2014). Physical and neural entrainment to rhythm: human sensorimotor coordination across tasks and effector systems. *Frontiers in Human Neuroscience*, *8*, 576. https://doi.org/10.3389/FNHUM.2014.00576

Rothwell, J. C. (2008). Physiology and Anatomy of Possible Oscillators in the Central Nervous System. *Movement Disorders*, *13*(S3), 24–28. https://doi.org/10.1002/mds.870131304

Ruigrok, T. J. H. (2013). Cerebellar influences on descending spinal motor systems. In *Handbook of the Cerebellum and Cerebellar Disorders* (pp. 497–528). Springer Netherlands. https://doi.org/10.1007/978-94-007-1333-8_23

Ruigrok, T. J. H., & Voogd, J. (2000). Organization of projections from the inferior olive to the cerebellar nuclei in the rat. *The Journal of Comparative Neurology*, *426*(2), 209–228. https://doi.org/10.1002/1096-9861(20001016)426:2<209::AID-CNE4>3.0.CO;2-0

Rummel, C., Abela, E., Andrzejak, R. G., Hauf, M., Pollo, C., Müller, M., Weisstanner, C., Wiest, R., & Schindler, K. (2015). Resected brain tissue, seizure onset zone and quantitative EEG measures: Towards prediction of post-surgical seizure control. *PLoS ONE*, *10*(10), e0141023.

https://doi.org/10.1371/journal.pone.0141023

Sakai, S. T. (2013). Cerebellar thalamic and thalamocortical projections. In *Handbook of the Cerebellum and Cerebellar Disorders* (pp. 529–548). Springer Netherlands. https://doi.org/10.1007/978-94-007-1333-8_24

Salemi, G., Savettieri, G., Rocca, W. A., Meneghini, F., Saporito, V., Morgante, L., Reggio, A., Grigoletto, F., & Di Perri, R. (1994). Prevalence of essential tremor: a door-to-door survey in Terrasini, Sicily. Sicilian Neuro-Epidemiologic Study Group. *Neurology*, *44*(1), 61–64. http://www.ncbi.nlm.nih.gov/pubmed/8290093

Santello, M., McDonagh, M. J. N., & Challis, J. H. (2001). Visual and non-visual control of landing movements in humans. *Journal of Physiology*, *537*(1), 313–327. https://doi.org/10.1111/j.1469-7793.2001.0313k.x

Saupe, K., Schröger, E., Andersen, S. K., & Müller, M. M. (2009). Neural mechanisms of intermodal sustained selective attention with concurrently presented auditory and visual stimuli. *Frontiers in Human Neuroscience*, *3*(NOV), 58–58. https://doi.org/10.3389/neuro.09.058.2009

Scherg, M. (1990). Fundamentals of dipole source potential analysis. *Auditory Evoked Magnetic Fields and Electric Potentials, Advances in Audiology*, *6*(1990), 40–69. http://apsychoserver.psychofizz.psych.arizona.edu/JJBAReprints/PSYC501A/Readings/Scherg_Fundamentals of Dipole Source Potentials_Auditory Evoked Agnetic Fileds_1990.pdf

Scherg, M., Berg, P., Nakasato, N., & Beniczky, S. (2019). Taking the EEG back into the brain: The power of multiple discrete sources. *Frontiers in Neurology*, *10*(JUL). https://doi.org/10.3389/fneur.2019.00855

Schnitzler, A., Münks, C., Butz, M., Timmermann, L., & Gross, J. (2009). Synchronized brain network associated with essential tremor as revealed by magnetoencephalography. *Movement Disorders*, *24*(11), 1629–1635. https://doi.org/10.1002/mds.22633

Schnitzler, A., Timmermann, L., & Gross, J. (2006). Physiological and pathological oscillatory networks in the human motor system. *Journal of Physiology-Paris*, *99*(1), 3–7. https://doi.org/10.1016/j.jphysparis.2005.06.010

Schreiber, T., & Schmitz, A. (1996). Improved surrogate data for nonlinearity tests. *Physical Review Letters*, *77*(4), 635–638. https://doi.org/10.1103/PhysRevLett.77.635

Shakkottai, V. G. (2014). Physiologic Changes Associated with Cerebellar Dystonia. In *Cerebellum* (Vol. 13, Issue 5, pp. 637–644). Springer New York LLC. https://doi.org/10.1007/s12311-014-0572-5

Sharifi, S., Luft, F., Verhagen, R., Heida, T., Speelman, J. D., Bour, L. J., & van Rootselaar, A.-F. (2017). Intermittent cortical involvement in the preservation of tremor in essential tremor. *Journal of Neurophysiology*, *118*(5), 2628–2635. https://doi.org/10.1152/jn.00848.2016

Sharifi, S., Nederveen, A. J., Booij, J., & Van Rootselaar, A. F. (2014). Neuroimaging essentials in essential tremor: A systematic review. *NeuroImage: Clinical*, *5*, 217–231. https://doi.org/10.1016/j.nicl.2014.05.003

Shatunov, A. (2006). Genomewide scans in North American families reveal genetic linkage of essential tremor to a region on chromosome 6p23. *Brain*, *129*(9), 2318–2331. https://doi.org/10.1093/brain/awl120

Sherman, S. M. (2007). The thalamus is more than just a relay. In *Current Opinion in Neurobiology* (Vol. 17, Issue 4, pp. 417–422). Elsevier Current Trends. https://doi.org/10.1016/j.conb.2007.07.003

Sheth, B. R., & Shimojo, S. (2002). How the lack of visuomotor feedback affects even the early stages of goal-directed pointing movements. *Experimental Brain Research*, *143*(2), 181–190. https://doi.org/10.1007/s00221-001-0977-5

Shih, L. C., & Pascual-Leone, A. (2017). Non-invasive brain stimulation for essential tremor. *Tremor and Other Hyperkinetic Movements*, *7*, 458. https://doi.org/10.7916/D8G44W01

Siapas, A. G., Lubenov, E. V., & Wilson, M. A. (2005). Prefrontal phase locking to hippocampal theta oscillations. *Neuron*, *46*(1), 141–151. https://doi.org/10.1016/j.neuron.2005.02.028

Silver, R. A., Momiyama, A., & Cull-Candy, S. G. (1998). Locus of frequency-dependent depression identified with multiple-probability fluctuation analysis at rat climbing fibre-Purkinje cell synapses. *The Journal of Physiology*, *510*(3), 881–902. https://doi.org/10.1111/j.1469-7793.1998.881bj.x

Singer, C., Sanchez-Ramos, J., & Weiner, W. J. (2004). Gait abnormality in essential tremor. *Movement Disorders*, *9*(2), 193–196. https://doi.org/10.1002/mds.870090212

Sjölund, B., Björklund, A., & Wiklund, L. (1977). The indolaminergic innervation of the inferior olive. 2. Relation to harmaline induced tremor. *Brain Research*, *131*(1), 23–37.

https://doi.org/10.1016/0006-8993(77)90026-9

Sollfrank, T., Hart, D., Goodsell, R., Foster, J., & Tan, T. (2015). 3D visualization of movements can amplify motor cortex activation during subsequent motor imagery. *Frontiers in Human Neuroscience*, *9*(AUGUST), 463. https://doi.org/10.3389/fnhum.2015.00463

Song, J., Davey, C., Poulsen, C., Luu, P., Turovets, S., Anderson, E., Li, K., & Tucker, D. (2015). EEG source localization: Sensor density and head surface coverage. *Journal of Neuroscience Methods*, *256*, 9–21. https://doi.org/10.1016/j.jneumeth.2015.08.015

Sotelo, C., & Angaut, P. (1973). The fine structure of the cerebellar central nuclei in the cat I. Neurons and neuroglial cells. *Experimental Brain Research*, *16*(4), 410–430. https://doi.org/10.1007/BF00233432

Spaak, E., de Lange, F. P., & Jensen, O. (2014). Local Entrainment of Alpha Oscillations by Visual Stimuli Causes Cyclic Modulation of Perception. *Journal of Neuroscience*, *34*(10), 3536–3544. https://doi.org/10.1523/JNEUROSCI.4385-13.2014

Splettstoesser, F., Bonnet, U., Wiemann, M., Bingmann, D., & Büsselberg, D. (2005). Modulation of voltage-gated channel currents by harmaline and harmane. *British Journal of Pharmacology*, *144*(1), 52–58. https://doi.org/10.1038/sj.bjp.0706024

Srinath, R., & Ray, S. (2014). Effect of amplitude correlations on coherence in the local field potential. *Journal of Neurophysiology*, *112*(4), 741–751. https://doi.org/10.1152/jn.00851.2013

Stefansson, H., Steinberg, S., Petursson, H., Gustafsson, O., Gudjonsdottir, I. H., Jonsdottir, G. A., Palsson, S. T., Jonsson, T., Saemundsdottir, J., Bjornsdottir, G., Böttcher, Y., Thorlacius, T., Haubenberger, D., Zimprich, A., Auff, E., Hotzy, C., Testa, C. M., Miyatake, L. A., Rosen, A. R., … Stefansson, K. (2009). Variant in the sequence of the LINGO1 gene confers risk of essential tremor. *Nature Genetics*, *41*(3), 277–279. https://doi.org/10.1038/ng.299

Steriade, M. (1995). Two channels in the cerebellothalamocortical system. *The Journal of Comparative Neurology*, *354*(1), 57–70. https://doi.org/10.1002/cne.903540106

Sternberg, E. J., Alcalay, R. N., Levy, O. A., & Louis, E. D. (2013). Postural and Intention Tremors: A Detailed Clinical Study of Essential Tremor vs. Parkinson's Disease. *Frontiers in Neurology*, *4*, 51. https://doi.org/10.3389/fneur.2013.00051

Stolze, H., Petersen, G., Raethjen, J., Wenzelburger, R., & Deuschl, G. (2001). The gait disorder of

advanced essential tremor. *Brain*, *124*(11), 2278–2286. https://doi.org/10.1093/brain/124.11.2278

Stone, K. D., Bullock, F., Keizer, A., & Dijkerman, H. C. (2018). The disappearing limb trick and the role of sensory suggestibility in illusion experience. *Neuropsychologia*, *117*, 418–427. https://doi.org/10.1016/j.neuropsychologia.2018.07.012

Stratton, S. E., Lorden, J. F., Mays, L. E., & Onmans, G. A. (1988). Spontaneous and Harmaline-Stimulated Purkinje Cell Activity in Rats with a Genetic Movement Disorder. *The Journal of Neuroscience*, *8*(9), 3327–3336.

Streng, M. L., Popa, L. S., & Ebner, T. J. (2018). Complex Spike Wars: a New Hope. In *Cerebellum* (Vol. 17, Issue 6, pp. 735–746). Springer New York LLC. https://doi.org/10.1007/s12311-018-0960-3

Stüttgen, M. (2020). *MLIB - toolbox for analyzing spike data , MATLAB Central File Exchange.*

Sudhakar, S. K., Torben-Nielsen, B., & De Schutter, E. (2015). Cerebellar Nuclear Neurons Use Time and Rate Coding to Transmit Purkinje Neuron Pauses. *PLoS Computational Biology*, *11*(12). https://doi.org/10.1371/journal.pcbi.1004641

Sugihara, I., Lang, E. J., & Llinás, R. (1995). Serotonin Modulation of Inferior Olivary Oscillations and Synchronicity: A Multiple-electrode Study in the Rat Cerebellum. *European Journal of Neuroscience*, *7*(4), 521–534. https://doi.org/10.1111/j.1460-9568.1995.tb00657.x

Sultan, F., & Glickstein, M. (2007). The cerebellum: Comparative and animal studies. *Cerebellum*, *6*(3), 168–176. https://doi.org/10.1080/14734220701332486

Takada, M., Tokuno, H., Hamada, I., Inase, M., Ito, Y., Imanishi, M., Hasegawa, N., Akazawa, T., Hatanaka, N., & Nambu, A. (2001). Organization of inputs from cingulate motor areas to basal ganglia in macaque monkey. *European Journal of Neuroscience*, *14*(10), 1633–1650. https://doi.org/10.1046/j.0953-816X.2001.01789.x

Tan, E. K., Prakash, K. M., Fook-Chong, S., Yih, Y., Chua, E., Lum, S. Y., Wong, M. C., Pavanni, R., & Zhao, Y. (2007). DRD3 variant and risk of essential tremor. *Neurology*, *68*(10), 790–791. https://doi.org/10.1212/01.wnl.0000256773.87498.2f

Tan, E. K., Teo, Y. Y., Prakash, K. M., Li, R., Lim, H. Q., Angeles, D., Tan, L. C., Au, W. L., Yih, Y., & Zhao, Y. (2009). Lingo1 variant increases risk of familial essential tremor. *Neurology*, *73*(14), 1161–1162. https://doi.org/10.1212/WNL.0b013e3181bacfc9

Tanji, J. (1994). The supplementary motor area in the cerebral cortex. In *Neuroscience Research* (Vol. 19, Issue 3, pp. 251–268). Elsevier. https://doi.org/10.1016/0168-0102(94)90038-8

Taylor, C. P. (1997). Mechanisms of action of gabapentin. In *Revue neurologique: Vol. 153 Suppl 1*. Rev Neurol (Paris). https://pubmed.ncbi.nlm.nih.gov/9686247/

Teune, T. M., Van Der Burg, J., Van Der Moer, J., Voogd, J., & Ruigrok, T. J. H. (2000). Topography of cerebellar nuclear projections to the brain stem in the rat. In *Progress in Brain Research* (Vol. 124). https://doi.org/10.1016/s0079-6123(00)24014-4

Thenganatt, M. A., & Jankovic, J. (2016). The relationship between essential tremor and Parkinson's disease. *Parkinsonism & Related Disorders*, *22*, S162–S165. https://doi.org/10.1016/J.PARKRELDIS.2015.09.032

Tio, M., & Tan, E. K. (2016). Genetics of essential tremor. *Parkinsonism and Related Disorders*, *22*, S176–S178. https://doi.org/10.1016/j.parkreldis.2015.09.022

Tokuno, H., & Tanji, J. (1993). Input organization of distal and proximal forelimb areas in the monkey primary motor cortex: A retrograde double labeling study. *Journal of Comparative Neurology*, *333*(2), 199–209. https://doi.org/10.1002/cne.903330206

Trillenberg, P., Führer, J., Sprenger, A., Hagenow, A., Kömpf, D., Wenzelburger, R., Deuschl, G., Heide, W., & Helmchen, C. (2006). Eye-hand coordination in essential tremor. *Movement Disorders*, *21*(3), 373–379. https://doi.org/10.1002/mds.20729

Tuleasca, C., Witjas, T., Najdenovska, E., Verger, A., Girard, N., Champoudry, J., Thiran, J. P., Van de Ville, D., Cuadra, M. B., Levivier, M., Guedj, E., & Régis, J. (2017). Assessing the clinical outcome of Vim radiosurgery with voxel-based morphometry: visual areas are linked with tremor arrest! *Acta Neurochirurgica*, *159*(11), 2139–2144. https://doi.org/10.1007/s00701-017-3317-7

Tuleasca, C., Witjas, T., Van de Ville, D., Najdenovska, E., Verger, A., Girard, N., Champoudry, J., Thiran, J. P., Cuadra, M. B., Levivier, M., Guedj, E., & Régis, J. (2018). Right Brodmann area 18 predicts tremor arrest after Vim radiosurgery: a voxel-based morphometry study. *Acta Neurochirurgica*, *160*(3), 603–609. https://doi.org/10.1007/s00701-017-3391-x

Turecek, J., Yuen, G. S., Han, V. Z., Zeng, X. H., Bayer, K. U., & Welsh, J. P. (2014). NMDA receptor activation strengthens weak electrical coupling in mammalian brain. *Neuron*, *81*(6), 1375–1388. https://doi.org/10.1016/j.neuron.2014.01.024

Udenfriend, S., Witkop, B., Redfield, B. G., & Weissbach, H. (1958). Studies with reversible inhibitors of monoamine oxidase: Harmaline and related compounds. *Biochemical Pharmacology*, *1*(2), 160–165. https://doi.org/10.1016/0006-2952(58)90025-X

Uemura, Y., Haque, T., Sato, F., Tsutsumi, Y., Ohara, H., Oka, A., Furuta, T., Bae, Y. C., Yamashiro, T., Tachibana, Y., & Yoshida, A. (2020). Proprioceptive thalamus receiving forelimb and neck muscle spindle inputs via the external cuneate nucleus in the rat. *Brain Structure and Function*, *225*(7), 2177–2192. https://doi.org/10.1007/s00429-020-02118-2

Vaillancourt, D. E., Sturman, M. M., Metman, L. V., Bakay, R. A. E., & Corcos, D. M. (2003). Deep brain stimulation of the VIM thalamic nucleus modifies several features of essential tremor. *Neurology*, *61*(7), 919–925. https://doi.org/10.1212/01.WNL.0000086371.78447.D2

van der Want, J. J. L., Wiklund, L., Guegan, M., Ruigrok, T. J. H., & Voogd, J. (1989). Anterograde tracing of the rat olivocerebellar system with phaseolus vulgaris leucoagglutinin (PHA-L). Demonstration of climbing fiber collateral innervation of the cerebellar nuclei. *The Journal of Comparative Neurology*, *288*(1), 1–18. https://doi.org/10.1002/cne.902880102

Venema, V., Ament, F., & Simmer, C. (2006). A Stochastic Iterative Amplitude Adjusted Fourier Transform algorithm with improved accuracy. In *Nonlin. Processes Geophys* (Vol. 13). www.nonlin-processes-geophys.net/13/321/2006/

Verstraelen, S., van Dun, K., Duque, J., Fujiyama, H., Levin, O., Swinnen, S. P., Cuypers, K., & Meesen, R. L. J. (2020). Induced Suppression of the Left Dorsolateral Prefrontal Cortex Favorably Changes Interhemispheric Communication During Bimanual Coordination in Older Adults–A Neuronavigated rTMS Study. *Frontiers in Aging Neuroscience*, *12*. https://doi.org/10.3389/fnagi.2020.00149

Walsh, E. G., & Wright, G. W. (1987). Inertia, resonant frequency, stiffness and kinetic energy of the human forearm. *Quarterly Journal of Experimental Physiology*, *72*(2), 161–170. https://doi.org/10.1113/expphysiol.1987.sp003060

West, T. O., Berthouze, L., Halliday, D. M., Litvak, V., Sharott, A., Magill, P. J., & Farmer, S. F. (2018). Propagation of beta/gamma rhythms in the cortico-basal ganglia circuits of the parkinsonian rat. *Journal of Neurophysiology*, *119*(5), 1608–1628. https://doi.org/10.1152/jn.00629.2017

Whaley, N. R., Putzke, J. D., Baba, Y., Wszolek, Z. K., & Uitti, R. J. (2007). Essential tremor: Phenotypic expression in a clinical cohort. *Parkinsonism and Related Disorders*, *13*(6), 333–339. https://doi.org/10.1016/j.parkreldis.2006.12.004

Wiklund, L., & Björklund, A. (1980). Mechanisms of regrowth in the bulbospinal serotonin system following 5,6-dihydroxytryptamine induced axotomy. II. Fluorescence histochemical observations. *Brain Research*, *191*(1), 129–160. https://doi.org/10.1016/0006-8993(80)90319-4

Wiklund, L., Sjolund, B., & Bjorklund, A. (1981). Morphological and functional studies on the serotoninergic innervation of the inferior olive. *Journal de Physiologie*, *77*(2–3), 183–186. https://europepmc.org/article/med/6169826

Wills, A. J., Jenkins, I. H., Thompson, P. D., Findley, L. J., & Brooks, D. J. (1994). Red nuclear and cerebellar but no olivary activation associated with essential tremor: A positron emission tomoraphic study. *Annals of Neurology*, *36*(4), 636–642. https://doi.org/10.1002/ana.410360413

Wlklund, L., Toggenburger, G., & Cuénod, M. (1984). Selective retrograde labelling of the rat olivocerebellar climbing fiber system with d-[3h]aspartate. *Neuroscience*, *13*(2), 441–468. https://doi.org/10.1016/0306-4522(84)90242-2

Wu, Y., & Raman, I. M. (2017). Facilitation of mossy fibre-driven spiking in the cerebellar nuclei by the synchrony of inhibition. *The Journal of Physiology*. https://doi.org/10.1113/JP274321

Yamawaki, N., & Shepherd, G. M. G. (2015). Synaptic circuit organization of motor corticothalamic neurons. *Journal of Neuroscience*, *35*(5), 2293–2307. https://doi.org/10.1523/JNEUROSCI.4023-14.2015

Yeo, C. H., Hardiman, M. J., & Glickstein, M. (1985). Classical conditioning of the nictitating membrane response of the rabbit - I. Lesions of the cerebellar nuclei. In *Experimental Brain Research* (Vol. 60, Issue 1). https://doi.org/10.1007/BF00237022

Yokoi, A., Arbuckle, S. A., & Diedrichsen, J. (2018). The role of human primary motor cortex in the production of skilled finger sequences. *Journal of Neuroscience*, *38*(6), 1430–1442. https://doi.org/10.1523/JNEUROSCI.2798-17.2017

Young, R. R., & Hagbarth, K. E. (1980). Physiological tremor enhanced by manoeuvres affecting the segmental stretch reflex. *Journal of Neurology Neurosurgery and Psychiatry*, *43*(3), 248–256. https://doi.org/10.1136/jnnp.43.3.248

Yu, M., Ma, K., Faust, P. L., Honig, L. S., Cortés, E., Vonsattel, J. P. G., & Louis, E. D. (2012). Increased number of Purkinje cell dendritic swellings in essential tremor. *European Journal of*

Neurology, *19*(4), 625–630. https://doi.org/10.1111/j.1468-1331.2011.03598.x

Zesiewicz, T. A., Shaw, J. D., Allison, K. G., Staffetti, J. S., Okun, M. S., & Sullivan, K. L. (2013). Update on Treatment of Essential Tremor. *Current Treatment Options in Neurology*, *15*(4), 410–423. https://doi.org/10.1007/s11940-013-0239-4

Zhan, X., & Graf, W. (2012). Harmaline Attenuates Voltage-Sensitive Ca2+ Currents in Neurons of the Inferior Olive. *Journal of Pharmacy &*. https://ejournals.library.ualberta.ca/index.php/JPPS/article/view/18370

Zhang, C., Zhou, P., & Yuan, T. (2016). The cholinergic system in the cerebellum: From structure to function. *Reviews in the Neurosciences*, *27*(8), 769–776. https://doi.org/10.1515/revneuro-2016-0008